The role of Helios in the hematopoietic stem and progenitor cell development

Giovanni Cova

UNIVERSITÉ DE STRASBOURG

ÉCOLE DOCTORALE DES SCIENCES DE LA VIE ET DE LA SANTÉ

INSTITUT DE GÉNÉTIQUE ET DE BIOLOGIE MOLÉCULAIRE ET CELLULAIRE (IGBMC)

THÈSE PRÉSENTÉE PAR:

Giovanni Cova

Soutenue publiquement le 25 Novembre 2019

Pour obtenir le grade de : **Docteur de l'université de Strasbourg**

Discipline/Spécialité : Aspects moléculaires et cellulaires de la biologie

THE ROLE OF HELIOS IN THE HEMATOPOIETIC STEM AND PROGENITOR CELL DEVELOPMENT

THÈSE DIRIGÉE PAR:
Dr. Susan Chan

EXAMINATEUR INTERNE
Dr. Irwin Davidson

RAPPORTEURS EXTERNES:
Dr. Hind Medyouf
Dr. Claus Nerlov

ACKNOWLEDGEMENTS

I would like to start by thanking Susan Chan and Philippe Kastner, who gave me the opportunity to work on such interesting and challenging project. I am grateful for all the support that they provided me during my PhD journey.

I thank Hind Medyouf, Claus Nerlov and Irwin Davidson for agreeing to judge my work, and particularly Hind Medyouf to be also part of my PhD mid-thesis committee and provide valuable scientific inputs.

I thank Peggy Kirstetter for all the inspiration and help over the past 4 years. I appreciated very much that she was always available to share part of the work by “fighting” and discussing with me.

A big thanks goes to all the members and friends of the lab, in particular: Céline for all the wise advices and kindness, Beate for organizing always amazing lab excursions, Célestine, Marie Céline, Chiara and Guillaume to be first friends and after colleagues. Lastly, a special thanks is for Patricia that always took care and helped me and every member of the lab.

I thank the whole IGBMC community: the way you can do science here is amazing! Special thanks go to: the FACS facility, and in particular Claudine Ebel and Muriel Philipps that shared with me many funny and also dramatic moments; the IGBMC mouse facility, and in particular Michael Gendron for all the kind help; the sequencing platform, and in particular Christelle Thibault for nice discussions and collaborations.

I am thankful to my friends: Annabella, Daniela, Federica, Rana, Rocio, Valentina, Federico, Nicla. This French adventure without you would not have been the same! You made my experience here the best of my life.

Towards the end, I want to thank my whole family for constant support from the beautiful Italy.

Last but not least, I want to mention the most important person, my girlfriend Chiara: thank you for your endless care and to be by my side.

TABLE OF CONTENTS

INTRODUCTION

HEMATOPOIESIS

Many different cell types with unique properties and functions, such as lymphocytes and myelocytes, circulate into the bloodstream. These cells have a limited lifespan and need to be replaced continuously throughout life. The developmental process that brings immature stem cells and progenitors to differentiate into more mature and specialized blood cells is called hematopoiesis. In humans and mice, adult hematopoietic stem and progenitor cells (HSPC) reside into the bone marrow (BM), where they can differentiate into mature cells that will either enter the bloodstream to accomplish their function or reach a secondary location to complete their differentiation (Zhang et al., 2018).

Hematopoiesis during ontogenesis

During ontogenesis, hematopoiesis takes place in different locations. In mouse, the first hematopoietic wave occurs in the yolk sack at embryonic (E) day 7.5, with the emergence of the first primitive erythrocytes. Later on, at E10.5, a second hematopoietic wave arises from the hemogenic endothelium (HE) of the aorta-gonad-mesonephros region (AGM), along with the emergence of the first pre-hematopoietic stem cell (HSC). Afterwards, pre-HSC matures into a definitive HSC and, around E12.5, migrates into fetal liver, where hematopoiesis takes place until birth (Ghosn et al., 2019; Kobayashi et al., 2019). After birth, hematopoiesis relocates into the BM where blood cells are produced for the entire life. During adulthood, proliferation and differentiation of BM HSPC are finely regulated, as they have to promote turnover of mature cells. Underlying this process, crucial roles are played by both hematopoietic and non-hematopoietic cells that regulate hematopoiesis by producing different regulatory molecules (Pinho and Frenette, 2019).

Hematopoiesis in the bone marrow

BM is a complex organ located in the cavity of long and axial bones. Two big categories of cells are found within the BM microenvironment: cells of hematopoietic origin and non-hematopoietic cells, such as stroma cells, endothelial cells, pericytes

and adipocytes (Ambrosi et al., 2017; Pinho and Frenette, 2019). The inner tissue around the bone marrow cavity is called endosteum and it is mainly composed by vasculature, osteoblasts and osteoclasts. Vasculature is highly dense all around the marrow with large arteries and veins mainly found in the central part of the marrow, branching to the peripheral endosteum into smaller arterioles and sinusoids. Wrapped around vascular cells there are pericytes and mesenchymal stem cells (MSC) able to differentiate into adipocytes, chondrocytes and osteoblasts. Moreover, within the marrow, are also found sympathetic noradrenergic fibers that can regulate hematopoietic cells in a circadian manner (**Fig. A**) (Pinho and Frenette, 2019; Zhao and Li, 2016).

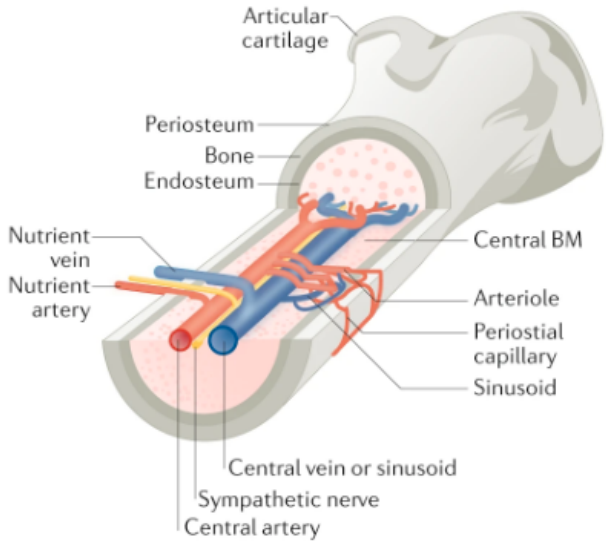

Figure A | The bone marrow cavity.
A representative tibia section is shown. Within the inner bone part, it is possible to recognize the endosteum, the marrow, the central blood vessels and the sympathetic nerve (Pinho and Frenette, 2019).

Hematopoietic cell hierarchy

Hematopoiesis is often represented with the help of an inverted tree-like diagram: the apex contains the multi-potent hematopoietic stem and progenitor cells (HSPC), they can self-renew and give rise to committed progenitors. In a second

layer, we find the committed progenitors that can be broadly divided into three sub-categories: *i)* the megakaryocyte and erythrocyte progenitors, originating red blood cells and platelets; *ii)* the myeloid progenitors that give rise to granulocyte, monocyte and also to dendritic cells *and iii)* the lymphoid progenitors generating B, T and also some dendritic cells (**Fig. B**).

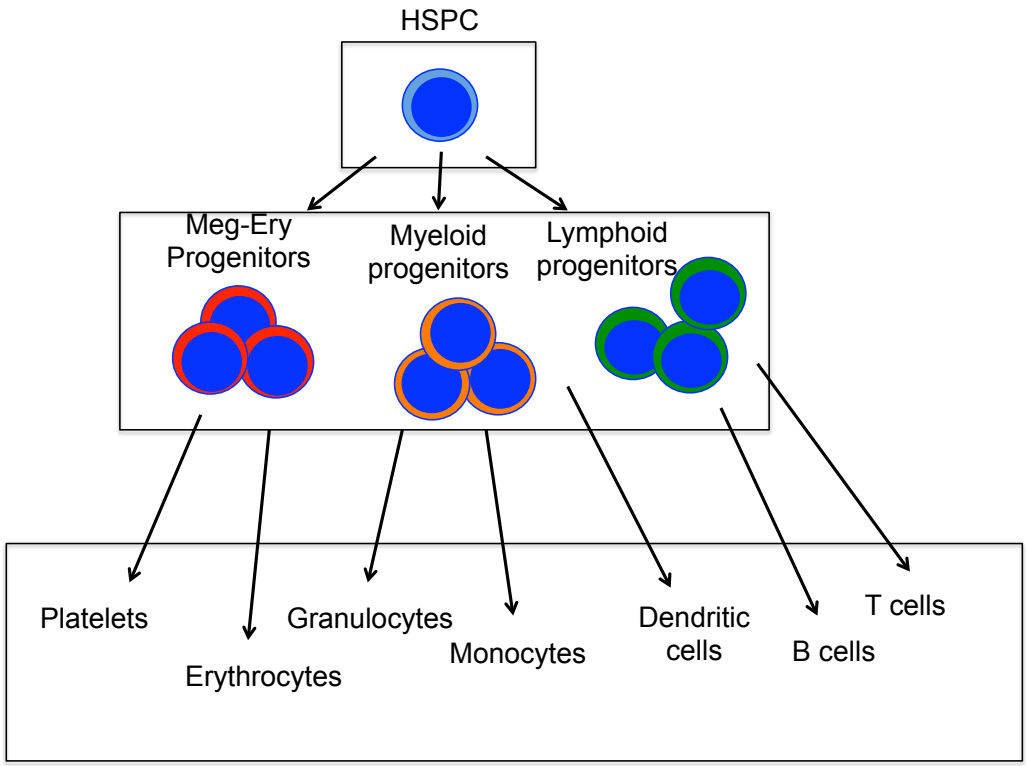

Figure B | Hierarchical hematopoietic structure.
Representation of the hematopoietic hierarchy. Starting from the top, HSPC give rise to the committed progenitors: megakaryocyte-erythrocyte (Meg-Ery), myeloid and lymphoid progenitors, which further differentiate in mature blood cells.

HOW TO STUDY HEMATOPOIESIS

Flow cytometry analysis

Flow cytometry is a routinely used technique to detect, quantify and classify cells based on their composition in either surface or intracellular markers. In particular, using a specific combination of fluorophore-conjugated antibodies directed

against “identifier” antigens, it is possible to recognize and therefore divide a heterogeneous BM population into phenotypically and functionally defined sub-populations. The flow cytometer scans high amounts of single cells in a relatively short time interval (~20.000 cells per second), allowing analyses even of small rare populations. Moreover, a relative high number of fluorophores, almost 15 in a single staining, can be used for a rapid and wide investigation of several populations (Adan et al., 2017; Cossarizza et al., 2017).

This technique has been extensively used in the past (and is still broadly employed), with the precise aim of discovering the antigen “combinations” necessary to divide total BM cells into distinct separate cell populations (Akashi et al., 2000; Kondo et al., 1997). In addition, the tool is particularly powerful when a researcher intends to study and quantify the effect of a specific genetic mutation (or intervention), as flow cytometry analysis allows for a fast and wide investigation. As mentioned before, it is also possible to stain cells for their intracellular content in DNA (cell cycle analyses), RNA, Ca^{2+}, Reactive Oxygen Species (ROS) and proteins (Darzynkiewicz et al., 2010; Hyman and Franz, 2012; Lovelace and Maecker, 2011; Soh and Wallace, 2018). Importantly, the staining of intracellular proteins, such as Transcription Factors (TFs), cytokines and cell cycle regulators, allows for their quantification at the single cell level, therefore permitting protein quantification also in small cell populations, otherwise inaccessible with other techniques that require higher amounts of cells (“high input techniques”).

Despite the great utility of this technology, some concerns need to be kept in mind to avoid result misinterpretation. It may happen that a given treatment or genetic mutation affects the expression of an identifier antigen used to mark a given cell population. In such case, the investigated population will appear reduced but only because cells lost expression of the representative antigen. This deceptive phenotype can finally lead to erroneous interpretation. To avoid such issue, it may be useful to analyze the same population looking at different identifiers whenever possible or, alternatively, to use another method of analysis.

Fluorescence Activated Cell Sorting (FACS) of a target population

Cells labeled either by fluorophore-conjugated antibody (directed to known surface antigens) or transgenic expression of a specific fluorescent protein can be

FACS purified and used for subsequent analyses (e.g. RNA-seq, ChIP-seq, cultures, etc.) (Cossarizza et al., 2017; Purton and Scadden, 2007). This tool is particularly useful when the cell population of interest is technically inaccessible because surrounded by other more abundant populations, as it is the case for HSC or progenitors (Frascoli et al., 2012; Oguro et al., 2013; Will and Steidl, 2010). An important issue to consider when sorting is cellular "contamination", which may arise when cell populations possess a similar pattern of antigen expression that prevents an efficient separation. In particular, experiments like mRNA-sequencing or CFU assays might typically suffer from such issue, as a contaminated pool of cells could bias the experimental outcome.

BM reconstitution assay

BM reconstitution assay represents a useful technique suitable to study HSC and progenitor (HSPC) functionality, reconstitution ability and differentiation potential. As only these cells engraft and reconstitute a hematopoietic depleted host system, these are the only cells appropriate for this assay. Based on reconstitution potential, HSPC can be divided into three groups: *(i)* Long Term reconstituting HSC (LT-HSC) that sustain hematopoiesis in a host environment for the whole life, *(ii)* Short-Term reconstituting HSC (ST-HSC) able to sustain hematopoiesis only for a few months and *(iii)* Multi-Potent Progenitors (MPP) capable to contribute to hematopoiesis in a host environment only for a few weeks (Grover et al., 2016; Kiel et al., 2005; Purton and Scadden, 2007).

Technically, HSPC donor cells, either FACS sorted or directly derived from total BM, can be injected into recipient host mice previously depleted of their endogenous hematopoietic system. If necessary, donor cells are typically injected along with helper BM cells, in order to sustain (during the first weeks) BM recovery and mouse survival. Donor HSPC and progeny are usually marked by the expression of an identifier surface antigen (e.g. CD45.2) that enables their distinction with respect to host cells (and helper cells), indeed marked by a different identifier (e.g. CD45.1 or both CD45.1 and CD45.2). This assay is particularly advantageous because it allows to study the HSC and progenitor function in an *in vivo* environment similar to the physiological one (Purton and Scadden, 2007).

In particular, this tool becomes powerful to uncover whether a given germ-line genetic mutation affects hematopoiesis intrinsically, as mutant hematopoietic cells can be transplanted into a WT environment. Furthermore, BM reconstitution assay can be performed in a competitive manner. For instance, WT and “mutant” BM cells can be co-injected into the same host recipient in order to directly compare their BM reconstitution ability in the same environment (Kwarteng and Heinonen, 2016). In a similar way, a defined number of control and “mutant” HSC can be purified and separately injected into different recipient mice, allowing in this case comparative analyses between the same amount of HSC (Beerman et al., 2014; Rossi et al., 2005). Lastly, BM reconstitution assay can be even performed with single injected LT-HSC, assessing in this way lineage potential at the single cell resolution (Carrelha et al., 2018).

Despite the idea that the host BM environment may represent the perfect “location” for studying HSPC behavior (because it is apparently identical to the physiological one), some concerns have to be considered. To make space into the BM and allow donor cell engraftment, the host hematopoietic system needs to be depleted, and this operation is often achieved through an invasive total body irradiation treatment. This process is known to be not specific and harmful for multiple non-hematopoietic tissues (like the BM microenvironment). When damaged, even only partially, those tissues may not be completely comparable to the initial healthy physiological state. Moreover, in contrast to the endogenous counterpart, transplanted HSPC need to extensively proliferate and differentiate in order to regenerate the depleted system, assuming a behavior which is different from, and not comparable to, the steady state one (Busch et al., 2015). Some new techniques have been recently developed in order to mitigate the aforementioned issue. Selective host HSPC depletion, achieved by using a specific antibody able to deliver toxic drugs to targeted cells, has been shown to be a good and mild strategy. Toxic targeted drug delivery allows elimination, through apoptosis, of endogenous HSPC (but in general of any cell type), thus creating an empty new space that allows the engraftment of donor injected HSPC (Czechowicz et al., 2019).

Colony forming unit (CFU) assay

When seeded into semisolid media containing appropriate cytokines, colony forming unit (CFU) cells, like HSC and progenitors, are able to proliferate and generate distinct separated colonies of mature hematopoietic cells. Each colony derives from a unique CFU cell and, as such, the final number of colonies will reflect the number of seeded progenitors (Purton and Scadden, 2007).

Several cytokine cocktails have been developed in order to stimulate the *in vitro* growth of progenitors or HSC. The general cocktail used to promote progenitor differentiation comprises SCF and IL3, which can be supplemented with more "lineage specific cytokines". IL-6 and GM-CSF stimulate myeloid progenitor differentiation, while EPO is required for CFU-erythroid (erythroid progenitor) development; TPO stimulates CFU-megakaryocyte (megakaryocyte progenitor) differentiation, whereas IL7 promotes pro-B cell expansion but only in the absence of IL-3 and the other mentioned lineage specific cytokines (Akashi et al., 2000; Kobayashi et al., 2019; Rieger et al., 2009; Young et al., 2016). Interestingly, HSC differentiation has slightly different requirements, as both SCF and TPO are necessary and colonies of all myeloid kinds can be obtained with the addition of either myeloid or erythroid specific cytokines (Akashi et al., 2000; Drissen et al., 2016; Grover et al., 2014; Mohrin et al., 2010). One of the greatest limitations of this assay is the impossibility to assess the myeloid and lymphoid HSC potential in the same medium, as lymphoid development requires unique and different culture conditions not compatible with the myeloid ones (Vieira and Cumano, 2004).

CFU assays can be performed by plating total BM cells; in this case, the assay is used to quantify the amount of specific CFU cells present in the BM. This approach represents an alternative quantification method with respect to flow cytometry analysis, as it allows progenitor quantification in a surface antigen independent manner. Alternatively, the assay can be applied to sorted HSC or progenitors in order to test their functionality. For example, by comparing sorted WT versus "mutant" HSC, it is possible to address whether an investigated mutation is able to affect the differentiation potential of such cells. Despite the fact that this assay provides a very advantageous tool of investigation, it is done in a synthetic *ex vivo* environment, which differs from the *in vivo* one; thus, the artificial condition could promote cellular behaviors that do not usually occur *in vivo*. In such respect, an externally provided cytokine cocktail may favor some paths instead of others, masking or biasing the real

potential of a given progenitor. Moreover, “ectopic” cytokine concentration could even force progenitors to accomplish certain differentiation pathways, which are not normally achieved *in vivo*, thus producing artificial outcomes.

Cell expansion in liquid culture

A common drawback when working with rare and sorted populations is the limited amount of material, which precludes the use of high input techniques. To overcome this problem, sorted cells can be seeded and expanded in an appropriate liquid culture medium. However, not all cell types can be easily grown: HSC, for instance, easily undergo differentiation (Wilkinson et al., 2019). In such cases, the researcher might want to genetically modify primary cells in order to obtain, whether possible, a homogeneous immortalized cell line. Specifically, HSPC cell line can be generated by transduction with genes able to increase their self-renewal ability (e.g. HoxB4 or Lhx2) (Antonchuk et al., 2002; Pinto do et al., 2001). Once transduced, the derived HSPC cell line can be extensively expanded within the appropriate medium condition. Interestingly, Wilkinson and colleagues recently described a new protocol for massive LT-HSC expansion, allowing for the use of primary cells instead of HSC derived cell lines. They expanded LT-HSC over the period of 1 month increasing the starting numbers by 800x. However, they also expanded a considerable high amount of progenitor cells (more than 95% of the cells are indeed progenitors), thus generating a heterogeneous cell population that need to be subsequently FACS purified (Wilkinson et al., 2019).

In conclusion, despite the fact that *in vitro* cellular expansion may represent a necessary tool, the method possesses some limitations and caution must be taken when such cellular models are used in replacement of endogenous primary cells. First, the *in vitro* condition may not fully reflect the *in vivo* context and lead to cellular epigenetic and functional changes. Second, genetic modification obtained for example by transgene insertion may drive dramatic cellular changes that render the *in vitro* cell system too different from the original one.

Cell tracking

Reporter genes encoding for fluorescent proteins (such as GFP, YFP and Td-Tomato) have been extensively used in hematopoietic research to study protein expression, localization and, in some cases, to track specific cell types otherwise inaccessible by surface antigen staining. For Treg identification, for instance, reporter genes under the control of the specific FoxP3 Regulatory Elements (REs) are extensively used (Li and Zheng, 2015).

Alternatively, constitutive expression of a reporter gene can be induced in a cell-type specific manner and used to track the derived progeny. For example, HSC specific REs can be used to drive expression of Cre recombinase fused to the Estrogen Receptor (Cre-ER transgene); upon tamoxifen injection, the Cre-ER protein can excide a lox-stop-lox cassette used to prevent constitutive expression of a given reporter gene of interest. Several REs have been chosen in order to trigger constitutive reporter expression in HSC and progeny, with the specific aim of uncovering their contribution to steady state hematopoiesis (Busch et al., 2015; Sawai et al., 2016). Despite being useful, one important limitation of this technique concerns the choice of the RE used to drive Cre-ER expression, since not always the chosen RE homogeneously drives Cre-ER expression in the population of interest. For example, Tie2 RE used to induce YFP expression in LT-HSC is active only in a little subset of LT-HSC (~1% of total LT-HSC) (Busch et al., 2015). On the contrary, other LT-HSC specific REs, like Pdzk1ip1 RE, induce Td-Tomato expression abundantly in LT-HSC, but they also “leak” into the more differentiated ST-HSC and MPP (Sawai et al., 2016).

Another strategy that allows the study of the progeny derived from a given cell is based on a more recent cellular barcoding technology (Pei et al., 2017; Rodriguez-Fraticelli et al., 2018). The generation of unique and permanent DNA barcodes, obtained for example by random transposition of a given DNA cassette or random recombination of a transgenic locus, allows the univocal reconstruction of the cellular hierarchy after barcode sequencing. With this method, HSC cells and the relative progeny will be identified because both share the same barcode sequence. The advantage of this technique, with respect to the gene reporter tool, is that each single cell is individually marked and, as such, single cell hierarchy can be estimated. Cell barcoding is usually achieved by using an inducible system, composed of a cell specific inducible protein, able to trigger random locus recombination or DNA

cassette transposition. Importantly, as mentioned before, the REs chosen to drive the expression of the “barcoding activating protein” constitute the main limitation, given that in some cases they can be active either too “strictly” or too “generously”. To overcome this drawback, Camargo and colleagues developed a system to “barcode” all hematopoietic cells in an inducible way. Some weeks after barcode induction (from 1 to 4), they were able to identify barcodes both specific for, and in common with, sorted HSC, progenitor and mature cells (Rodriguez-Fraticelli et al., 2018). This second approach overcomes the main limitation of the previous one because it is “promoter unbiased” and, thus, all the hematopoietic trajectories can be effectively detected. Importantly, in order to comprehensively track the LT-HSC contribution without underestimating it, the entire hematopoietic system (HSC, progenitor and mature cells) needs to be sorted from a single mouse.

High-throughput techniques

High-throughput technologies allow for a global assessment of molecular changes. RNA sequencing techniques detect transcriptional changes at the population level (bulk RNA-seq) or even at the single cell level (scRNA-seq). DNA sequencing-based techniques, such as ATAC-seq and ChIP-seq, serve to study nucleosome density, epigenetic modifications and TF-DNA binding (Jiang and Mortazavi, 2018). On the other hand, mass spectrometry represents the high throughput approach in the proteomic field. Interestingly, a hybrid flow cytometry – mass spectrometry machine, called Cy-TOF, has been recently developed and allows for the quantification of approximately hundred target proteins at the single cell resolution (Bendall et al., 2011).

While the value of these techniques is undisputed, some concerns need to be kept in mind. Chromatin immunoprecipitation, for example, possesses an intrinsic limitation, as it does not perform efficiently with small cell populations. Novel alternative low input approaches, like ChIPmentation, Cut and Run or ChIL-seq, have been recently developed in order to drastically reduce the amount of required input material (Harada et al., 2019; Schmidl et al., 2015; Skene and Henikoff, 2017). However, despite this great improvement, the starting material necessary for profiling TF binding to DNA is extremely variable and, in some cases, high amounts of cells are still required.

Single cell RNA sequencing (scRNA-seq) revolutionized the field of developmental biology, as the precise assessment of mRNA differences between single cells allows for the identification of cellular trajectories and heterogeneity with unprecedented high resolution. However, even scRNA-seq presents some limitations: high noise and “zero count”, due to partial mRNA capture, complicated differential gene expression analysis between small or “too similar” groups of cells, making bulk mRNA-seq more suitable for such aim (Hwang et al., 2018).

THE HEMATOPOIETIC CELLS

Mature cells

Mature hematopoietic cells can be broadly divided into lymphoid and myeloid cells. Myeloid cells, literally cells residing within the BM, are a heterogeneous group of mature cells. The definition of myeloid cells is vague and sometimes confusing. In the present thesis, the term myeloid cells will be used to indicate only granulocyte and monocyte cells, while the term pan-myeloid cells will be used to group erythrocyte, megakaryocyte, granulocyte, monocyte and dendritic cells.

Megakaryocytes and platelets

Platelets are small, rounded and anucleated cells originating from larger megakaryocytes. Similar to granulocytes, platelets contain cytoplasmic granules that can be liberated after platelet activation, called alpha granules, delta granules and lysosomal granules. Platelets are mostly known for their role in blood vessel haemostasis, as endothelial injury promotes their accumulation aimed at damage repair. In particular, after endothelial damage, extracellular matrix proteins like collagen and Vwf are exposed and bound by circulating platelets. Once bound, platelets become activated and secrete bioactive molecules to promote further platelet recruitment and activation and, consequently, blood vessel plug formation and bleeding cessation (Golebiewska and Poole, 2015).

In addition to their well-known roles in haemostasis, platelets were more recently described to participate in pathogen clearance. They accumulate rapidly to the site of infection and promote pathogen removal by many means: directly, by

releasing antimicrobial peptides or indirectly, acting as docking and activation site for other immune cells, such as T and B lymphocytes, dendritic cells and granulocytes (Yeaman, 2014). Moreover, in addition to their classical platelet progenitor roles, megakaryocytes possess HSC regulatory functions: BM megakaryocytes localize in close proximity to HSC and can partially regulate their quiescence by secreting high amounts of TGF-β1 (Bruns et al., 2014; Zhao et al., 2014).

Erythrocytes

Erythrocytes, also known as red blood cells (RBCs), are small, anucleated cells with a biconcave shape. They contain hemoglobin, a globular tetrameric protein composed of two α chains and two β chains. All globin chains are linked to a prostatic heme group containing an iron atom in the middle of the structure. The iron atom confers to the hemoglobin the ability to bind oxygen. RBCs circulate into the bloodstream and, once reached the lung capillaries, they bind oxygen and release CO_2. On the contrary, they release oxygen and pick up CO_2 when approaching peripheral tissues (Alam et al., 2017).

Granulocytes

Granulocytes are a class of myeloid cells morphologically characterized by the presence of cytoplasmic granules and a specific nuclear shape, as they can be either bi-lobed or tri-lobed. Granulopoiesis occurs in the BM and, once terminally differentiated, granulocytes leave the bone and enter into the bloodstream, circulating until inflamed tissues request them. Based on the content of their granules, granulocytes can be divided into 3 categories: basophils, eosinophils and neutrophils (Koenderman et al., 2014).

Basophils

Basophils are the least abundant granulocyte population in the blood, as they represent <1% of circulating leukocytes. They are characterized by the presence of basophilic granules, several Pattern Recognition Receptors (PRRs) and the strong expression of the Fragment crystallizable (Fc) Receptor (R) epsilon (FcεR), the immunoglobulin E receptor. With critical roles in allergy-related inflammation processes, basophils can be activated either in an Immunoglobulin (Ig) E mediated

way or in cytokine-related manners. Furthermore, basophils can also be important immune regulatory cells, as they secrete large amounts of IL4, a potent Th2 stimulatory cytokine (Siracusa et al., 2013).

Mast cells

Mast cells are mainly found in mucosal and epithelial tissues and, under physiological conditions, do not circulate into the bloodstream. They share many functional features with basophils, such as granules containing histamine and heparin, as well as the ability to bind IgE (Chirumbolo, 2012; Krystel-Whittemore et al., 2015).

Eosinophils

Eosinophils are rare blood circulating cells characterized by bi-lobed nuclei, large acidophil granules and expression of several PRRs. In contrast to other granulocytes, they highly express specific receptors like IL5Rα, CCR3 and SIGLEC-F. Among all the eosinophil regulatory cytokines, IL5 plays a major role in promoting their development, activation and survival. They express several Fc receptors that allow them to bind several immunoglobulin Fc chains. Furthermore, accumulating evidence have shown that eosinophils can act as antigen presenting cells (Akuthota et al., 2010; Rosenberg et al., 2013).

Neutrophils

Neutrophils are the most abundant granulocytes circulating into the bloodstream and their main function is to eliminate pathogen microorganisms. Neutrophils can directly recognize pathogens by their PRRs or, alternatively, be recruited and activated to the site of inflammation. They eliminate pathogenic microorganisms by different mechanisms: 1) recognizing antibody coated cells through their FcγR, they can perform phagocytosis; 2) moreover, they are able to kill pathogens by releasing granules containing bactericidal protein and Reactive Oxygen Species (ROS); 3) finally, under certain conditions, neutrophils might enhance their response by secreting a neutrophil extracellular trap. In addition to their classical role in innate immunity, neutrophils can trans-differentiate into antigen presenting cells and modulate T cell activation, when required (Koenderman et al., 2014; Li and Tablin, 2018; Mortaz et al., 2018).

Monocytes and macrophages

Monocytes and macrophages are mononuclear phagocytes that can be found either circulating into the bloodstream or resident into tissues. Like granulocytes, they express diverse PRRs and Fc receptors that help them to recognize and phagocyte pathogens. Once the inflammatory reaction is triggered, BM derived monocytes infiltrate the inflamed tissue and differentiate into macrophages. Macrophages activated by Pathogen Associated Molecular Patterns (PAMPs), Damage Associated Molecular Patterns (DAMPs) and inflammatory cytokines develop the pro-inflammatory M1 phenotype. Conversely, anti-inflammatory cytokines such as IL-10, IL-4 and IL-13 induce the M2 phenotype.

In contrast to the macrophages derived from BM monocytes, embryonic-derived, tissue resident macrophages have been shown to play major roles in regulating organ function and tissue homeostasis (Hirayama et al., 2017). Interestingly, it has been found that some macrophages marked by the surface antigen CD169 regulate BM to blood HSC migration and blood to BM HSC homing in antagonism to the sympathetic nervous system. Moreover, macrophages have essential roles in regulating erythrocyte maturation and enucleation (Chow et al., 2011).

Dendritic cells

Dendritic cells (DCs) are specialized Antigen Presenting Cells (APC) that operate at the interface between the innate and the adaptive immunity. They promote both T cell polarization and B cell activation, by presenting them foreign antigens. Three main subsets of BM-derived dendritic cells have been so far recognized: two conventional dendritic cell subtypes (cDCs), cDC1 and cDC2, and plasmacytoid dendritic cell (pDC).

cDCs reside in both lymphoid and non-lymphoid tissues and express high levels of the Major Histocompatibility Complex II (MHCII): type 1 cDC cells are recognizable because express the CD8a antigen, whereas type 2 cDC cells are CD11b positive (with splenic cDC2 also CD4 positive). Conventional DC 1 and 2 are considered the classical APC: they have a stellate morphology, express a wide range of PRRs, have strong antigen up-taking, processing and presenting capabilities, as well as the faculty, once stimulated by pathogen particles, to

migrate to draining lymph nodes in order to activate both T and B cells. On the other hand, pDCs represent a small subset of DCs that resides in BM and lymphoid organs, characterized by a plasma cell-like morphology and specialized in virus recognition. Once activated by viral particles, that are recognized by the TLR 7 and 9, pDCs start to produce vast amounts of anti-viral type I Interferon (IFN α, β and ω) and become able to internalize, process and expose foreign antigen peptides on the MHCII complex (Eisenbarth, 2019; Schlitzer and Ginhoux, 2014).

These three DC subsets, in contrast to the embryonic-derived DCs (such as Langerhans cells), are continuously produced within the BM and arise from the Macrophage Dendritic cell Progenitor populations (MDP) that possess both monocyte and DC potentials. MDP cells further differentiate into Common Dendritic cell Progenitors (CDP), that lack monocyte potential and give rise to: *i)* pre-pDC, the pDC precursor and *ii)* pre-DC, the precursor of cDC 1 and 2 (Puhr et al., 2015; Schraml and Reis e Sousa, 2015).

B lymphocytes

B cells are roundish nucleated cells mainly found in the bloodstream, bone marrow, spleen and lymph node. They recognize pathogens through their B cell receptor (BCR) or via PRRs. The BCR is constituted of a membrane bound Immunoglobulin (like IgD or IgM) responsible for the antigen binding, and by a transmembrane Igα and Igβ responsible for the signal transduction. Binding of the foreign antigen to the BCR triggers B cell activation. Immediately after binding, a cascade leading to the internalization, processing and presentation of the foreign antigen is started. The processed antigen is exposed on the MHCII and presented to lymph node or spleen naïve T cells. The B and T cell crosstalk promotes T cell polarization as well as B cell immunoglobulin class switch recombination, proliferation and terminal maturation. Terminally differentiated B cells, known as plasma cells, are devoted to secrete high amounts of soluble IgG, IgA and IgE used to opsonize pathogens (Tarlinton, 2019; Yuseff et al., 2013).

T lymphocytes

T lymphocytes are roundish nucleated cells mainly found in the bloodstream, thymus, spleen and lymph node. They derive from the bone marrow Earliest Thymic Progenitors (ETP), which migrate into the thymus and generate naïve T cells. T cells

can be divided into two classes: CD4 T helper (Th) and CD8 effector (Te) (Shah and Zuniga-Pflucker, 2014).

CD4$^+$ cells

Each naïve CD4$^+$ cell is characterized by the expression of a unique T cell receptor (TCR). The TCR recognizes antigens presented by the MHCII on activated APCs. Based on the nature and affinity of the antigen, the kind of co-receptors involved in the signaling as well as the type of released cytokines, naïve T cells can be polarized into functionally diverse Th cells.

The better characterized Th effector subtypes are: Th1 cells, promoting cellular immunity and characterized by the secretion of IL-2, IFN-γ and TNFα; Th2 cells, stimulating humoral response by producing IL-4, IL-5 and IL-13; Th17 cells, characterized by the secretion of IL-17 and able to support host defense against bacteria, fungi and viruses (Zhu et al., 2010). Another kind of activated CD4$^+$ cells, involved in self-tolerance maintenance, are FoxP3 expressing T regulatory cells (Treg), which secrete anti-inflammatory mediators that suppress APC cell functions as well as T cell activation. Recent work highlighted new roles for Treg, as they can also regulate homeostasis of non-lymphoid tissues (Burzyn et al., 2013). In relation to hematopoiesis, Tregs have been recently found to be a functional component of the Hematopoietic Stem and Progenitor Cell (HSPC) niche, where they suppress inflammation and promote lymphoid progenitor differentiation (Hirata et al., 2018; Pierini et al., 2017).

CD8$^+$ cells

Similar to CD4$^+$ cells, naïve CD8$^+$ cells are generated in the thymus. However, they recognize antigen exposed on the MHCI, expressed by all nucleated cells, and play a major role in fighting against intracellular pathogen infection. Once activated by APC, CD8$^+$ cells undergo expansion and migrate to the site of infection, where they can kill the infected cells by using different strategies: *i)* secreting anti-viral and microbial cytokines like IFNγ and TNFα, *ii)* releasing cytotoxic granules containing perforin and granzymes as well as *iii)* inducing cell apoptosis by exposing FAS-ligand (Schurch et al., 2014; Zhang and Bevan, 2011).

Innate lymphoid cells

Innate lymphoid cells (ILC) are a newly described cellular component of the immune system. In contrast to B and T lymphocytes, they do not possess specific antigen receptors. However, despite the inability to be activated by specific antigens, they possess some T cell-like features and, based on that, they were divided into four main groups: ILC1 resembling Th1 cells, ILC2 resembling Th2 cells, ILC3 resembling Th17 cells and natural killer (NK) cells resembling cytotoxic CD8 cells (Vivier et al., 2018).

Progenitor cells

Committed progenitors

"Committed progenitors" is a generic term used to group cells with common functional features:

(1) the ability to expand and generate colonies of mature cells when plated *ex vivo* (in the appropriate condition);

(2) reduced potency, as they can generate only a few (or even a unique) hematopoietic lineages (Boyer et al., 2019; Pronk et al., 2007);

(3) reduced BM reconstitution ability, as they can sustain hematopoiesis only for a few weeks when transplanted into lethally irradiated mice (Boyer et al., 2019).

Megakaryocyte progenitor (MkP)

MkP is defined as: lineage$^-$, c-Kit$^+$, Sca1$^-$ (LK), CD150$^+$ and CD41$^+$. FACS sorted MkPs plated in SCF, IL3, and TPO enriched medium generate colonies containing mature megakaryocytes (Pronk et al., 2007).

Erythroid progenitors (Ery-P)

Two erythroid progenitors, called preCFU-E and CFU-E, were identified in 2007 by the group of Weissman. Pre-CFU-E are considered the upstream progenitors, as they are able to give rise to more and bigger erythroid colonies than CFU-E, when cultured in media containing SCF, IL-3 and EPO. Phenotypically, they are defined as LK with a distinction: the preCFU-E are CD150$^+$ and CD105$^+$, whereas the CFU-E are CD150$^-$ and CD105$^+$ (Pronk et al., 2007).

Megakaryocyte-Erythrocyte progenitor (MEP)

A megakaryocyte erythrocyte bi-potent progenitor population was initially identified as LK, FcγR$^-$ and CD34$^-$ (Akashi et al., 2000). However, additional studies further divided this heterogeneous group into three populations, mainly composed of uni-potent erythroid and megakaryocyte progenitors, and a small bi-potent population called preMEP (Pronk et al., 2007).

PreMEP are LK CD150$^+$ CD105$^-$. Despite having both megakaryocyte and erythroid potential, it is currently not clear whether this population comprises bi-potent progenitors or rather it is a mixture of multiple, not separated, uni-potent progenitors. Some clues come from recent work where the MEP progenitor mRNA content was profiled at the single cell level. Paul and colleagues did not observe the presence of any bi-potent progenitor expressing both megakaryocyte and erythroid transcripts, while uni-lineage primed cells were mostly detected (Paul et al., 2016) (**Fig. C**). These observations support a view where the megakaryocyte and erythrocyte progenitor compartment is mainly composed of uni-potent erythroid and megakaryocyte progenitors; however, functional validations are still required to further confirm this view.

Granulocyte-Monocyte progenitor (GMP)

GMP is a bi-potent population defined as LK, FcγR$^+$, CD34$^+$ and CD150$^-$. Cultured GMP in media enriched with SCF, IL3 and GM-CSF give rise to either mixed or single colonies of mature granulocytes and monocytes (Akashi et al., 2000; Pronk et al., 2007). As for preMEP, the bi-potent nature of the GMP population has been recently reviewed by the group of Grimes (Olsson et al., 2016). In particular, sc-mRNA sequencing analysis identified two main cell clusters within the GMP pool: one cluster expressing Irf8 and monocyte transcripts, and a second one expressing Gfi1 and granulocyte signatures. The author further purified these 2 populations, using Gfi1 and Irf8 reporters and they tested their potential using *in vitro* CFU assay. It emerged that Gfi1-positive GMP generate only granulocyte colonies, while Irf8-positive GMP give rise exclusively to monocytes.

These findings strongly support the idea that the GMP population is mainly composed of uni-potent committed progenitors. In addition, the authors claimed the existence of an extra, rare bi-potent population co-expressing both monocyte and granulocyte signatures and capable of generating both lineages *in vitro* (Olsson et

al., 2016). However, there might be the possibility of an experimental artefact due to difficulties to clearly FACS separate this rare population. It is indeed located at the boarder of the abundant Gfi1 and Irf8 positive populations, raising the risk that the sorted cells represent just a contaminated pool of Gfi1 and Irf8 neighboring cells.

Common lymphoid progenitor (CLP)

CLP was the first identified hematopoietic progenitor and, in contrast to the myeloid progenitor, it does not belong to the LK population. CLP is Lineage$^-$, IL7rα^+, Flt3$^+$, Sca1^{mid} and Kit^{mid}. It possesses the ability to generate, *in vitro* as well as *in vivo*, lymphoid B and T mature cells. On the contrary, it is depleted of any myeloid reconstitution potential (Karsunky et al., 2008; Kondo et al., 1997). Recent work further sub-divided the CLP within 2 additional populations: Ly6D$^-$ CLP called All Lymphoid Progenitor (ALP), and a Ly6D$^+$ CLP renamed B cell biased Lymphoid Progenitor (BLP). The ALP has both B cell and T cell potentials and it is considered the BLP precursor, mainly devoted to produce B cells (Ghaedi et al., 2016; Inlay et al., 2009).

Common myeloid progenitor (CMP)

- Discovery of a common myeloid progenitor

A common myeloid progenitor (CMP) population was identified in 2000 by the group of Weissman. CMP are lineage$^-$, c-kit$^+$, Sca1$^-$, CD34$^+$ and FcγR^{low} cells. Cultured CMP give rise to colonies of all myeloid kinds (pan-myeloid): granulocytes, monocytes, erythrocytes and megakaryocytes (Akashi et al., 2000) (**Fig. Db**). Some years later, the idea of multi-potent pan-myeloid CMP was challenged by the same group, as the CMP was further split into two distinct bi-potent populations: one CD150$^+$ and CD105$^-$, called preMEP with megakaryocyte-erythroid potential and another one, CD150$^-$ and CD105$^-$, called preGM which possesses restricted granulocyte-monocyte potential. These observations prompted a view where the separation between megakaryocyte-erythroid and granulocyte-monocyte lineages occurred before reaching the CMP stage (Pronk et al., 2007) (**Fig. Dc**).

- CMP in the single cell era

Single cell (sc) qPCR first and, more recently, scRNA sequencing experiments provided massive help in uncovering the nature of the myeloid progenitors (Paul et

al., 2016). In particular, scRNA-seq of purified progenitors (CMP, GMP and MEP) described a gradual transcriptional heterogeneity within the myeloid progenitor compartment (**Fig. C**), revealing:

1) a well separated “peripheral” population composed of transcriptionally committed cells, clustering far away from each other and mainly part of the GMP and MEP populations;

2) a smaller pool of transcriptionally inter-connected cells belonging to the CMP population (**Fig. C**).

Interestingly, the CMP populations were themselves found to be heterogeneous, although transcriptionally more similar. Five main clusters were identified, each of them composed of transcriptionally primed pan-myeloid progenitors. Within these clusters, the authors identified erythroid, megakaryocyte, granulocyte, monocyte and DC primed progenitors, based on their RNA content. On the contrary, they never observed any cell cluster potentially belonging to a transcriptionally bi-potent state (Paul et al., 2016). In summary, these findings depicted a pan-myeloid progenitor compartment mainly comprising a pool of cells already transcriptionally primed towards single pan-myeloid fates, although these different populations have not been yet validated for their effective potential and function.

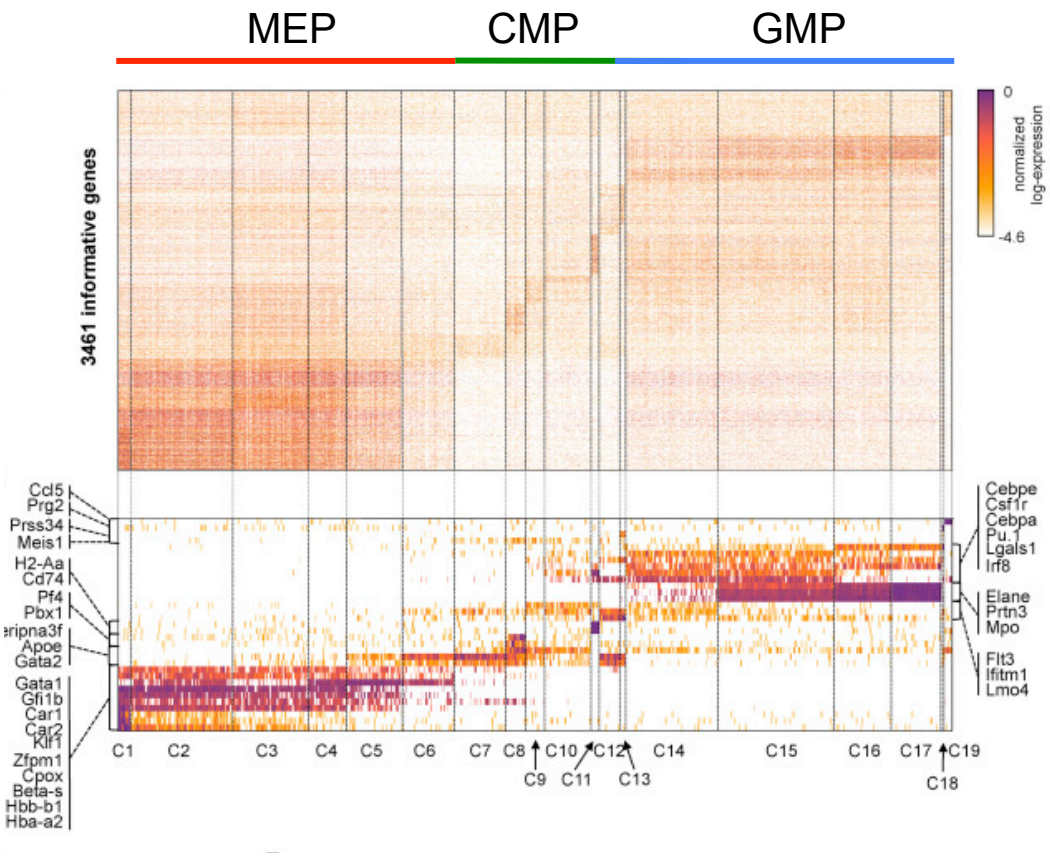

Figure C | The myeloid progenitor transcriptome at the single cell resolution.
Single cell mRNA transcriptome-based heatmap of differentially expressed genes across purified CMP, GMP and MEP cells. Five CMP clusters are located within the middle part of the heatmap, while the more committed MEP- and GMP-derived clusters are found at the periphery of the map (Paul et al., 2016).

- *A new bifurcation in the preGM*

In parallel, using a similar approach (scRNA-seq), Drissen and colleagues further recognized an additional branch separation within the pre granulo-monocyte progenitor (preGM) population, identifying: one preGM pool marked by the expression of Gata1 and a second one expressing Flt3. Furthermore, they functionally validated this bifurcation, uncovering that $Gata1^{+}$ preGM were composed of eosinophil-basophil progenitors, while $Flt3^{+}$ preGM were neutrophil-monocyte restricted progenitors (**Fig. Da,d**) (Drissen et al., 2016).

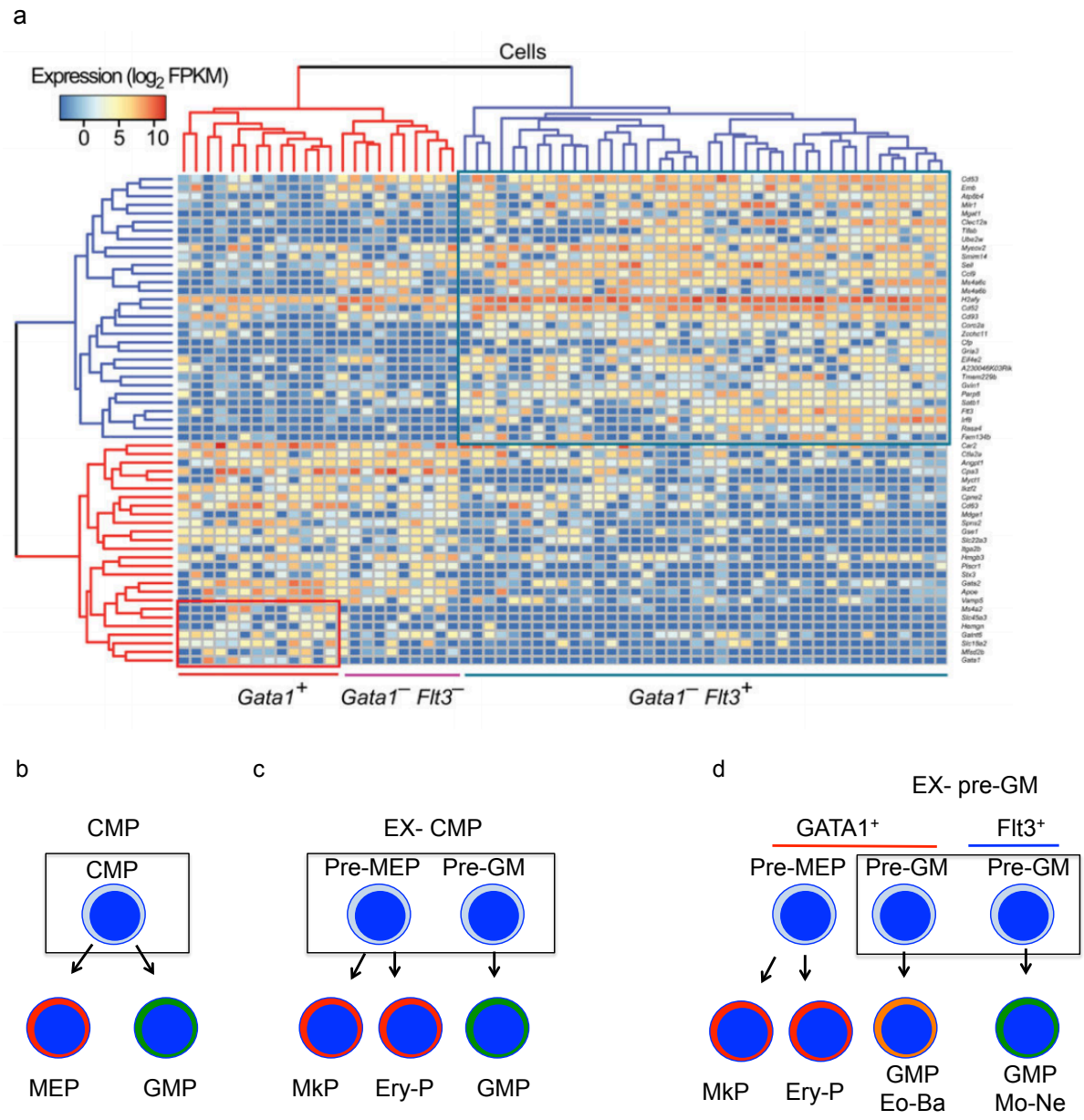

Figure D | Refining the myeloid progenitor hierarchy.
(**a**) Hierarchical clustering of differentially expressed genes between single pre-GM cells. Two main clusters marked by Gata1 and Flt3 expression can be identified: the pre-GM eosinophil and basophil progenitors (Gata1^{+}) and the monocyte / neutrophil progenitors (Flt3^{+}) (Drissen et al., 2016). (**b**) Myeloid progenitor hierarchy based on studies performed in 2000 (Akashi et al., 2000): a multi-potent CMP gives rise to bi-potent MEP and GMP. (**c**) Myeloid progenitor hierarchy based on Pronk and colleague findings (Pronk et al., 2007): the CMP population is split in pre-GM and pre-MEP populations. (**d**) Myeloid progenitor hierarchy from 2016: the pre-GM population is further divided in pre-GM Gata1^{+} and pre-GM Flt3^{+} progenitors (Drissen et al., 2016).

- To be a progenitor: a permanent state or a transient condition?

As discussed above, scRNA-seq analysis divided the CMP compartment into discrete clusters of lineage-primed cells. However, it remains unknown whether this transcriptional priming mostly represents a stable condition or rather a transient state. A recent publication from the Nerlov group has provided some hints. They showed that Gata1^{+} preGM cells retain the ability to differentiate *in vitro* into megakaryocyte and erythroid cells; similarly, Flt3^{+} preGM cells retain some lymphoid potential when cultured in a lymphoid cytokine enriched medium (Drissen et al., 2016). These results, even if performed in a synthetic *in vitro* context, seem to suggest that a certain degree of plasticity may exist within these transcriptionally primed cellular entities and that some developmental trajectories may be more interlinked with respect to others.

Taken together, both old and new findings provide support to a scenario in which the progenitor compartment is mainly composed of lineage primed cells, potentially able to maintain a partial degree of plasticity and multipotency (although with some limitations).

Multipotent progenitors (MPP)

Multipotent progenitors are Lineage^{-}, Sca1^{+}, c-Kit^{+} and CD48^{+} cells, with the unique ability to give rise to 1) all pan-myeloid and lymphoid lineages when transplanted into lethally irradiated mice and 2) all hematopoietic lineages when cultured in the appropriate *in vitro* condition (Oguro et al., 2013). MPP possess a limited BM reconstitution ability, which remains however greater than that of CLP and CMP cells (Boyer et al., 2019).

More recently, based on the expression of the CD150 and Flt3 surface markers, heterogeneity was identified within the MPP population, with some MPP exclusively expressing the surface antigen Flt3 while others the surface antigen CD150. Based on these features, 3 subpopulations of lineage biased MPP, with not well-established borders, have been identified: MPP2, MPP3 and MPP4 (Pietras et al., 2015). Moreover, scRNA-seq analysis of MPP revealed that such population is mainly constituted by a continuum of cell states in which one extremity is composed of Flt3^{+} lymphoid biased cells, whereas the other edge by CD150^{+} megakaryocyte-erythrocyte biased progenitors (Pietras et al., 2015; Rodriguez-Fraticelli et al., 2018).

MPP2

MPP2 are the first recognizable and immature megakaryocyte-erythrocyte biased progenitors. They are defined as $CD48^+$ and $CD150^+$, while they do not express the surface marker Flt3. *In vivo*, when transplanted into sub-lethally irradiated mice, they generate megakaryocytes and erythrocytes. Similarly, when plated *in vitro*, they produce mainly megakaryocyte-erythrocyte colonies (**Fig. E**) (Pietras et al., 2015).

MPP3

MPP3 are granulocyte-monocyte biased progenitors. In the context of their antigen expression, they are "located" in between MPP2 and MPP4 as they express low levels of Flt3 and CD150. Similarly, at the transcriptional level they also cluster in between MPP2 and MPP4 cells, as they express both MPP2 and MPP4 transcripts. *In vivo*, when transplanted into sub-lethally irradiated mice, they generate mainly mature granulocytes and monocytes. When plated *in vitro*, in a similar way, they generate granulo-monocyte colonies (**Fig. E**) (Pietras et al., 2015).

MPP4

MPP4 are lymphoid biased progenitors. They are marked by the high expression of Flt3 while, on the contrary, they do not express the antigen CD150. When MPP4 are transplanted into sub-lethally irradiated mice, they generate mainly mature lymphoid cells as well as also a minor percentage of myeloid cells. In line with the *in vivo* results, once plated *in vitro*, MPP4 can very efficiently generate lymphoid colonies, while retaining a partial granulo-monocyte potential. This mixed lymphoid and myeloid potential may derive from difficulties to properly separate MPP3 and MPP4 using flow cytometry techniques, as these two populations are "attached" to each other and do not possess well-defined borders (**Fig. E**) (Pietras et al., 2015; Young et al., 2016).

- MPP: primed or multi-potent progenitors?

As mentioned, recent work depicted an MPP population composed of 3 separate and biased cellular states. However, MPP properties were extrapolated based on *in vitro CFU assays* and *in vivo* transplantation experiments, conditions in

which MPP were “forced” to differentiate in small time windows. As such, these experiments do not provide information on the real MPP behavior at the steady state. Moreover, despite the described differences, MPP2, MPP3 and MPP4 still retain high degree of transcriptional similarity, greater than the one observed for example within CMP cells; for this reason, it might be hypothesized that they may retain a certain level of multipotency.

Suggestions supporting such scenario came from a recent publication. Rodriguez-Fraticelli and colleagues generated an inducible cellular barcoding system, in order to track the HSC and MPP steady state hematopoietic contribution (Rodriguez-Fraticelli et al., 2018). The author triggered random barcode transposition in all hematopoietic cells and they monitored the appearance of MPP specific barcodes within the more mature populations. Within the first two weeks, they noticed that each MPP was producing only one (or a few) mature cell lineage, a behavior expected from uni-potent cells. However, later on, unique MPP barcodes were abundantly found on different mature cells types, suggesting that MPP can indeed behave as plastic multi-potent cells in a long-term perspective.

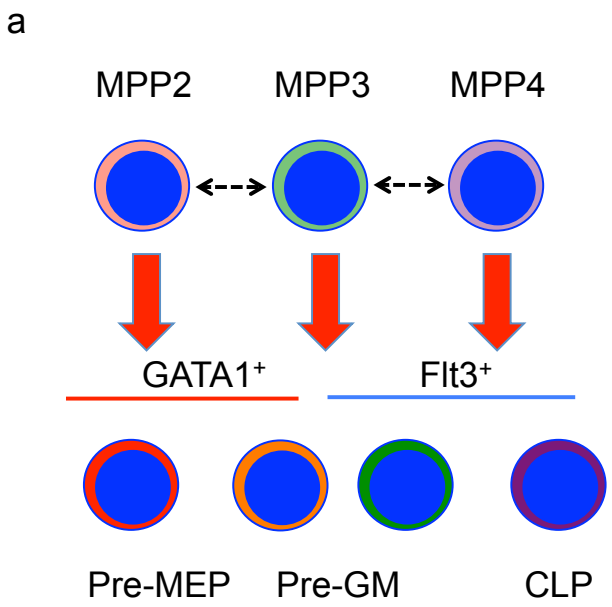

Figure E | The pool of biased MPP.
A schematic representation of the MPP hierarchy shows that MPP2 preferentially generate megakaryocyte and erythrocyte progeny (e.g. MEP), MPP3 originate myeloid progenitors (e.g. Pre-GM), while Flt3^{+} MPP4 mainly give rise to lymphoid lineages (e.g. CLP). The horizontal arrows suggest a possible scenario where MPP behave as partially inter-convertible plastic entities.

Hematopoietic stem cells (HSC)

HSC are placed at the apex of the hematopoietic hierarchy, as they fulfill unique and peculiar features:

1) *high quiescence*, resulting from their attitude to divide rarely;

2) *multi-potency*, as they can generate all hematopoietic lineages;

3) *self-renewal*, as they can reconstitute and maintain the entire hematopoietic system when injected into lethally irradiated mice. Based on this specific property, they are divided into two functional groups: *(i)* Long Term repopulating HSC (LT-HSC), belonging to the LSK, $CD34^-$, $CD48^-$ $CD150^+$ population and able to sustain hematopoiesis for the whole life; *(ii)* Short Term repopulating HSC (ST-HSC), enriched in the LSK, $CD34^+$, $CD48^-$ $CD150^-$ population and responsible to sustain hematopoiesis only for a few months after transplantation (Bernitz et al., 2016; Oguro et al., 2013).

-HSC: a heterogeneous multi-potent population

LT-HSC are undoubtedly real multi-potent cells, given that even a single LT-HSC can reconstitute several, if not all, hematopoietic lineages upon transplantation into lethally irradiated recipient mice (Bernitz et al., 2016; Oguro et al., 2013). Despite multi-potent, LT-HSC are not as homogeneous as it could be expected: subpopulations of functionally distinct LT-HSC have been identified in the past few years. In a recent elegant work, Carrelha and colleagues injected single LT-HSC into lethally irradiated mice and analyzed their progeny over a period of four months. They described five novel functional groups of LT-HSC with a stereotypical behavior. Specifically, ~10% of total LT-HSC are platelets lineage restricted (P), a limited ~5% is composed of platelets- (P) and erythrocytes- (E) restricted LT-HSC (PE), ~15% of LT-HSC are pan-myeloid- (PEM), a bigger fraction corresponding to the ~20% of the total LT-HSC produces pan-myeloid and B cell lineages (PEMB), while the remaining ~50% are multi-lineage reconstituting LT-HSC (**Fig. F**) (Carrelha et al., 2018).

Although the authors provided this detailed functional classification, an equivalent detailed phenotypical classification is currently not available. Through surface marker analysis it is only possible to roughly distinguish three broader groups: *i)* platelets biased LT-HSC, Vwf $^{+}$ and CD41^{+}, *ii)* pan-myeloid biased LT-HSC mainly CD150^{+} and *iii)* lymphoid biased (or equilibrated) CD150^{low} LT-HSC (Gekas and Graf, 2013; Morita et al., 2010; Sanjuan-Pla et al., 2013). Moreover, no evidence of such functional heterogeneity have been recognized via scRNA sequencing analysis, as all LT-HSC tend to cluster close to each other without showing any sign of lineage priming (Olsson et al., 2016; Rodriguez-Fraticelli et al., 2018). Interestingly, an exception is represented by old LT-HSC that acquired a peculiar platelet biased gene expression profile (Grover et al., 2016; Olsson et al., 2016).

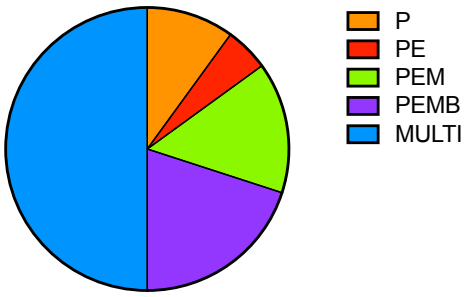

Figure F | The LT-HSC pool.
Schematic pie chart representing the LT-HSC repartition based on their *in vivo* single cell reconstitution potential: P are Platelets biased LT-HSC, PE are erythroid and platelet restricted LT-HSC, PEM are pan-myeloid LT-HSC, PEMB are pan-myeloid and B cell potent LT-HSC, while MULTI represents the more abundant population of multi-lineage reconstituting LT-HSC. Modified from (Carrelha et al., 2018).

- Contribution of LT-HSC to adult steady state hematopoiesis

As previously mentioned, LT-HSC greatly contribute to hematopoiesis in transplantation context. However, it is currently not clear to which extent they participate in hematopoiesis maintenance at homeostasis. Several researchers made use of inducible systems to tackle the question. Typically, a Cre-ER transgene is placed under control of regulatory elements (REs) specifically active in LT-HSC and, after tamoxifen injection, constitutive reporter gene expression is triggered in LT-HSC

and maintained throughout the cell progeny. However, contradictory results have been collected over the past few years, and the debate is far to be closed.

Busch and colleagues drove Cre-ER expression under the control or Tie2 REs and traced the LT-HSC progeny, marked by the expression of YFP, for several months. 34 weeks after tamoxifen injection, they found that only 1% of mature cells were YFP positive, suggesting that LT-HSC poorly contribute to steady state hematopoiesis (Busch et al., 2015). In stark contrast, the groups of Reizis and Nakada, using a similar tracking system, found that LT-HSC massively contribute to steady state hematopoiesis, however they drove LT-HSC specific Cre-ER expression using different REs (Chapple et al., 2018; Sawai et al., 2016). The explanation for these contrasting results may reside in the degree of HSC specificity of the different REs employed to trigger Cre-ER expression and reporter gene activation. Tie2-CreER was expressed only in a limited subset of LT-HSC (~1 % of total LT-HSC), raising the question whether enough LT-HSC were marked. On the contrary, the other Cre-ER system was also ectopically expressed in ST-HSC and MPP, suggesting that the observed contribution was mediated by more proliferating progenitors. Interestingly, independently from the level of LT-HSC contribution, all two groups found that LT-HSC preferentially renew the megakaryocyte-platelet lineage.

A third research group tried to address this question undertaking a different approach, in order to overcome the intrinsic limitations behind the promoter choice. Specifically, the group of Camargo labeled all hematopoietic cells using an unbiased barcode system and, over time, quantified the LT-HSC specific barcodes in common to the mature lineages. The authors found that LT-HSC strongly contributed to the megakaryocyte lineage replenishment and little to the myeloid and lymphoid renewal. Moreover, most of LT-HSC (~94.5%) were inactive, with no barcode shared with any mature cells (Rodriguez-Fraticelli et al., 2018). This experiment seems to propose, in a more unbiased and conclusive way, that LT-HSC provide little contribution to the steady state hematopoiesis, exception made for megakaryocyte lineage.

- LT-HSC niche

LT-HSC activity, such as self-renewal, differentiation and migration, needs to be precisely regulated and relies on regulatory inputs provided by a specific “niche” in which both hematopoietic and non-hematopoietic cells reside (Pinho and Frenette,

2019; Zhao and Li, 2016) (**Fig. G**). LT-HSC and their niche are homogeneously distributed along the cavity of the bone marrow, although their concentration increases moving from the central vein to the endosteum (Kunisaki et al., 2013). LT-HSC closely associate with endothelial cells (EC) and: ~ 80% of HSC are located close to sinusoids, while a smaller ~20% are found in close proximity to arterioles. Endothelial cells, and in particular arteriolar EC, are an important source of pro-hematopoietic factors like: stem cell factor (SCF), which regulates HSC maintenance, and Dll4 modulating lymphoid progenitor development (Asada et al., 2017; Kunisaki et al., 2013; Xu et al., 2018). In addition, in close proximity to endothelial cells there are perivascular pericytes^{myh11+}, producing an important regulator of HSC maintenance and egress, CXCL12 (Asada et al., 2017).

Leptin Receptor Positive Mesenchymal Stem Cells (LepR^{+} MSC) represent another important niche component, reported to be a heterogeneous population of adipocyte-primed and osteoblast-primed cells, both able of produce high levels of SCF and CXCL12 (Asada et al., 2017; Mendez-Ferrer et al., 2010). In addition, some MSC can also produce IL-7, a crucial cytokine that stimulates lymphoid progenitor survival and development (Cordeiro Gomes et al., 2016; Tikhonova et al., 2019). Moreover, wrapped around blood vessel and MSC, are found sympathetic adrenergic fibers that can regulate HSC and MPP differentiation by stimulating MSC through the β2 and β3 Adrenergic Receptors (AR): β2AR induces MSC to produce IL-6 that, in turn, skews HSPC differentiation towards a myeloid-megakaryocyte fate. On the contrary, β3AR stimulation weakens myeloid-megakaryocyte differentiation (Ho et al., 2019; Maryanovich et al., 2018).

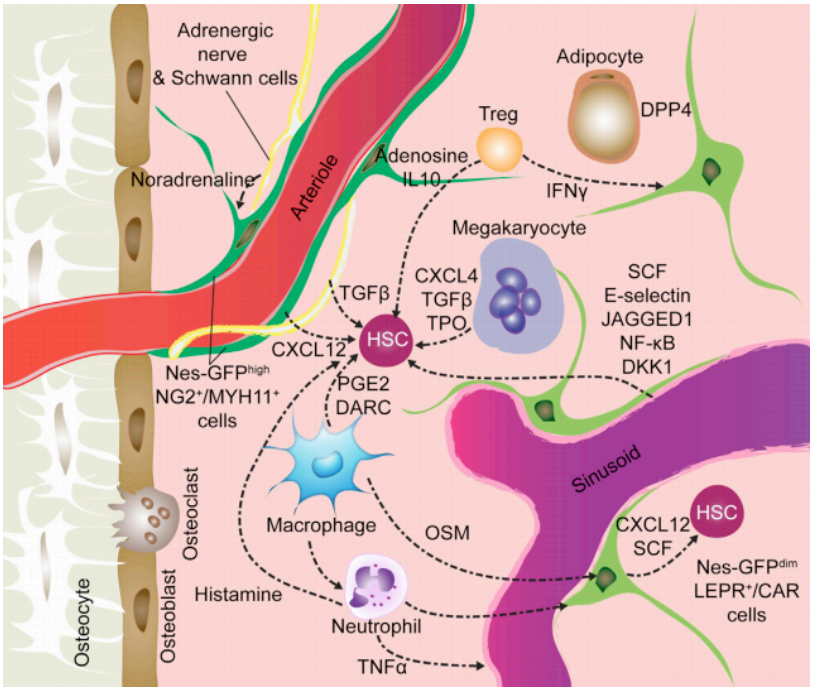

Figure G | The bone marrow LT-HSC niche.
Representative scheme of a typical BM LT-HSC niche architecture. LT-HSC localize close to vasculature, MSC and pericytes. Within the BM cavity, mature hematopoietic cells, such as megakaryocytes, macrophages and T cells, along with extra-hematopoietic cells, regulate LT-HSC activity. Modified from (Wei and Frenette, 2018).

AGING OF THE HEMATOPOIETIC SYSTEM

The old hematopoietic system

Hematopoiesis in mouse (and human) occurs throughout the entire life, however the composition of the system changes with respect to the age. Old mice have reduced B cells, while producing more granulocytes, monocytes and platelets. Interestingly, the progenitor compartment changes in the same direction, as old mice have reduced MPP4 and CLP, as well as increased MPP3, GMP and MkP (Rossi et al., 2005; Young et al., 2016). Also, LT-HSC become affected by the aging process, as they:

- accumulate DNA damage (Beerman et al., 2014; Flach et al., 2014);
- increase in number (Rossi et al., 2005);
- lessen their reconstitution ability (Pietras et al., 2015; Rossi et al., 2005);
- start to express megakaryocyte specific genes (Grover et al., 2016);
- acquire a myeloid and platelet skewed potential (Pietras et al., 2015).

LT-HSC aging

Old LT-HSC become less functional, as they reconstitute less efficiently lethally irradiated mice with respect to the young counterpart. Moreover, when transplanted, old LT-HSC reconstitute an old like hematopoietic system, with fewer B lymphoid cells and more granulocyte-monocyte cells (Pietras et al., 2015; Rossi et al., 2005). These findings suggested that LT-HSC might represent the major source of hematopoietic aging.

A defective myeloid biased pool of LT-HSC expands in old mice

The LT-HSC compartment expands in old mice and, in particular, the pool of $CD150^{+}$ and $CD41^{+}$ megakaryocyte and myeloid biased LT-HSC (here called myLT-HSC) expands more than the lineage equilibrated $CD150^{low}$ $CD41^{-}$ pool (also called lymphoid biased LT-HSC). Furthermore, only the injection of old myLT-HSC into lethally irradiated mice reproduces the aging phenotype, while injection of old $CD150^{low}$ LT-HSC alone does not generate an old system. These findings showed that a selective accumulation of “defective” megakaryocyte and myeloid biased LT-HSC takes place in the BM of old mice (Gekas and Graf, 2013; Pietras et al., 2015).

-How do old myeloid biased LT-HSC accumulate?

It has been proposed that myLT-HSC accumulate in old mice with a mechanism of clonal expansion (Pietras et al., 2015; Yamamoto et al., 2018). Although this could be possible, it is hard to explain why and how a specific pool of HSC should expand more than another one. Moreover, the myLT-HSC pool is little (and quiescent) in young mice and it seems unlikely that it can expand so much to overcome the more abundant pool of lineage equilibrated LT-HSC. Alternatively, it can be assumed that a gradual age-dependent “conversion” at the epigenetic and transcriptional levels transforms lineage equilibrated young LT-HSC into old myLT-HSC. Recent studies showed that some stimuli, like inflammation and DNA damage, can indeed convert young stem cells into old-like LT-HSC (Chang et al., 2016; Mirantes et al., 2014). The HSC compartment changes phenotype when mice are treated with agents able to trigger an inflammatory response, such as lipopolysaccharides (LPS) and polyinosinic: polycytidylic acids (polyI:C). LT-HSC from treated mice rapidly acquire a platelet biased $CD41^{+}$ phenotype and start to express genes that are typically up-regulated in old LT-HSC. These findings provide

evidence that inflammatory stimuli are potentially able to affect the LT-HSC phenotype (Haas et al., 2015; Mann et al., 2018).

Another potential aging driving force is DNA damage accumulation, which has been shown to dramatically increase in aged HSC (Beerman et al., 2014; Flach et al., 2014). Several studies showed that DNA damage induced upon treatment (e.g. by gamma or X-ray irradiation) can convert young HSC into old ones. DNA damaged young HSC reconstitute an “old-like” hematopoietic system when injected into lethally irradiated mice, suggesting that DNA injury intrinsically and permanently generates an old LT-HSC phenotype (Chang et al., 2016). However, despite these results seem to indicate a critical role of DNA damage in driving HSC aging, it cannot be excluded that acute DNA damage may drive a myLT-HSC positive selection (and a negative one for lineage equilibrate HSC), rather than a young to old HSC conversion.

Epigenetic and transcriptional changes occur in old LT-HSC

In order to understand the differences between old and young LT-HSC, epigenetic and transcriptomic analyses have been performed. Old LT-HSC have an altered DNA methylome when compared to young HSC. Specifically, Sun and colleagues reported that some lymphoid genes, like Flt3, were hypermethylated and repressed, while myeloid genes such as Gata2 and Runx1 showed the opposite pattern, suggesting a model where old HSC may “reprogram” their epigenome in order to be primed towards the myeloid fate, instead of the lymphoid one (Sun et al., 2014). However, it should be noticed that the genes identified in this study represent only a very small fraction of the total lymphoid and myeloid genes. Moreover, recent mRNA-seq experiments did not arrive to the same conclusion when comparing young and old LT-HSC transcriptomes: gene set enrichment analysis (GSEA) did not show any significant depletion of lymphoid gene signatures in old LT-HSC (Grover et al., 2016). Interestingly, from this work it also emerged that old LT-HSC have an enrichment in megakaryocyte signatures (Grover et al., 2016), even though the functional relevance of such changes remains largely unknown and the mechanisms leading to the megakaryocyte and myeloid skewing still need a proper investigation.

- Are old LT-HSC alone sufficient for promoting the aging of the hematopoietic system?

As mentioned before, old LT-HSC are able to promote hematopoietic aging when injected into lethally irradiated mice. However, given that LT-HSC contribution to the steady state hematopoiesis seems to be limited (Busch et al., 2015; Chapple et al., 2018; Sawai et al., 2016), it could be argued that also their contribution to hematopoietic aging will be partial and limited. In a such scenario, what may drive hematopoietic age? Recent studies suggested that aged BM microenvironment may have a central role in shaping the old hematopoietic system.

BM microenvironment and hematopoietic aging

The BM microenvironment undergoes gradual changes during mouse aging. The vasculature becomes depleted of arterioles, whereas the density of sinusoids and capillaries has been reported to increase. MSC expand in number, although they decrease the production of pro-hematopoietic factors like SCF, CXCL12 and Angiopoietin (Ho et al., 2019; Maryanovich et al., 2018). Discordant results have been described for the sympathetic nervous system, as some groups detected increased amounts of nervous fibers, while another team reported nerve degeneration. However, both groups agreed that adrenergic signals from sympathetic BM fibers can regulate LT-HSC transition towards a myeloid-megakaryocyte biased state (Ho et al., 2019; Maryanovich et al., 2018). Furthermore, the amount of pro-inflammatory cytokines like IL1α/β, IL-6 and IFNγ, able to favor myeloid progenitor differentiation, increased in old BM. Nevertheless, the identity of the cells producing such cytokines, during aging, is not well defined (Ho et al., 2019; Maeda et al., 2005; Matatall et al., 2014; Mirantes et al., 2014).

Despite many studies have shown that the microenvironment and, particularly, chronic inflammatory conditions can shape the hematopoietic system in an aged-related manner, an old BM environment alone seems to be not sufficient to age the hematopoietic system. In particular, young LT-HSC transplanted into lethally irradiated old mice generate a “young-like” hematopoietic system, despite the old microenvironment and, the other way around, old LT-HSC transplanted into young recipients generate an old-like system despite the young microenvironment. Thus, it becomes clear that the LT-HSC state dominates over the microenvironment,

probably suggesting that intrinsic LT-HSC alterations may be somehow the primary cause of hematopoietic aging (Ergen et al., 2012; Rossi et al., 2005).

In light of these facts, the main question stays the same: how do LT-HSC promote the hematopoietic aging? While a clear and definitive answer cannot be addressed, it is possible to propose some hypotheses. In the first scenario, LT-HSC could directly contribute to hematopoietic aging by generating a biased progeny. However, as mentioned before, the most recent studies argue against this model, given that LT-HSC poorly contribute to steady state hematopoiesis. Alternatively, epigenetic changes may occur in LT-HSC and similarly within MPP, leading to a skewed myeloid differentiation outcome that is mainly supported by both HSC and MPP. Additionally, a third possibility envisions that old LT-HSC may become able to shape their own niche and affect the closest MPP.

THE TRANSCRIPTIONAL CONTROL OF HEMATOPOIESIS

The hematopoietic transcription factors

Extracellular signals are crucial mediators of cellular plasticity, as they for example regulate the stemness of the HSPC pool, as well as their commitment and further progenitor maturation. Elaboration of such environmental stimuli often converges on Transcription Factor (TF) activity, which in turn shapes gene expression. TFs represent the first layer of gene expression regulation, they are *trans*-acting factors able to bind short *cis*-DNA regulatory elements (REs) to positively or negatively affect gene expression. In particular, it has long been appreciated that TFs shape gene expression patterns by working in cooperation with other TFs; therefore, activation of a given gene network requires the joint activity of several TFs (Reiter et al., 2017). Importantly, acquisition of a specific TF "combination" is the key event that drives and support lineage specification. In hematopoiesis, for instance, erythroid specification requires GATA1, Sox6 and KLf1 TFs; myeloid progenitors need CEBPα, CEBPε and SPI1, whereas the lymphoid branch wants Pax5, Ikaros and EBF1. The presence of each member of a given TF combination is essential to guarantee a specific cellular fate, and even small changes in TF composition can

lead to phenotypic differences (Dore and Crispino, 2011; Wilson et al., 2011; Yu et al., 2017).

While it is clear that specific combinations of TFs are exploited to generate different cellular lineages, it remains obscure how these different combinations are assembled during the process of HSPC differentiation. A model of stochastic switches between cross-antagonistic TFs has been proposed to be the primary force underlying HSC differentiation (Hoppe et al., 2016): random fluctuations of the erythroid master TF GATA1 and the myeloid master TF SPI1 were suggested to determine HSC fate choice. In order to challenge this model, Hope and colleagues cloned two different reporter genes under the control of GATA1 and SPI1 REs. They sorted and seeded LT-HSC in media containing cytokines, promoting both erythrocyte-megakaryocyte and myeloid cell differentiation. They monitored by *in vivo* staining the differentiation process for one week, looking at the emergence of myeloid preGM and MEP cells. In parallel, they measured by real time immunofluorescence the levels of GATA1 and SPI1. This experiment showed that when GATA1 was detectable (after 3 days of culture), HSC or progenitors differentiate into megakaryocyte and erythroid cells independently of SPI1 levels. On the contrary, GATA1 was never detected when HSC undergo myeloid differentiation.

In conclusion, the authors denied the existence of a GATA1 versus SPI1 cross-antagonism in HSC, as: *i)* the two TFs are not expressed together within the multipotent HSC; *ii)* GATA1 becomes expressed only later, independently of SPI1 starting levels; *iii)* similarly, SPI1 is expressed at low levels in HSC and bursts only when the myeloid path is activated. The authors proposed that these two TFs were not involved in HSC fate choice but rather they were reinforcing their relative lineage pathways once the decision was already taken (Hoppe et al., 2016). This study does not exclude the strength of a model in which TFs with cross antagonistic effects may lead to HSC fate determination; however, it does exclude that this specific behavior is performed by GATA1 and SPI1.

Ikaros family of TFs provides a useful tool to study hematopoiesis

Several approaches have been applied in order to uncover the mechanisms underlying cell decision, commitment and maturation. Among others, TF “manipulation” has emerged since many years as an advantageous tool, as it allowed

researchers to explore some of the networks and pathways that are crucial to accomplish a given cellular function. However, how could we select a good TF candidate? A promising candidate gene can be chosen by undertaking an experimental screening approach or, alternatively, because a certain TF may possess an intriguing expression pattern fitting with a given biological question. Once appointed, the TF is usually “manipulated” (often deleted but also overexpressed) in order to evaluate whether its removal or its ectopic induction causes any interesting phenotype. It must be noted that this first step represents a bottleneck, as not always the targeted TF shows an obvious and interesting phenotype. However, in case of a manifested phenotype, this mutation becomes a fruitful tool to characterize TF-regulated networks and finally lead to the identification of the molecular and cellular mechanisms underlying the process object of study.

Several TFs have been used as models to study different aspects at the basis of hematopoietic development. One remarkable example is given by the Ikaros TFs, belonging to a family containing four homologous members: Ikaros (IKZF1), Helios (IKZF2), Aiolos (IKZF3) and Eos (IKZF4). These four genes encode proteins with similar structure and a peculiar pattern of expression (**Fig. H**). Different knockout (KO) mouse models of these hematopoietic specific TFs have been generated and helped to uncover gene networks, pathways and mechanisms fundamental to accomplish HSPC development, lymphoid differentiation, maturation and leukemogenesis avoidance (Georgopoulos, 2017; Heizmann et al., 2018).

Ikaros:

In contrast to the other members of the family, Ikaros has a broad expression pattern: it is expressed in HSPC, progenitors and mature cells. Its KO causes a vast range of defects in the hematopoietic system and it represents the best-studied member of the family (Georgopoulos, 2017; Heizmann et al., 2018).

- In HSPC

Germline Ikaros KO has a strong impact on hematopoiesis, as several lineages are affected at different stages of development. Specifically, Yoshida and colleagues found an important involvement of Ikaros regulation as early as at the HSPC stage, where it promotes proper HSPC differentiation. Mice bearing an Ikaros germline loss of function mutation indeed show reduced LMPP (also known as MPP4) and CLP

(Yoshida et al., 2006). Furthermore, transcriptome analysis of Ikaros KO LSK, in comparison to WT LSK, revealed a depletion of lymphoid gene signatures, with concomitant increased expression of stem cell-like genes (Ng et al., 2009). The authors concluded that Ikaros directly primes lymphoid gene expression in LSK or HSC. However, this interpretation may be not completely accurate, as at the time of this study the LSK pool was not well defined and it was studied as total bulk population. It is therefore difficult to distinguish whether the observed lymphoid gene depletion was directly mediated by Ikaros or, rather, it was an indirect consequence of an altered MPP composition. Today, given that the heterogeneity within the LSK population has been better resolved and great improvement has been achieved in low input and single cell-based techniques, it will be possible to investigate more accurately the mechanisms underlying Ikaros control of HSC differentiation.

- In B cells

Ikaros is required also in early B cell development, as highlighted by its conditional deletion in pro-B cells. Lymphoid progenitor development requires adhesion to $IL7^+$ MSC, while further maturation demands an efficient detachment (Freitas et al., 2017). Ikaros null pro-B cells showed a differentiation block at the early IL7 dependent pre-B cell stage and up-regulated genes involved in the IL-7 and Integrin dependent pathways (Heizmann et al., 2013; Joshi et al., 2014). Furthermore, ChIP-seq experiments showed that Ikaros directly binds and represses REs of cell adhesion coding genes, whereas it directly activates genes necessary for pre-B cell maturation (Hu et al., 2016).

- In T cells

Immature Double Negative (DN) thymocytes carrying a hypomorphic Ikaros mutation ($Ikaros^{L/L}$) have altered H3k27 tri-methylation landscape along with entropic gene expression up-regulation. ChIP-seq experiments showed that Ikaros directly binds and represses enhancers typically active in immature HSC and progenitors. Consequently, $Ikaros^{L/L}$ thymocytes progress their maturation with an inefficient and delayed repression of ectopic HSPC genes (Freitas et al., 2017). However, despite these alterations, $Ikaros^{L/L}$ thymocytes manage to reach the final CD8 and CD4 stage, while remaining defective and able to develop leukemia (Dumortier et al., 2006; Oravecz et al., 2015).

Aiolos:

In contrast to Ikaros, Helios and Eos, Aiolos is the Ikaros member exclusively expressed in mature B and T cells. Aiolos KO mice have specific defects only during late B cell maturation: small pre-B cell compartment is expanded, highlighting a block of differentiation at this stage of B cell development (Wang et al., 1998). ChIP-seq experiments performed on pre-B cells showed that almost all Ikaros-bounded genes were also bounded by Aiolos (Hu et al., 2016). Despite this could suggest the existence of functional redundancy between the two factors, overexpression of Aiolos alone into Ikaros KO pre-B cells does not rescue the differentiation phenotype, suggesting that these factors may possess unique and different features, despite being very similar (unpublished data from our lab).

Helios:

Helios is characterized by a peculiar expression pattern, with high mRNA levels detected in HSPC as well as in more differentiated Treg cells. While there is a large body of literature on its role in Treg cells, Helios contribution to HSPC biology has not been fully addressed yet. Helios KO mice do not show any alteration in T cell development, although Treg functionality appears to be compromised (Kim et al., 2015; Liu et al., 2012). Kim and colleagues reported that Helios KO Treg are not as efficient as WT Treg in suppressing T helper cell activation; moreover, mice depleted of Helios activity are prone to develop autoimmunity with aging. These findings have been partially reviewed by the group of Shevach, which confirmed a role of Helios in regulating Treg suppressive function without however reporting the emergence of any autoimmune phenotype (Sebastian et al., 2016). Kharas and colleagues recently found that Helios is additionally involved in leukemic stem cell regulation, as its removal decreases their self-renewal capability while supporting their myeloid differentiation. Besides those aspects, to our surprise they found Helios to be dispensable for normal HSPC function (Park et al., 2019).

Ikaros structure and partners

As mentioned before, Ikaros, Helios, Aiolos and Eos encode proteins that are structurally highly similar: in the N-terminus, they all possess 4 kruppel-type zinc

finger domains, important for the binding to the a/gGGAA DNA core motif, while the C-terminal part of the protein encompasses 2 additional zinc-fingers engaged in protein-protein interaction, allowing contacts between family members (**Fig. H**) (Heizmann et al., 2018).

Ikaros and Helios were found to predominantly and abundantly interact with the Nucleosome Remodeling and Deacetylase (NuRD) Complex, either by co-immunoprecipitation or mass-spectrometry analyses. Additional co-factors, like the SMARCA4 and PRC2 complexes, have been also pulled down by Ikaros in co-immunoprecipitation assay. However, mass spectrometry analyses never detected such interaction, thus suggesting that they may represent minor partners (Kim et al., 1999; Oravecz et al., 2015; Sridharan and Smale, 2007).

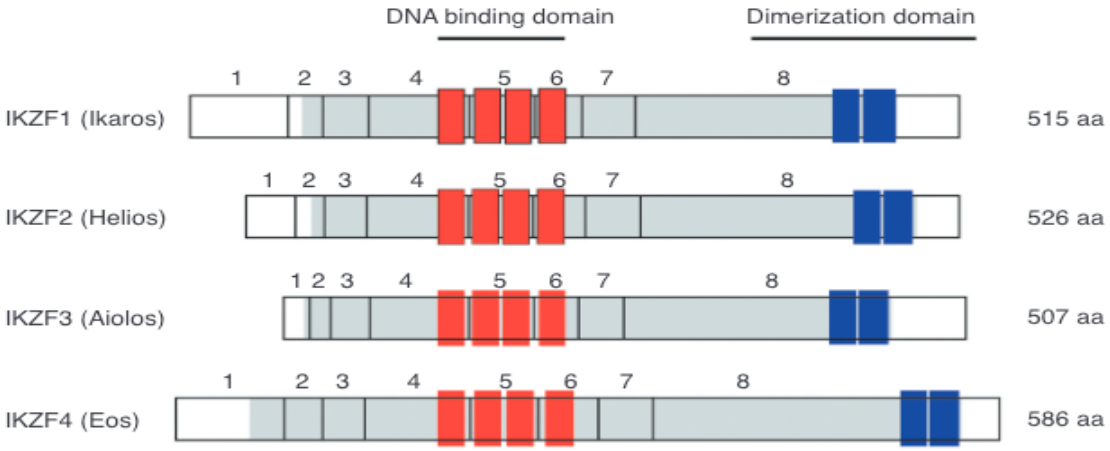

Figure H | High degree of homology between IKAROS proteins.
Representation of the main structural domains shared among the four TF homologous family members: 4 N-terminal kruppel-type zinc finger domains (red) are crucial to mediate TF-DNA binding, while 2 zinc-finger domains in the C-terminus (blue) are used for dimerization.

NuRD multi-protein complex

Involved in chromatin remodeling and catalysis of histone deacetylation, NuRD is a multi-protein complex composed of several subunits: one SWI/SNF ATPase chromatin remodeling subunit called CHD4; one zinc finger protein GATAd2a or GATAd2b; one MDB3 or MDB2 subunit acting as a bridge in order to link the “chromatin remodeling side” to the “histone deacetylase edge”, containing in turn the protein HDAC1/2, the two histone chaperones Rbb4/Rbb7 and two MTA proteins (Mta1, Mta2 and/or Mta3) (**Fig. I**). It has been proposed that TFs, such as the Ikaros

members, function by guiding NuRD to the DNA target sites. However, recent studies challenged this idea. In particular, NuRD is broadly found across all active enhancers/promoters in a variety of cell types and it has been suggested that its recruitment to given chromatin regions is primarily mediated by its affinity for open chromatin and for histone tail modifications (like H3k9ac) while, on the contrary, TF interaction may be important to then trigger NuRD activity (Bornelov et al., 2018; Tencer et al., 2017).

The NuRD complex is very likely used to fine tune gene expression, as the removal of its main components only moderately affects gene expression levels (with most of gene expression changes around ~2 fold). On a functional level, it can act either as positive gene activator or rather as a repressor by reducing chromatin accessibility. Several groups found that NuRD regulates enhancer/promoter activity primarily through its chromatin remodeling action and, only later, by changing histone acetylation levels. Moreover, Liang and colleagues found that deacetylation activity was not necessary to establish Ikaros/NuRD-mediated pre-B gene down-regulation, and they proposed that deacetylation may serve to stabilize an already acquired repressive state (probably through PRC2 complex recruitment) (Bornelov et al., 2018; Liang et al., 2017).

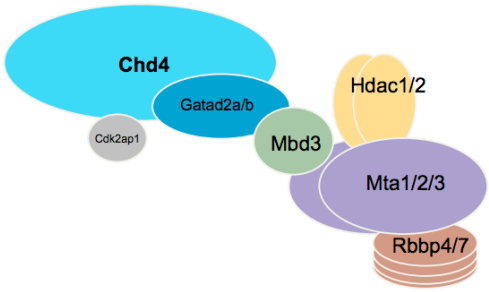

Figure I | The NuRD complex subunits.
Schematic representation of the NuRD structure. Starting from the left: Chd4, the chromodomain helicase protein; Mdb3, the subunit that links the chromatin remodeling NuRD side to the histone deacetylase part containing HDAC1/2. Modified from (Bornelov et al., 2018).

The polycomb repressive complex 2 (PRC2)

The Polycomb Repressive Complex 2 is a multi-protein complex comprising the core subunits SUZ12, EEC, RBBP4/7 and the methyltransferase subunit EZH2 or 1.

PRC2 is the only complex able to mono-, di- and tri-methylate H3 on lysine27 (H3k27me1, H3k27me2 and H3k27me3). However, only H3K27me3 is associated with detectable PRC2 binding and found on repressed enhancers/promoters. The mechanism through which PRC2 is recruited to chromatin in order methylate histones and trigger chromatin compaction is matter of intensive study and still need to be properly understood. Several researches highlight that PRC2 non-core subunits, TFs and PRC1 may cooperate to stabilize PRC2 binding. Furthermore, unmethylated CpG islands and lncRNAs have been reported to facilitate PRC2 binding (Laugesen et al., 2019; Oravecz et al., 2015).

SMARCA4 (BRG1)

SMARCA4 is one of the two mutually exclusive ATPase subunits of the SWI/SNF complex (the other one is called SMARCA2); it hydrolyzes ATP to promote nucleosome mobilization. SMACA4 loss of function in MEFs causes either an increase or decrease of H3k27 acetylation levels across enhancers/promoters, with consequent changes in expression of the neighboring genes. Similar results were obtained also in other cellular systems, where ablation of the SMARCA4 SWI/SNF function was found to affect gene expression either positively or negatively. These findings suggest that SWI/SNF complex is able to act either as transcriptional activator or repressor (Alver et al., 2017; Bossen et al., 2015). However, while the mechanisms promoting REs activation by enhancing chromatin accessibility are known, the basis of SMARCA4 SWI/SNF repressive function remains poorly characterized.

- Ikaros interacts with many partners: which one is the predominant one?

Given that Ikaros deletion results in either REs activation or repression, it has been proposed the following: *i)* its repressive activity is mediated through NuRD or PRC2 interactions, as these two complexes were considered repressive, while *ii)* Ikaros-mediated activation is accomplished through SMARCA4 binding, given that SMARCA4 was considered an activator. However, this view has been recently revisited. On the one hand, several groups reported that NuRD acts both as activator and repressor. Bornelov and colleagues experimentally tracked genome wide enhancer accessibility and histone modification by MNase-seq and ChIP-seq, after inducing NuRD complex assembly; they found that half of the REs were activated

upon NuRD assembly, while the other half was repressed, thus revealing a dual functional nature of NuRD. On the other hand, Liang and colleagues showed that Ikaros and SMARCA4 complex function in a mutual antagonistic logic in pre-B cells, with genes that are activated or repressed by Ikaros found to be, on the opposite, repressed or activated by SMARCA4. Supporting such scenario, Liang and colleagues observed that some pre-B cell specific enhancers (e.g. Myc and Igll1 enhancers) require efficient Ikaros-NuRD interaction in order to achieve nucleosome compaction (repression) and SMARCA4 eviction. SMARCA4 deletion, on the contrary, caused Myc down-regulation in pre-B cells, confirming the antagonistic role of SMARCA4 versus Ikaros-NuRD complex mentioned before (Bossen et al., 2015; Liang et al., 2017).

In conclusion, SMARCA4-Ikaros interaction appears less abundant, not always detected, and associated with a reciprocal antagonistic role, proposing that: *i)* SMARCA4 is not a relevant Ikaros partner, perhaps found to interact with it only because localized in close proximity, and *ii)* SMARCA4 and Ikaros interact only to regulate a limited subset of REs, even though evidence of a functional Ikaros-SMARCA4 cooperation are mostly missing. In addition, our laboratory has shown that repression of stem cell genes in thymocyte progenitors requires the interaction between Ikaros and the PRC2 complex. Ikaros loss of function in thymocyte progenitors results indeed in decreased PRC2 binding, decreased H3k27 tri-methylation and stem cell gene up-regulation. Importantly, PRC2-Ikaros binding occurs mainly in NuRD depleted regions and represents ~20% of the total Ikaros binding activity. On the contrary, more than 60% of Ikaros bound regions are found to be in association with the NuRD complex (Oravecz et al., 2015).

These findings propose NuRD as the main Ikaros partner, mediator of both its repressive and activating functions. On the contrary, PRC2 may represent a “secondary” partner whose recruitment may occur on REs that need to be stably repressed. It can be hypothesized that PRC2-Ikaros binding localizes to site previously deacetylated on H3K27 by Ikaros-NuRD, thus facilitating PRC2 recruitment, methylation and further repression.

AIM OF STUDY

As introduced, the Ikaros family of TFs represents a group of critical hematopoietic regulators. They control several aspects of the development of lymphoid B, T cells as well as dendritic cells (Heizmann et al., 2018; Mastio et al., 2018). One of the most interesting features of these TFs is their unique pattern of expression. In such respect, Helios is the Ikaors factor whose expression has been shown to be restricted within HSPC and mature Treg cells. Moreover, its expression is dynamically regulated during aging, with its down-regulation occurring specifically in old LT-HSC. Notably, while Helios role within Treg cells has been recently characterized (Kim et al., 2015), little is currently available on its function within the HSPC.

HSPC population comprises self renewing HSC and lineage biased MPP: MPP2, MPP3 and MPP4. The phenotipical and functional composition of the HSPC compartment has been extensively studied in the past few years (Pietras et al., 2015). However, molecular mechanisms and players involved in the initial steps of hematopoietic diversification remain mainly obscure.

In our work, we aimed at elucidating the role of Helios within the HSPC population, in order to uncover how this Ikaros member is eventually able to shape HSPC differentiation and aging.

MATERIALS AND METHODS

Mouse lines

Helios germline knockout mice were generated as described in (Cai et al., 2009). Briefly, Helios exon 7 was replaced by a 1.8-kb floxed PGK-neo-poly(A) cassette in order to remove the C-terminal part of the Helios protein, that encodes for two sets of zinc fingers. The vector used for the homologous recombination was transfected into P1 129/Sv embryonic stem cells and the recombination event was detected by Southern Blot. A positive clone was selected for injection into the C57BL/6 blastocyst to produce chimeric mice. Germline transmission was verified by PCR on tail or finger extracted genomic DNA using the primers P1, P2 and P3 (P1-P2 for the WT allele, P1-P3 for the knockout allele). The mouse used for the experiments in the present study were backcrossed six times onto the B6 background.

T cell conditional knockout was obtained by crossing mice bearing IKZF2 loxP flanked (f/f) insertion on exon 7 (Sebastian et al., 2016) with mice expressing the CRE recombinase under the control of the CD4 regulatory elements (Lee et al., 2001). Germline transmission was verified by PCR on tail or finger extracted genomic DNA using the primer set P4and P5 to interrogate Helios deletion and the primer pair P6 and P7 for Cre recombinase transmission. Additionally, Helios conditional deletion was analyzed by BM Treg Helios intracellular staining. All mice were bred and maintained under pathogen free conditions in the animal facility of the Institut de Génétique et de Biologie Moléculaire et Cellulaire (IGBMC). Both males and females were used for the described experiments and mice were sacrificed at 6, 10 and 20 week-of-age.

Genotyping primer list:

P1: 5′-TCTATTAGTGTCAGCTTTTTGACAGTTT-3′
P2: 5′-GATGAATTCCTTATAGATGTCCTTCAGAGAGCC-3′
P3: 5′-ATCTGCACGAGACTAGTGAGACG-3′
P4: 5′-CTGAGCCTCACACAATTGGA-3′
P5: 5′-TATGTGACCACACAAAGGGG-3′
P6: 5′-GTTCGCAAGAACCTGATGGACA-3′
P7: 5′-CTAGAGCCTGTTTTGCACGTTC-3′

Flow cytometry analyses

Total bone marrow cells were prepared by crushing on a mortar 2 tibias, 2 femurs, 2 pelvis, the sternum and the spine. Bone marrow derived cell suspension was incubated in 0.15M NH_4Cl water solution for 2 minutes at RT in order to eliminate mature red blood cells. The cell suspension was further filtered using a 100um cell strainer. The following antibodies were used in the described experiments: CD3e (145-2C11), CD4 (RM4-5), CD8 (53-6.7), CD11b (M1/70) CD11c (HL3), CD16/32 (2.4G2), CD19 (6D5), CD25 (PC61.5), CD41 (MWReg30), CD45 (30-F11), CD45.1 (A20), CD45.2 (104.2), B220 (RA3-6B2), CD48 (HM48-1), CD71 (R17217), CD105 (MJ7/18), c-KIT (2B8), CD127 (A7-R34), Flt3 (A2F10), CD150 (TC15-12F12.2), FoxP3 (FJK-16S), GR1 (RB6-8C5), Helios (D8W4X), IFNg (XMG1.2), IL10 (JES5-16E3), SCA1 (D7), Ter119 (TER-119), AN2 (1E6.4), CD31 (390), IL-2 (JES6-5H4).

~$5x10^6$ cells were incubated with 2-5ug/ml of specific fluorophore or biotin conjugate antibodies. Biotinylated antibodies were detected with fluorochrome conjugated streptavidin. For intracellular protein staining, ~$5x10^6$ of previously surface stained BM cells were incubated o/n at 4°C in Fixation-Permeabilization solution (eBioscence 00-5523-00), permeabilized in permeabilization buffer (eBioscence 00-5523-00) and stained with primary antibodies 1h at RT, and with an eventual secondary antibody 1h on ice. Populations were defined as follow:
Lineage staining $(lin)^+$: (CD3, CD4, CD8, CD11b, CD11c, B2200, CD19, Ter119, $CD71)^+$; LT-HSC: Lin^-, $SCA1^+$, $c\text{-}KIT^+$, $CD150^+$, $CD48^-$; ST-HSC: Lin^-, $SCA1^+$, $c\text{-}KIT^+$, $CD150^-$, $CD48^-$; MPP: Lin-, $SCA1^+$, $c\text{-}KIT^+$, CD150, $CD48^+$; mkLT-HSC: Lin^-, $SCA1^+$, $c\text{-}KIT^+$, $CD150^+$, $CD48^-$, $CD41^+$; MPP2: Lin-, $SCA1^+$, $c\text{-}KIT^+$, $CD150^+$, $CD48^+$; MPP3: Lin^-, $SCA1^+$, $c\text{-}KIT^+$, $CD150^-$, $CD48^+$, $Flt3^-$; MPP4: Lin^-, $SCA1^+$, $c\text{-}KIT^+$, $CD150^-$, $CD48^+$,$Flt3^+$; CLP: Lin^-, $SCA1^{low}$, $c\text{-}KIT^{low}$, $CD127^+$,$Flt3^+$; MkP: Lin^-, $SCA1^-$, $c\text{-}KIT^+$, $CD150^+$, $CD105^-$, $CD41^+$; GMP: Lin^-, $SCA1^-$, $c\text{-}KIT^+$, $CD150^-$, $CD16/32^+$; CMP: Lin^-, $SCA1^-$, $c\text{-}KIT^+$, $CD34^+$, $CD16/32^{low}$; EryP: Lin^-, $SCA1^-$, $c\text{-}KIT^+$, $CD150^+$, $CD105^-$, $CD41^-$; pre MEP: Lin^-, $SCA1^-$, $c\text{-}KIT^+$, $CD150^+$, $CD105^-$, $CD41^-$; pre-GM: Lin^-, $SCA1^-$, $c\text{-}KIT^+$, $CD150^-$, $CD105^-$, $CD41^+$, $CD16/32^-$; Erythrocytes: $Ter119^+$,$CD71^{+/low}$; Myeloid cells: $GR1^+$,$CD11b^+$; B cells: $B220^+$,$CD19^+$; $CD4^+$ T cells: $CD4^+$,$CD8^-$; Treg : $CD4^+$, $FoxP3^+$; $CD8^+$ T cells: $CD4^-$,$CD8^+$. Samples were acquired on BD LSRII, LSR Fortessa and analyses were performed using Flowjo10 analysis software (TreeStar).

Fluorescence-activated cell sorting (FACS)

BM cells were prepared as described above, incubated for 20 minutes at 4°C with rat (CD3, CD4, CD8, CD11b, CD11c, B2200, CD19, Ter119, CD71) antibodies (rat IgG). Lineage positive stained cells were magnetically separated using anti-rat conjugated magnetic immunobeads (Dynabeads™ Sheep Anti-Rat IgG 11035). Depleted cells were stained as previously described and samples were acquired and sorted on BD FACS ARIA II or FACS ARIA Fusion.

Colony forming unit (CFU) assays and single cell cultures

BM colony forming unit assay: 150.000 unfractionated BM cells were added to either 3ml of complete MethoCult™ media (3434) containing 50ng/ml SCF, 3U/ml EPO, 10ng/ml IL-3, 10ng/ml IL-6 or 3ml of MethoCult™ media (3134) supplemented with the following cytokine: 50ng/ml SCF, 50/ml TPO, 20ng/ml IL-3. 2 out of the 3 ml of media containing cells were further split, by using a 5ml syringe equipped with a 19 gauge needle, into two distinct 30mm petri dish (1ml each). The Petri dishes were finally accommodated, along with an extra distilled water filled dish, inside to a larger dish in order to avoid medium evaporation. Cells were incubated in a 5% CO_2 humidified (95%) chamber incubator at 37°C. 8 days after cell seeding, colony morphology and number were scored using a Leica stereo microscope. Megakaryocyte containing colonies were defined as colonies containing large and light diffracting cells. Positive megakaryocyte and myeloid colonies were separately collected for cytospin preparation and May Grünwald Giemsa (MGG) staining to further confirm cellular identity.

Single cell cultures of purified MPP: 120 single MPP were sorted onto 2 separated U-shaped 96 well plates, containing 50ul of complete MethoCult™ media (3434). The external wells of the 96 well plates were all filled with deionized water, in order to avoid media evaporation. Cells were incubated as previously described. Colony morphology and number found in positive wells were evaluated using a Leica stereo microscope 8 days after cell seeding.

Single cell culture of purified LT-HSC: 100 single LT-HSC were sorted onto 2 separated U-shaped 96 well plates containing StemSpan™ SFEM (STEMCELL Technologies), 20% FCS, 1% β-mercaptoethanol (Sigma, 0.1nM), 1% penicillin / streptomycin, 50ng/ml SCF, 20ng/ml IL-3 and 50ng/ml TPO. The external wells of the

96 well plates were all filled with deionized water, in order to avoid media evaporation. Cells were incubated as previously described. Colony morphology and number found in positive wells were evaluated using a Leica stereo microscope 8 days after cell seeding. Positive megakaryocyte and myeloid colonies were separately collected for cytospin preparation and MGG staining to further determine the presence of megakaryocytes, granulocytes and monocytes.

$CD4^+$ T cell stimulation and cytokine staining

BM cells were prepared as previously described and $CD4^+$ cell enrichment was obtained through immunomagnetic mature lineage cell depletion. Briefly, BM cell suspension was incubated with the following rat antibodies, CD11b, B220, CD8, Ter119, for 20' at 4°C. Antibody bounded cells were magnetically separated using anti-rat conjugated magnetic immunobeads (Dynabeads™ Sheep Anti-Rat IgG 11035). ~$5x10^6$ $CD4^+$ enriched BM cells were further incubated in IMDM containing: Glutamax, 10% iFCS, non-essential amino acids, Sodium Pyruvate (1 mM), Penicillin Streptomycin (100U/ml), Hepes 10mM, beta Mercaptoethanol (57,2uM); further addition of Phorbol 12-Myristate 13-Acetate (PMA, 0.5 ug/ml), Ionomycin (0.5 ug/ml) and Golgi plug (1/1000, BD Biosciences) allowed to stimulate cytokine production while avoiding their release. Cells were stimulated for 2 hours in a 5% CO_2 humidified (95%) chamber at 37°C. After stimulation, cells were stained with an anti-CD4 fluorophore conjugated antibody, fixed for 30 minutes at 4°C in Fixation-Permeabilization solution (eBioscence 00-5523-00), permeabilized in Permeabilization buffer and stained o/n with IFNγ, FoxP3, Il-2, Il-10 fluorophore conjugated antibodies. Samples were acquired on BD LSRII, LSR Fortessa and analyses were performed using Flowjo10 analysis software (TreeStar).

BM reconstitution assay

BM competitive transplantation: donor (CD45.2) unfractionated BM cells from either WT or $He^{-/-}$ 10/15 week-old sex-matching mice were mixed in IMDM along with the same amount of competitor cells derived from age-matching CD45.1 mice. 150.000 donor cells were injected in the presence of the same amount of competitor cells, within the tail vein of lethally irradiated (9Gy) CD45.1 and CD45.2 5/6 week-old

recipient congenic mice. Seven to nine recipient mice per donor genotype were used for each experiment. Reconstitution was analyzed 2 and 4 months after injection.

LT-HSC reconstitution assay: donor (CD45.2) WT and $He^{-/-}$ LT-HSC from age- (10/15 week-old) and sex- matching mice were sorted and mixed in IMDM along with unfractionated helper BM cells. 100 LT-HSC were co-injected together with 500.000 helper unfractionated BM cells, within the tail vein of lethally irradiated (9Gy) CD45.1 and CD45.2 5/6 week-old recipient congenic mice. Seven to nine recipient mice per donor genotype were used for each experiment. Peripheral blood reconstitution was analyzed 2 and 4 months after injection.

MPP3 and MPP4 *in vivo* differentiation assay: donor (CD45.2) sorted MPP4 and MPP3 cells from either WT or $He^{-/-}$ age- (15 week-old) and sex- matching mice were separately mixed in IMDM. 5000 MPP3 were injected within the tail vein of lethally sub-irradiated (6.5Gy) CD45.1 and CD45.2 5/6 week-old congenic recipient mice. In the same way, 5000 MPP4 were injected into sub-lethally irradiated (6.5Gy) CD45.1, CD45.2 congenic recipient mice. Four to five recipient mice per donor MPP3 or MPP4 genotype were used for each experiment. Peripheral blood reconstitution was analyzed 2 weeks after transplantation. Mice reconstituted with less than 0.5% donor cells were excluded from the analyses (4 mice out of 60 were excluded).

Peripheral blood preparation and staining: 200ul of peripheral blood extracted from the tail vein or directly from the heart of euthanized mice were collected into microtubes containing 50ul of 50mM EDTA and scaled up to 500ul with PBS. 500ul of 2% dextran was further added to the blood suspension in order to obtained a final 1% dextran solution, that was then incubated for 30' at 37°C. The upper phase was taken, centrifuged at 500g for 5' and the pellet was lysed into 0.15M NH_4Cl water solution for 2 minutes at RT, in order to eliminate residual mature red blood cells.
White blood cells were stained with the following antibodies: B220, CD11b, CD4, CD8, CD45.1 and CD45.2. Donor/competitor myeloid and B lymphoid cells were defined as: donor B cells: % of $B220^+$, $CD11b^-$ within the $CD45.2^+$ $ter119^-$ population; donor myeloid cells: % of $B220^-$, $CD11b^+$ within the $CD45.2^+$ $ter119^-$ population; donor T cells: % of $B220^-$, $CD11b^-$ $CD4\text{-}8^+$ within the $CD45.2^+$ $ter119^-$ population; competitor B cells: % of $B220^+CD11b^-$ within the $CD45.1^+$ $ter119^-$ population; competitor myeloid cells: % of $B220^-$, $CD11b^+$ within the $CD45.2^+$ $ter119^-$ population.

RNA extraction and bulk mRNA sequencing

Total RNA was extracted from 10.000 to 40.000 sorted WT and $He^{-/-}$ LT-HSC, MPP3 and MPP4 cells. Total RNA extraction was performed using the RNeasy Plus Micro Kit (Qiagen 74034). Libraries were prepared with the Clonotech SMART-seq v4 Ultra Low Input RNA Kit for Sequencing. Libraries were sequenced on Illumina HiSeq 4000 sequencer (1x50 bases). Reads were pre-processed in order to remove adapter, poly(A) and low-quality sequences (Phred quality score below 20). After this pre-processing, reads shorter than 40 bases were discarded for further analysis. These pre-processing steps were performed using cutadapt version 1.10. Reads were mapped onto the mm10 assembly of Mus musculus genome using STAR version 2.5.3a. Gene expression quantification was performed from uniquely aligned reads using htseq-count version 0.6.1p1, with annotations from Ensembl version 94 and "union" mode. Differential gene expression analysis were performed using the Bioconductor package DESeq2 version 1.16.1 on R 3.3.2. Wald statistical test was used to identified gene significantly differentially expressed among the following comparison: LT-HSC WT versus $He^{-/-}$; MPP3 WT versus $He^{-/-}$ and MPP4 WT versus $He^{-/-}$.

WT versus $He^{-/-}$ heatmaps on differentially expressed gene with a False Discovery Rate <0.1 (FDR<0.1) were created by using Cluster and Java TreeView software. Gene set enrichment analyses (GSEA) were performed using the GSEA software (http://software.broadinstitute.org/gsea/index.jsp). Up- and down-regulated genes identified by comparing WT versus $He^{-/-}$ transcriptomes of LT-HSC, MPP3 or MPP4 respectively (p-value < 0.05 and $\log_2$ fold change > 0.5) have been used to create the ranked lists. CLP and MkP, gene signatures(Grover et al., 2016) were tested over the LT-HSC, MPP3 or MPP4 ranked lists. Old LT-HSC gene signature were obtained from data published by the Goodell lab (Sun et al., 2014). Old LT-HSC transcripts were selected by picking the 450 highest (highest fold change) up- or down-regulated genes. Pathways analyses were performed on LT-HSC differentially expressed genes (p-value < 0.05 and $\log_2$ fold change > 0.5) using the Metascape website (http://metascape.org/gp/index.html#/main/step1).

Single cell mRNA sequencing

Libraries preparation

35.000 LSK were FACS purified from 4 total mice: 2 WT and 2 $He^{-/-}$. Each LSK pool was uniquely labeled with a different anti-CD45 HasTag Oligo (HTO) conjugated antibody (following the Cell Hashing protocol; (Stoeckius et al., 2018) (TotalSeq-A0301 Hashtag 1, TotalSeq-A0302 Hashtag 2, TotalSeq-A0303 Hashtag 3, TotalSeq-A0304 Hashtag 4) In order to multiplex together the four samples. Moreover, all the four LSK pool were stained with common anti- CD150, CD48, CD41 and Flt3 HTO conjugated antibodies for cell population identification (TotalSeq 133937 antiCD41, TotalSeq 115945 antiCD150, TotalSeq 135316 antiCD135 and TotalSeq 103477 antiCD48), as reported for the CITE-seq protocol (Stoeckius et al., 2017). 10.000 total cells (2500 from each LSK pool) were selected for library preparation. mRNA and HTO libraries were prepared by using the 10x Genomics Single Cell 3' v2 technology. Briefly, following cell lysis inside droplets, cellular mRNA and antibody-derived oligos were reverse-transcribed and indexed with a shared cellular barcode by using the Chromium Single Cell 3' Reagent kits v2 (10X Genomics). Indexed cDNA were then pooled and amplified by PCR according to 10X Genomics protocol with the addition of supplementary primers in order to amplify also the antibody-derived cDNA (CITE-seq and Cell Hashing). SPRI bead size selection was then performed in order to separate both the mRNA-derived cDNA (>300bp) and the tagged antibody-derived cDNAs (180bp). For the mRNA derived cDNA library preparation, we further proceeded with standard 10x Genomics protocol. For tagged antibody-derived library, we used the 2x KAPA HiFi PCR Master Mix with the following program and primers:

- Cite-seq library = 10 cycles: 95°C for 3'; 95°C for 20'', 60°C for 30'', 72°C for 20''; final elongation 72°C 5'.
- Cell Hashing library = 10 cycles: 95°C for 3'; 95°C for 20'', 64°C for 30'', 72°C for 20''; final elongation 72°C 5'.
- primers :
- 10x Genomics SI-PCR primer (for 10x Genomics Single Cell 3P v2)
- 5'AATGATACGGCGACCACCGAGATCTACACTCTTTCCCTACACGACGCTC

- Illumina Small RNA RPI1 primer (for **ADT amplification**; i7 index 1, 5'CAAGCAGAAGACGGCATACGAGATCGTGATGTGACTGGAGTTCCTTGGCACCCGAGAATTCCA
- Illumina TruSeq D701_s primer (for **HTO amplification**; i7 index 1, shorter than the original D701 Illumina sequence) 5'CAAGCAGAAGACGGCATACGAGATCGAGTAATGTGACTGGAGTTCAGACGTGTGC

Libraries were sequenced on Illumina HiSeq 4000 sequencer (2x100 bases).
Read 1: barcode and UMI; Read 2 cDNA.

Gene expression and library analysis

3' mRNA-seq library reads were processed using Cell Ranger count pipeline version 3.0.2 from 10x Genomics on mm10 *Mus musculus* assembly and Ensembl version 93. HTO and ADT library reads were merged together and processed with 3' mRNA-seq library using Feature Barcoding Analysis option. Hashtag identification was performed using the approach proposed in (Stoeckius et al., 2018) with Seurat R package (Butler et al., 2018; Stuart et al., 2019) version 3.0.0 and R version 3.5.1 on HTO counts. Furthermore, Cell Ranger has been used to filter out outlier cells possessing: more than >5% read count belonging to mitochondrial genes, having more than 32,883 total count in 3'mRNA-seq library, having more than 740 read count in ADT library, having more than 3,234 read count in HTO library or belonging to none or more than one hashtag categories. Resulting file was further analyzed using 10x Genomics Loupe Cell Browser.

LT-HSC were defined as cell expressing CD150 HTO (log_2 expression >100 counts) and not expressing CD48 HTO (log_2 expression < 100 counts). MPP were defined as cell expressing CD48 HTO (log_2 expression > 100 counts). HSC-MPP2 cells were defined as Mpl positive (log_2 expression > 0.1 counts) and Flt3 negative (log_2 expression < 0.1 counts). MPP4 cells were defined as Flt3 positive (log_2 expression > 0.1 counts) and Mpl negative (log_2 expression < 0.1 counts). MPP3 were defined as not HSC-MPP2 and MPP4 cells expressing Sox4 (log_2 expression > 0.1 counts). K-mean clustering was performed using the K-mean clustering option present in the 10x Genomics Loupe Cell Browser, using a K=3 set-up. Genes enriched in each K mean cluster were computed and extracted using the 10x

Genomics Loupe Cell Browser and enriched pathway terms uncovered using the online Medscape application (metascape.org).

Heatmap generation

Cell Ranger Graph-Based t-SNE was rotated of -20° on the x-axis and then fragmented in a defined number of segments. Gene expression mean, for all transcripts was calculated taking into account all cells belonging to a given segment. Informative genes were further filtered out: for a given transcript, we calculated mean expression in the central segment, if the gene expression value was higher than 0.5 (in log2 scale) within the segments at the right or at the left of the central segment, the gene was selected for heatmap representation. Outlier transcripts were further manually excluded.

RESULTS

1) ANALYSIS OF HELIOS PROTEIN LEVELS ACROSS BM CELL POPULATIONS

Helios protein is highly expressed in Hematopoietic Stem and Progenitor Cells (HSPC)

It has been shown that Helios mRNA is abundantly expressed within Hematopoietic Stem and Progenitor Cells (HSPC) and also within regulatory T (Treg) cells (data from Immunological Genome Project (ImmGen,http://www.immgen.org); however, information on its protein levels are still missing. To shed light on Helios protein expression pattern in BM hematopoietic cells, and to uncover in which cell types Helios might operate, we performed flow cytometry analysis.

We distinguished different mouse Bone Marrow (BM) populations by performing cell surface antigen stainings (and also intracellular for FoxP3$^+$ Treg cells) and we evaluated Helios expression by intracellular staining using an anti-Helios antiboby. This strategy provided some advantages with respect to the microarray experiments performed by the ImmGen consortium: first, our technique allowed the detection of the protein and, as such, provided a better readout of Helios expression in comparison to the mRNA (as mRNA levels do not always correlate with protein levels); second, flow cytometry analysis allowed to detect Helios protein at the single cell level, thus permitting to uncover whether this transcription factor is homogeneously or heterogeneously expressed within a given population of interest.

We found Helios to be expressed in more than ~97% of LSK, LT-HSC, ST-HSC and MPP cells (**Fig. 1a,b**). Moreover, we also detected the protein in most of the committed LK, GMP, MEP and MkP populations, with over ~88% of Helios-positive cells (**Fig. 1a,c,d**). These results contrast with the low Helios mRNA expression detected in committed cells by the ImmGen consortium (as shown in the discussion section). On the other hand, Helios expression is reduced in total Lin$^-$Sca1$^-$c-kit$^-$ (LSK$^-$) cells, as only ~10% of such cells express Helios, showing that its expression progressively decreases with cell maturation (**Fig. 1a**). In agreement, no Helios protein was detected in B cells, myeloid cells and erythrocytes (**Fig. 1e,f**). On the contrary, CD4$^+$ and CD8$^+$ T cells are the only mature BM populations expressing this

transcription factor (**Fig. 1g**), with high levels specifically detected in the Treg Foxp3$^+$ CD4$^+$ cells (**Fig. 1h**).

In order to evaluate and compare Helios levels among different BM cell types, we analyzed its median fluorescence intensity (MFI) within the different hematopoietic populations. We found that Helios MFI is ~2000 in HSC (both LT and ST –HSC) and around 4000 in MPP2, MPP3 and MPP4 (**Fig. 1i**). In committed progenitors, Helios MFI remains the highest in the GMP (~4000), while in the MkP, MEP and CLP we found roughly the same expression than HSC (MFI ~2000; **Fig. 1i**). Moreover, the myeloid, B and erythroid cells showed almost no expression of this transcription factor (MFI <100; **Fig. 1i**). Notably, we also analyzed Helios expression within non-hematopoietic cells, such as Mesenchymal Stem Cells (MSC) and Endothelial Cells (EC), as they represent an important component of the BM microenvironment where they regulate HSPC maintenance and differentiation. Interestingly, Helios is mostly absent in the non-hematopoietic population (CD45$^-$) and has low MFI in both EC and MSC (**Fig. 1l,m**), suggesting that Helios may specifically operate only within hematopoietic cells.

Intriguingly, by analyzing transcriptomics data from recent publications comparing LT-HSC isolated from young and old mice, we found that Helios mRNA levels decrease during the process of aging (Grover et al., 2016; Sun et al., 2014). This motivated us to understand whether Helios downregulation: 1) also occurs at the protein level in LT-HSC and 2) is specific to the LT-HSC or occurs more generally in all Helios-expressing progenitor cells. To address these questions, we performed Helios intracellular staining in BM HSPC and committed progenitor cells using both old and young mice. Interestingly, we showed that Helios MFI decreases significantly only in LT-HSC (1.5X) and MkP (1.4X), whereas Helios age-related changes were not observed in ST-HSC, MPP2, MPP3, MPP4, GMP and MEP populations (**Fig. 1n,o**). In addition, we noticed a correlation between the low Helios expression level and a high expression of CD41, a typical cell surface marker known to be up-regulated in aged myeloid-megakaryocyte-biased LT-HSC (**Fig. 1o**) (Gekas and Graf, 2013).

In view of these results, we concluded that Helios is homogeneously and abundantly expressed by HSC and progenitor cells, whereas Helios protein is absent in mature B, myeloid, erythrocyte and non-hematopoietic (CD45$^-$) cells (except for some T cells). Intriguingly, the decreasing level of Helios expression in aged LT-HSC

prompts the possibility that this transcription factor participates in the aging process. Altogether, these findings motivated us to research Helios role in HSCP biology, development and aging.

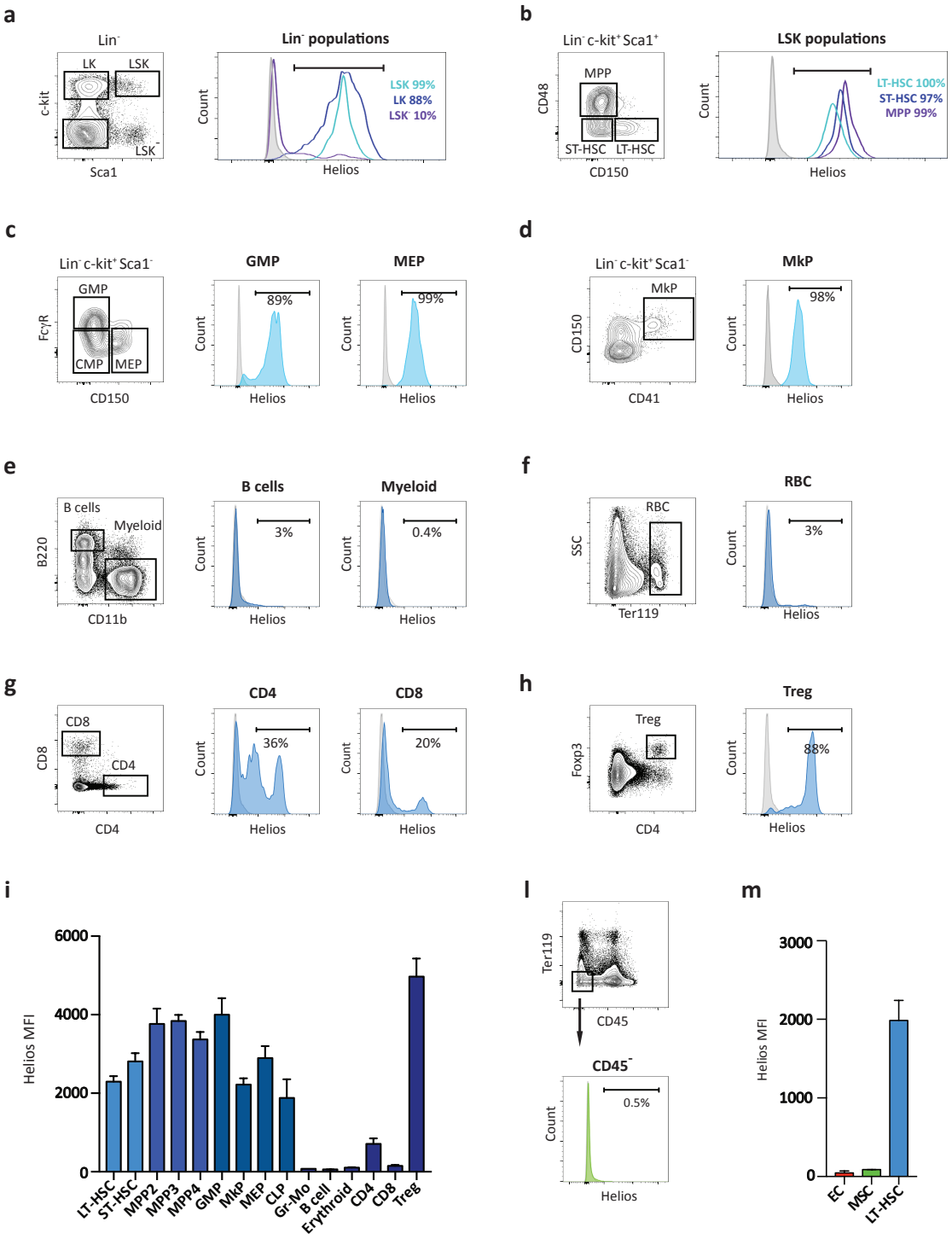

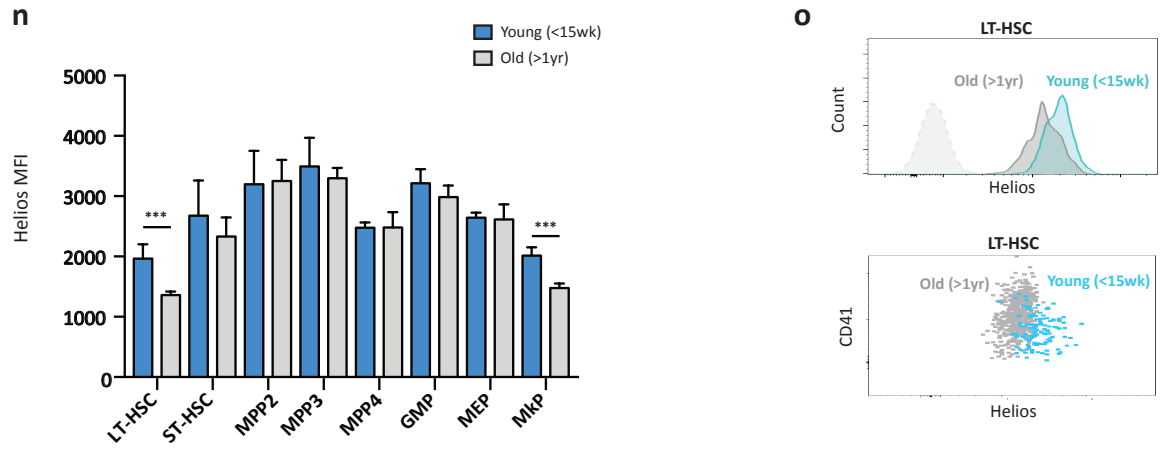

Figure 1 | Helios is highly expressed in HSPC and down-regulated with age in LT-HSC. **(a-d)** On the left, representative contour plots depicting different BM populations defined by surface antigen expression. On the right, representative flow cytometry histograms showing the intracellular Helios protein levels within the indicated populations. As negative control, cells were stained only with the secondary antibody and its intracellular signal was detected within the same BM population. Flow cytometry analysis of Helios expression in: **(a)** LSK ($Lin^-Sca^+c\text{-}Kit^+$), LK ($Lin^-Sca^-c\text{-}Kit^+$), LSK^- ($Lin^-Sca^-c\text{-}Kit^-$) cells; **(b)** long-term hematopoietic stem cells ($Lin^-Sca^+c\text{-}Kit^+CD150^+CD48^-$; LT-HSC), short term hematopoietic stem cells ($Lin^-Sca^+c\text{-}Kit^+CD150^-CD48^-$; ST-HSC); multipotent progenitors ($Lin^-Sca^+c\text{-}Kit^+CD150^-CD48^+$; MPP); **(c)** granulocyte-monocyte progenitors ($Lin^-Sca^-c\text{-}Kit^+CD150^-CD16/32^+$; GMP), megakaryocyte-erythrocyte progenitors ($Lin^-Sca^-c\text{-}Kit^+CD150^+CD41^-CD105^-$; MEP); **(d)** megakaryocyte progenitors ($Lin^-Sca^-c\text{-}Kit^+CD150^+CD41^+$; MkP); **(e)** B cells ($B220^+CD11B^-$), myeloid cells ($B220^-CD11B^+$); **(f)** erythrocytes (Ery) or Red Blood Cells ($Ter119^+$; RBC); **(g)** $CD4^+$ T cells, $CD8^+$ T cells; **(h)** Treg cells ($CD4^+FoxP3^+$). **(i)** Helios Median Fluorescence Intensity (MFI) within different BM populations. **(l)** Representative contour plot (top) of BM non-hematopoietic cells ($CD45^-$ and $Ter119^-$) and their relative Helios levels (bottom), in comparison to control intracellular staining (secondary antibody alone). **(m)** Helios MFI in BM Endothelial Cells ($CD45^-CD31^+Ng2^-$; EC), Mesenchymal Stem Cells ($CD45^-CD31^-Ng2^+$; MSC) and LT-HSC. **(n)** Helios MFI in hematopoietic BM populations derived from young (blue) and old (gray) mice. **(o)** Representative flow cytometry histograms (top) of Helios expression in old (grey) and young (blue) LT-HSC, in comparison to control intracellular staining (secondary antibody alone). Dot plot (bottom) representing Helios expression in old (grey) and young (blue) LT-HSC, considering the CD41 antigen level. Mean±SD from 3-4 independent experiments. Statistical significance was calculated using an unpaired two tailed t-test, * $p<0.05$, ** $p<0.01$ and *** $p<0.01$.

2) EFFECT OF HELIOS DELETION IN MATURE HEMATOPOIETIC CELLS AND COMMITTED PROGENITORS

A) MYELOID AND LYMPHOID CELLS

Helios knockout ($He^{-/-}$) mice acquire a myeloid skewed hematopoietic system

In order to understand the role of Helios in hematopoiesis, we made use of a Helios germline knockout mouse line ($He^{-/-}$), that we always subjected to experiments in comparison to control WT mice. In general, $He^{-/-}$ mice are slightly smaller in size than WT animals (**Fig. S1a**) and possess a peculiar eye phenotype, as they have a narrow eye opening. Important for our experiments, $He^{-/-}$ mice show only a mild tendency to possess less BM cells, with respect to WT mice. Moreover, we found that BM cellularity is often highly variable between experiments (**Fig S1b**). For this reason, in the present study, we represented data in percentages (% of a given cell population within the BM), without considering absolute numbers. In this way, we managed to correct for the high BM cellular variability.

We started our analysis by characterizing the myeloid and lymphoid progenitor and mature cell compartments by using flow cytometry analysis. Specifically, we collected BM cells from WT and $He^{-/-}$ mice at 6, 10 and 20 weeks of age, in order to comprehensively capture early but also eventual later hematopoietic defects happening during growth. Interestingly, across the entire investigated time window, we observed that $He^{-/-}$ mice have ~1.6 times less Common Lymphoid Progenitors (CLP) and ~1.5 times less mature B lymphoid cells, in comparison to WT BM (**Fig. 2a, S2a, S2c**). On the contrary, the $He^{-/-}$ myeloid compartment is increased, but only 10- and 20- week-old animals bear such changes. Starting from 10 weeks, $He^{-/-}$ bone contains 1.2 times more GMP, while mature myeloid cells increase significantly only around 20 weeks (**Fig. 2b, S2b, S2c**). It must be noted that, in contrast to the B cell and myeloid compartments, $CD4^+$ and $CD8^+$ lymphoid cells are unaffected in $He^{-/-}$ mice, as their percentages did not change with respect to the WT counterpart (**Fig. 2c**). Altogether, these results highlighted that Helios loss causes a bias in the production of hematopoietic cells, with a gain of myeloid derived cells and a reduction in the B lymphoid cell compartment.

To more directly confirm these findings, we quantified the number of myeloid progenitors using an alternative *in vitro* Colony Forming Unit (CFU) assay. We

seeded WT and $He^{-/-}$ BM cells into a semisolid media containing SCF, IL3, IL6 and EPO cytokines optimal to promote granulo-monocyte and erythroid progenitor expansion (MethoCult 3434 containing; **Fig. 2d**). Eight days after cell seeding, we counted the number of granulocyte/monocyte colonies, that we were able to distinguish from the erythroid ones based on chromatic features (erythroid colonies are red). Interestingly, we observed that $He^{-/-}$ BM possesses more myeloid colony forming unit cells, in both culture conditions, with respect to WT bones (**Fig. 2e**).

In conclusion, these results showed that Helios deletion caused a reduction in the B lymphoid lineage, while progressively skewed the hematopoietic system towards the myeloid fate, by mainly acting at the level of committed progenitors (CLP, GMP). Interestingly, the hematopoietic system conformation observed in $He^{-/-}$ mice is reminiscent of that observed in old mice (Rossi et al., 2005).

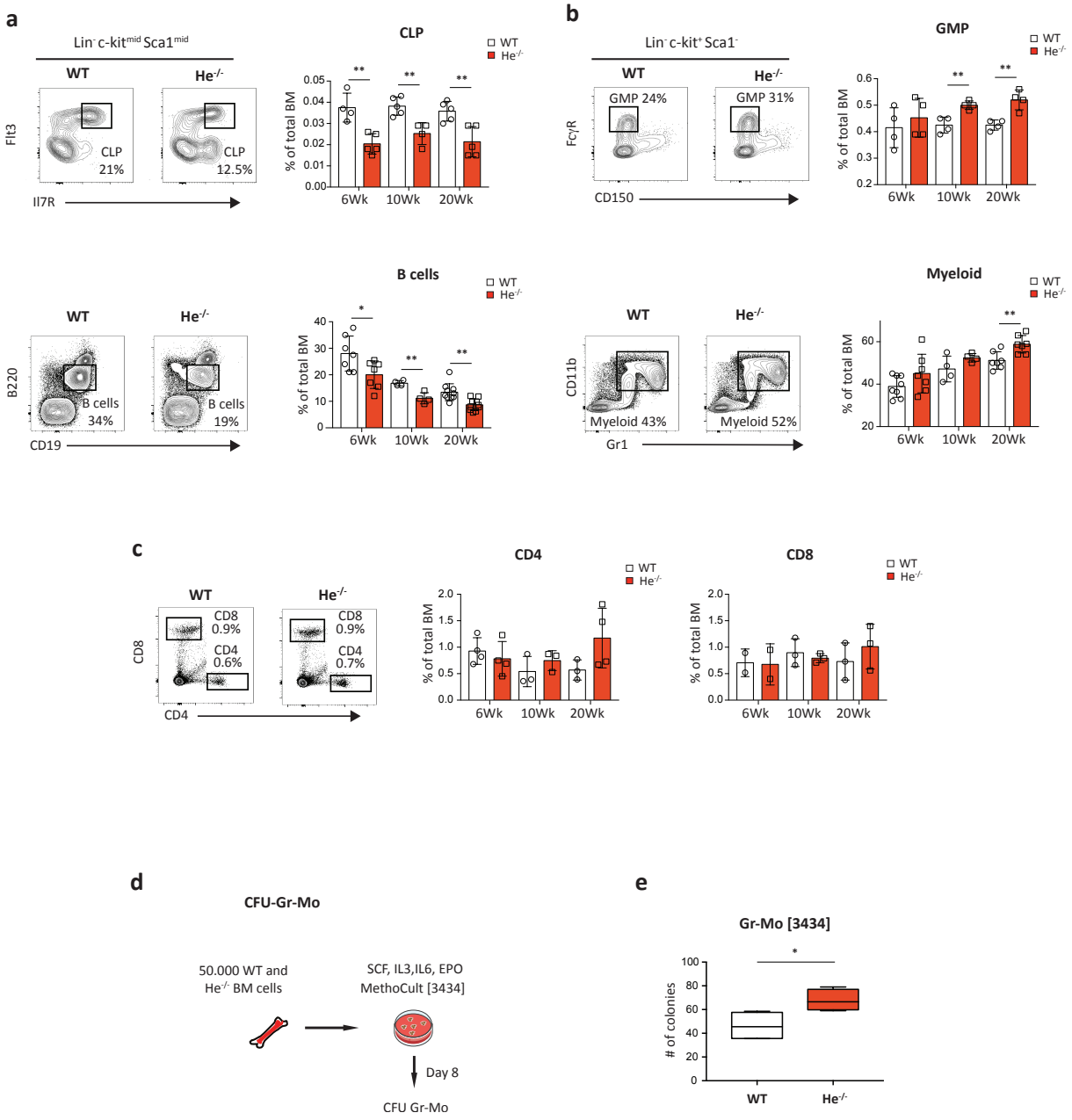

Figure 2 | Myeloid and lymphoid progenitor abundance is altered in He$^{-/-}$ mice.
(a-c) Left – Representative contour plots of BM surface stained WT and He$^{-/-}$ populations. Right – Percentage of the indicated populations within the BM of 6-, 10- and 20- week-old WT or He$^{-/-}$ mice. **(a)** Flow cytometry analysis of Common Lymphoid Progenitor (CLP) and mature B cells. **(b)** Flow cytometry analysis of granulocyte and monocyte progenitors (GMP) and mature myeloid cells. **(c)** Flow cytometry analysis of CD4^{+} and CD8^{+} T cells. Mean ±SD from 3-7 independent experiments per mouse age. Statistical significance was calculated using an unpaired two tailed t-test, * $p<0.05$ and ** $p<0.01$. **(d)** Myeloid Colony Forming Unit (CFU) assay strategy: 50.000 unfractionated BM cells from WT or He$^{-/-}$ 10- and 20-week-old mice were seeded in MethoCult cytokine complete medium (10ng/ml IL-3, 10ng/ml IL-6, 50ng/ml SCF and 3U/ml EPO) [3434]. **(e)** Box plot representing the number of granulocyte and monocyte (Gr-Mo) colonies after 8 days of culture. Mean ±SD from 4 independent experiments. Each experiment was performed in technical

duplicate. Statistical significance was calculated using an unpaired two tailed t-test, * $p<0.05$ and ** $p<0.01$.

B) MEGAKARYOCYTE AND ERYTHROID CELLS

Increased megakaryocyte progenitor pool in $He^{-/-}$ BM

The premature aging phenotype that emerged in the absence of Helios encouraged us to analyze also the megakaryocyte and erythrocyte lineages. We performed flow cytometry analysis of BM megakaryocyte progenitors, erythroid progenitors as well as mature erythrocytes. We found a mild reduction in mature erythrocytes in $He^{-/-}$ 20-week-old mice, in comparison to the WT counterpart; however, such changes were not significant (**Fig. 3a, S3a**). In agreement with this result, we also did not observe a significant difference between WT and $He^{-/-}$ erythroid progenitors at all the investigated ages (**Fig. 3b, S3b**). On the contrary, $He^{-/-}$ BM showed a significant and gradual megakaryocyte progenitor expansion (**Fig. 3c**), a typical feature observed also during hematopoietic aging.

In order to independently confirm this last result, we quantified megakaryocyte progenitor abundance using an *in vitro* CFU assay. We seeded total BM cells from WT and $He^{-/-}$ mice, on IL3, SCF and TPO cytokine-containing semisolid media (MethoCult 3134) (**Fig. 3d**). After eight days of culture, we counted the number of megakaryocyte colonies characterized by the presence of large megakaryocyte cells (5-to-10 times larger than monocyte and granulocyte cells; **Fig. 3f**). Furthermore, to confirm the reliability of our analysis, we performed May Grünwald Giemsa (MGG) staining on the scored colonies (**Fig. 3g**). In line with the previous results, we detected three times more megakaryocyte colonies (~90) in $He^{-/-}$ mice (**Fig. 3e**), with respect to the WT counterpart (~25), highlighting that loss of Helios correlates with an expansion of megakaryocyte progenitors**.**

In summary, our exploration of the mature and committed progenitor BM compartments revealed that $He^{-/-}$ mice have a lymphoid progenitor (CLP) reduction from an early age, along with a gradual accumulation of megakaryocyte and myeloid progenitors. Interestingly, these peculiar phenotypes are reminiscent of the main features found within the BM of old mice.

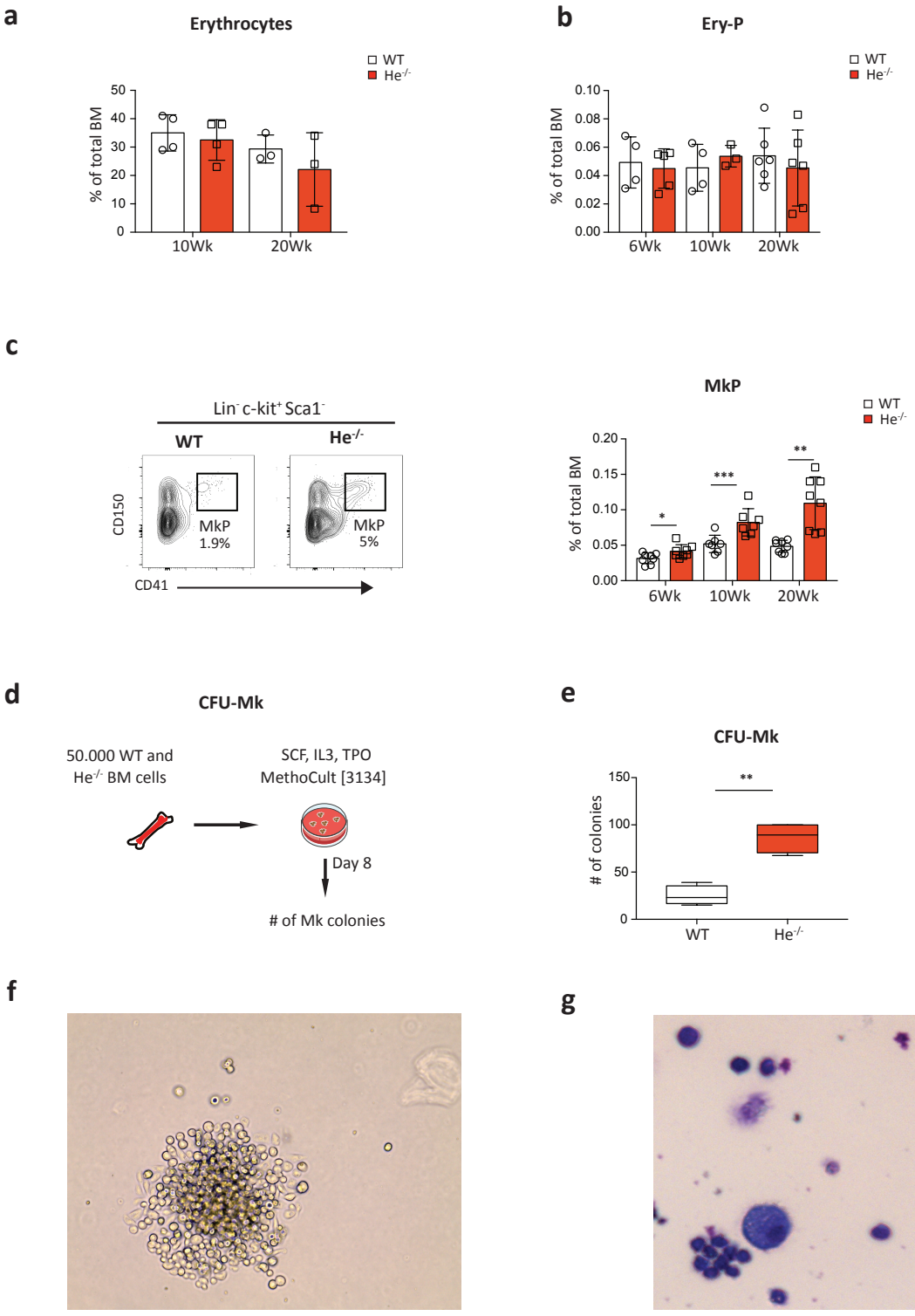

Figure 3 | Increase of megakaryocyte progenitors in He$^{-/-}$ mice.
(a) Percentage of BM erythrocytes (Ter119^{+}) and **(b)** Erythroid Progenitors (Ery-P; Lin^{-}c-kit^{+}Sca1^{-} CD105^{+}) in 6-, 10- and 20- week-old WT and He$^{-/-}$ mice. **(c)** Representative gating strategy to identify Megakaryocyte Progenitors (MkP); on the left, percentage of MkP within the BM of 6-, 10- and 20-week-old WT and He$^{-/-}$ mice. Means ± SD from 3 to 8 independent experiments per mouse age. Statistical significance was calculated using an unpaired two tailed t-test, * $p<0.05$, **$p<0.01$ and ***$p<0.001$. **(d)** Megakaryocyte CFU assay strategy: 50.000 total BM cells derived from 10- and 20-week-old WT and He$^{-/-}$ mice were seeded in MethoCult medium [3134] with the

addition of the following cytokines: 50ng/ml SCF, 20ng/ml IL3 and 50ng/ml TPO. Large megakaryocyte colonies were scored after 8 days. **(e)** Box plot showing the number of megakaryocyte colonies after 8 days of culture. **(f)** Representative picture of a megakaryocyte colony. **(g)** May Grünwald Giemsa (MGG) staining of BM derived colonies. Mean ±SD from 4 independent experiments. Each experiment was performed in technical duplicate. Statistical significance was calculated using an unpaired two tailed t-test, * $p<0.05$ and ** $p<0.01$.

3) EFFECT OF HELIOS DELETION ON MULTIPOTENT PROGENITORS AND HEMATOPOIETIC STEM CELLS

A) MPP3 AND MPP4

Reduced lymphoid potential in $He^{-/-}$ LSK cells

To gain insights into the origin of the altered myeloid-to-lymphoid ratio in $He^{-/-}$ mice, and discriminate between a defect disturbing the more committed progenitors or the stem cell and MPP levels, we analyzed by flow cytometry different MPP subpopulations, with a focus on myeloid-biased MPP3 and lymphoid-biased MPP4. Starting from 6 weeks of age, we found that the MPP4 compartment was significantly reduced (1.6X) in $He^{-/-}$ mice, in contrast to a global increase of the MPP3 population (1.2X) (**Fig. 4a, S4a**).

Given that Flt3 represents the MPP4 identifier antigen, we wanted to understand whether our observation was genuine and not due to an eventual Flt3 down-regulation. Thus, we evaluated the MPP3 abundance (and indirectly also the MPP4 percentage) within the total MPP population, undertaking the *ex vivo* approach. We purified single WT and $He^{-/-}$ MPP cells into a 96 well plate and cultured them with medium containing cytokines stimulating myeloid cell proliferation (MethoCult 3434 containing SCF, IL3, IL6, EPO). Eight days after cell plating, we tallied the wells containing a myeloid colony (**Fig. 4b**). $He^{-/-}$ MPP generated significantly more myeloid colonies (1.2X) with respect to the WT MPP (**Fig. 4c**), therefore confirming, with a different approach, that $He^{-/-}$ MPP3 predominate over the lymphoid biased MPP4.

In addition, we further investigated the MPP potential using an *in vivo* transplantation approach. We purified WT and $He^{-/-}$ donor MPP3 and MPP4 cells (marked by the surface antigen polymorphism CD45.2), and we separately

transplanted them into sub-lethally irradiated recipient mice (marked by surface antigen polymorphism CD45.1 and CD45.2) (**Fig. 4d**). Two weeks after MPP3 and MPP4 transfer, we quantified blood B lymphoid and myeloid cells derived from WT and $He^{-/-}$ donors. We uncovered that donor $He^{-/-}$ MPP4 cells repopulate the B lymphoid compartment less efficiently (1.7X) than the WT counterpart and partially differentiate towards the myeloid lineage ($CD11b^{+}$) (1.7X) (**Fig. 4e, S4b**). On the contrary, no differences were observed in the behavior of the MPP3, as both WT and $He^{-/-}$ MPP3 cells specifically give rise to equal amounts of myeloid cells (**Fig. 4f, S4c**). These results corroborated the validity of our previous observation and, moreover, showed that $He^{-/-}$ MPP4 are less efficient in producing lymphoid B cells, with respect to the WT counterpart.

Altogether, these findings revealed that Helios deletion affects lymphoid and myeloid development as early as the MPP stage, given that $He^{-/-}$ BM contains more MPP3 and less functional MPP4.

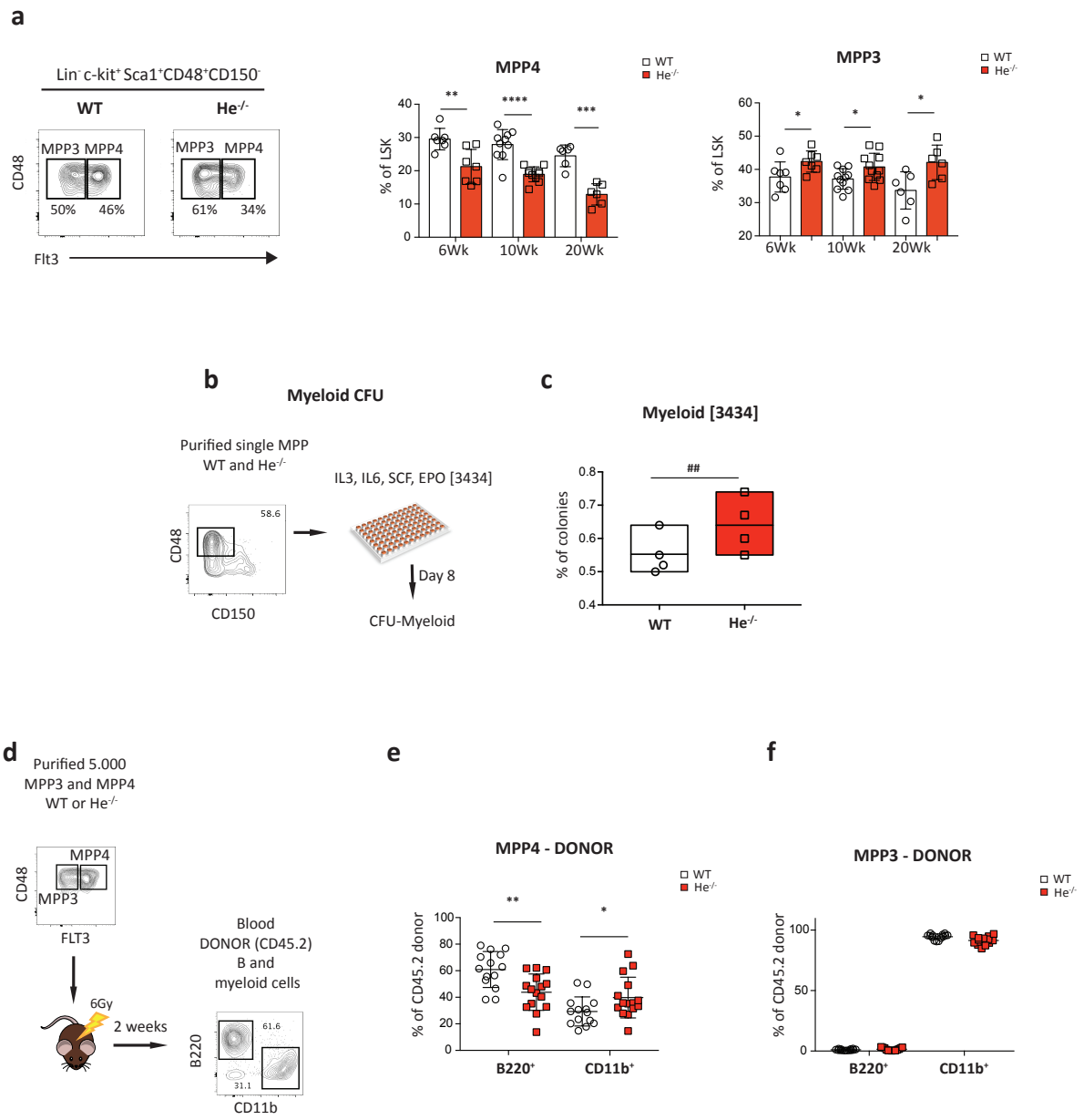

Figure 4 | Decreased lymphoid potential in multipotent progenitors of He$^{-/-}$ mice.
(a) Left - Representative contour plots depicting WT and He$^{-/-}$ BM MPP3 (Lin$^-$Sca$^+$c-kit$^+$CD150$^-$ CD48$^+$Flt3$^-$) and MPP4 (Lin$^-$Sca$^+$c-kit$^+$CD150$^-$CD48$^+$Flt3$^+$). Right – Percentage of MPP3 and MPP4 within the LSK compartment of 6-, 10- and 20-week old mice. Means ± SD from 3 to 7 independent experiments per mouse age. Statistical significance was calculated using an unpaired two tailed t-test, * p<0.05, **p<0.01 and ***p<0.001. **(b)** Schematic strategy underlying the myeloid CFU assay: sorted MPP from WT or He$^{-/-}$ BM were seeded into 96 well plates (one cell per well) containing MethoCult cytokine complete medium (10ng/ml IL-3, 10ng/ml IL-6, 50ng/ml SCF and 3U/ml EPO) [3434]. Myeloid colonies were tallied after 8 days of culture. **(c)** Percentage of myeloid colonies originated from WT and He$^{-/-}$ MPP. Means ± Max/Min from 4 independent experiments performed in duplicate. Statistical significance was calculated using paired two tailed t-test, # p<0.05 and ## p<0.01. **(d)** Experimental strategy for MPP3 and MPP4 transplantation: 5000 purified MPP3 and MPP4 from donor WT or He$^{-/-}$ (CD45.2$^+$) BM were separately transplanted into sub-lethally (6.5Gy) irradiated recipient mice (CD45.1 and CD45.2).

Blood myeloid ($CD11B^+$) and B ($B220^+$) cell reconstitution was measured 2 weeks after transplantation. **(e-f)** Percentage of blood myeloid and B cells, within the $CD45.2^+$ population, derived from WT and $He^{-/-}$ **(e)** MPP4 or **(f)** MPP3. Mean ± SD of 4 independent experiments with 3-4 recipient mice per genotype. Statistical significance was calculated using an unpaired two tailed t-test, * $p<0.05$ and **$p<0.01$.

B) MPP2 AND HSC

$He^{-/-}$ HSC are megakaryocyte biased

Give that the myeloid / lymphoid ratio was affected already at the MPP level, we wondered whether also the megakaryocyte expansion observed in $He^{-/-}$ mice was caused by a defect occurring in their more upstream precursors: MPP2 or LT-HSC (Rodriguez-Fraticelli et al., 2018). Flow cytometry analyses showed that MPP2 and LT-HSC percentages are unchanged in $He^{-/-}$ mice with respect to the WT counterpart, at all investigated mouse ages (**Fig. 5a,b, S5a**).

In order to deeply investigate the LT-HSC and MPP2 compartments, we further looked at the expression of the surface antigen CD41, that has been already shown to specifically mark platelet biased LT-HSC (Gekas and Graf, 2013). In this case, we found that around 60% of both LT-HSC (**Fig. 5c**, red bars) and MPP2 (**Fig. 5d**, red bars) derived from $He^{-/-}$ mice were $CD41^+$, a much larger fraction (3X) with respect to the WT LT-HSC and MPP2 counterpart (**Fig. 5c,d, S5b**). These findings suggest a scenario where Helios deletion causes a LT-HSC and MPP2 platelet-oriented phenotype.

An *in vitro* culture approach allowed us to test whether LT-HSC were indeed functionally platelet biased. We isolated single LT-HSC from WT and $He^{-/-}$ mice and seeded each of them into 96 well plates (one cell per well) containing medium supplemented with SCF, IL3 and TPO cytokines specific for megakaryocyte but also myeloid cell development. Eight days after the seeding, we tallied the wells containing megakaryocytes, recognizable because of their large cell size, and those containing only granulo-monocyte colonies (Gr-Mo only colonies) depleted of large cells (**Fig. 5e**). Furthermore, to validate our finding we performed MGG staining on megakaryocyte positive and myeloid only colonies; as expected, we found megakaryocytes (recognizable by morphology) only within megakaryocyte positive wells (**Fig. S5c**). Our result showed that $He^{-/-}$ LT-HSC give rise to significantly more megakaryocyte containing colonies (1.5X) when compared to WT stem cells;

conversely, WT LT-HSC generate more “megakaryocyte depleted” colonies (1.4X) (**Fig. 5f**).

Taken together, these results suggest that Helios is able to affect megakaryopoiesis as early as the LT-HSC stage, in a way reminiscent of the phenotype observed in old LT-HSC.

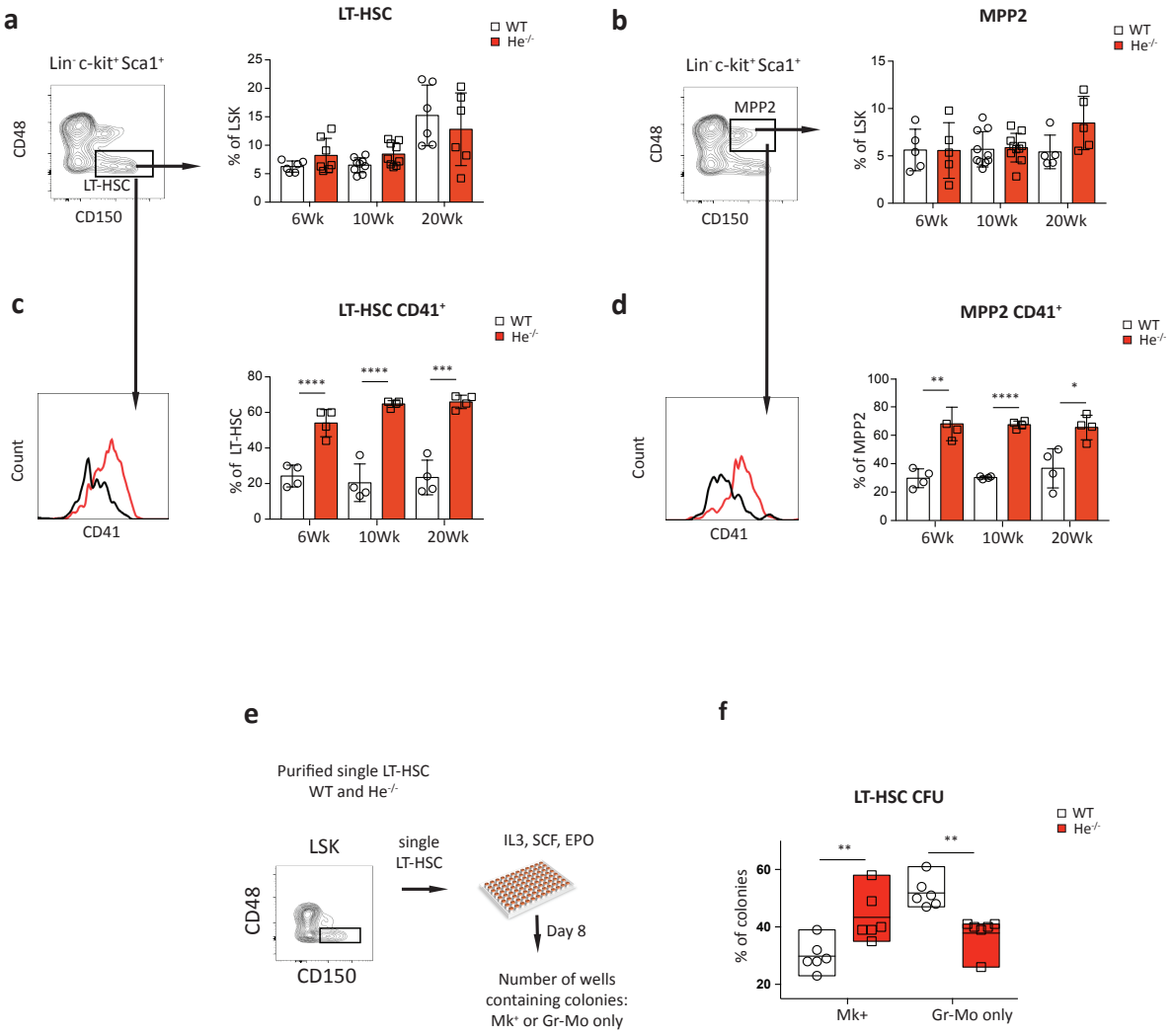

Figure 5 | He$^{-/-}$ LT-HSC are biased towards the megakaryocyte lineage.
(a) Representative FACS plot of BM LT-HSC and their LSK percentage in WT and He$^{-/-}$ 6-, 10- and 20- week-old mice. **(b)** Representative FACS plot of BM Lin^{-}Sca^{+}c-Kit^{+}CD150^{+}CD48^{+} MPP2 and their LSK percentage in WT and He$^{-/-}$ 6-, 10- and 20- week-old mice. **(c)** Representative flow cytometry histogram showing the CD41 levels within LT-HSC cells of WT and He$^{-/-}$ mice. Right panel - percentage of CD41 positive LT-HSC in WT and He$^{-/-}$ 6-, 10- and 20- week-old animals. **(d)** Representative flow cytometry histogram showing the CD41 levels within MPP2 cells of WT and He$^{-/-}$ mice. Right panel - percentage of CD41 positive MPP2 in WT and He$^{-/-}$ 6-, 10- and 20-

week-old animals. Means ± SD from 3 to 7 independent experiments per mouse age. Statistical significance was calculated using an unpaired two tailed t-test, * p<0.05, **p<0.01 and ***p<0.001. **(e)** Schematic strategy underlying the megakaryocyte-myeloid single cell culture assay: single LT-HSC from WT or $He^{-/-}$ BM were seeded into 96 well plates (one cell per well) containing StemSpan SFEM supplemented with the following cytokines: 50ng/ml SCF, 20ng/ml IL3 and 50ng/ml TPO. Megakaryocyte containing colonies (Mk^{+}) and "granulo-monocyte only" colonies (Gr-Mo only) were tallied 8 days later. **(f)** Percentage of megakaryocyte or "granulo-monocyte only" colonies derived from WT and $He^{-/-}$ LT-HSC. Each dot represents the mean ± Max/Min of 4 independent experiments all performed in technical duplicates. Statistical significance was calculated using unpaired two tailed t-test, * p<0.05 and ** p<0.01.

4) INTRINSIC VERSUS EXTRINSIC HELIOS EFFECT ON HSPC REGULATION

A) TESTING THE HELIOS HSPC EXTRINSIC ROLE: INFLAMMATION IN THE BONE MARROW MICROENVIRONMENT

Th1-like inflammation takes place in $He^{-/-}$ bone marrow

Accumulating evidence have shown that in old BM there is an increased concentration of pro-inflammatory cytokines, like interferon (IFN)-γ and interleukin (IL)-6 (Ho et al., 2019). Such pro-inflammatory cytokines can suppress lymphoid progenitor development and favor a myeloid and megakaryocyte bias (Ho et al., 2019; Mirantes et al., 2014). Moreover, when acute inflammation is ectopically triggered in young mice, LSK are rapidly affected and undergo dramatic expansion (~5X) (Haas et al., 2015; Mirantes et al., 2014; Schurch et al., 2014). In similar way, $He^{-/-}$ mice have less lymphoid progenitors (MPP4 and CLP), more megakaryocyte and myeloid biased MPP and undergo an age related LSK expansion (around week 20), with respect to the WT counterpart (**Fig. 6a,b**). These findings suggest that a kind of pro-inflammatory condition might be present in $He^{-/-}$ BM. Furthermore, Helios is highly expressed in $CD4^{+}$ $Foxp3^{+}$ Treg cells, where it has been recently described to regulate their suppressive function (Kim et al., 2015). Interestingly, recent publications highlighted that $FoxP3^{+}$ Treg cells are located close to LT-HSC in the BM and that their selective depletion promoted LSK expansion and lymphoid lineage restriction (Pierini et al., 2017). These pieces of data give space to a scenario in which Helios indirectly regulates HSPC development by promoting Treg suppressive

ability: defective BM Treg suppression may indeed trigger T cell-mediated inflammation and finally skew HSPC towards a megakaryocyte and myeloid direction.

To investigate further this possibility, we explored whether a T cell-mediated inflammation was indeed present in the BM of $He^{-/-}$ mice. To match such goal, we incubated $CD4^+$ enriched BM cells in media containing PMA and ionomycin and Golgi-plug, in order to enhance cytokine production and avoid their release. After two hours of stimulation we evaluated, by flow cytometry, the intracellular levels of IFN-γ, IL-10 and IL-2, typical Th1 cytokines. Within the $He^{-/-}$ $CD4^+$ effector T cell pool, we found an enhanced production of IFN-γ (4.5X), IL10 (3.5X) and IL2 (1.5X) Th1 cytokines, with respect to the WT counterpart **(Fig. 6c,d)**. On the contrary, cytokine production was not affected in $CD4^+$ $FoxP3^+$ regulatory T cells (data not shown). These findings highlighted that a Th1-like inflammation condition is present within the $He^{-/-}$ BM, reinforcing the idea that T cell-mediated inflammation may have a role in regulating the Helios dependent HSPC phenotype.

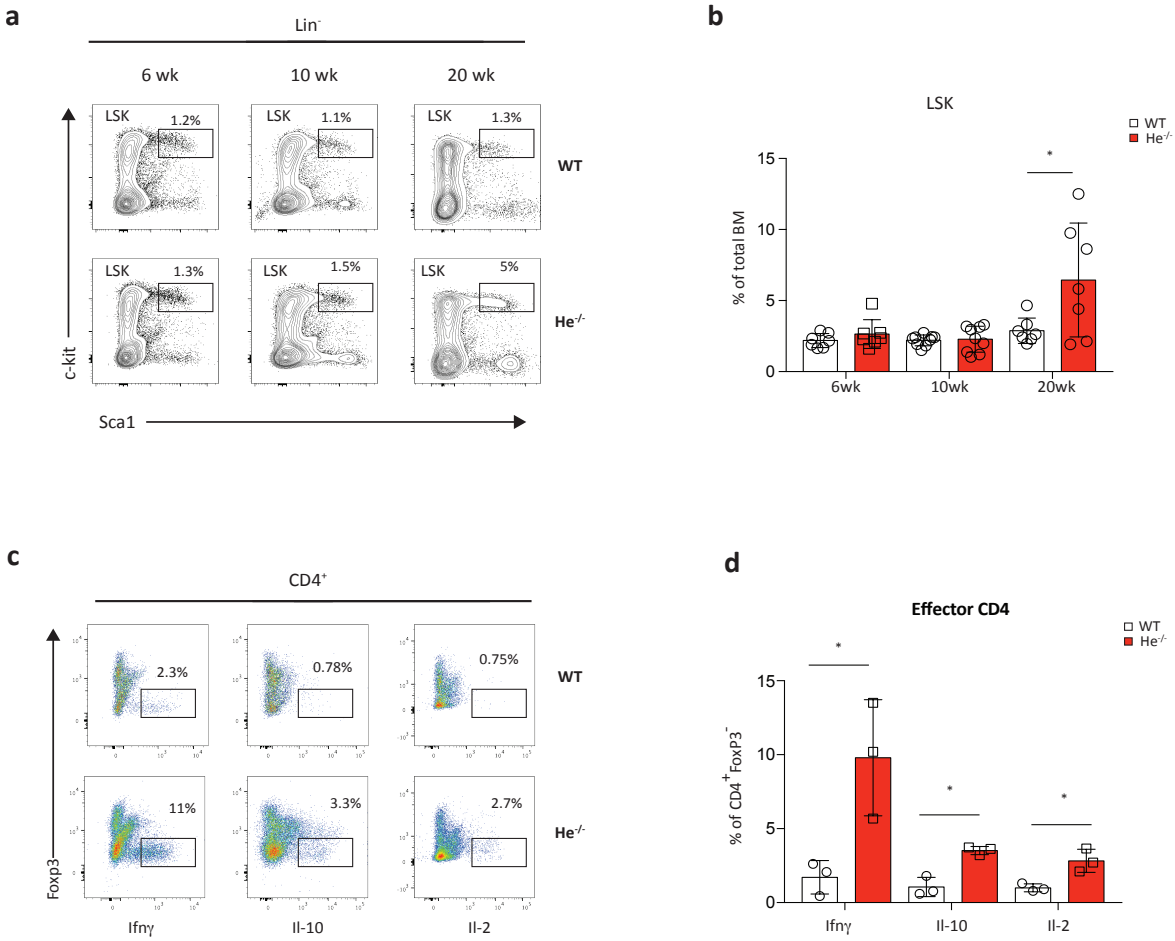

Figure 6 | **Th1-like inflammation in $He^{-/-}$ BM.**
(a) Representative contour plots of LSK cells and **(b)** their BM frequency in WT and $He^{-/-}$ mice at 6, 10 and 20 weeks of age. Means ± SD from 3 to 7 independent experiments per mouse age. Statistical significance was calculated using an unpaired two tailed t-test, * $p<0.05$. **(c)** Representative pseudo-contour plots of WT and $He^{-/-}$ $CD4^+$ BM T cells, intracellularly stained for Foxp3, IFN-γ, IL-10 and IL-2. **(d)** Percentage of positive IFN-γ, IL-10 and IL-2 cells within the $CD4^+FoxP3^-$ population of WT and $He^{-/-}$ 20-week-old mice. Means ± SD from 3 to 4 mice per genotype. Statistical significance was calculated using an unpaired two tailed t-test, * $p<0.05$.

B) TESTING THE HELIOS HSPC EXTRINSIC ROLE: CONSEQUENCES OF ITS DELETION ON T CELLS

Helios knockout in T cells marginally affects hematopoiesis

In order to understand whether the myeloid-to-lymphoid MPP bias, as well as the Th1-like inflammation were caused by Helios loss in T cells, we decided to ablate

Helios specifically in this cell population. To achieve this goal, we crossed a mouse line expressing the Cre recombinase transgene under the control of the CD4 regulatory elements (CD4-Cre) (Lee et al., 2001) with a second mouse line carrying the Helios gene flanked by two LoxP sites ($He^{f/f}$; kindly provided by the Shevach laboratory). In this way, we obtained CD4-Cre^{+} expressing mice in which Helios is constitutively deleted in both CD8 and CD4 cells (CD4-$He^{-/-}$) (**Fig. 7a**). We assessed the Helios specific deletion in T cells by performing intracellular staining with an anti-Helios antibody. As control, we stained Helios positive HSPC where we recovered normal Helios expression as expected (data not shown).

We analyzed the BM B lymphoid, myeloid and HSPC compartments of CD4-$He^{-/-}$ and control CD4-$He^{f/f}$ mice using flow cytometry. We observed an identical amount of mature B and myeloid cells (**Fig. 7b,c**) and, furthermore, we did not detect any difference in MkP, $CD41^{+}$ LT-HSC and MPP3 abundance (**Fig. 7d,e,f,g**). We only detected a mild, however not significant, reduction in MPP4 and CLP percentages (**Fig. 7g,h**). More in detail, we observed a trend where around half of the investigated CD4-$He^{-/-}$ mice showed decreased amounts of MPP4 (**Fig. 7g**, dashed lines).

In addition, $CD4^{+}$ effector T cells derived from CD4-$He^{-/-}$ mice produced more IFNγ, in comparison to control mice (**Fig. 7i**). However, this phenotype was highly variable across CD4-$He^{-/-}$ animals, with a trend similar to that observed within MPP4 (**Fig. 7g**). Indeed, roughly two groups of mice could be recognized (**Fig. 7i**, dashed lines): half of them producing abundant IFNγ, whereas the other half expressing low IFNγ, to an extent almost comparable to control mice. Given that several studies highlighted the importance of IFNγ in regulating the HSPC myeloid versus lymphoid skewing (reviewed in (Mirantes et al., 2014), we wondered whether high IFNγ production could explain the low MPP4 abundance observed in some CD4-$He^{-/-}$ animals (**Fig. 7g**, lower dashed line). We thus divided the CD4-$He^{-/-}$ mice into two separate groups, one of them containing the four mice showing the highest IFNγ production ($IFN\gamma^{high}$) and a second group containing the four mice showing the lower IFNγ secretion ($IFN\gamma^{low}$; **Fig. 7i,l**). Interestingly, we found that $IFN\gamma^{high}$ mice had significantly less MPP4, with respect to control mice (1.5X), while $IFN\gamma^{low}$ animals displayed MPP4 amounts comparable to that of control mice (**Fig. 7m**).

In conclusion, these findings revealed that Helios expressing T cells are dispensable for: *i)* LT-HSC megakaryocyte priming, *ii)* megakaryocyte progenitor and

MPP3 expansion, as well as *iii)* myeloid cell augmentation and mature B cell reduction. Notably, it is rather possible that Helios expressing T cells may play partial roles in controlling the MPP4 compartment (although the phenotype is not fully penetrant). However, in contrast to CD4-He$^{-/-}$ animals, 100% of germline Helios knockout mice showed MPP4 reduction, implying that the main mechanism underlying lymphoid progenitor diminution may be HSPC intrinsic, and probably only partially contributed by Helios deletion in T cells.

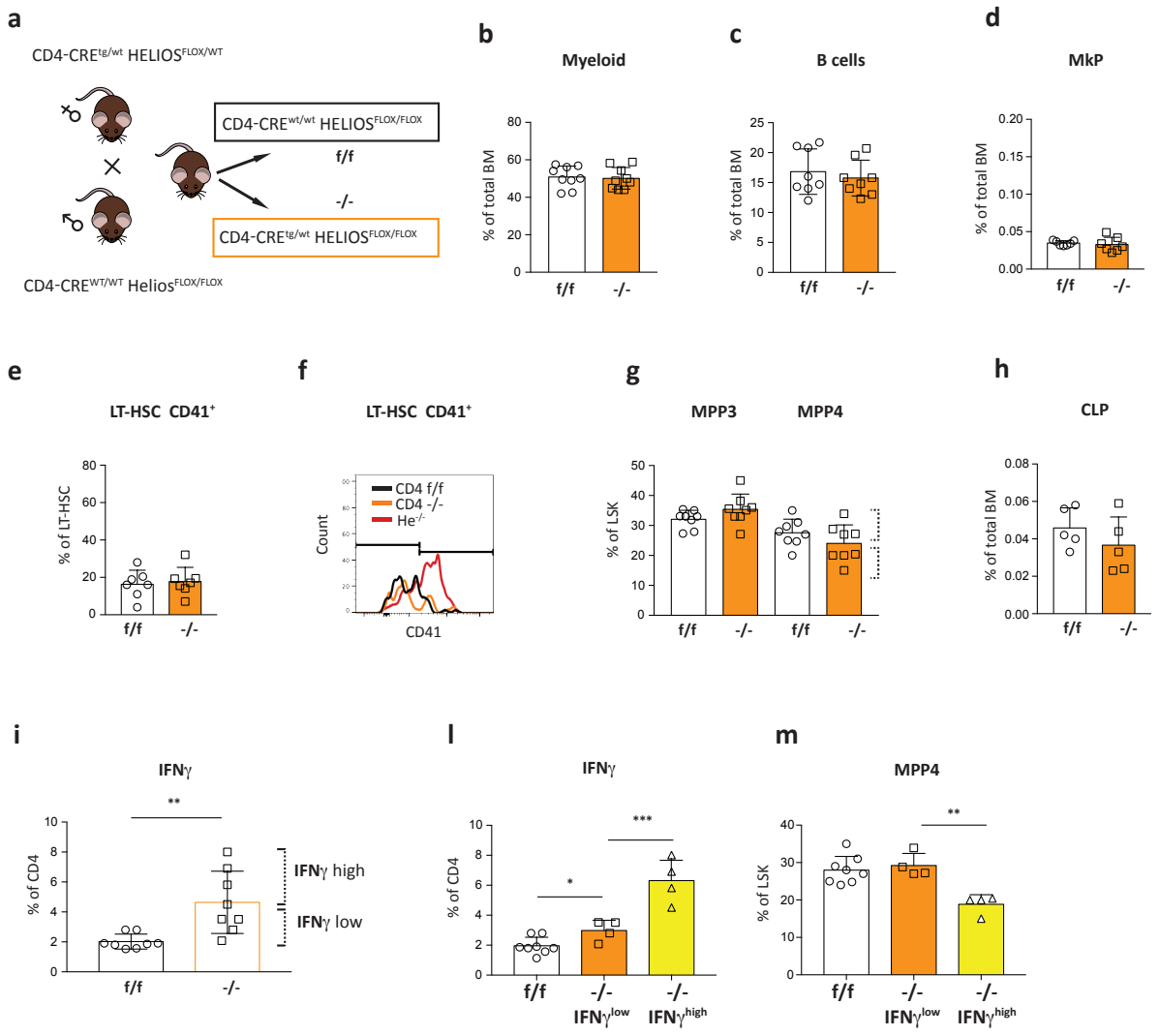

Figure 7 | Analyses of mice bearing a Helios conditional deletion in T cells.
(a) Schematic breeding strategy used to obtain CD4-specific Helios deletion. Mice carrying the CD4-Cre transgene and the LoxP floxed Helios gene in heterozygosis were crossed to animals bearing the two Helios floxed alleles. The following mice were generated and used for our analyses: CD4-Cre^{+}; He$^{f/f}$ (-/-) experimental animals and control CD4-Cre^{-}; He$^{f/f}$ (f/f) mice. Sex-

(both males and females) and age- (10-week-old) matched mice were used for the described experiments. **(b)** Percentage of mature myeloid and **(c)** B cells in the BM of CD4-$He^{-/-}$ and CD4-$He^{f/f}$ mice. **(d)** Percentage of MkP in the BM of CD4-$He^{-/-}$ and CD4-$He^{f/f}$ mice. **(e)** Percentage of CD41 positive LT-HSC in the BM of CD4-$He^{-/-}$ and CD4-$He^{f/f}$ mice. **(f)** Representative flow cytometry histogram showing the CD41 levels in LT-HSC of CD4-$He^{-/-}$, CD4-$He^{f/f}$ and Helios germline KO mice. **(g)** Percentage of MPP3 and MPP4 cells within the LSK compartment of CD4-$He^{-/-}$ and CD4-$He^{f/f}$ mice. **(h)** Percentage of CLP in the BM of CD4-$He^{-/-}$ and CD4-$He^{f/f}$ mice. **(i)** Percentage of IFNγ positive cells within the BM $CD4^+$ $Foxp3^-$ population of CD4-$He^{-/-}$ and CD4-$He^{f/f}$ mice. **(l)** Percentage of IFNγ positive cells within the $CD4^+FoxP3^-$ populations of CD4-$He^{f/f}$, CD4-$He^{-/-}$ $IFN\gamma^{low}$ and CD4-$He^{-/-}$ $IFN\gamma^{high}$ mice. **(m)** Percentage of MPP4 within the LSK population of CD4-$He^{f/f}$, CD4-$He^{-/-}$ $IFN\gamma^{low}$ and CD4-$He^{-/-}$ $IFN\gamma^{high}$ mice. Means ± SD from 3 to 7 independent experiments. Statistical significance was calculated using an unpaired two tailed t-test, * $p<0.05$, ** $p<0.01$ and *** $p<0.001$.

C) TESTING THE HELIOS HSPC INTRINSIC ROLE: $He^{-/-}$ HSPC IN A WILD TYPE ENVIRONMENT

Helios regulates the myeloid versus lymphoid bias in a hematopoietic intrinsic manner

Given that Helios deletion is present in all cells of the organism (since it is a germline mutation), we wanted to test whether its removal was intrinsically affecting the hematopoietic system. To address this point, we injected $He^{-/-}$ LT-HSC into a WT environment, in order to selectively evaluate the consequences of Helios deletion exclusively within the hematopoietic system. In particular, we injected into lethally irradiated WT recipient mice (CD45.1 and CD45.2) 100 purified LT-HSC (donor CD45.2) either from $He^{-/-}$ or WT control mice, along with 500.000 helper BM cells (CD45.1) able to sustain hematopoiesis during the first weeks after irradiation. We let the donor stem cells reconstitute the host hematopoietic system for two months and, afterwards, we analyzed their blood donor reconstitution (**Fig. 8a**). $He^{-/-}$ donor LT-HSC generated significantly less B lymphocytes (2.3X), more myeloid cells (2.3X) as well as equal amounts of T cells, with respect to the WT donor counterpart (**Fig. 8b,c**). This result showed that $He^{-/-}$ LT-HSC possess the ability to generate a myeloid versus lymphoid biased system in a WT environment, further suggesting that Helios operates intrinsically in hematopoietic cells.

At this point, it was important to discriminate whether Helios acts directly, probably within HSPC, or rather its mutation affects mature cells (e.g. T cells) able, in

turn, to exert a negative feedback on HSPC. In order to address this point, we performed competitive BM transplantation experiments. In such setup, we injected equal amounts of WT (competitor) and $He^{-/-}$ donor cells within the same lethally irradiated recipient mouse. If Helios acts directly on HSPC, only the $He^{-/-}$ donor counterpart is going to be perturbed, whereas if Helios deletion affects HSPC indirectly, also the co-hosted WT competitor cells would result equally affected. More in detail, we injected 150.000 BM donor $He^{-/-}$ (CD45.2) cells along with the same amount of WT competitor BM cells (CD45.1) into lethally irradiated recipient mice (CD45.1 and CD45.2). As control, we generated a parallel system where we injected donor WT cells together with WT competitors (**Fig. 8d**). Two months after transplantation, we observed that competitor cells (CD45.1), injected along with $He^{-/-}$ donors (CD45.2), gave rise to a normal B lymphoid and myeloid ratio: ~60% of B cells and ~20% of myeloid cells (**Fig. 8e**, gray). On the contrary, $He^{-/-}$ donor cells generated a myeloid skewed system composed of roughly the same amount (~40%) of both B and myeloid cells (**Fig. 8e**, red). As expected, no differences in reconstitution ability were observed between WT donor and WT competitor cells (**Fig. 8f**). Altogether, these findings support a scenario in which Helios intrinsically affects hematopoiesis, most likely by acting on uncommitted HSPC cells.

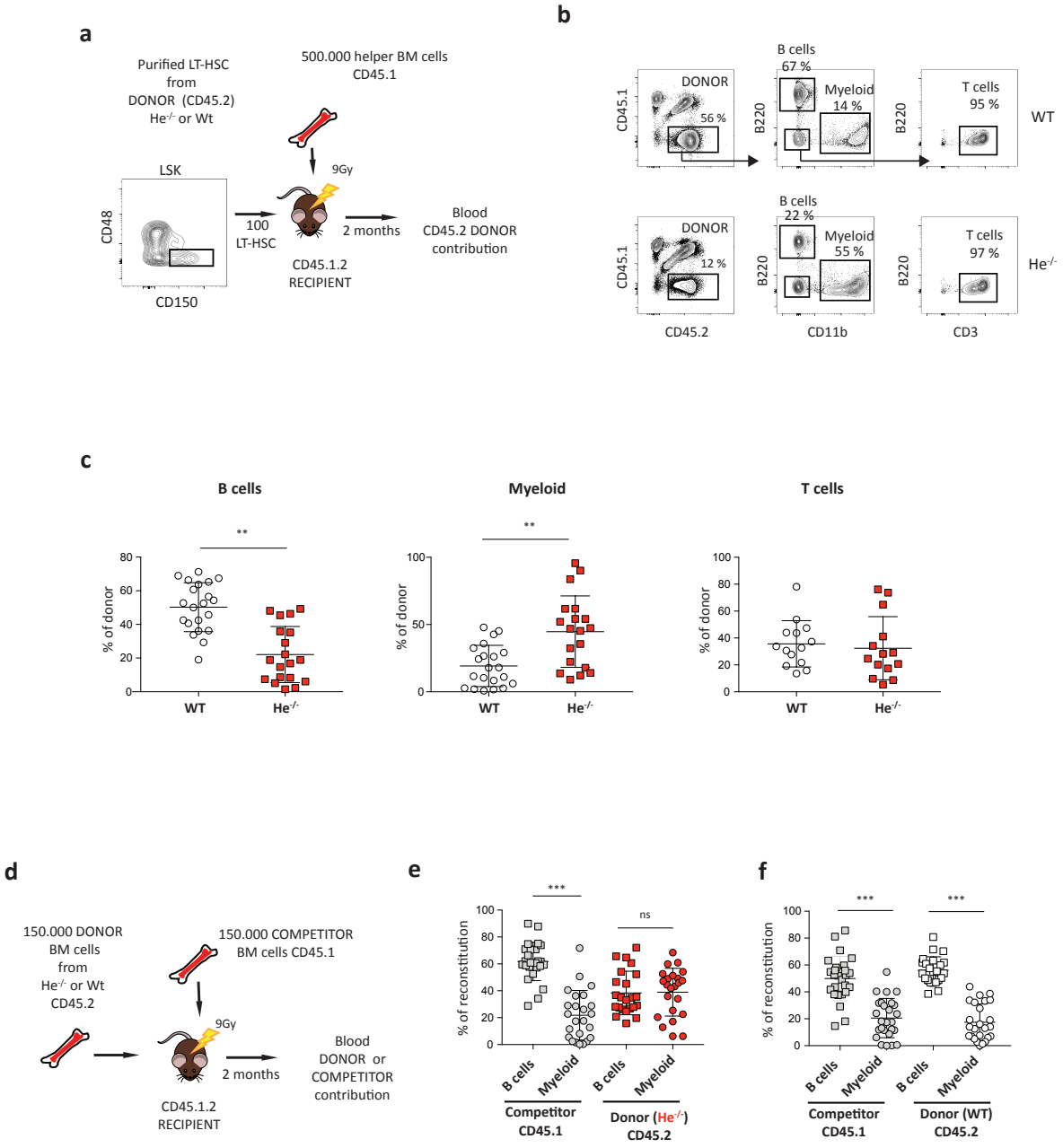

Figure 8 | Transplantation of donor WT and He$^{-/-}$ hematopoietic cells into lethally irradiated recipient mice.

(a) Schematic strategy of LT-HSC transplantation assay: 100 donor WT or He$^{-/-}$ sorted LT-HSC were injected into lethally irradiated recipient mice along with 500.000 helper BM cells. **(b)** Blood donor B, T and myeloid cell reconstitution was assessed by flow cytometry two months later. **(c)** Percentage of blood myeloid and B cells within the CD45.2^{+} population derived from WT and He$^{-/-}$ LT-HSC. Means ± SD from 3 independent experiments with 6-7 recipient mice per genotype (for B and myeloid cells). Means ± SD from 2 independent experiments with 6-7 recipient mice per genotype (for T cells). Statistical significance was calculated using an unpaired two tailed t-test, * p<0.05, **p<0.01 and ***p<0.001. **(d)** Strategy for competitive BM transplantation assay: 150.000 donor WT or He$^{-/-}$ BM cells were injected into lethally irradiated recipient mice together with 150.000 WT competitor BM cells. Blood B and myeloid cell reconstitution was assessed two months later. **(e)** In gray, percentage of blood myeloid and B cells within the CD45.1^{+} population

(derived from the WT BM competitor) and in red, percentage of blood myeloid and B cells within the CD45.2^{+} population (derived from He$^{-/-}$ donor BM cells). Both BM populations, CD45.1^{+} and CD45.2^{+}, were co-transplanted into the same lethally irradiated recipient mice. **(f)** In gray, percentage of blood myeloid and B cells within the CD45.1^{+} population (derived from the WT BM competitor) and in white, percentage of blood myeloid and B cells within the CD45.2^{+} population (derived from WT donor BM cells). Both BM populations, CD45.1^{+} and CD45.2^{+}, were co-transplanted into the same lethally irradiated recipient mice. Means ± SD from 4 independent experiments with 6-7 recipient mice per genotype. Statistical significance was calculated using an unpaired two tailed t-test, * p<0.05, **p<0.01 and ***p<0.001.

5) HELIOS HSPC REGULATED GENES

Helios deletion affects HSPC transcription, with a stronger impact on LT-HSC population

HSPC cells are functionally and phenotypically affected in He$^{-/-}$ mice but we still miss information about the molecular profile of this cell population. In order to uncover genes potentially mis-regulated in absence of Helios, we performed mRNA sequencing on purified LT-HSC, MPP3 and MPP4 (from 10-week-old mice), which represent the most affected populations in He$^{-/-}$ BM. Hierarchical clustering of differentially expressed genes between He$^{-/-}$ and the WT counterpart showed that LT-HSC are the most perturbed cells, with approximately 400 mis-regulated genes (FDR<0.1). On the contrary, only a few genes were affected in MPP3 (46 genes, FDR<0.1) and MPP4 (26 genes, FDR<0.1) populations (**Fig. 9a,b**).

In order to understand which kind of gene signatures were affected by Helios deletion, we performed gene set enrichment analysis (GSEA) on WT versus He$^{-/-}$ Differentially Expressed Genes (DEG) with a p-value < 0.05. We found that He$^{-/-}$ LT-HSC up-regulated transcripts were enriched for genes typically overexpressed in old LT-HSC and for signatures characteristic of megakaryocyte progenitors (Grover et al., 2016; Sun et al., 2014). Moreover, He$^{-/-}$ LT-HSC down-regulated mRNAs were enriched for transcripts typically down-regulated in old LT-HSC (**Fig. 9c**). These findings well correlate with the increased LT-HSC megakaryocyte bias potential observed *in vivo* and *in vitro*, and also with the premature aging phenotype observed in He$^{-/-}$ mice. Similarly, we found enrichment of megakaryocyte progenitor signatures on up-regulated He$^{-/-}$ MPP3 genes (**Fig. 9d**), whereas the lymphoid (CLP) signatures were enriched on the down-regulated transcripts of both He$^{-/-}$ MPP3 and MPP4 (**Fig.**

9d,e). These results revealed, on a genome wide scale, that the lymphoid transcriptional priming is negatively regulated in $He^{-/-}$ MPP.

Given that LT-HSC underwent the largest changes in their gene expression profile, we decided to further explore the affected pathways. For this aim, Metascape analysis was performed on up- and down- regulated LT-HSC genes. Platelet activation resulted to be the best represented category within the up-regulated genes, along with other categories still related to platelet biology and activation (**Fig. 9f**) (Nakamura-Ishizu et al., 2018). Regarding the down-regulated genes, the affected categories were more heterogeneous, with cell adhesion, cell projection assembly and microtubule-based processes being the most recurrent terms (**Fig. 9f**).

In conclusion, comparison of the mRNA profiles across HSPC populations revealed that LT-HSC are the most affected cells by Helios deletion. $He^{-/-}$ LT-HSC acquired an old-like gene expression profile, along with the overexpression of genes involved in megakaryocyte development and platelet activation.

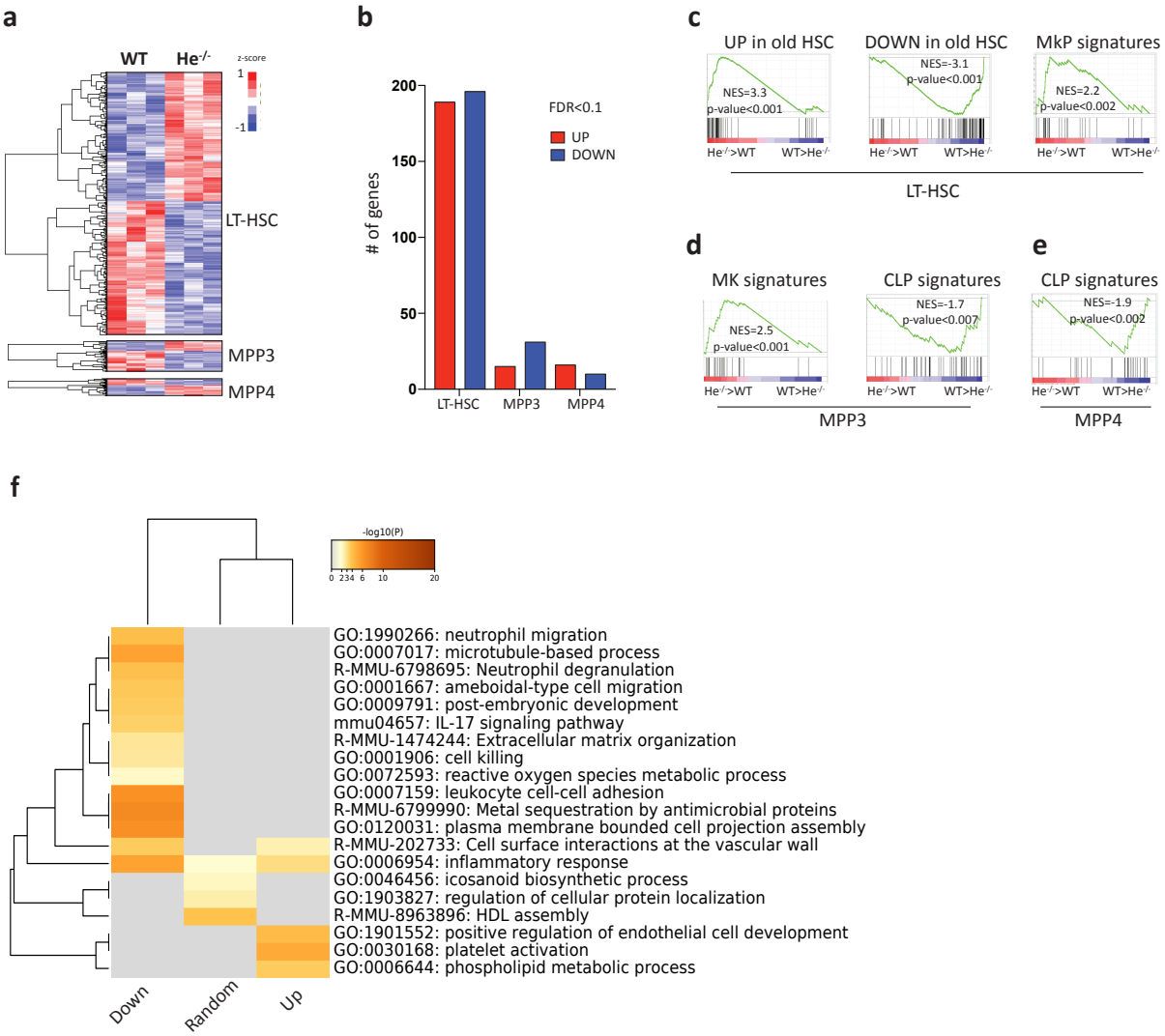

Figure 9 | Transcriptome analysis of He$^{-/-}$ HSPC.
(a) Heatmap derived from hierarchical clustering of WT versus He$^{-/-}$ LT-HSC, MPP3 and MPP4 up- and down- regulated mRNAs. **(b)** Number of genes (FDR<0.1) up- and down-regulated in He$^{-/-}$ LT-HSC, MPP3 and MPP4. **(c)** GSEA using a ranked list comprising up- and down- regulated genes in He$^{-/-}$ LT-HSC ($p < 0.05$). The signature list is composed of: up-regulated genes in old LT-HSC (450 genes), down-regulated genes in old LT-HSC (450 genes) (Sun et al., 2014), gene signatures of MkP progenitors (Grover et al., 2016). **(d)** GSEA using a ranked list comprising up- and down- regulated genes in He$^{-/-}$ MPP3 ($p < 0.05$). The signature list is composed of MkP progenitor and CLP signatures (Grover et al., 2016). **(e)** GSEA using a ranked list comprising up- and down- regulated genes in He$^{-/-}$ MPP4 ($p < 0.05$). The signature list is composed of CLP progenitor signatures (Grover et al., 2016) **(f)** Metascape heatmap of enriched terms (e.g. Gene Ontology terms), colored by p-value, across He$^{-/-}$ up-regulated, down-regulated and randomly selected LT-HSC input genes (as negative control).

6) SINGLE CELL ANALYSES OF HSPC

HSPC heterogeneity revealed by single cell mRNA sequencing analyses

In order to more comprehensively explore Helios function within HSPC and understand how the compartment is globally shaped by its deletion, we decided to probe the whole molecular heterogeneity within WT and $He^{-/-}$ LSK, looking at single cell resolution. As illustrated in **Fig. 10a**, to achieve this goal we FACS purified LSK cells from WT and $He^{-/-}$ mice in biological duplicates (analyzing two animals for each genotype). Importantly, immediately after cellular sort we labeled cells from each distinct sample with a unique HasTag Oligo (HTO)-tagged antibody directed against the CD45 surface protein, as described in the recently published Cell Hashing protocol (Stoeckius et al., 2018). This provided us the advantage of pooling the four samples together, as they can be later on demultiplexed. Labeled LSK were additionally stained using the CITE-seq protocol (Stoeckius et al., 2017), in order to specifically distinguish the HSC and MPP2-4 populations upon sequencing. In particular, for LT-HSC identification we used the CD150 and CD41 HTO conjugated antibodies, while for MPP2, MPP3 and MPP4 detection we added CD48 and Flt3 HTO conjugated antibodies. We then collected 10.000 total cells (2.500 from each sample) that we used to prepare mRNA and HTO libraries using the 10X chromium technology. After library sequencing and further bioinformatics cell analyses, we confidentially identified 3470 single cells (**Fig. 10a**), on top of which we performed all the following analyses.

First, taking advantage of the Cell Hashing derived HTO sequences, we identified the relative WT and $He^{-/-}$ cells within the total pool of LSK cells, recovering: 554 and 824 cells belonging to the two $He^{-/-}$ samples; 1175 and 914 cells derived from the two WT samples. In a next step, we wanted to detect and separate cell sub-populations within the total LSK pool. For this, we applied two main different clustering strategies to our transcriptomic data (illustrated in the form of T-distribute Stochastic Neighbor Embedding (t-SNE) plots in **Fig. 10b,c**): one based on the K-mean unsupervised machine learning algorithm (**Fig. 10b**) and a second approach relying on the cell specific expression of CITE-seq-derived CD150, CD41, CD48 and Flt3 HTO (**Fig.10c**).

Applying the K-mean clustering (with n=3), we reliably identified 3 populations separated mainly based on differences in cell cycle and DNA replication genes (**Fig.**

10b, S6a). The more “quiescent” cells, which are depleted of DNA replication and cell cycle transcripts, are located at the bottom part of the t-SNE plot within the so called Cluster Q (blue); the middle cluster accommodates less quiescent cells expressing genes like CDK1 and MCM3 (Cluster M, orange); finally, the “active” and proliferating cells localize at the top of the t-SNE plot as part of the Cluster A (green), marked for example by the cell cycle gene Mki67 (**Fig. 10b, S6a**).

While K-mean clustering helped to separate cells based on their proliferative status, we used the 4 CITE-seq derived HTO (CD150, CD41, CD48 and Flt3) to assess the HSPC composition in LT-HSC, MPP2-4 (**Fig. 10c**). Unfortunately, we were not able to technically detect a clear signal over the background for the Flt3 and CD41 HTO. On the contrary, we succeeded to obtain a strong and clear signal for the HTO CD150 and CD48 markers. By selecting cells possessing high CD150 and low CD48 expression we identified LT-HSC, mainly localized within the left bottom part of the t-SNE plot (**Fig 10c**, orange), while by selecting cells expressing only high CD48 HTO we retrieved the MPP pool, more homogeneously distributed to the opposite side of the plot (**Fig. 10c**, blue).

Interestingly, by combining both clustering analyses (**Fig. 10b,c**), we could realize that the majority of LT-HSC populate the K-mean Q cluster comprising quiescent cells; of note, a small percentage of LT-HSC, perhaps less quiescent, are also found within the K-mean cluster M, probably reflecting the existence of two pools of LT-HSC: one more quiescent and a second one more active. On the contrary, MPP cells were more homogeneously distributed across all K-mean clusters.

Given the technical impossibility to identify the MPP2-4 populations by using our HTO-based system, we decided to rather identify such populations by using selected marker mRNAs derived from our transcriptomic data (**Fig. 9a**), in combination with the available ImmGen dataset. As expected, several megakaryocyte lineage-related genes, known to be expressed by MPP2 (Pietras et al., 2015), were also found in HSC (e.g. Mpl, Gata2; **Fig. 10d**). On the contrary, lymphoid related genes were enriched within MPP4 (e.g.Flt3; **Fig. 10d**). Unexpectedly, while we were able to identify cell specific signatures for HSC and MPP4, this was not the case for MPP3 cells, whose genes are shared with HSC (e.g CD63, Vamp5 and Sdsl) and more often with MPP4 (e.g. Sox4, Spi1 and Cebpa; **Fig 10d**). Based on this, among the identified markers we specifically selected the Mpl, Sox4 and Flt3 “population specific” genes for our next analyses, as they were the

best captured transcripts within our single cell transcriptome (**Fig. S6b,c,d**). In particular, we defined: *i)* HSC and MPP2 as cells positive for Mpl and negative for Flt3; *ii)* MPP4 as cells expressing Flt3 but negative for Mpl; *iii)* MPP3 as Sox4 expressing cells, non-overlapping with MPP4 and HSC-MPP2 (**Fig. 10d**, bold).

By applying these criteria of "cell separation" (**Fig. 10e**), we identified a "vertical patterned" distribution of the three cell populations, encompassing the whole height of the t-SNE plot. Starting from the left, we found HSC-MPP2 (**Fig. 10e**, red) followed by MPP3 in the middle part (**Fig. 10e**, green) and finally by MPP4 on the right side (**Fig. 10e**, blue). Furthermore, based on the expression of the well characterized MPP2 specific TF Gata1 (ImmGen), we additionally identified MPP2 cells within the HSC-MPP2 cluster as $Gata1^{+}$ cells (**Fig. S6b**). Interestingly, $Gata1^{+}$ MPP2 localize almost exclusively within the K-mean M and A clusters (**Fig. S6b**), whereas MPP3 and MPP4 are abundantly present within all three K-mean clusters (**Fig. 10e**). The surprising discovery that several MPP3 and MPP4 reside within the K-mean cluster Q, along with many LT-HSC, reveals the existence of "quiescent stem cell-like" MPP, that we envision may represent the more upstream biased multi-potent progenitors.

In conclusion, by superimposing molecular mRNA signatures on single cell transcriptome data, we identified three "vertical" HSC/MPP2, MPP3 and MPP4 populations (**Fig. 10e**). On the contrary, by using the K-mean clustering strategy we uncovered three "horizontal" clusters based on cell cycle and proliferative properties (**Fig 10b**).

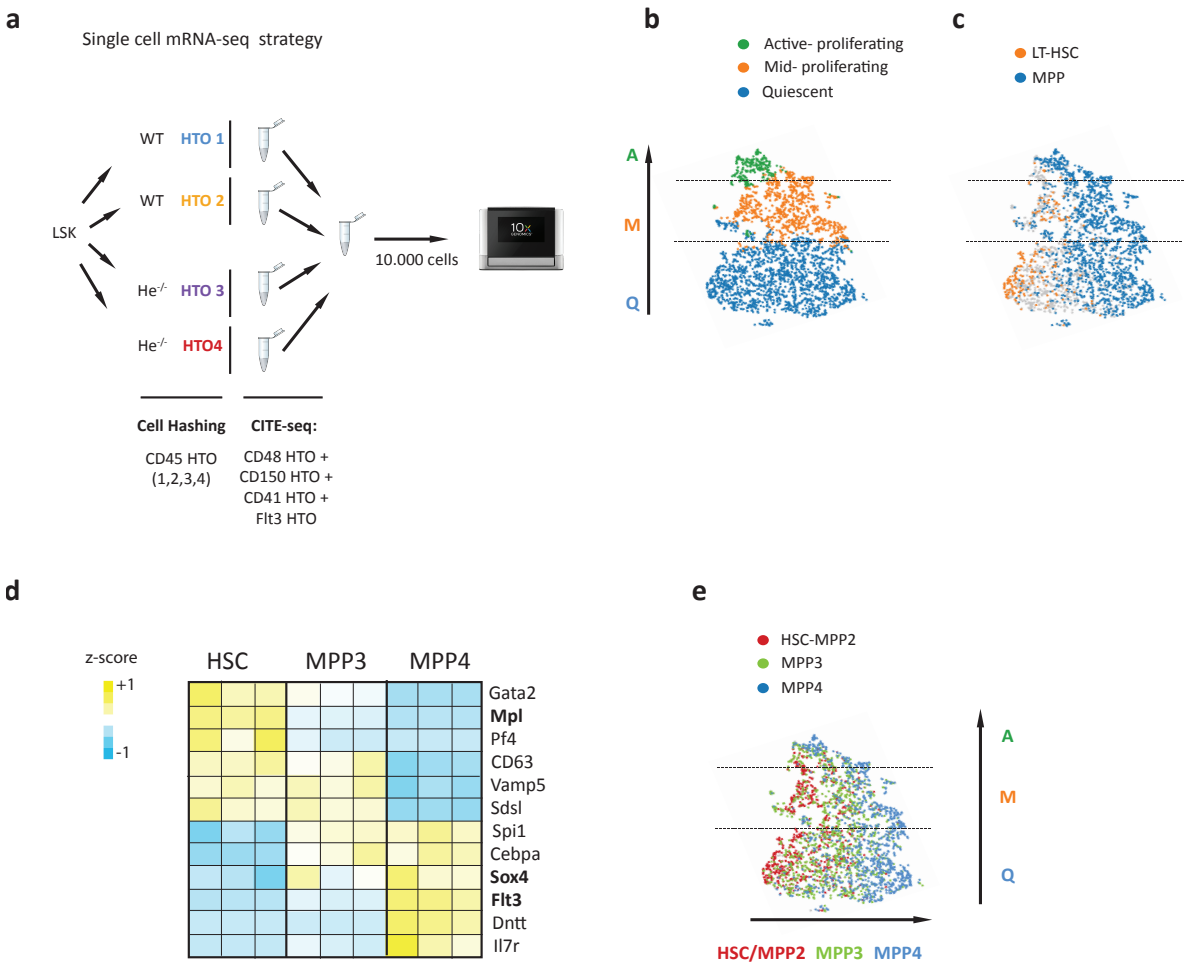

Figure 10 | Single cell mRNA sequencing of WT and He$^{-/-}$ HSPC.
(a) Schematic strategy of the single cell mRNA-seq experiment. LSK cells were purified from 2 WT and 2 He$^{-/-}$ mice. Each pool of LSK cells was labeled with a unique HasTag Oligo (HTO) conjugated anti-CD45 antibody (for a total of 4 uniquely tagged antibodies), following the Cell Hashing protocol described in (Stoeckius et al., 2018). In order to identify cell populations, the 4 LSK samples were additionally labeled with a common mix of HTO conjugated anti- CD150, CD48, CD41 and Flt3 antibodies (as described in the CITE-seq protocol from (Stoeckius et al., 2018). After antibody incubation, 2500 LSK cells from each pool were collected and the total 10.000 cells were processed for library preparation using the 10X chromium technology. **(b)** LSK t-distributed Stochastic Neighbor Embedding (t-SNE) plot of color-coded K-mean clusters (K=3): cluster Q (blue) = quiescent cells; cluster M (orange) = less quiescent cells; cluster A (green) = proliferative cells. Dashed lines delimit borders of the 3 K-mean derived clusters. **(c)** LSK t-SNE plot of color-coded CITE-seq-derived populations. CD150 and CD48 HTO levels define the LT-HSC and MPP clusters as follows: LT-HSC have high levels of CD150 HTO (read counts > 100) and low levels of CD48 (read count < 100); MPP express high levels of CD48 HTO (read counts > 100). Dashed lines delimit borders of the 3 K-mean derived clusters. **(d)** Representative heatmap showing: selected genes specifically expressed within LT-HSC and MPP4. MPP3 enriched transcripts are also shared between LT-HSC or MPP4. **(e)** LSK t-SNE depicting HSC-MPP2, MPP3 and MPP4 populations defined based on the expression levels of three marker genes: Mpl, Sox4 and Flt3. HSC-MPP2 are defined as positive for Mpl (read counts > 0.1) and negative for Flt3 (read counts <0.1); MPP4 cells are defined as positive for Flt3 (read counts >

0.1) and negative for Mpl (read counts <0.1); MPP3 are defined as Sox4 positive cells (read count > 0.1), non-overlapping with HSC-MPP2 and MPP4 clusters. Dashed lines delimit borders of the 3 K-mean derived clusters.

Helios acts on a small pool of quiescent HSPC

Our ability to properly dissect the heterogeneous nature of HSPC pool organization offered us the unique opportunity to carefully "map" the impact of the Helios deletion. In order dissect the HSPC Helios effect, we compared and analyzed the WT and $He^{-/-}$ HSPC populations taking into account their heterogeneity: the proliferative heterogeneity described by the three K-mean clusters (**Fig 10b**) and the "cell population" heterogeneity described by our mRNA markers (**Fig 10e**). For this reason, we superimposed our three mRNA derived HSPC groups HSC-MPP2, MPP3 and MPP4 to the three quiescent/proliferative Q, M and A clusters and evaluated eventual changes in the amounts of HSC-MPP2, MPP3 and MPP4 within individual K-mean clusters, comparing the WT and $He^{-/-}$ conditions (**Fig. 11a,b,c**). Interestingly, we found that the $He^{-/-}$ HSC-MPP2 population is increased by 1.5 fold within the Q cluster, with respect to the WT counterpart (**Fig. 11a**, red), and such Helios-dependent HSC-MPP2 augmentation is offset by a concomitant reduction (1.6X) of MPP4 percentage within the same cluster (**Fig. 11a**, blue). On the contrary, no obvious changes in abundance were detected within both WT and $He^{-/-}$ MPP3 in the Q cluster (**Fig. 11a**, green).

Surprisingly, we did not observe a remarkable trend within the proliferative M and A clusters (**Fig. 11b,c**): $He^{-/-}$ HSC-MPP2 belonging to cluster M were only marginally increased (1.15X; **Fig. 11b**, red), while $He^{-/-}$ MPP4 slightly reduced (1.18X; **Fig. 11b**, blue). Finally, no big differences were observed comparing $He^{-/-}$ and WT populations within the cluster A (**Fig. 11c**), although variability between replicates in the WT background complicates a clear interpretation of these experiments.

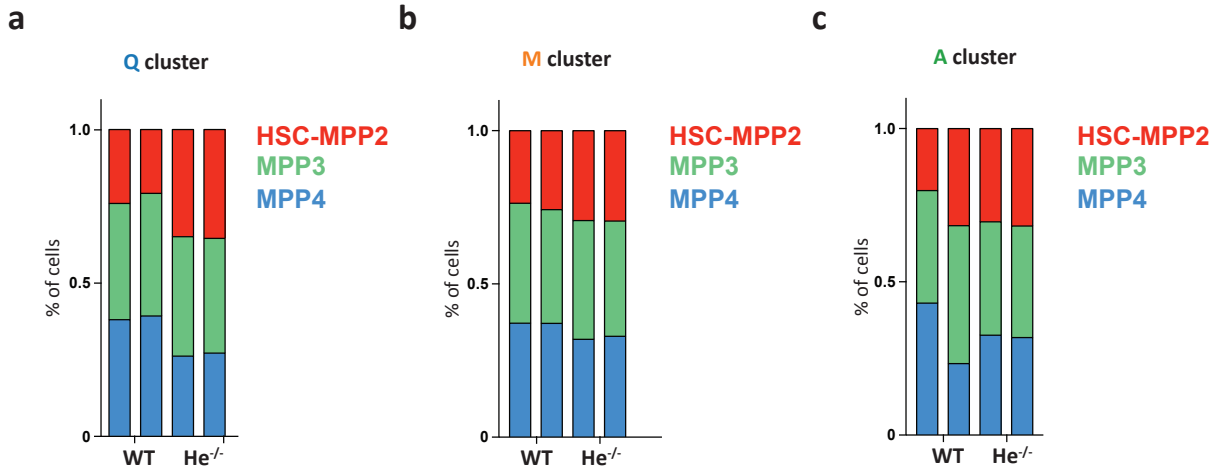

Figure 11 | Comparison of WT and He$^{-/-}$ HSPC at the single cell level.
(a-c) WT and He$^{-/-}$ HSC-MPP2, MPP3 and MPP4 quantification across the three K-mean clusters: Q, M and A. **(a)** Percentage of HSC-MPP2, MPP3 and MPP4 within the cluster Q. **(b)** Percentage of HSC-MPP2, MPP3 and MPP4 within the cluster M. **(c)** Percentage of HSC-MPP2, MPP3 and MPP4 within the cluster A.

In order to corroborate our findings in a more unbiased way and without a prior arbitrary HSC-MPP2, MPP3 and MPP4 definition, we decided to analyze our single cell mRNA data undertaking a different clustering approach. Given that HSC, MPP3 and MPP4 cells are distributed in a progressive fashion, across the entire "left to right axis" of our t-SNE representation (**Fig. 10e**), we decided to subdivide the t-SNE plot into arbitrary, equally sized, vertical segments. This criterion allowed us to cover the entire HSC to MPP4 progression with high resolution and without a prior population definition. Moreover, we further took into account the three K-mean proliferative clusters, in order to separately analyze quiescent cells from more proliferative cells and increase in this way the resolution of our analysis (**Fig. 12a**). Based on this logic, we ended up with 45 final vertical segments: 23 within the cluster Q, 16 contained within the cluster M and 6 coming from the cluster A (**Fig. 12a**).

To identify the identity of each segment, we computationally extracted genes responsible for the left to right separation. We found that segments on the left, as expected, are enriched in genes typically expressed in HSC and MPP2 (e.g. Gata2, Mpl; **Fig 12b**, red); the middle segments possess both HSC and MPP4 lymphoid-like signatures, therefore likely reflecting an MPP3 identity (**Fig 12b**, green); finally, the

extreme right segments express exclusively MPP4 lymphoid genes (e.g. Flt3, Dntt; **Fig 12b**, blue). Interestingly, our heatmap depicted a sort of "left to right developmental gradient": on the left we found cells enriched in megakaryocyte-like transcripts that, progressively, loose their marker genes while acquiring novel lymphoid-like signatures. In such view, we decided to quantify WT and $He^{-/-}$ cell percentage within each segment, in order to understand which classes of segments were more affected by Helios removal. By comparing WT and $He^{-/-}$ cell abundance within the Q cluster segments, we found that $He^{-/-}$ cells are homogeneously more abundant within HSC-MPP2 and some MPP3 segments, while homogeneously less profuse within the lymphoid MPP4 columns (**Fig. 12c**). On the contrary, such sinusoidal pattern was not identified within the segments belonging to the M and A clusters, where $He^{-/-}$ enriched and depleted segments are randomly distributed along the developmental gradient (**Fig. 12d,e,f,g)**.

Such results, in line with our previous findings, showed that Helios deletion affects a limited pool of quiescent HSPC.

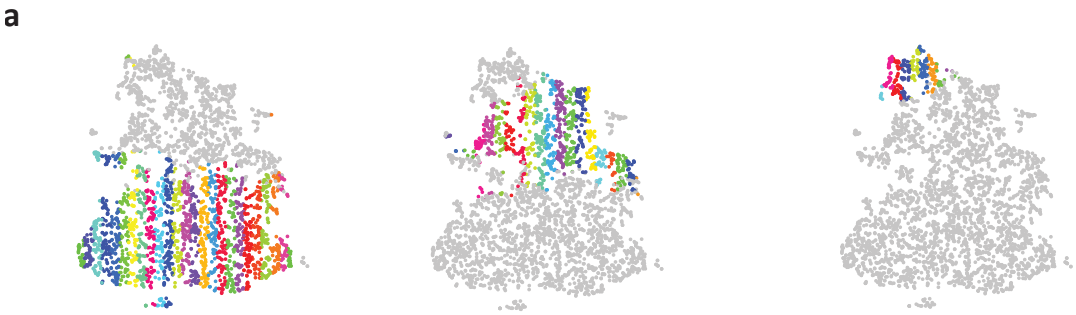

b

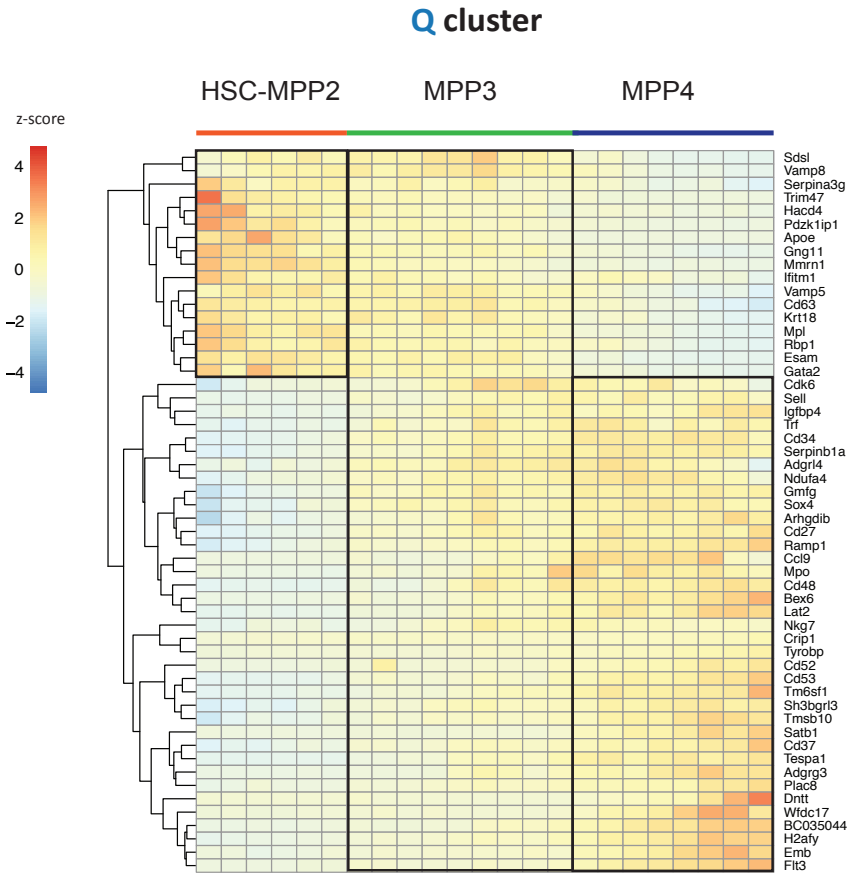
Q cluster
HSC-MPP2
MPP3
MPP4
z-score
4
2
0
−2
−4
Sdsl
Vamp8
Serpina3g
Trim47
Hacd4
Pdzk1ip1
Apoe
Gng11
Mmrn1
Ifitm1
Vamp5
Cd63
Krt18
Mpl
Rbp1
Esam
Gata2
Cdk6
Sell
Igfbp4
Tif
Cd34
Serpinb1a
Adgrl4
Ndufa4
Gmfg
Sox4
Arhgdib
Cd27
Ramp1
Ccl9
Mpo
Cd48
Bex6
Lat2
Nkg7
Crip1
Tyrobp
Cd52
Cd53
Tm6sf1
Sh3bgrl3
Tmsb10
Satb1
Cd37
Tespa1
Adgrg3
Plac8
Dntt
Wfdc17
BC035044
H2afy
Emb
Flt3

c

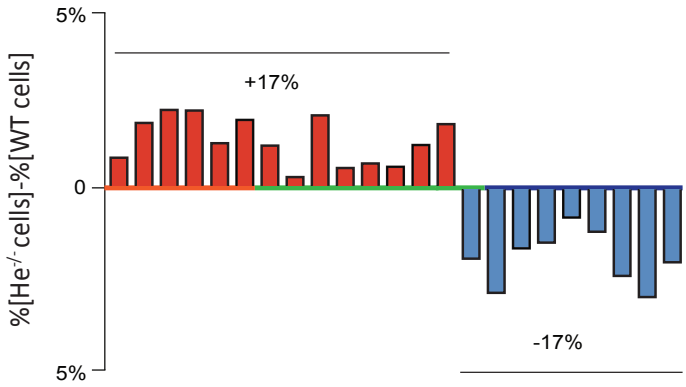
5%
+17%
0
%[He-/- cells]-%[WT cells]
-17%
5%

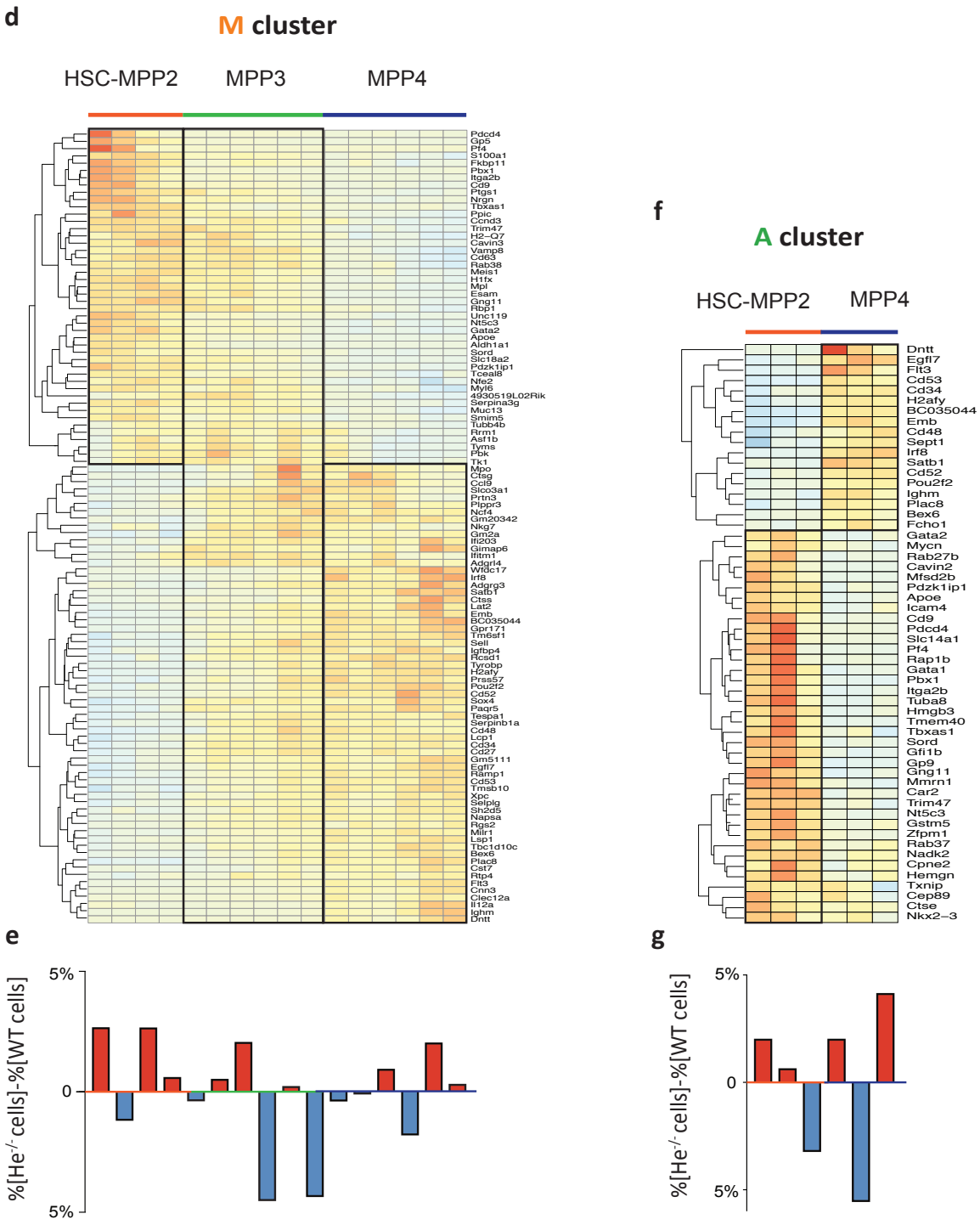

Figure 12 | Helios deletion affects a pool of quiescent HSPC.
(a) 45 equally spaced segments were chosen to divide the t-SNE plot across the left-to-right axis: 23 segments divided the Q cluster, 16 segments the M cluster and 6 segments the A cluster. Each segment was considered as a cell population and mean expression values were calculated for each gene. **(b,d,f)** Heatmaps depicting gene expression differences across segments: differentially expressed transcripts across the left-to-right axis have been selected in order to identify HSC-MPP2, MPP3 and MPP4 specific segments. **(b)** Q cluster derived heatmap:

segments are classified as HSC-MPP2, MPP3 and MPP4 based on their expression profile. **(c)** Quantification of $He^{-/-}$ and WT cellularity across the 23 single segments of the Q cluster. For each WT and $He^{-/-}$ segment we calculated the relative cell percentage. For WT cells, we divided the number of cells in a given segment by the total number of WT cells within the Q cluster. The same operation was performed for the $He^{-/-}$ segments. Upon this calculation we performed the following operation: %of $He^{-/-}$ cells (within a given segment) - % of WT cells (within the same segment), in this way we identified the $He^{-/-}$ enriched segments and the $He^{-/-}$ depleted segments. **(d)** M cluster derived heatmap: each segment is classified as HSC-MPP2, MPP3 and MPP4 based on its expression profile. **(e)** The analyses described in (c) were performed also for the 16 segments of the M cluster. **(f)** Cluster A derived heatmap: each segment is classified as HSC-MPP2 and MPP4 segment based on its expression profile. **(g)** The analyses described in (c) were performed also for the 6 segments of the A cluster.

7) SUPPLEMENTARY RESULTS

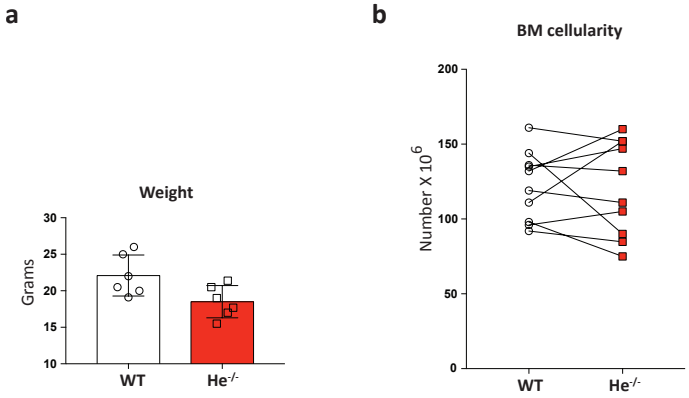

Figure S1 | BM cellularity within WT and $He^{-/-}$ mice.
(a) Body weight (grams) of WT and $He^{-/-}$ 10-week-old mice (both males and females are represented in the graph). **(b)** Number of BM cells within WT and $He^{-/-}$ 10-week-old mice (both females and males are represented in the graph). BM cells were derived from 2 tibia, 2 femurs, 2 pelvis and sternum.

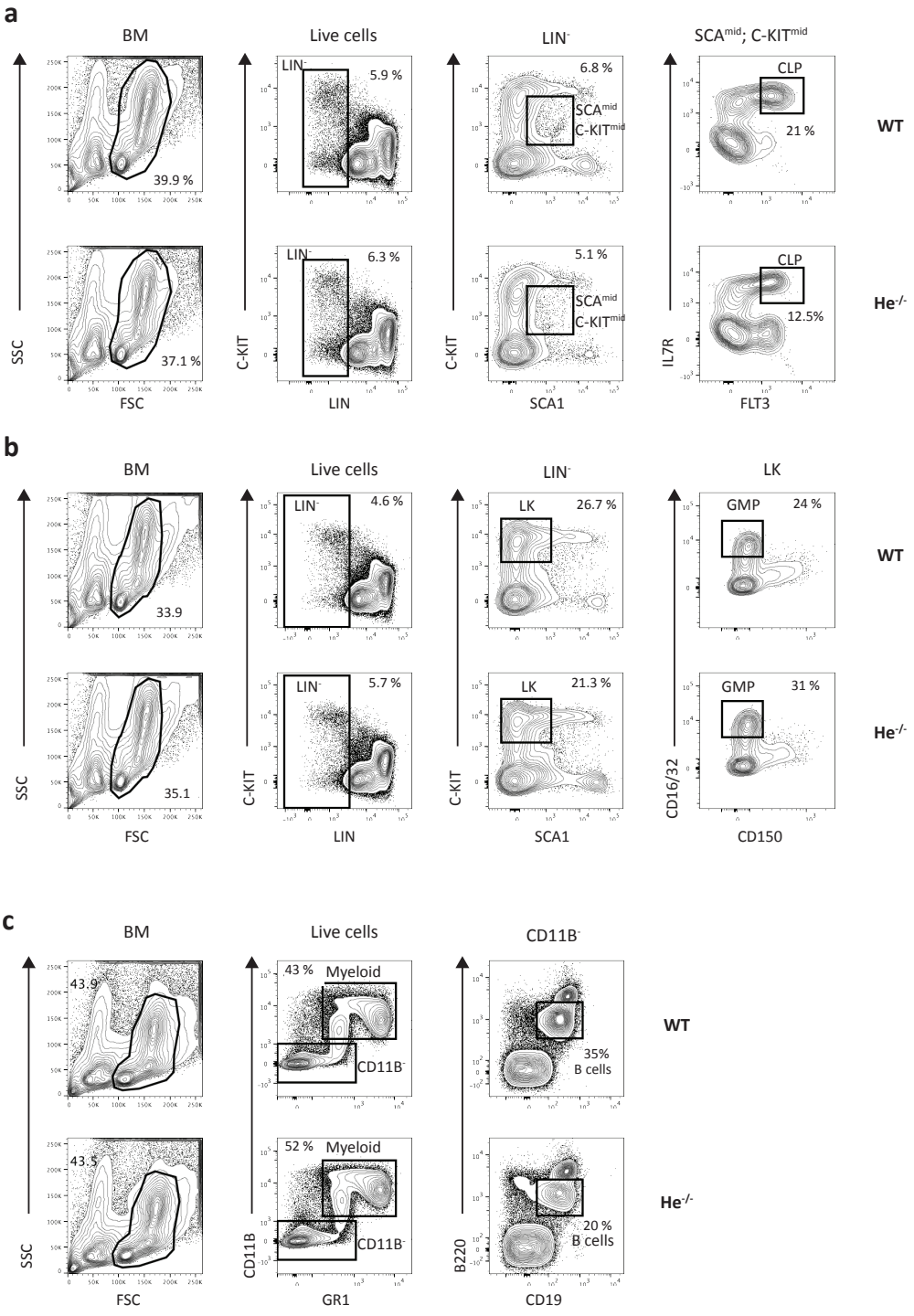

Figure S2 | Gating strategy for myeloid and lymphoid cell identification by flow cytometry. **(a-c)** Representative gating strategy for the identification of WT and $He^{-/-}$: **(a)** Common Lymphoid Progenitor (CLP); **(b)** Granulocyte Monocyte Progenitor (GMP); **(c)** mature myeloid and B cells.

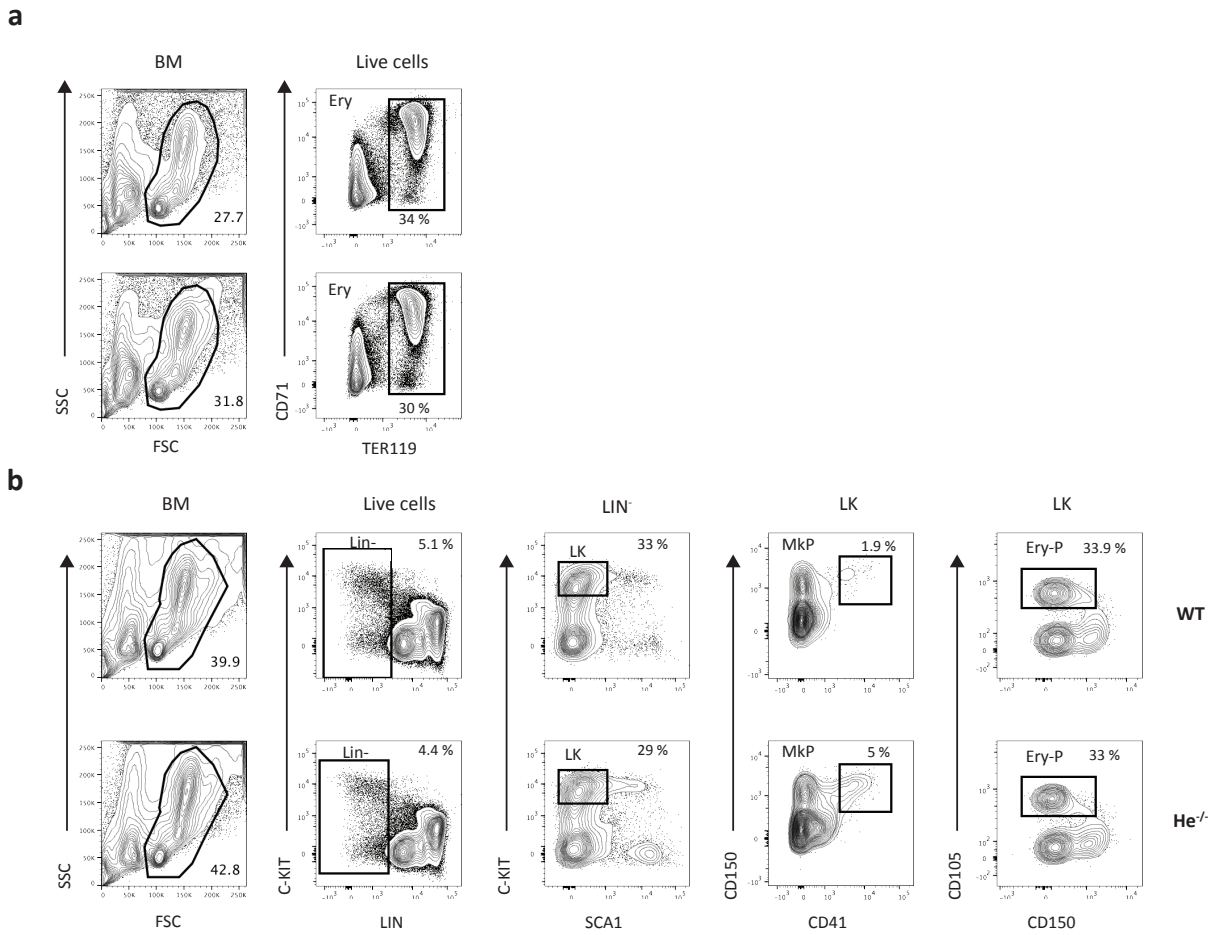

Figure S3 | Gating strategy for megakaryocyte and erythrocyte progenitor cell identification by flow cytometry.

(a-b) Representative gating strategy for the identification of WT and $He^{-/-}$: **(a)** Erythroid cell (Ery); **(b)** Megakaryocyte Progenitor (MkP) and Erythroid Progenitor (Ery-P).

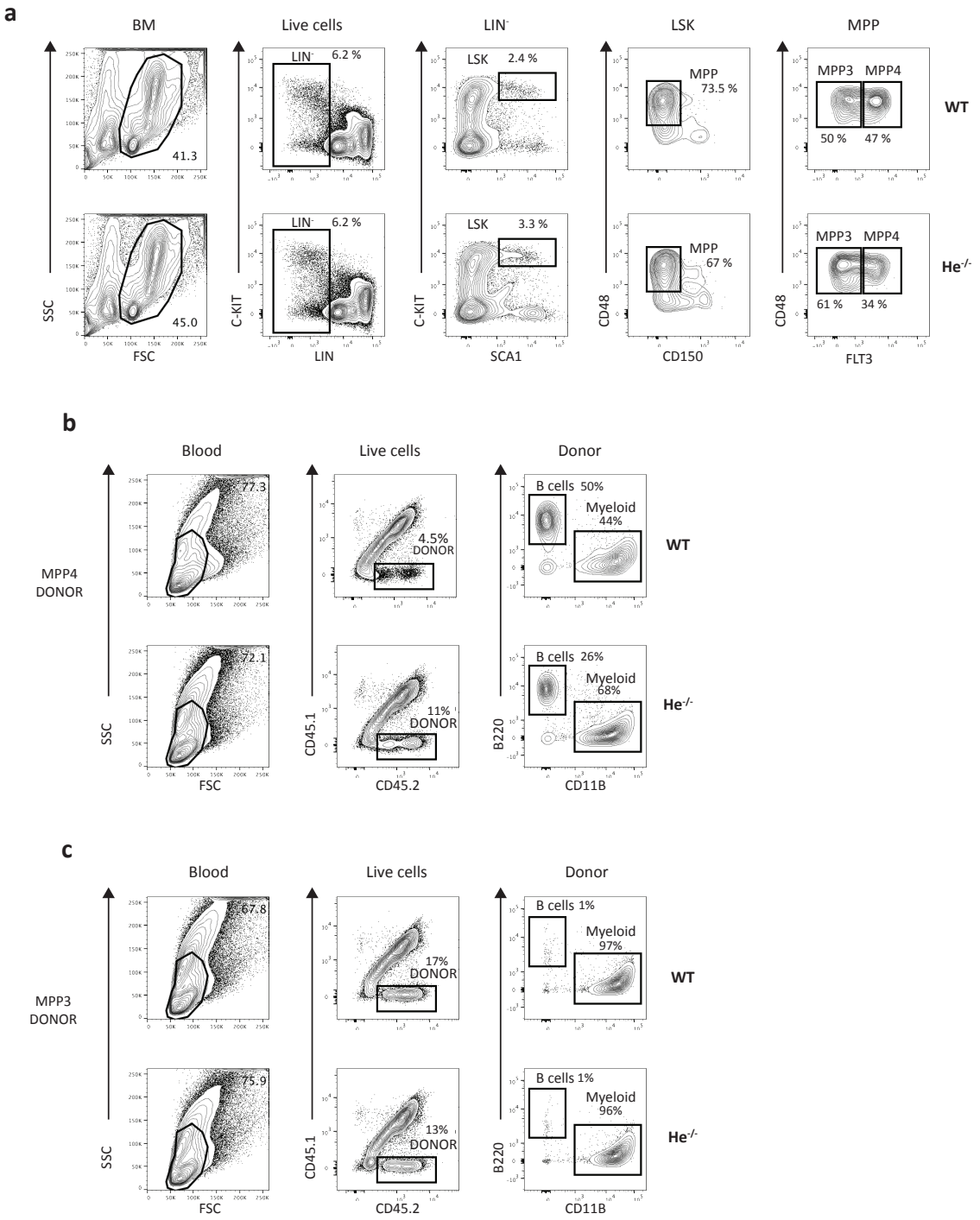

Figure S4 | Gating strategy for BM MPP3 and MPP4 identification by flow cytometry.
(a) Representative gating strategy for the identification of WT and $He^{-/-}$ MPP3 and MPP4. **(b-c)** Representative gating strategy for the identification of blood B and myeloid cells derived from WT and $He^{-/-}$ **(b)** MPP4 and **(c)** MPP3.

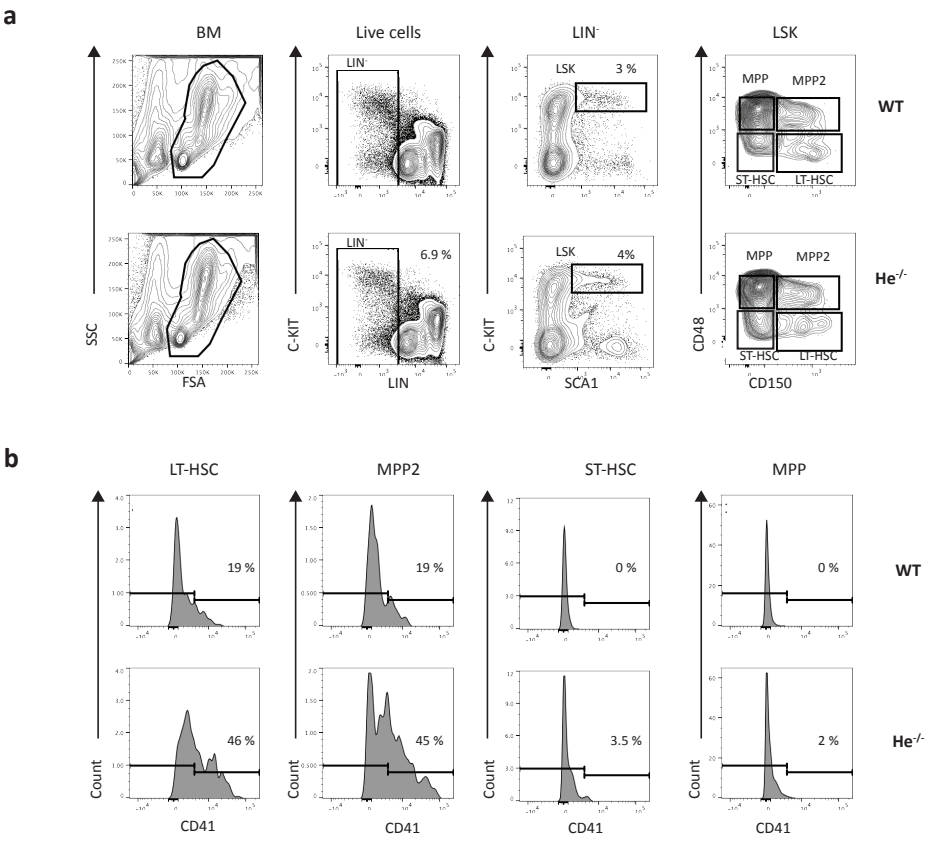
a
BM
Live cells
LIN-
LSK
WT
He-/-
SSC
FSA
C-KIT
LIN
SCA1
CD48
CD150
MPP
MPP2
ST-HSC
LT-HSC
3 %
6.9 %
4%
b
LT-HSC
MPP2
ST-HSC
MPP
19 %
0 %
46 %
45 %
3.5 %
2 %
Count
CD41

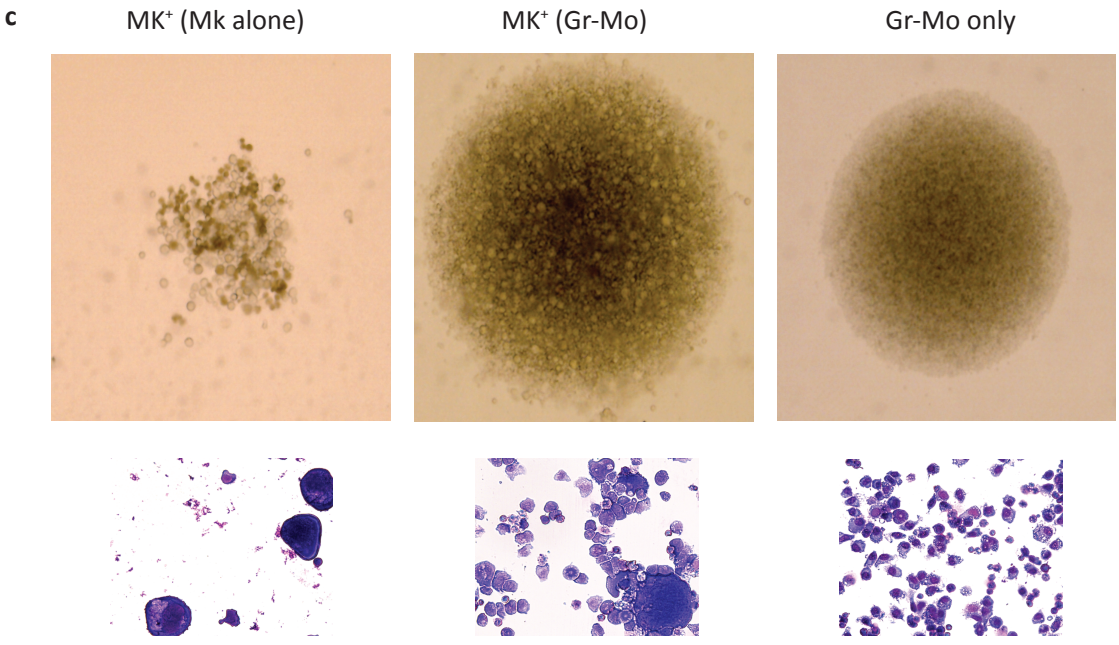
c
MK+ (Mk alone)
MK+ (Gr-Mo)
Gr-Mo only

Figure S5 | Gating strategy for LT-HSC and MPP2 identification by flow cytometry. (a) Representative gating strategy for the identification of WT and $He^{-/-}$ LT-HSC, ST-HSC, MPP and MPP2. **(b)** Representative flow cytometry histogram depicting the CD41 levels in LT-HSC, MPP2, ST-HSC and MPP. CD41 positive cells were defined using WT MPP as negative reference. **(c)** Top - Representative pictures of megakaryocyte-containing colonies (Mk^+): MK^+ only (left) and Mk^+ + Gr-Mo cells, middle) and a "granulocyte-monocyte only" colony (Gr-Mo only, right). Bottom - MGG staining of the upper described colonies.

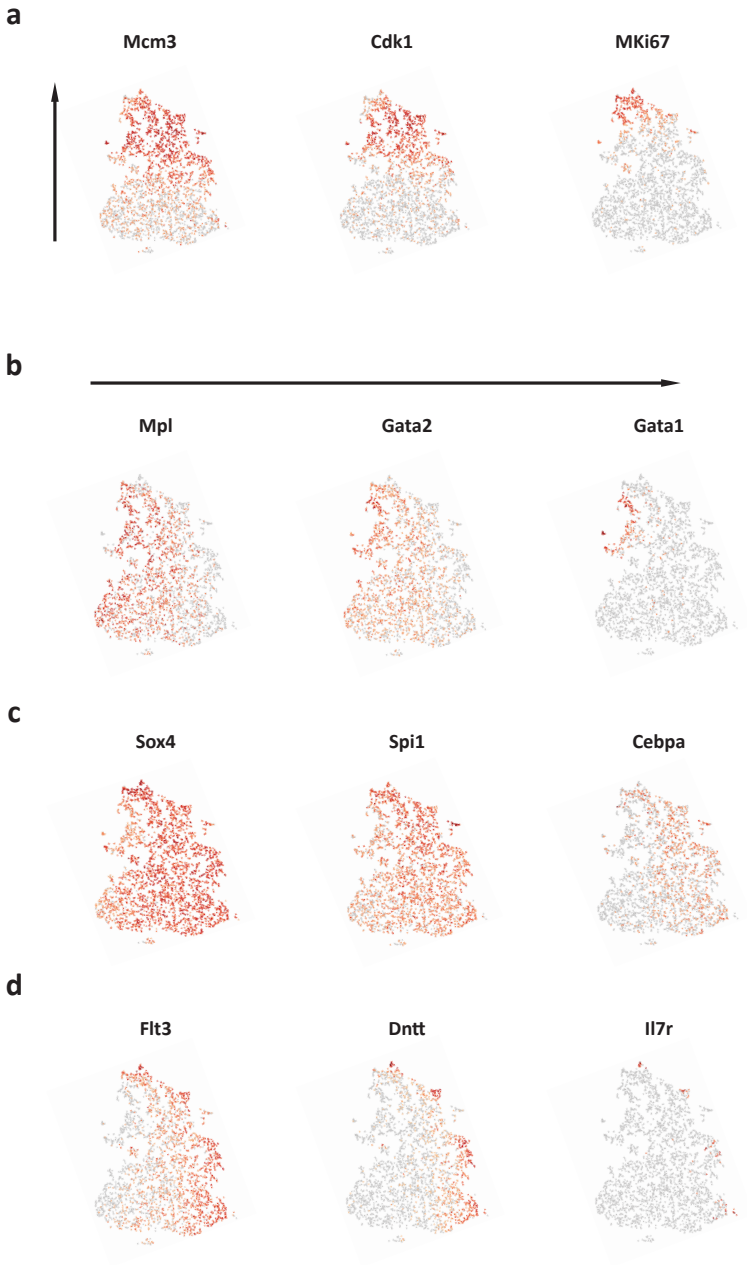

Figure S6 | Expression pattern of selected genes within single HSPC.
(a) Mcm3, Cdk1 and Mki67 expressing cells (orange) within the t-SNE plot. **(b)** HSC-MPP2 specific genes Mpl, Gata2 and Gata1 and their expression patterns (orange) within the t-SNE plot. **(c)** MPP3 and MPP4 specific genes Sox4, Spi1 and Cebpα and their expression pattern (orange) within the t-SNE plot. **(d)** MPP4 specific genes Flt3, Dntt and Il7r and their expression pattern (orange) within the t-SNE plot.

DISCUSSION

Helios is differentially expressed across hematopoietic populations

During our investigation, we evaluated Helios protein levels in several BM cell populations. We observed that Helios is almost absent in non-hematopoietic $CD45^-$ cells, as well as in mature B, myeloid and erythroid cells, most likely excluding a Helios extra hematopoietic and mature cell-related role (exception made for Treg cells). As expected, we detected Helios proteins in HSPC and, surprisingly, also in committed progenitor cells (e.g. GMP, MEP and CLP) where low mRNA levels were detected by transcriptomic analysis (**Fig. 13a**). These data may suggest that Helios regulation at the post-transcriptional levels is highly exploited by progenitors that, in turn, need to compensate for their low rate of transcription. In addition, another interesting aspect concerns the fact that Helios levels do not completely correlate with the amplitude of its knockout phenotype: the more affected HSC have less Helios expression, with respect to some committed progenitors (e.g. GMP), that showed a milder and delayed phenotype (as better discussed in the following paragraph). One possible reason behind this Helios level/function discrepancy might be that Helios production within progenitor cells does not translate into a functional output, or perhaps its loss can be partially compensated by other highly homologous Ikaros members. Alternatively, Helios activity and its ability to bind DNA may be uncoupled from its expression level, depicting a scenario in which cells with lower Helios expression may “paradoxically” benefit of an augmented capacity of Helios to bind DNA and regulate a broader spectrum of gene array. Such kind of behavior may result from post-transcriptional modifications that can affect Helios nuclear localization (as described for Ikaros (Song et al., 2011; Uckun et al., 2012)) or rather its dimerization efficiency.

Remarkably, we also found Helios to be down-regulated specifically in LT-HSC and MkP during the aging process, suggesting the existence of an age-dependent pathway able to modulate Helios expression. We envision that such pathway could work at the epigenetic or transcriptional level, as in aged LT-HSC Helios promoter becomes hyper-methylated and its mRNA is reduced (**Fig 13b**) (Grover et al., 2016; Sun et al., 2014). In such view, it would be extremely useful to further characterize the aging input able to affect Helios expression. We hypothesize that DNA damage,

oxidative stress or chronic inflammation could be important aging-related stimuli able to cause Helios repression. In line with this hypothesis, we are currently planning to test the contribution of such stimuli on Helios mRNA and protein expression, using either *in vivo* or *ex vivo* approaches (e.g. by directly exposing mice or purified LT-HSC to agents able to trigger inflammation or stimulate the DNA damage response).

a)

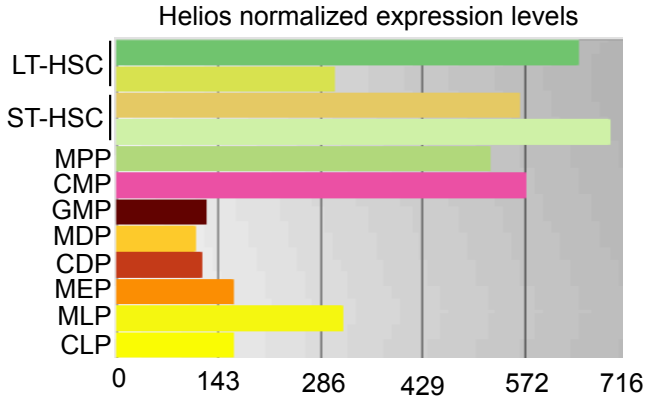

b)

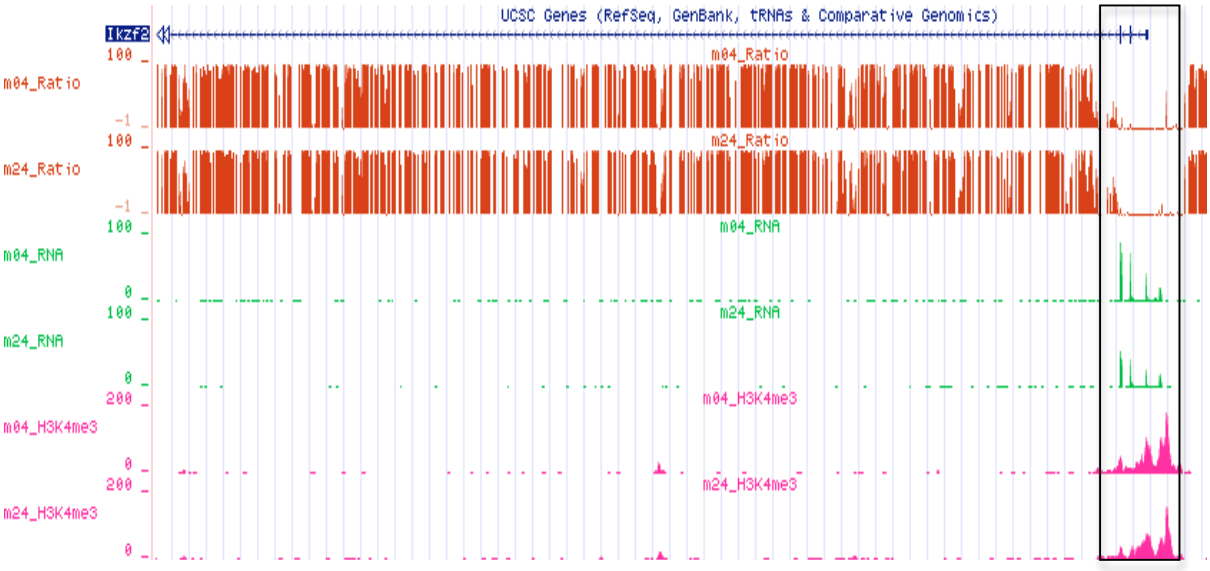

Fig. 13 | Helios expression and regulation
(**a**) IKZF2 normalized mRNA expression across different hematopoietic progenitor populations (microarray data from ImmGen). Two LT- and ST-HSC gating strategies were used to identify such cells. (**b**) UCSC Genome browser view of the IKZF2 gene body (blue). The boxed area highlights IKZF2 promoter. Features associated with IKZF2 gene body are shown in color: purple tracks show the methylation profile within the IKZF2 gene body in young (m04) and old (m24) LT-HSC; green tracks indicate the IKZF2 mRNA levels in young (m04) and old (m24) LT-HSC; pink

tracks refer to the H3k4me3 levels within IKZF2 gene body in young (m04) and old (m24) LT-HSC (Sun et al., 2014).

Helios deletion affects mainly HSPC

While we would tend to exclude a Helios involvement in mature hematopoietic cell biology (exception made for Treg cells, which will be proper discussed in the following paragraph), we only have indirect suggestions supporting Helios dispensability within the more committed progenitor populations. We observed that in the absence of Helios the abundance of both GMP and MkP progenitors looks overall affected during mouse growth, especially towards the adult stages (from 10 to 20 weeks of age; **Fig. 2, 3**). On the contrary, MPP3 and megakaryocyte-biased HSC and MPP2 augmentation occurs earlier, already at the first investigated time point (6-week-old mice), with a rather homogeneous and larger increase (**Fig. 4, 5**). Altogether, these findings lead us to hypothesize that the Helios-dependent MkP and GMP augmentation could be caused by upstream MPP3 and LT-HSC alterations. In such view, $He^{-/-}$ biased HSC and MPP would be the first affected population that, in turn, will favor the MkP and GMP accumulation. However, the reasons behind the gradual GMP and MkP accumulation are still obscure: indeed, if HSC and MPP are early biased, it is expected also that they generate a biased progeny from early on. The fact that this is mainly not observed at the early stage could be explained by other mechanisms (maybe related to the BM microenvironment), perhaps responsible for an initial compensation that, however, cannot last for long time. Interestingly, Ergen and colleagues found that a young BM microenvironment does not support myeloid differentiation as efficiently as an old microenvironment (Ergen et al., 2012). These findings may explain why GMP and MkP accumulate later in $He^{-/-}$ mice: the MkP and GMP “niches” may be saturated in young mice, while older BM may have increased tolerance for a surplus of myeloid progenitor production.

On the other hand, $He^{-/-}$ committed lymphoid progenitors are affected already in 6-week-old mice, although also in this case their decrease is preceded by an upstream MPP4 reduction (**Fig. 2, 4**). Thus, once again, the committed progenitor phenotype is preceded by alterations within the upstream HSPC compartment,

further supporting that the root of the phenotype must reside at the top of the hierarchy, with the only difference that the early lymphoid progenitor reduction cannot be compensated.

It should be noted that, although these data support a Helios specific HSPC role, we still cannot rule out Helios function within committed progenitors. Some indirect corroborations to this view come from our transcriptomic data, where we found that Helios deletion mainly affects quiescent HSPC (**Fig. 11, 12**), without interfering with the group of more proliferating HSPC. Thus, these data not only confirm the importance of Helios within the HSPC population, but also restrict Helios function to a smaller target HSPC pool. Despite we did not directly analyzed committed progenitors using mRNA sequencing, we think that an eventual Helios role in such compartment is quite unlikely. Indeed, we would expect that the committed and proliferative GMP, MkP and CLP progenitors would behave more similarly to the more proliferative and marginally affected $He^{-/-}$ HSPC, with respect to the highly perturbed quiescent HSPC.

Some more additional hints come from our *in vitro* CFU assay, where we found more myeloid and megakaryocyte CFU cells by plating $He^{-/-}$ BM, with respect to WT bone (starting from 10 weeks of age; **Fig. 2e, 3e**). Importantly, the numerous colonies were all characterized by similar size, suggesting, once again, a model in which Helios mainly acts by shaping the CFU cell composition (progenitors), rather than affecting downstream progenitor proliferation and self-renewal. Indeed, if Helios would act on GMP self-renewal, we would expect to see not only more myeloid CFU cells but also larger and dense colonies.

Helios acts in a HSPC intrinsic way

It was already shown that Helios is abundantly expressed by Treg cells, where it provides support to their suppressive function (Kim et al., 2015; Sebastian et al., 2016). In the present study, we observed that Helios CD4 conditional deletion does not seem to affect HSC and their megakaryocyte phenotypes. However, we found that MPP4 were reduced in half of the cases (**Fig. 7m**). Interestingly, this MPP4 reduction correlates with increased INFγ production. Based on this, we suggested that Helios deficient $FoxP3^{+}$ Treg cells suppress less efficiently BM T cell mediated inflammation that, in turn, indirectly triggers lymphoid progenitor reduction (similarly

to what is described in (Pierini et al., 2017). Importantly, this phenotype is not 100% penetrant, implying that Helios function is also T cell independent.

A further confirmation that lymphoid restriction exists independently on Helios T cell function came from the competitive BM transplantation assay. In such case, only $He^{-/-}$ donor cells have a defective lymphoid repopulation capability, in contrast to the co-hosted competitors (**Fig. 8,e,f**). This result showed in an indirect way that Helios HSPC phenotype is not triggered by any mature cell (e.g. T cell) defect, as otherwise also competitor HSPC would be equally perturbed. In addition, by transplanting WT and $He^{-/-}$ LT-HSC, we showed that Helios function is most probably hematopoietic cell intrinsic, as the WT host environment did not rescue the lymphoid differentiation defect (**Fig. 8c**). Notably, we cannot exclude that transplanted LT-HSC at the moment of the transplantation were already irreversibly converted to a myeloid biased state, for example by endogenous unknown stimuli. However, we would tend to exclude such possibility as: *i)* Helios expression is not detected in extra hematopoietic BM cells and *ii)* unlikely an eventual systemic defect is going to selectively affect only quiescent HSPC, without affecting other cell types of the system (even very similar cell-like active MPP).

In conclusion, these results support a scenario where Helios acts in a hematopoietic intrinsic way. Moreover, considering the Helios expression pattern, together with its knockout phenotype and transcriptome profile, we can assume that most probably Helios TF acts intrinsically on HSPC.

Helios regulates a small pool of quiescent HSPC

Total mRNA-seq analysis on LT-HSC, MPP3 and MPP4 showed that the more severally affected $He^{-/-}$ population is represented by the LT-HSC (**Fig. 9a,b**). Only smaller changes, in terms of number of affected genes and mRNA fold changes, were observed between WT and $He^{-/-}$ MPP3 and MPP4. In parallel, scRNA-seq analysis highlighted that the $He^{-/-}$ LSK compartment is mainly affected at the level of quiescent HSC and MPP (**Fig. 11, 12**). Moreover, by combining both single cell and bulk RNA-seq experiments, we found enrichment in cells expressing myeloid and megakaryocyte genes (e.g. Gata2 and Mpl) and depletion in cells expressing typical lymphoid markers (e.g. Flt3 and Dntt; **Fig. 11, 12**). However, a question remains unanswered: why is only a pool of HSPC affected by Helios deletion? We might

hypothesize that proliferative MPP may not require Helios anymore because other Ikaros dimers (e.g. Ikaros-Ikaros or Ikaros-Aiolos) could take over the Helios function. Alternatively, Helios deletion may be better compensated in proliferative HSPC (perhaps due to higher expression of Ikaros), while less efficiently in the quiescent ones.

What is the Helios contribution to the physiological hematopoietic aging?

As just mentioned, $He^{-/-}$ LT-HSC represent the most affected population at the transcriptional level, suggesting that they might be the main players of our phenotype. However, can Helios bias the hematopoietic system in an age-related manner, by acting only in LT-HSC? We envision 3 possible scenarios, taking into account that LT-HSC more likely poorly contribute to steady state hematopoiesis (Rodriguez-Fraticelli et al., 2018) and, in transplantation assays, drive hematopoietic aging in a dominant manner bypassing the nature of the environment (e.g. young LT-HSC generate a “young-like” hematopoietic system in the context of an old recipient mouse and vice-versa) (Ergen et al., 2012; Rossi et al., 2005).

1) Old LT-HSC unlikely give rise to an old biased system

In a first model, we propose a Helios LT-HSC direct role and we imagine that, during physiological aging, LT-HSC down-regulate Helios expression and acquire the classic aging phenotype. In such scenario, LT-HSC would unlikely be able to directly give rise to a mature myeloid biased compartment at the steady state (in contrast to a transplantation context). Their hematopoietic contribution would be minimal, exception made for the megakaryocyte compartment, which is the only one highly renewed by LT-HSC (Rodriguez-Fraticelli et al., 2018). In this logic, Helios role during aging would be marginal and mainly relegated to the megakaryocyte lineage. On the contrary, global hematopoietic changes would be mostly explained by a Helios independent role.

2) Old LT-HSC can indirectly generate an old biased system

If old LT-HSC alone are unlikely going to generate a biased hematopoietic system, we can imagine an alternative scenario where old LT-HSC drive hematopoietic aging by indirectly affecting the downstream MPP compartment (that

more prominently contribute to steady state hematopoiesis (Rodriguez-Fraticelli et al., 2018). In such view, upon acquisition of the characteristic old phenotype triggered by Helios down-regulation, LT-HSC may start to affect the neighbor niche and MPP cells. Following this logic, old LT-HSC might not directly give rise to a biased progeny but rather bias a preexisting MPP compartment through indirect means.

However, how do LT-HSC become able to affect adjacent cells? Some clues may come from carefully observing the old LT-HSC transcriptome profile. Indeed, old LT-HSC (but also $He^{-/-}$ LT-HSC) acquire a characteristic platelet-like pro-inflammatory phenotype (**Fig. 8c,f**) and, similar to inflammatory platelets, LT-HSC may become able to recruit granulocytes and dendritic cells (as well as the platelets themselves), in part by overexpressing proteins like VWF and SELP (Grover et al., 2016; Morrell et al., 2014). DC and granulocyte recruitment may finally lead to a LT-HSC localized inflammation reaction, potentially able to reach and bias the adjacent MPP compartment (Pietras, 2017). Such eventual “dominant negative” LT-HSC effect may be for example addressed by their selective removal. Using for instance anti-CD41 or anti-CD150 antibody-mediated saporin delivery, we could trigger LT-HSC apoptosis and assess whether their removal can rejuvenate the MPP compartment (Czechowicz et al., 2019).

3) HSC and MPP together can give rise to an old hematopoietic system

In a third model, we hypothesize a Helios “extended” MPP role, assuming that hematopoietic aging is promoted by Helios down-regulation on both HSC and also MPP. We imagine a scenario where Helios is able to directly up-regulate genes important for the MPP4 lymphoid identity and repress “megakaryocyte lineage” genes important for HSC, MPP2 and partial MPP3 specification. Helios would be thus required by both HSC and MPP (most probably the quiescent MPP), in order to: *i)* maintain active the lymphoid genes while shutting down the megakaryocyte transcripts within MPP4, and *ii)* decrease "megakaryocyte-like” gene expression while favoring the beginning of a lymphoid priming within HSC.

However, the statement of such hypothesis clashes with the experimental evidence that $He^{-/-}$ MPP are only modestly affected at the transcriptional level (**Fig. 9a,b**). Therefore, how can this model, that postulates a Helios direct role in HSC but also MPP aging, fit with our results? Such apparent paradox can be explained taking into consideration that we may have underestimated Helios function within MPP. Two

main mechanisms or “effects” can properly illustrate the reasons behind a transcriptional underestimation of Helios role within MPP: “dilution effect” and “LSK shift effect”.

For the first mechanism, it is important to notice that not all MPP3 and MPP4 cells are touched by Helios deletion. For instance, Helios removal seems to mainly affect a limited subset of quiescent MPP, while proliferating MPP look overall unperturbed (**Fig. 11, 12**). Therefore, differential gene expression analysis between WT and $He^{-/-}$ MPP3 and MPP4 may suffer from a “dilution effect”, given that unaffected proliferating MPP3 and MPP4 would mask transcriptional changes occurring within the quiescent MPP (**Fig. 14a**), thus contributing to wrong or rather inaccurate interpretations of Helios cellular function.

For the second mechanism, that I called “LSK shift effect”, we have to postulate that Helios directly up-regulates lymphoid genes necessary for the MPP4 identity and down-regulates megakaryocyte signatures important for HSC, MPP2 and MPP3 specification. In such scenario, Helios depletion in MPP4 would cause down-regulation of their lymphoid genes and, in parallel, up-regulation of megakaryocyte transcripts, conferring to MPP4 a novel “shifted” identity, which is more similar to that of MPP3, or eventually HSC. The same logic can be applied to the next cellular pool: up-regulation of megakaryocyte-like signatures triggered by Helios ablation in MPP3 would make them, in turn, more similar to HSC and divergent from MPP4. This shift effect then continues until the last upstream population, the LT-HSC (**Fig. 14b**): $He^{-/-}$ LT-HSC would acquire the most extreme megakaryocyte potential (with the lowest lymphoid one) and thus, when comparing them to WT LT-HSC, we will be able to recover only there the entire Helios effect, that cannot be masked anymore by a more upstream population (**Fig. 14b**).

Both these effects would help us to explain why we may have underestimated the Helios effect within the MPP pool. However, one problem remains: how does Helios affect MPP during aging, if its down-regulation only occurs within old LT-HSC and not in old MPP (**Fig. 1n**)? In line with the mentioned Helios dependent LSK shift effect, there might be the possibility for some of the old MPP (likely the quiescent ones) to shift identity towards a more megakaryocyte and less lymphoid phenotype upon Helios down-regulation, preventing us from measuring changes of Helios expression within MPP. In light of the described mechanisms, some credibility might be attributed also to the last described Helios dependent HSPC aging model.

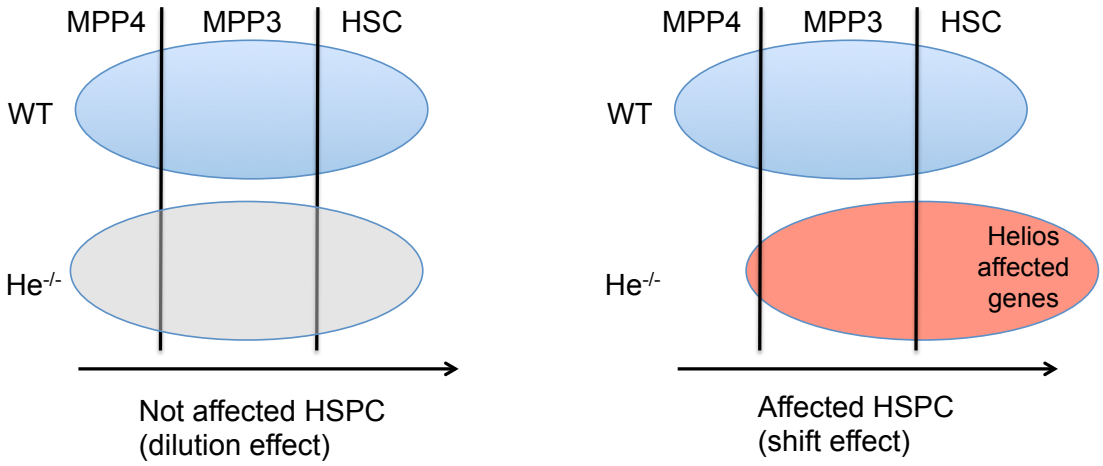

Fig. 14 | Dilution and LSK shift effects.
Schematic of WT and $He^{-/-}$ LSK pools. The vertical black lines define the borders between MPP4, MPP3 and HSC populations. The WT LSK compartment is represented in blue. On the left, the gray circle represents the unaffected $He^{-/-}$ LSK population ("dilution compartment"); on the right, the red circle shows the affected shifted $He^{-/-}$ LSK compartment.

The Helios targeted genes

The investigation of genes that are bound by Helios TF may help to gain further insights into whether Helios acts only in HSC or in both HSC and MPP. In other words, the identification of Helios binding sites would allow us to understand whether Helios binds only the regulated LT-HSC specific genes or also lymphoid MPP4 genes. However, it must be noted the existence of technical challenges underlying the research of HSPC Helios binding sites, as these cells are rare and only few techniques allow such investigation starting from low input material. Thus, we decided to set up the first Helios ChIP-seq experiments using cell line-based models as HSPC alternative systems.

We have preliminary results from two different hematopoietic cell lines: the HPC7 progenitor cell line and a second BH1 pre-B cell line generated in our laboratory (Heizmann et al., 2013). By using BH1 cells, Marie Celine Deau (PhD student in our team) identified several thousand Helios binding sites including HSC megakaryocyte genes and MPP4 lymphoid specific genes. On the contrary, using the HPC7 cell line (which resembles a mixture of LK and LSK $CD48^{+}$ cells) we did not recover the same binding profile. Indeed, Helios targets relatively few genes (~200), many of which are related to neither megakaryocyte nor lymphoid function (data not

shown). In BH1 cells, we recovered a more predictable Helios binding profile, although the cell line should be far from LSK cells. On the other hand, while HPC7 should be "closer" to LSK cells, the Helios binding profile weakly correlates with our transcriptomic data.

In order to more comprehensively access the Helios binding profile enigma, we planned to look at other cell systems. One strategy that we are going to adopt is based on LT-HSC (and also MPP) *in vitro* expansion (Wilkinson et al., 2019). Hopefully, this strategy will provide us the closest model with respect to the *in vivo* counterpart. Alternatively, we are currently searching for low input ChIP-seq like methods able to detect TF binding on freshly isolated LSK.

We already tried the newly described Cut and Run (CεR) and Cut and Tag (CεT) protocols, but unfortunately these techniques worked efficiently in my hands only on histone modifications (e.g. H3k27me3, H3k4me1), while CεR/T performed on Helios TF never gave the expected enrichment over the isotope control antibody (Kaya-Okur et al., 2019; Skene and Henikoff, 2017). For this reason, we have been trying to apply other low input methodologies such as ChIP-mentation and CHIL-seq, that may be more appropriate to match our goal as they both include a cross-link step that should favor the stabilization of TF-DNA interaction (Harada et al., 2019; Schmidl et al., 2015).

FINAL CONSIDERATIONS

The HSPC TF networks

Several TFs have been so far identified as critical hematopoietic lineage regulators. Among them, we can define: *i)* "*peripheral* TFs" that act on already committed progenitors, where they reinforce lineage-specific decisions while repressing alternative fates. Examples of such factors are Gata1, Cebpα and Pax5 (Dahl et al., 2003; Dore and Crispino, 2011; Paul et al., 2016). On the other hand, we can find *ii)* "*HSPC* TFs" dedicated to control the lineage-priming of multipotent HSC and MPP. Some examples of early hematopoietic TFs are represented by Gata2, Spi1 and Ikaros (Huang et al., 2009; Menendez-Gonzalez et al., 2019). Interestingly, two main antagonistic networks seem to exist within the HSPC population: a Gata2-

related network for the activation of pan-myeloid genes (Huang et al., 2009; Menendez-Gonzalez et al., 2019) and an Ikaros-Spi1 network important for lymphoid gene priming and pan-myeloid program repression (Pang et al., 2018; Yoshida et al., 2006). In such context, our study proposed Helios as a novel "*HSPC specific* TF" and collocated its function within the Ikaros and Spi1 network. As such, it is possible that these TFs may collaborate together in order to coordinate the expression of common gene batteries. Interestingly, all the three factors bind to a very similar 'GGAA' DNA motif, suggesting that their synergistic roles might be even mediated by protein-protein interaction. Notably, as mentioned in the introduction, Helios and Ikaros are indeed well described partners (while their interaction with Spi1 has not been validated yet); therefore, it does not surprise that they may possess similar, overlapping and maybe redundant roles.

In this context, it would be interesting to understand the nature of this family member cooperation. Starting from the observation that Helios and Aiolos possess a restricted pattern of expression, while Ikaros is broadly expressed across several lineages, we tried to hypothesize two scenarios: 1) Helios, Aiolos and Ikaros play similar roles and their "split" pattern of expression may serve to confer robustness to the system at particular (and maybe critical) stages of the hematopoietic development. Alternatively, 2) Helios and Aiolos may represent the Ikaros "regulatory partners" and, in such scenario, they may serve to turn on/off Ikaros activity in a spatio-temporal regulated manner. However, it is also important to notice that Ikaros role within the HSPC population was identified several years ago, when HSPC cells were not functionally characterized as they are nowadays. For this reason, an updated characterization of Ikaros function would be important in order to understand whether Helios and Ikaros have overlapping roles or rather they regulate different HSPC populations.

Single cell mRNA-seq considerations

The HSPC single cell mRNA sequencing allowed us to visualize, to a large scale, the molecular heterogeneity within HSC and MPP populations. We identified a continuum gradient of differentiation: the more extreme lineages are represented by HSC-MPP2 and MPP4, while in the middle there are MPP3 that possess both HSC-MPP2 and MPP4 features (**Fig. 11, 12**). Surprisingly, we discovered a pool of stem

cell-like quiescent MPP that we hypothesized may represent the more apical progenitors.

We speculate that HSC may give rise to MPP3 and MPP4 at the beginning of BM ontogenesis. Once the HSPC system is established, quiescent HSC are co-opted as long-lived megakaryocyte progenitors (a sort of upstream MPP2), quiescent MPP3 as myeloid precursors and quiescent MPP4 as permanent lymphoid mature cell source. This would in part explain why LT-HSC mainly acts as megakaryocyte progenitors at the steady state, while they poorly contribute to either MPP or mature cell renew (with the exception of megakaryocytes). We further speculate that the proliferating HSPC pool may represent a second layer of progenitors more prone to differentiate and less able to renew themselves.

Is Helios dispensable for HSPC differentiation?

A recent publication from the group of Kharas examined the role of Helios within HSPC and leukemic stem cells by using VAV-Cre conditional Helios knockout mice (He^{cKO}). In contrast to our findings, they concluded Helios to be dispensable for steady state hematopoiesis, while its deletion would only be crucial for leukemic stem cell self-renewal (Park et al., 2019). However, this apparent inconsistency between our and their conclusions can be understood and explained. Indeed, Park and colleagues restricted their analysis to only He^{cKO} 7-week-old mice and investigated exclusively their GMP, CMP, MEP, LSK and MPP (total MPP without MPP2-4) populations, all cell types that we also did not find affected in 6-week-old $He^{-/-}$ mice. On the contrary, they did not look at the $He^{-/-}$ BM populations that we described as the most affected, such as $CD41^{+}$ HSC, MPP2-MPP4, CLP and MkP. Similarly to us, they observed a mature B cell reduction within the BM of He^{cKO} mice, however their data did not reach statistical significance probably because of high mouse-to-mouse B cell variability and the minimal numbers of analyzed samples (n=4). On the contrary, we analyzed more mice (n=7) and, despite the B cell mouse-to-mouse variability, that we noticed is higher in 6-week-old mice with respect to 10-20-week-old mice (**Fig. 2a**), we managed to obtain significant results. Additionally, they performed non-competitive BM transplantation assays without finding any difference between WT and He^{cKO} blood lineages reconstitution. Notably, it is important to consider how they analyzed the results. For instance, when they measured B cell

reconstitution (but this is also true for the myeloid one), they looked at the % of donor positive cells within the pool of total B220 cells; however, given that the mouse was composed mainly (if not only) by donor cells, they always recovered around 90% of donor chimerism in both WT and He^{cKO} condition. This type of set-up most probably did not allow them to properly quantify the real lymphoid lineage potential of the He^{cKO} HSPC.

In conclusion, in my opinion our and their results are not dissimilar and the main differences reside in both the analyzed populations and the experimental set-up of the BM reconstitution assay. Moreover, we cannot exclude that their He^{cKO} model could be partially different from our $He^{-/-}$ model (although the Helios deletions are very similar); however, given that our analyses differ from each other, we cannot neither exclude nor refute this possibility.

REFERENCES

Adan, A., Alizada, G., Kiraz, Y., Baran, Y., and Nalbant, A. (2017). Flow cytometry: basic principles and applications. Crit Rev Biotechnol *37*, 163-176.

Akashi, K., Traver, D., Miyamoto, T., and Weissman, I.L. (2000). A clonogenic common myeloid progenitor that gives rise to all myeloid lineages. Nature *404*, 193-197.

Akuthota, P., Wang, H., and Weller, P.F. (2010). Eosinophils as antigen-presenting cells in allergic upper airway disease. Curr Opin Allergy Clin Immunol *10*, 14-19.

Alam, M.Z., Devalaraja, S., and Haldar, M. (2017). The Heme Connection: Linking Erythrocytes and Macrophage Biology. Front Immunol *8*, 33.

Alver, B.H., Kim, K.H., Lu, P., Wang, X., Manchester, H.E., Wang, W., Haswell, J.R., Park, P.J., and Roberts, C.W. (2017). The SWI/SNF chromatin remodelling complex is required for maintenance of lineage specific enhancers. Nat Commun *8*, 14648.

Ambrosi, T.H., Scialdone, A., Graja, A., Gohlke, S., Jank, A.M., Bocian, C., Woelk, L., Fan, H., Logan, D.W., Schurmann, A.*, et al.* (2017). Adipocyte Accumulation in the Bone Marrow during Obesity and Aging Impairs Stem Cell-Based Hematopoietic and Bone Regeneration. Cell Stem Cell *20*, 771-784 e776.

Antonchuk, J., Sauvageau, G., and Humphries, R.K. (2002). HOXB4-induced expansion of adult hematopoietic stem cells ex vivo. Cell *109*, 39-45.

Asada, N., Kunisaki, Y., Pierce, H., Wang, Z., Fernandez, N.F., Birbrair, A., Ma'ayan, A., and Frenette, P.S. (2017). Differential cytokine contributions of perivascular haematopoietic stem cell niches. Nat Cell Biol *19*, 214-223.

Beerman, I., Seita, J., Inlay, M.A., Weissman, I.L., and Rossi, D.J. (2014). Quiescent hematopoietic stem cells accumulate DNA damage during aging that is repaired upon entry into cell cycle. Cell Stem Cell *15*, 37-50.

Bendall, S.C., Simonds, E.F., Qiu, P., Amir el, A.D., Krutzik, P.O., Finck, R., Bruggner, R.V., Melamed, R., Trejo, A., Ornatsky, O.I.*, et al.* (2011). Single-cell mass cytometry of differential immune and drug responses across a human hematopoietic continuum. Science *332*, 687-696.

Bernitz, J.M., Kim, H.S., MacArthur, B., Sieburg, H., and Moore, K. (2016). Hematopoietic Stem Cells Count and Remember Self-Renewal Divisions. Cell *167*, 1296-1309 e1210.

Bornelov, S., Reynolds, N., Xenophontos, M., Gharbi, S., Johnstone, E., Floyd, R., Ralser, M., Signolet, J., Loos, R., Dietmann, S.*, et al.* (2018). The Nucleosome Remodeling and Deacetylation Complex Modulates Chromatin Structure at Sites of Active Transcription to Fine-Tune Gene Expression. Mol Cell *71*, 56-72 e54.

Bossen, C., Murre, C.S., Chang, A.N., Mansson, R., Rodewald, H.R., and Murre, C. (2015). The chromatin remodeler Brg1 activates enhancer repertoires to establish B cell identity and modulate cell growth. Nat Immunol *16*, 775-784.

Boyer, S.W., Rajendiran, S., Beaudin, A.E., Smith-Berdan, S., Muthuswamy, P.K., Perez-Cunningham, J., Martin, E.W., Cheung, C., Tsang, H., Landon, M.*, et al.* (2019). Clonal and Quantitative In Vivo Assessment of Hematopoietic Stem Cell Differentiation Reveals Strong Erythroid Potential of Multipotent Cells. Stem Cell Reports *12*, 801-815.

Bruns, I., Lucas, D., Pinho, S., Ahmed, J., Lambert, M.P., Kunisaki, Y., Scheiermann, C., Schiff, L., Poncz, M., Bergman, A.*, et al.* (2014). Megakaryocytes regulate hematopoietic stem cell quiescence through CXCL4 secretion. Nat Med *20*, 1315-1320.

Burzyn, D., Benoist, C., and Mathis, D. (2013). Regulatory T cells in nonlymphoid tissues. Nat Immunol *14*, 1007-1013.

Busch, K., Klapproth, K., Barile, M., Flossdorf, M., Holland-Letz, T., Schlenner, S.M., Reth, M., Hofer, T., and Rodewald, H.R. (2015). Fundamental properties of unperturbed haematopoiesis from stem cells in vivo. Nature *518*, 542-546.

Butler, A., Hoffman, P., Smibert, P., Papalexi, E., and Satija, R. (2018). Integrating single-cell transcriptomic data across different conditions, technologies, and species. Nat Biotechnol *36*, 411-420.

Cai, Q., Dierich, A., Oulad-Abdelghani, M., Chan, S., and Kastner, P. (2009). Helios deficiency has minimal impact on T cell development and function. J Immunol *183*, 2303-2311.

Carrelha, J., Meng, Y., Kettyle, L.M., Luis, T.C., Norfo, R., Alcolea, V., Boukarabila, H., Grasso, F., Gambardella, A., Grover, A.*, et al.* (2018). Hierarchically related lineage-restricted fates of multipotent haematopoietic stem cells. Nature *554*, 106-111.

Chang, J., Wang, Y., Shao, L., Laberge, R.M., Demaria, M., Campisi, J., Janakiraman, K., Sharpless, N.E., Ding, S., Feng, W.*, et al.* (2016). Clearance of senescent cells by ABT263 rejuvenates aged hematopoietic stem cells in mice. Nat Med *22*, 78-83.

Chapple, R.H., Tseng, Y.J., Hu, T., Kitano, A., Takeichi, M., Hoegenauer, K.A., and Nakada, D. (2018). Lineage tracing of murine adult hematopoietic stem cells reveals active contribution to steady-state hematopoiesis. Blood Adv *2*, 1220-1228.

Chirumbolo, S. (2012). State-of-the-art review about basophil research in immunology and allergy: is the time right to treat these cells with the respect they deserve? Blood Transfus *10*, 148-164.

Chow, A., Lucas, D., Hidalgo, A., Mendez-Ferrer, S., Hashimoto, D., Scheiermann, C., Battista, M., Leboeuf, M., Prophete, C., van Rooijen, N.*, et al.* (2011). Bone marrow CD169+ macrophages promote the retention of hematopoietic stem and progenitor cells in the mesenchymal stem cell niche. J Exp Med *208*, 261-271.

Cordeiro Gomes, A., Hara, T., Lim, V.Y., Herndler-Brandstetter, D., Nevius, E., Sugiyama, T., Tani-Ichi, S., Schlenner, S., Richie, E., Rodewald, H.R.*, et al.* (2016). Hematopoietic Stem Cell Niches Produce Lineage-Instructive Signals to Control Multipotent Progenitor Differentiation. Immunity *45*, 1219-1231.

Cossarizza, A., Chang, H.D., Radbruch, A., Akdis, M., Andra, I., Annunziato, F., Bacher, P., Barnaba, V., Battistini, L., Bauer, W.M.*, et al.* (2017). Guidelines for the use of flow cytometry and cell sorting in immunological studies. Eur J Immunol *47*, 1584-1797.

Czechowicz, A., Palchaudhuri, R., Scheck, A., Hu, Y., Hoggatt, J., Saez, B., Pang, W.W., Mansour, M.K., Tate, T.A., Chan, Y.Y.*, et al.* (2019). Selective hematopoietic stem cell ablation using CD117-antibody-drug-conjugates enables safe and effective transplantation with immunity preservation. Nat Commun *10*, 617.

Dahl, R., Walsh, J.C., Lancki, D., Laslo, P., Iyer, S.R., Singh, H., and Simon, M.C. (2003). Regulation of macrophage and neutrophil cell fates by the PU.1:C/EBPalpha ratio and granulocyte colony-stimulating factor. Nat Immunol *4*, 1029-1036.

Darzynkiewicz, Z., Halicka, H.D., and Zhao, H. (2010). Analysis of cellular DNA content by flow and laser scanning cytometry. Adv Exp Med Biol *676*, 137-147.

Dore, L.C., and Crispino, J.D. (2011). Transcription factor networks in erythroid cell and megakaryocyte development. Blood *118*, 231-239.

Drissen, R., Buza-Vidas, N., Woll, P., Thongjuea, S., Gambardella, A., Giustacchini, A., Mancini, E., Zriwil, A., Lutteropp, M., Grover, A.*, et al.* (2016). Distinct myeloid progenitor-differentiation pathways identified through single-cell RNA sequencing. Nat Immunol *17*, 666-676.

Dumortier, A., Jeannet, R., Kirstetter, P., Kleinmann, E., Sellars, M., dos Santos, N.R., Thibault, C., Barths, J., Ghysdael, J., Punt, J.A.*, et al.* (2006). Notch activation is an early and critical event during T-Cell leukemogenesis in Ikaros-deficient mice. Mol Cell Biol *26*, 209-220.

Eisenbarth, S.C. (2019). Dendritic cell subsets in T cell programming: location dictates function. Nat Rev Immunol *19*, 89-103.

Ergen, A.V., Boles, N.C., and Goodell, M.A. (2012). Rantes/Ccl5 influences hematopoietic stem cell subtypes and causes myeloid skewing. Blood *119*, 2500-2509.

Flach, J., Bakker, S.T., Mohrin, M., Conroy, P.C., Pietras, E.M., Reynaud, D., Alvarez, S., Diolaiti, M.E., Ugarte, F., Forsberg, E.C.*, et al.* (2014). Replication stress is a potent driver of functional decline in ageing haematopoietic stem cells. Nature *512*, 198-202.

Frascoli, M., Proietti, M., and Grassi, F. (2012). Phenotypic analysis and isolation of murine hematopoietic stem cells and lineage-committed progenitors. J Vis Exp.

Freitas, C., Wittner, M., Nguyen, J., Rondeau, V., Biajoux, V., Aknin, M.L., Gaudin, F., Beaussant-Cohen, S., Bertrand, Y., Bellanne-Chantelot, C.*, et al.* (2017).

Lymphoid differentiation of hematopoietic stem cells requires efficient Cxcr4 desensitization. J Exp Med *214*, 2023-2040.

Gekas, C., and Graf, T. (2013). CD41 expression marks myeloid-biased adult hematopoietic stem cells and increases with age. Blood *121*, 4463-4472.

Georgopoulos, K. (2017). The making of a lymphocyte: the choice among disparate cell fates and the IKAROS enigma. Genes Dev *31*, 439-450.

Ghaedi, M., Steer, C.A., Martinez-Gonzalez, I., Halim, T.Y.F., Abraham, N., and Takei, F. (2016). Common-Lymphoid-Progenitor-Independent Pathways of Innate and T Lymphocyte Development. Cell Rep *15*, 471-480.

Ghosn, E., Yoshimoto, M., Nakauchi, H., Weissman, I.L., and Herzenberg, L.A. (2019). Hematopoietic stem cell-independent hematopoiesis and the origins of innate-like B lymphocytes. Development *146*.

Golebiewska, E.M., and Poole, A.W. (2015). Platelet secretion: From haemostasis to wound healing and beyond. Blood Rev *29*, 153-162.

Grover, A., Mancini, E., Moore, S., Mead, A.J., Atkinson, D., Rasmussen, K.D., O'Carroll, D., Jacobsen, S.E., and Nerlov, C. (2014). Erythropoietin guides multipotent hematopoietic progenitor cells toward an erythroid fate. J Exp Med *211*, 181-188.

Grover, A., Sanjuan-Pla, A., Thongjuea, S., Carrelha, J., Giustacchini, A., Gambardella, A., Macaulay, I., Mancini, E., Luis, T.C., Mead, A.*, et al.* (2016). Single-cell RNA sequencing reveals molecular and functional platelet bias of aged haematopoietic stem cells. Nat Commun *7*, 11075.

Haas, S., Hansson, J., Klimmeck, D., Loeffler, D., Velten, L., Uckelmann, H., Wurzer, S., Prendergast, A.M., Schnell, A., Hexel, K.*, et al.* (2015). Inflammation-Induced Emergency Megakaryopoiesis Driven by Hematopoietic Stem Cell-like Megakaryocyte Progenitors. Cell Stem Cell *17*, 422-434.

Harada, A., Maehara, K., Handa, T., Arimura, Y., Nogami, J., Hayashi-Takanaka, Y., Shirahige, K., Kurumizaka, H., Kimura, H., and Ohkawa, Y. (2019). A chromatin integration labelling method enables epigenomic profiling with lower input. Nat Cell Biol *21*, 287-296.

Heizmann, B., Kastner, P., and Chan, S. (2013). Ikaros is absolutely required for pre-B cell differentiation by attenuating IL-7 signals. J Exp Med *210*, 2823-2832.

Heizmann, B., Kastner, P., and Chan, S. (2018). The Ikaros family in lymphocyte development. Curr Opin Immunol *51*, 14-23.

Hirata, Y., Furuhashi, K., Ishii, H., Li, H.W., Pinho, S., Ding, L., Robson, S.C., Frenette, P.S., and Fujisaki, J. (2018). CD150(high) Bone Marrow Tregs Maintain Hematopoietic Stem Cell Quiescence and Immune Privilege via Adenosine. Cell Stem Cell *22*, 445-453 e445.

Hirayama, D., Iida, T., and Nakase, H. (2017). The Phagocytic Function of Macrophage-Enforcing Innate Immunity and Tissue Homeostasis. Int J Mol Sci *19*.

Ho, Y.H., Del Toro, R., Rivera-Torres, J., Rak, J., Korn, C., Garcia-Garcia, A., Macias, D., Gonzalez-Gomez, C., Del Monte, A., Wittner, M.*, et al.* (2019). Remodeling of Bone Marrow Hematopoietic Stem Cell Niches Promotes Myeloid Cell Expansion during Premature or Physiological Aging. Cell Stem Cell.

Hoppe, P.S., Schwarzfischer, M., Loeffler, D., Kokkaliaris, K.D., Hilsenbeck, O., Moritz, N., Endele, M., Filipczyk, A., Gambardella, A., Ahmed, N.*, et al.* (2016). Early myeloid lineage choice is not initiated by random PU.1 to GATA1 protein ratios. Nature *535*, 299-302.

Hu, Y., Zhang, Z., Kashiwagi, M., Yoshida, T., Joshi, I., Jena, N., Somasundaram, R., Emmanuel, A.O., Sigvardsson, M., Fitamant, J.*, et al.* (2016). Superenhancer reprogramming drives a B-cell-epithelial transition and high-risk leukemia. Genes Dev *30*, 1971-1990.

Huang, Z., Dore, L.C., Li, Z., Orkin, S.H., Feng, G., Lin, S., and Crispino, J.D. (2009). GATA-2 reinforces megakaryocyte development in the absence of GATA-1. Mol Cell Biol *29*, 5168-5180.

Hwang, B., Lee, J.H., and Bang, D. (2018). Single-cell RNA sequencing technologies and bioinformatics pipelines. Exp Mol Med *50*, 96.

Hyman, L.M., and Franz, K.J. (2012). Probing oxidative stress: Small molecule fluorescent sensors of metal ions, reactive oxygen species, and thiols. Coord Chem Rev *256*, 2333-2356.

Inlay, M.A., Bhattacharya, D., Sahoo, D., Serwold, T., Seita, J., Karsunky, H., Plevritis, S.K., Dill, D.L., and Weissman, I.L. (2009). Ly6d marks the earliest stage of B-cell specification and identifies the branchpoint between B-cell and T-cell development. Genes Dev *23*, 2376-2381.

Jiang, S., and Mortazavi, A. (2018). Integrating ChIP-seq with other functional genomics data. Brief Funct Genomics *17*, 104-115.

Joshi, I., Yoshida, T., Jena, N., Qi, X., Zhang, J., Van Etten, R.A., and Georgopoulos, K. (2014). Loss of Ikaros DNA-binding function confers integrin-dependent survival on pre-B cells and progression to acute lymphoblastic leukemia. Nat Immunol *15*, 294-304.

Karsunky, H., Inlay, M.A., Serwold, T., Bhattacharya, D., and Weissman, I.L. (2008). Flk2+ common lymphoid progenitors possess equivalent differentiation potential for the B and T lineages. Blood *111*, 5562-5570.

Kaya-Okur, H.S., Wu, S.J., Codomo, C.A., Pledger, E.S., Bryson, T.D., Henikoff, J.G., Ahmad, K., and Henikoff, S. (2019). CUT&Tag for efficient epigenomic profiling of small samples and single cells. Nat Commun *10*, 1930.

Kiel, M.J., Yilmaz, O.H., Iwashita, T., Yilmaz, O.H., Terhorst, C., and Morrison, S.J. (2005). SLAM family receptors distinguish hematopoietic stem and progenitor cells and reveal endothelial niches for stem cells. Cell *121*, 1109-1121.

Kim, H.J., Barnitz, R.A., Kreslavsky, T., Brown, F.D., Moffett, H., Lemieux, M.E., Kaygusuz, Y., Meissner, T., Holderried, T.A., Chan, S.*, et al.* (2015). Stable inhibitory activity of regulatory T cells requires the transcription factor Helios. Science *350*, 334-339.

Kim, J., Sif, S., Jones, B., Jackson, A., Koipally, J., Heller, E., Winandy, S., Viel, A., Sawyer, A., Ikeda, T.*, et al.* (1999). Ikaros DNA-binding proteins direct formation of chromatin remodeling complexes in lymphocytes. Immunity *10*, 345-355.

Kobayashi, M., Tarnawsky, S.P., Wei, H., Mishra, A., Azevedo Portilho, N., Wenzel, P., Davis, B., Wu, J., Hadland, B., and Yoshimoto, M. (2019). Hemogenic Endothelial Cells Can Transition to Hematopoietic Stem Cells through a B-1 Lymphocyte-Biased State during Maturation in the Mouse Embryo. Stem Cell Reports *13*, 21-30.

Koenderman, L., Buurman, W., and Daha, M.R. (2014). The innate immune response. Immunol Lett *162*, 95-102.

Kondo, M., Weissman, I.L., and Akashi, K. (1997). Identification of clonogenic common lymphoid progenitors in mouse bone marrow. Cell *91*, 661-672.

Krystel-Whittemore, M., Dileepan, K.N., and Wood, J.G. (2015). Mast Cell: A Multi-Functional Master Cell. Front Immunol *6*, 620.

Kunisaki, Y., Bruns, I., Scheiermann, C., Ahmed, J., Pinho, S., Zhang, D., Mizoguchi, T., Wei, Q., Lucas, D., Ito, K.*, et al.* (2013). Arteriolar niches maintain haematopoietic stem cell quiescence. Nature *502*, 637-643.

Kwarteng, E.O., and Heinonen, K.M. (2016). Competitive Transplants to Evaluate Hematopoietic Stem Cell Fitness. J Vis Exp.

Laugesen, A., Hojfeldt, J.W., and Helin, K. (2019). Molecular Mechanisms Directing PRC2 Recruitment and H3K27 Methylation. Mol Cell *74*, 8-18.

Lee, P.P., Fitzpatrick, D.R., Beard, C., Jessup, H.K., Lehar, S., Makar, K.W., Perez-Melgosa, M., Sweetser, M.T., Schlissel, M.S., Nguyen, S.*, et al.* (2001). A critical role for Dnmt1 and DNA methylation in T cell development, function, and survival. Immunity *15*, 763-774.

Li, R.H.L., and Tablin, F. (2018). A Comparative Review of Neutrophil Extracellular Traps in Sepsis. Front Vet Sci *5*, 291.

Li, X., and Zheng, Y. (2015). Regulatory T cell identity: formation and maintenance. Trends Immunol *36*, 344-353.

Liang, Z., Brown, K.E., Carroll, T., Taylor, B., Vidal, I.F., Hendrich, B., Rueda, D., Fisher, A.G., and Merkenschlager, M. (2017). A high-resolution map of transcriptional repression. Elife *6*.

Liu, P., Ge, Z., Lin, Z.K., Qian, S.X., Qiao, C., Zhang, J.F., Wu, Y.J., Qiu, H.R., Zhu, G.R., and Li, J.Y. (2012). [Expression characteristics of isoforms of Ikaros and Helios in patients with leukemia and their mechanism]. Zhongguo Shi Yan Xue Ye Xue Za Zhi *20*, 812-817.

Lovelace, P., and Maecker, H.T. (2011). Multiparameter intracellular cytokine staining. Methods Mol Biol *699*, 165-178.

Maeda, K., Baba, Y., Nagai, Y., Miyazaki, K., Malykhin, A., Nakamura, K., Kincade, P.W., Sakaguchi, N., and Coggeshall, K.M. (2005). IL-6 blocks a discrete early step in lymphopoiesis. Blood *106*, 879-885.

Mann, M., Mehta, A., de Boer, C.G., Kowalczyk, M.S., Lee, K., Haldeman, P., Rogel, N., Knecht, A.R., Farouq, D., Regev, A.*, et al.* (2018). Heterogeneous Responses of Hematopoietic Stem Cells to Inflammatory Stimuli Are Altered with Age. Cell Rep *25*, 2992-3005 e2995.

Maryanovich, M., Zahalka, A.H., Pierce, H., Pinho, S., Nakahara, F., Asada, N., Wei, Q., Wang, X., Ciero, P., Xu, J.*, et al.* (2018). Adrenergic nerve degeneration in bone marrow drives aging of the hematopoietic stem cell niche. Nat Med *24*, 782-791.

Mastio, J., Simand, C., Cova, G., Kastner, P., Chan, S., and Kirstetter, P. (2018). Ikaros cooperates with Notch activation and antagonizes TGFbeta signaling to promote pDC development. PLoS Genet *14*, e1007485.

Matatall, K.A., Shen, C.C., Challen, G.A., and King, K.Y. (2014). Type II interferon promotes differentiation of myeloid-biased hematopoietic stem cells. Stem Cells *32*, 3023-3030.

Mendez-Ferrer, S., Michurina, T.V., Ferraro, F., Mazloom, A.R., Macarthur, B.D., Lira, S.A., Scadden, D.T., Ma'ayan, A., Enikolopov, G.N., and Frenette, P.S. (2010). Mesenchymal and haematopoietic stem cells form a unique bone marrow niche. Nature *466*, 829-834.

Menendez-Gonzalez, J.B., Vukovic, M., Abdelfattah, A., Saleh, L., Almotiri, A., Thomas, L.A., Agirre-Lizaso, A., Azevedo, A., Menezes, A.C., Tornillo, G.*, et al.* (2019). Gata2 as a Crucial Regulator of Stem Cells in Adult Hematopoiesis and Acute Myeloid Leukemia. Stem Cell Reports *13*, 291-306.

Mirantes, C., Passegue, E., and Pietras, E.M. (2014). Pro-inflammatory cytokines: emerging players regulating HSC function in normal and diseased hematopoiesis. Exp Cell Res *329*, 248-254.

Mohrin, M., Bourke, E., Alexander, D., Warr, M.R., Barry-Holson, K., Le Beau, M.M., Morrison, C.G., and Passegue, E. (2010). Hematopoietic stem cell quiescence promotes error-prone DNA repair and mutagenesis. Cell Stem Cell *7*, 174-185.

Morita, Y., Ema, H., and Nakauchi, H. (2010). Heterogeneity and hierarchy within the most primitive hematopoietic stem cell compartment. J Exp Med *207*, 1173-1182.

Morrell, C.N., Aggrey, A.A., Chapman, L.M., and Modjeski, K.L. (2014). Emerging roles for platelets as immune and inflammatory cells. Blood *123*, 2759-2767.

Mortaz, E., Alipoor, S.D., Adcock, I.M., Mumby, S., and Koenderman, L. (2018). Update on Neutrophil Function in Severe Inflammation. Front Immunol *9*, 2171.

Nakamura-Ishizu, A., Matsumura, T., Stumpf, P.S., Umemoto, T., Takizawa, H., Takihara, Y., O'Neil, A., Majeed, A., MacArthur, B.D., and Suda, T. (2018). Thrombopoietin Metabolically Primes Hematopoietic Stem Cells to Megakaryocyte-Lineage Differentiation. Cell Rep *25*, 1772-1785 e1776.

Ng, S.Y., Yoshida, T., Zhang, J., and Georgopoulos, K. (2009). Genome-wide lineage-specific transcriptional networks underscore Ikaros-dependent lymphoid priming in hematopoietic stem cells. Immunity *30*, 493-507.

Oguro, H., Ding, L., and Morrison, S.J. (2013). SLAM family markers resolve functionally distinct subpopulations of hematopoietic stem cells and multipotent progenitors. Cell Stem Cell *13*, 102-116.

Olsson, A., Venkatasubramanian, M., Chaudhri, V.K., Aronow, B.J., Salomonis, N., Singh, H., and Grimes, H.L. (2016). Single-cell analysis of mixed-lineage states leading to a binary cell fate choice. Nature *537*, 698-702.

Oravecz, A., Apostolov, A., Polak, K., Jost, B., Le Gras, S., Chan, S., and Kastner, P. (2015). Ikaros mediates gene silencing in T cells through Polycomb repressive complex 2. Nat Commun *6*, 8823.

Pang, S.H.M., de Graaf, C.A., Hilton, D.J., Huntington, N.D., Carotta, S., Wu, L., and Nutt, S.L. (2018). PU.1 Is Required for the Developmental Progression of Multipotent Progenitors to Common Lymphoid Progenitors. Front Immunol *9*, 1264.

Park, S.M., Cho, H., Thornton, A.M., Barlowe, T.S., Chou, T., Chhangawala, S., Fairchild, L., Taggart, J., Chow, A., Schurer, A.*, et al.* (2019). IKZF2 Drives Leukemia Stem Cell Self-Renewal and Inhibits Myeloid Differentiation. Cell Stem Cell *24*, 153-165 e157.

Paul, F., Arkin, Y., Giladi, A., Jaitin, D.A., Kenigsberg, E., Keren-Shaul, H., Winter, D., Lara-Astiaso, D., Gury, M., Weiner, A.*, et al.* (2016). Transcriptional Heterogeneity and Lineage Commitment in Myeloid Progenitors. Cell *164*, 325.

Pei, W., Feyerabend, T.B., Rossler, J., Wang, X., Postrach, D., Busch, K., Rode, I., Klapproth, K., Dietlein, N., Quedenau, C.*, et al.* (2017). Polylox barcoding reveals haematopoietic stem cell fates realized in vivo. Nature *548*, 456-460.

Pierini, A., Nishikii, H., Baker, J., Kimura, T., Kwon, H.S., Pan, Y., Chen, Y., Alvarez, M., Strober, W., Velardi, A.*, et al.* (2017). Foxp3(+) regulatory T cells maintain the bone marrow microenvironment for B cell lymphopoiesis. Nat Commun *8*, 15068.

Pietras, E.M. (2017). Inflammation: a key regulator of hematopoietic stem cell fate in health and disease. Blood *130*, 1693-1698.

Pietras, E.M., Reynaud, D., Kang, Y.A., Carlin, D., Calero-Nieto, F.J., Leavitt, A.D., Stuart, J.M., Gottgens, B., and Passegue, E. (2015). Functionally Distinct Subsets of Lineage-Biased Multipotent Progenitors Control Blood Production in Normal and Regenerative Conditions. Cell Stem Cell *17*, 35-46.

Pinho, S., and Frenette, P.S. (2019). Haematopoietic stem cell activity and interactions with the niche. Nat Rev Mol Cell Biol *20*, 303-320.

Pinto do, O.P., Wandzioch, E., Kolterud, A., and Carlsson, L. (2001). Multipotent hematopoietic progenitor cells immortalized by Lhx2 self-renew by a cell nonautonomous mechanism. Exp Hematol *29*, 1019-1028.

Pronk, C.J., Rossi, D.J., Mansson, R., Attema, J.L., Norddahl, G.L., Chan, C.K., Sigvardsson, M., Weissman, I.L., and Bryder, D. (2007). Elucidation of the phenotypic, functional, and molecular topography of a myeloerythroid progenitor cell hierarchy. Cell Stem Cell *1*, 428-442.

Puhr, S., Lee, J., Zvezdova, E., Zhou, Y.J., and Liu, K. (2015). Dendritic cell development-History, advances, and open questions. Semin Immunol *27*, 388-396.

Purton, L.E., and Scadden, D.T. (2007). Limiting factors in murine hematopoietic stem cell assays. Cell Stem Cell *1*, 263-270.

Reiter, F., Wienerroither, S., and Stark, A. (2017). Combinatorial function of transcription factors and cofactors. Curr Opin Genet Dev *43*, 73-81.

Rieger, M.A., Hoppe, P.S., Smejkal, B.M., Eitelhuber, A.C., and Schroeder, T. (2009). Hematopoietic cytokines can instruct lineage choice. Science *325*, 217-218.

Rodriguez-Fraticelli, A.E., Wolock, S.L., Weinreb, C.S., Panero, R., Patel, S.H., Jankovic, M., Sun, J., Calogero, R.A., Klein, A.M., and Camargo, F.D. (2018). Clonal analysis of lineage fate in native haematopoiesis. Nature *553*, 212-216.

Rosenberg, H.F., Dyer, K.D., and Foster, P.S. (2013). Eosinophils: changing perspectives in health and disease. Nat Rev Immunol *13*, 9-22.

Rossi, D.J., Bryder, D., Zahn, J.M., Ahlenius, H., Sonu, R., Wagers, A.J., and Weissman, I.L. (2005). Cell intrinsic alterations underlie hematopoietic stem cell aging. Proc Natl Acad Sci U S A *102*, 9194-9199.

Sanjuan-Pla, A., Macaulay, I.C., Jensen, C.T., Woll, P.S., Luis, T.C., Mead, A., Moore, S., Carella, C., Matsuoka, S., Bouriez Jones, T.*, et al.* (2013). Platelet-biased stem cells reside at the apex of the haematopoietic stem-cell hierarchy. Nature *502*, 232-236.

Sawai, C.M., Babovic, S., Upadhaya, S., Knapp, D., Lavin, Y., Lau, C.M., Goloborodko, A., Feng, J., Fujisaki, J., Ding, L.*, et al.* (2016). Hematopoietic Stem Cells Are the Major Source of Multilineage Hematopoiesis in Adult Animals. Immunity *45*, 597-609.

Schlitzer, A., and Ginhoux, F. (2014). Organization of the mouse and human DC network. Curr Opin Immunol *26*, 90-99.

Schmidl, C., Rendeiro, A.F., Sheffield, N.C., and Bock, C. (2015). ChIPmentation: fast, robust, low-input ChIP-seq for histones and transcription factors. Nat Methods *12*, 963-965.

Schraml, B.U., and Reis e Sousa, C. (2015). Defining dendritic cells. Curr Opin Immunol *32*, 13-20.

Schurch, C.M., Riether, C., and Ochsenbein, A.F. (2014). Cytotoxic CD8+ T cells stimulate hematopoietic progenitors by promoting cytokine release from bone marrow mesenchymal stromal cells. Cell Stem Cell *14*, 460-472.

Sebastian, M., Lopez-Ocasio, M., Metidji, A., Rieder, S.A., Shevach, E.M., and Thornton, A.M. (2016). Helios Controls a Limited Subset of Regulatory T Cell Functions. J Immunol *196*, 144-155.

Shah, D.K., and Zuniga-Pflucker, J.C. (2014). An overview of the intrathymic intricacies of T cell development. J Immunol *192*, 4017-4023.

Siracusa, M.C., Kim, B.S., Spergel, J.M., and Artis, D. (2013). Basophils and allergic inflammation. J Allergy Clin Immunol *132*, 789-801; quiz 788.

Skene, P.J., and Henikoff, S. (2017). An efficient targeted nuclease strategy for high-resolution mapping of DNA binding sites. Elife *6*.

Soh, K.T., and Wallace, P.K. (2018). RNA Flow Cytometry Using the Branched DNA Technique. Methods Mol Biol *1678*, 49-77.

Song, C., Li, Z., Erbe, A.K., Savic, A., and Dovat, S. (2011). Regulation of Ikaros function by casein kinase 2 and protein phosphatase 1. World J Biol Chem *2*, 126-131.

Sridharan, R., and Smale, S.T. (2007). Predominant interaction of both Ikaros and Helios with the NuRD complex in immature thymocytes. J Biol Chem *282*, 30227-30238.

Stoeckius, M., Hafemeister, C., Stephenson, W., Houck-Loomis, B., Chattopadhyay, P.K., Swerdlow, H., Satija, R., and Smibert, P. (2017). Simultaneous epitope and transcriptome measurement in single cells. Nat Methods *14*, 865-868.

Stoeckius, M., Zheng, S., Houck-Loomis, B., Hao, S., Yeung, B.Z., Mauck, W.M., 3rd, Smibert, P., and Satija, R. (2018). Cell Hashing with barcoded antibodies enables multiplexing and doublet detection for single cell genomics. Genome Biol *19*, 224.

Stuart, T., Butler, A., Hoffman, P., Hafemeister, C., Papalexi, E., Mauck, W.M., 3rd, Hao, Y., Stoeckius, M., Smibert, P., and Satija, R. (2019). Comprehensive Integration of Single-Cell Data. Cell *177*, 1888-1902 e1821.

Sun, D., Luo, M., Jeong, M., Rodriguez, B., Xia, Z., Hannah, R., Wang, H., Le, T., Faull, K.F., Chen, R.*, et al.* (2014). Epigenomic profiling of young and aged HSCs reveals concerted changes during aging that reinforce self-renewal. Cell Stem Cell *14*, 673-688.

Tarlinton, D. (2019). B cells still front and centre in immunology. Nat Rev Immunol *19*, 85-86.

Tencer, A.H., Cox, K.L., Di, L., Bridgers, J.B., Lyu, J., Wang, X., Sims, J.K., Weaver, T.M., Allen, H.F., Zhang, Y.*, et al.* (2017). Covalent Modifications of Histone H3K9 Promote Binding of CHD3. Cell Rep *21*, 455-466.

Tikhonova, A.N., Dolgalev, I., Hu, H., Sivaraj, K.K., Hoxha, E., Cuesta-Dominguez, A., Pinho, S., Akhmetzyanova, I., Gao, J., Witkowski, M.*, et al.* (2019). The bone marrow microenvironment at single-cell resolution. Nature *569*, 222-228.

Uckun, F.M., Ma, H., Zhang, J., Ozer, Z., Dovat, S., Mao, C., Ishkhanian, R., Goodman, P., and Qazi, S. (2012). Serine phosphorylation by SYK is critical for nuclear localization and transcription factor function of Ikaros. Proc Natl Acad Sci U S A *109*, 18072-18077.

Vieira, P., and Cumano, A. (2004). Differentiation of B lymphocytes from hematopoietic stem cells. Methods Mol Biol *271*, 67-76.

Vivier, E., Artis, D., Colonna, M., Diefenbach, A., Di Santo, J.P., Eberl, G., Koyasu, S., Locksley, R.M., McKenzie, A.N.J., Mebius, R.E.*, et al.* (2018). Innate Lymphoid Cells: 10 Years On. Cell *174*, 1054-1066.

Wang, J.H., Avitahl, N., Cariappa, A., Friedrich, C., Ikeda, T., Renold, A., Andrikopoulos, K., Liang, L., Pillai, S., Morgan, B.A.*, et al.* (1998). Aiolos regulates B cell activation and maturation to effector state. Immunity *9*, 543-553.

Wei, Q., and Frenette, P.S. (2018). Niches for Hematopoietic Stem Cells and Their Progeny. Immunity *48*, 632-648.

Wilkinson, A.C., Ishida, R., Kikuchi, M., Sudo, K., Morita, M., Crisostomo, R.V., Yamamoto, R., Loh, K.M., Nakamura, Y., Watanabe, M.*, et al.* (2019). Long-term ex vivo haematopoietic-stem-cell expansion allows nonconditioned transplantation. Nature *571*, 117-121.

Will, B., and Steidl, U. (2010). Multi-parameter fluorescence-activated cell sorting and analysis of stem and progenitor cells in myeloid malignancies. Best Pract Res Clin Haematol *23*, 391-401.

Wilson, N.K., Calero-Nieto, F.J., Ferreira, R., and Gottgens, B. (2011). Transcriptional regulation of haematopoietic transcription factors. Stem Cell Res Ther *2*, 6.

Xu, C., Gao, X., Wei, Q., Nakahara, F., Zimmerman, S.E., Mar, J., and Frenette, P.S. (2018). Stem cell factor is selectively secreted by arterial endothelial cells in bone marrow. Nat Commun *9*, 2449.

Yamamoto, R., Wilkinson, A.C., Ooehara, J., Lan, X., Lai, C.Y., Nakauchi, Y., Pritchard, J.K., and Nakauchi, H. (2018). Large-Scale Clonal Analysis Resolves Aging of the Mouse Hematopoietic Stem Cell Compartment. Cell Stem Cell *22*, 600-607 e604.

Yeaman, M.R. (2014). Platelets: at the nexus of antimicrobial defence. Nat Rev Microbiol *12*, 426-437.

Yoshida, T., Ng, S.Y., Zuniga-Pflucker, J.C., and Georgopoulos, K. (2006). Early hematopoietic lineage restrictions directed by Ikaros. Nat Immunol *7*, 382-391.

Young, K., Borikar, S., Bell, R., Kuffler, L., Philip, V., and Trowbridge, J.J. (2016). Progressive alterations in multipotent hematopoietic progenitors underlie lymphoid cell loss in aging. J Exp Med *213*, 2259-2267.

Yu, X., Wu, C., Bhavanasi, D., Wang, H., Gregory, B.D., and Huang, J. (2017). Chromatin dynamics during the differentiation of long-term hematopoietic stem cells to multipotent progenitors. Blood Adv *1*, 887-898.

Yuseff, M.I., Pierobon, P., Reversat, A., and Lennon-Dumenil, A.M. (2013). How B cells capture, process and present antigens: a crucial role for cell polarity. Nat Rev Immunol *13*, 475-486.

Zhang, N., and Bevan, M.J. (2011). CD8(+) T cells: foot soldiers of the immune system. Immunity *35*, 161-168.

Zhang, Y., Gao, S., Xia, J., and Liu, F. (2018). Hematopoietic Hierarchy - An Updated Roadmap. Trends Cell Biol *28*, 976-986.

Zhao, M., and Li, L. (2016). Dissecting the bone marrow HSC niches. Cell Res *26*, 975-976.

Zhao, M., Perry, J.M., Marshall, H., Venkatraman, A., Qian, P., He, X.C., Ahamed, J., and Li, L. (2014). Megakaryocytes maintain homeostatic quiescence and promote post-injury regeneration of hematopoietic stem cells. Nat Med *20*, 1321-1326.

Zhu, J., Yamane, H., and Paul, W.E. (2010). Differentiation of effector CD4 T cell populations (*). Annu Rev Immunol *28*, 445-489.

ARTICLE

STATUS: Released Pubication
PLoS Genet. 2018 Jul 12;14(7):e1007485. doi: 10.1371/journal.pgen.

AUTHORS: Jerome Mastio, Celestine Simand, Giovanni Cova, Philippe Kastner, Susan Chan, Peggy Kirstetter

TITLE: Ikaros cooperates with Notch activation and antagonizes TGFβ signaling to promote pDC development

PLOS GENETICS

RESEARCH ARTICLE

Ikaros cooperates with Notch activation and antagonizes TGFβ signaling to promote pDC development

Jérôme Mastio[1¤], Célestine Simand[1☯], Giovanni Cova[1☯], Philippe Kastner[1,2*], Susan Chan[1*], Peggy Kirstetter[1*]

1 Institut de Génétique et de Biologie Moléculaire et Cellulaire (IGBMC), INSERM U1258, CNRS UMR 7104, Université de Strasbourg, Illkirch, France, **2** Faculté de Médecine, Université de Strasbourg, Strasbourg, France

☯ These authors contributed equally to this work.
¤ Current address: Wistar Institute, Philadelphia, PA, United States of America
* scpk@igbmc.fr (PKa); scpk@igbmc.fr (SC); kirstett@igbmc.fr (PKi)

Citation: Mastio J, Simand C, Cova G, Kastner P, Chan S, Kirstetter P (2018) Ikaros cooperates with Notch activation and antagonizes TGFβ signaling to promote pDC development. PLoS Genet 14(7): e1007485. https://doi.org/10.1371/journal.pgen.1007485

Editor: Hamish S. Scott, Centre for Cancer Biology, SA Pathology, AUSTRALIA

Received: February 23, 2018

Accepted: June 13, 2018

Published: July 12, 2018

Data Availability Statement: All the transcriptomic and the Chip-seq data held on Gene Expression Omnibus (GEO) repository repository (accession numbers GSE 114108, GSE114629 and GSE61148).

Funding: This work was supported by grants from the Agence Nationale de la Recherche (ANR-07-MIME-018-02 to PKa), the Conférence de Coordination Inter-Régionale du Grand-Est of the Ligue contre le Cancer (CCIRGE-2014 to PKi and 0001K-2016 to SC) and institutional funds from

Abstract

Plasmacytoid and conventional dendritic cells (pDCs and cDCs) arise from monocyte and dendritic progenitors (MDPs) and common dendritic progenitors (CDPs) through gene expression changes that remain partially understood. Here we show that the Ikaros transcription factor is required for DC development at multiple stages. Ikaros cooperates with Notch pathway activation to maintain the homeostasis of MDPs and CDPs. Ikaros then antagonizes TGFβ function to promote pDC differentiation from CDPs. Strikingly, Ikaros-deficient CDPs and pDCs express a cDC-like transcriptional signature that is correlated with TGFβ activation, suggesting that Ikaros is an upstream negative regulator of the TGFβ pathway and a repressor of cDC-lineage genes in pDCs. Almost all of these phenotypes can be rescued by short-term in vitro treatment with γ-secretase inhibitors, which affects both TGFβ-dependent and -independent pathways, but is Notch-independent. We conclude that Ikaros is a crucial differentiation factor in early dendritic progenitors that is required for pDC identity.

Author summary

Dendritic cells (DCs) are an important component of the immune system, and exist as two major subtypes: conventional DCs (cDCs) which present antigen via major histocompatibility class II molecules, and plasmacytoid DCs (pDCs) which act mainly as producers of type-I interferon in response to viral infections. Both types of DCs derive from a common dendritic progenitor (CDP), but the genetic pathways that influence their development are not completely understood. A better understanding of these pathways is important, which may lead to protocols for generating specific DCs in culture, depending on the need. In this study, we have discovered important roles for the Ikaros transcription factor in DC development. We found that: (i) Ikaros cooperates with the Notch pathway to promote the development or homeostasis of CDPs; (ii) Ikaros controls pDC differentiation from CDPs through a γ-secretase sensitive pathway; and (iii) Ikaros antagonizes the

INSERM, CNRS, University of Strasbourg and the ANR-10-LABX-0030-INRT grant. JM received pre-doctoral fellowships from the Ministry of Technology and Research and Fondation ARC; CS a master fellowship from the Fondation pour la Recherche Médicale (FRM-DEA20140630557) and GC a pre-doctoral fellowship from the IGBMC PhD programme (ANR-10-LABX-0030-INRT). The funders had no role in study design, data collection and analysis, decision to publish, or preparation of the manuscript.

Competing interests: The authors have declared that no competing interests exist.

TGFβ pathway to inhibit cDC differentiation. Our results thus identify Ikaros as a key player in the early steps of DC development.

Introduction

Dendritic cells (DCs) are essential modulators of the immune response [1]. They can be broadly divided into conventional DCs (cDC), which are required for antigen presentation, and plasmacytoid DCs (pDC), which secrete high quantities of type-I interferon (IFN-α, -β, -ω) upon certain viral infections [2, 3]. cDCs are further divided into cDC1 ($CD8^+$) and cDC2 ($CD11b^+$) subsets. Both DC lineages develop in the bone marrow. Monocyte and dendritic progenitors (MDPs) are the earliest known DC precursors, and they give rise to monocytes and common dendritic progenitors (CDPs) [4–6]. In turn, CDPs differentiate into pDCs and pre-cDCs, the latter of which migrate to the periphery to become cDCs. The molecular circuits regulating DC cell fate have been intensively studied, and some transcriptional regulators (Ikaros, E2.2, PU.1, IRF8, GFI1, NFIL3, BATF3, BCL11a) and canonical signaling pathways (TGFβ, Notch, Wnt) have been identified [3, 7–12]. However, the relationships and interactions between these players remain unclear, and this is important to understand if we wish to manipulate DC function.

Deficiency of the Ikaros zinc finger DNA-binding protein and tumor suppressor, encoded by the *Ikzf1* gene, is associated with profoundly impaired DC development. Mice homozygous for a dominant-negative (dn) *Ikzf1* mutation lack all cDCs, while animals with a null mutation predominantly lack cDC2s [13]. In contrast, mice carrying the hypomorphic $Ik^{L/L}$ mutation show a selective block in bone marrow (BM) pDC development, leading to an absence of peripheral pDCs, although cDCs appear normal [14]. These studies highlight the sensitivity of the DC lineages to Ikaros levels, where pDC development requires more Ikaros function than cDCs. In man, patients with germline *IKZF1* mutations also exhibit reduced pDC, but not cDC numbers, indicating a conserved role for Ikaros in DC development [15]. Interestingly, *IKZF1* deletions are associated with blastic plasmacytoid dendritic cell neoplasms (BPDCN), a malignancy of pDC precursors with poor prognosis [16–18]. Thus Ikaros is required for DC development, but little is known about its molecular mechanisms.

Here we show that Ikaros deficiency leads to multiple defects in pDC and cDC development. In particular, Ikaros is required for CDP development, where it antagonizes TGFβ function to promote pDC differentiation. We further show that Ikaros cooperates with Notch pathway activation to support the homeostasis of DC progenitors. Lastly, we show that a transient incubation of bone marrow cells with γ-secretase inhibitors rescues pDC development from WT and Ikaros-deficient BM progenitors, revealing a potentially novel way to enhance pDC function.

Results

Ikaros is required for CDP differentiation

To determine how pDC differentiation is affected by Ikaros deficiency, we evaluated DC progenitor populations in $Ik^{L/L}$ mice. $Ik^{L/L}$ cells express functional Ikaros proteins at ~10% of WT levels, and although $Ik^{L/L}$ mice die from Notch-dependent T cell leukemias at 4–6 months of age, the animals studied (6–8 weeks of age) showed no signs of transformation (normal CD4/CD8 profiles, T cell receptor chain usage, Notch pathway activation) [19–21].

Successive stages of DC development were analyzed, which included BM $Lin^-Sca1^-CD135^+$ cells, containing $CD117^{hi}CD115^+$ MDPs and $CD117^{lo}CD115^+$ CDPs, as well as the more

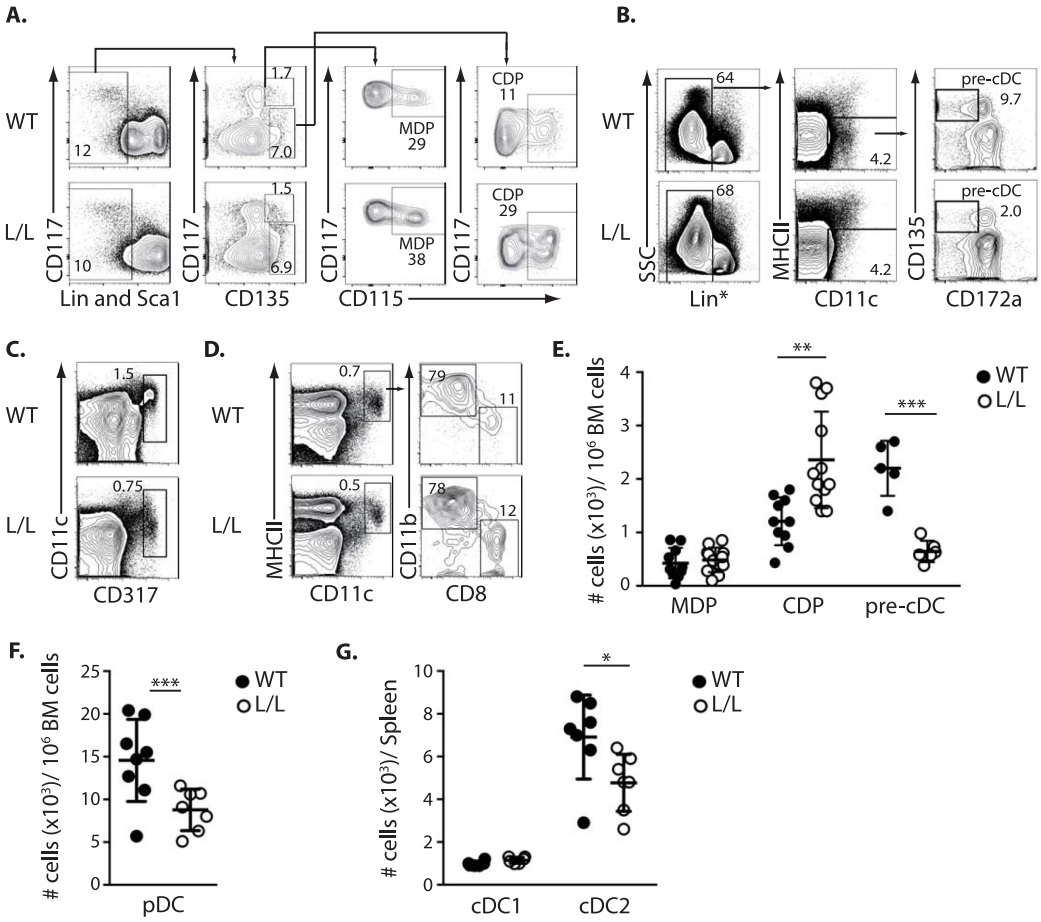

Fig 1. Ikaros regulates DC progenitor development. (A) Representative analysis of MDPs, CDPs, **(B)** pre-cDCs, and **(C)** pDCs from $Ik^{L/L}$ (L/L) and WT BM, by flow cytometry. **(D)** Representative analysis of splenic cDCs ($CD11c^+MHCII^+$). **(E)** Relative numbers of BM MDPs, CDPs and pre-cDCs (as gated in A and B), **(F)** BM pDCs (as gated in C), and **(G)** splenic cDCs (as gated in D). Mean±SD of 4–12 animals per group. $^*p\leq0.05$; $^{**}p\leq0.01$; $^{***}p\leq0.001$ (Student's t-test).

https://doi.org/10.1371/journal.pgen.1007485.g001

downstream BM $CD11c^+CD317^+$ pDCs and $CD11c^+CD135^+MHCII^-CD172a^-$ pre-cDCs, and splenic cDCs (Fig 1) [4–6, 22]. In the BM, CDP numbers were significantly increased and pDC and pre-cDC numbers were significantly decreased in $Ik^{L/L}$ mice, suggesting that $Ik^{L/L}$ DC differentiation is blocked at the CDP stage (Fig 1A–1C, 1E and 1F). In the spleen, $Ik^{L/L}$ animals had no detectable pDCs, as previously reported [13, 14], fewer cDC2s, but similar numbers of cDC1s compared with WT (Fig 1D and 1G). Thus Ikaros deficiency results in the specific accumulation of BM CDPs.

The Notch pathway is activated in Ikaros-deficient pDCs

We previously observed in a genome-wide study that genes associated with the Notch pathway (eg. *Hes1*, *Ptcra*, *Uaca*) are upregulated in the BM pDCs of $Ik^{L/L}$ mice [14]. Higher Hes1 and Ptcra mRNA levels were confirmed by RT-qPCR (Fig 2A). To determine if Ikaros deficiency results in Notch activation throughout pDC development, we crossed $Ik^{L/L}$ mice with animals carrying a *Hes1-GFP* knock-in (KI) reporter [23]. Total BM cells from $Ik^{+/+}$ (WT) and $Ik^{L/L}$ Hes1-GFP KI mice contained similar frequencies of GFP^+ cells (mostly $CD19^+$ B cells) (Fig 2B and 2C). In contrast, GFP^+ cells were nearly absent in WT BM pDCs, but they were present in a fraction of $Ik^{L/L}$ pDCs (7–35%). $Ik^{L/L}$ GFP^+ pDCs were mostly $SiglecH^+CCR9^{lo}$, suggesting an immature phenotype (Fig 2D) [24, 25]. $CCR9^{lo}$ pDCs from WT Hes1-GFP KI mice did not express GFP. These data indicated that the *Hes1* locus, and perhaps the Notch pathway, are ectopically activated during pDC development in the mutant mice.

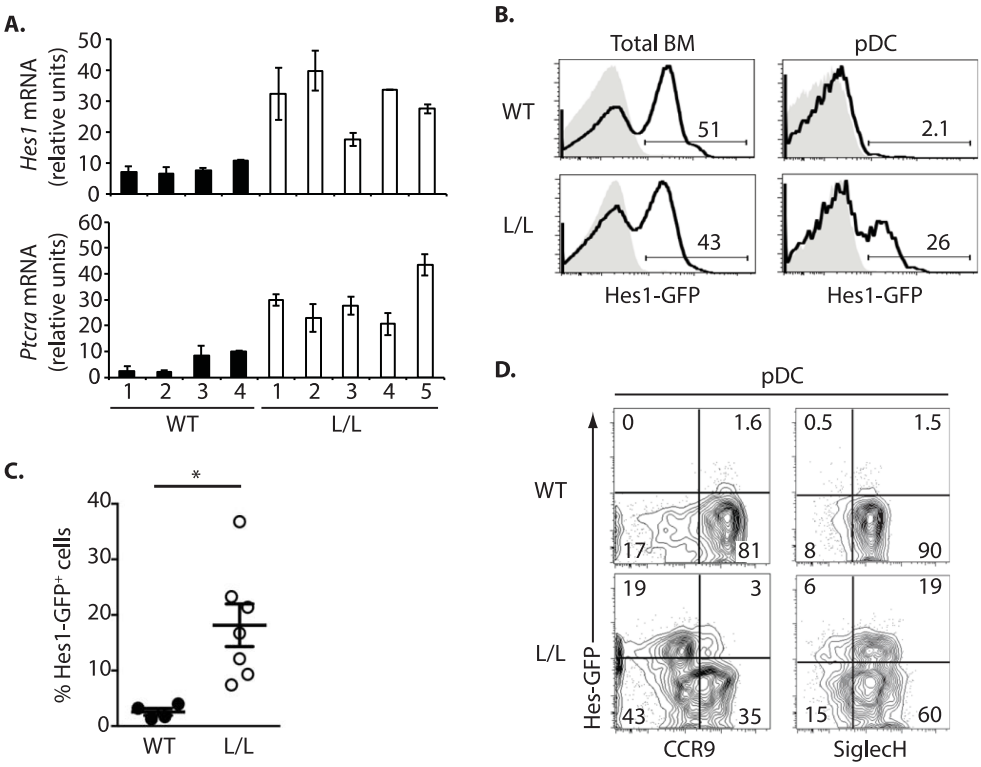

Fig 2. Notch pathway activation in $Ik^{L/L}$ pDCs. (A) *Hes1* and *Ptcra* mRNA expression in BM pDCs from 4 WT and 5 ($Ik^{L/L}$) mice, as analyzed by RT-qPCR and normalized to *Hprt* mRNA levels (mean±SD of triplicate data). **(B)** GFP reporter expression (black line) in total BM cells and BM pDCs ($CD11c^+CD317^+$) from Hes1-GFP^+ WT and $Ik^{L/L}$ mice, by flow cytometry. Grey histograms correspond to control cells from mice lacking the Hes1-GFP reporter. **(C)** Percentage of GFP^+ BM pDCs ($CD11c^+CD317^+$) from Hes1-GFP^+ WT and $Ik^{L/L}$ mice, as analyzed in (B). $^*p \leq 0.05$ (Student's t-test). **(D)** CCR9 and SiglecH vs. GFP expression in BM pDCs from Hes1-GFP^+ WT and $Ik^{L/L}$ mice. Representative of 3 independent experiments.

https://doi.org/10.1371/journal.pgen.1007485.g002

γ-secretase inhibitors rescue $Ik^{L/L}$ CDP differentiation in vitro and in vivo

To determine if ectopic Notch activation interferes with pDC differentiation in $Ik^{L/L}$ mice, we first blocked Notch signaling in Flt3L-supplemented cultures of total BM cells, using a γ-secretase inhibitor (GSI, Compound E) [26, 27]. As γ-secretase is required to cleave and activate ligand-bound Notch receptors, GSIs are potent inhibitors of Notch function. In the absence of GSI (DMSO), WT cultures generated robust numbers of $CD11c^+CD137^+CD11b^-$ pDCs over an 8-day period, while $Ik^{L/L}$ cultures did not (Fig 3A). Strikingly, GSI treatment significantly enhanced WT pDC differentiation, and rescued pDC development in the $Ik^{L/L}$ cultures to levels of WT cells. This occurred early, as GSI treatment at day 0 was both necessary and sufficient to rescue $Ik^{L/L}$ pDC development (Fig 3B and 3C). Similar results were obtained with other GSI compounds (DAPT and MRK003). In addition, early GSI treatment resulted in an increase in total cell numbers (Fig 3D), which correlated with an expansion of immature $CD11c^-$ cells, particularly in the $Ik^{L/L}$ cultures (Fig 3B). The pDCs produced in the GSI-treated cultures were more immature, and expressed low levels of CCR9 and Ly49Q (Fig 3E); B220 levels, however, remained unchanged after GSI treatment. Importantly, the GSI-rescued WT and $Ik^{L/L}$ pDCs expressed mRNA for *Ifna* following TLR9 stimulation in vitro with CpG ODN 1885 (Fig 3F), suggesting functionality. Because GSI treatment at day 0 of culture was sufficient to induce differentiation, GSI was added only once at the onset of culture in subsequent experiments.

To identify the DC progenitor cells sensitive to GSI, we co-cultured WT and $Ik^{L/L}$ total BM cells, purified Lin^-Sca1^- cells, MDPs or CDPs (all $CD45.2^+$), with $CD45.1^+$ supporting WT BM cells, in the presence of GSI and Flt3L, for 8 days (Fig 4A). The ability of the different $CD45.2^+$ populations to give rise to pDCs was evaluated. GSI treatment consistently increased pDC differentiation from $Ik^{L/L}$ CDPs (Fig 4B). On the contrary, GSI did not affect WT MDPs (2 out of 3 experiments) and CDPs, even though it enhanced pDC development from total WT BM cells. We also analyzed $Lin^-Sca1^-CD117^{lo}CD135^+CD115^-$ cells ("$CD115^-$ CDPs") in these assays, as they were reported to contain pDC-specific precursors [28], even though they existed in similar numbers in WT and $Ik^{L/L}$ BM (S1A and S1B Fig); GSI did not affect the pDC production from either WT or $Ik^{L/L}$ $CD115^-$ CDPs (S1C and S1D Fig), and these cells were not studied further. These results therefore suggested that Ikaros negatively regulates a γ-secretase-sensitive pathway mainly in ($CD115^+$) CDPs.

To determine if transient GSI treatment rescues $Ik^{L/L}$ pDC development in vivo, we adoptively transferred GSI-treated BM cells into recipient mice. WT and $Ik^{L/L}$ BM cells ($CD45.2^+$) were cultured with Flt3L and GSI for 2 days, and then transplanted into irradiated hosts ($CD45.1^+CD45.2^+$) along with $CD45.1^+$ supporting WT BM cells. BM and spleen cells were analyzed 9 days later for $CD45.2^+$ pDCs (Fig 4C and 4D). In the BM, $Ik^{L/L}$ cells generated few $CD11c^+CD137^+CD11b^-$ pDCs, regardless of GSI treatment (S2 Fig). However, in the spleen, GSI-treated $Ik^{L/L}$ cells generated $CD11c^+CD137^+CD11b^-$ pDCs while the DMSO-treated cells did not (Fig 4C and 4D). WT cells generated slightly more pDCs after GSI treatment compared with DMSO. Importantly, the $CD45.1^+$ supporting cells produced similar frequencies of pDCs in all conditions, indicating that GSI treatment enhanced $Ik^{L/L}$ and WT pDC differentiation in a cell-intrinsic manner.

Collectively, our results indicated that γ-secretase inhibitors rescue Ikaros-deficient pDC development in vitro and in vivo.

GSI promotes CDP differentiation via Notch-independent pathways

Because γ-secretase inhibitors affect other pathways in addition to Notch, we tested the role of Notch activation in pDC development by genetic means. $Ik^{L/L}$ mice were crossed with animals

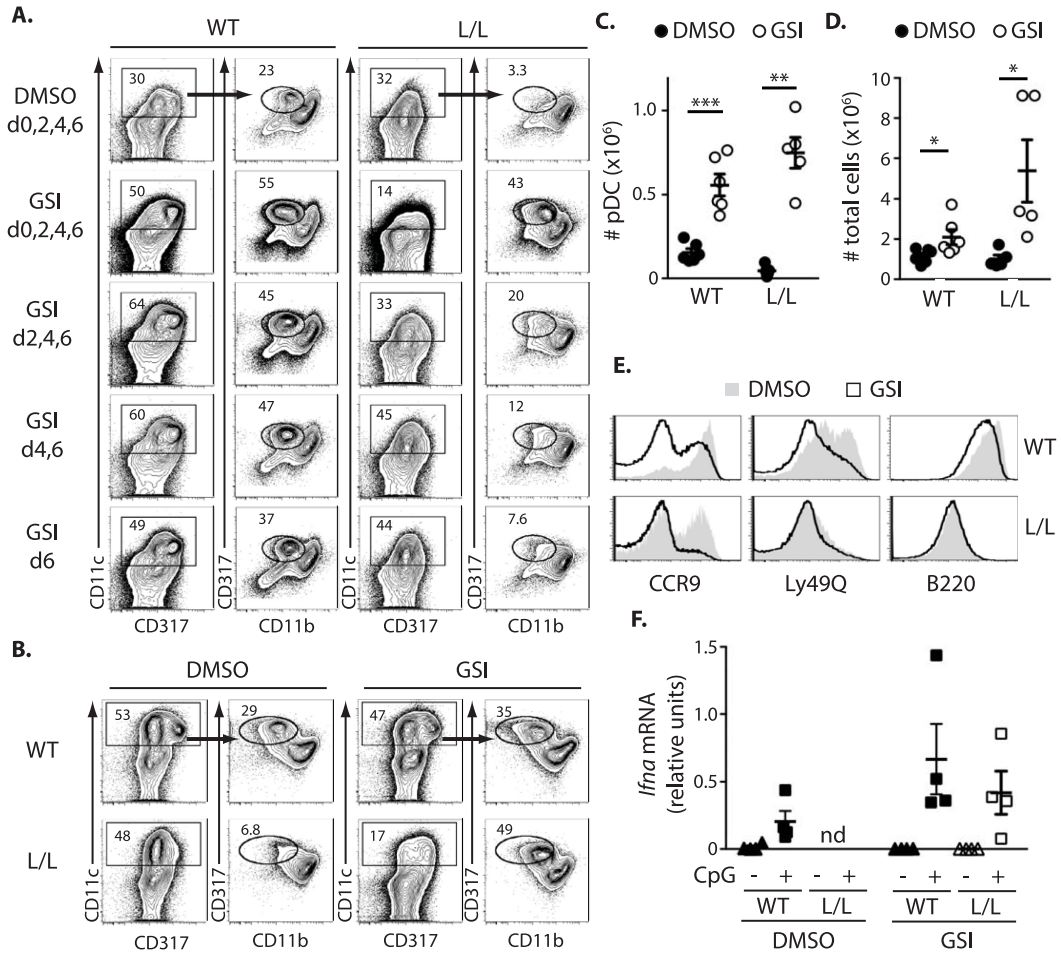

Fig 3. Inhibition of γ-secretase rescues $Ik^{L/L}$ pDC differentiation in vitro. (A) Percentage of $CD11c^{+}CD317^{+}CD11b^{-}$ pDCs after 8 days of Flt3L-supplemented WT and $Ik^{L/L}$ BM cultures, treated with GSI or vehicle (DMSO) at the indicated days of culture. Representative of >5 independent experiments. **(B)** Percentage of pDCs from Flt3L-supplemented WT and $Ik^{L/L}$ BM cultures, treated with GSI or DMSO at day 0 and analyzed at day 8. **(C, D)** Numbers of pDCs (C) and total cell numbers (D) obtained from cultures described in (B). $^{*}p \leq 0.05$; $^{**}p \leq 0.01$; $^{***}p \leq 0.001$ (Student's t-test). **(E)** CCR9, Ly49Q and B220 expression on pDCs cultured as in (B). Representative of 3 independent experiments. **(F)** RT-qPCR analysis of *Ifna* expression induced from pDCs after in vitro culture. WT and $Ik^{L/L}$ pDCs were sorted at d8 of culture, after GSI treatment at day 0, and stimulated for 16h with CpG ODN 1585. *Ifna* mRNA levels were measured by RT-qPCR and normalized to *Ubb* mRNA. nd: not done.

https://doi.org/10.1371/journal.pgen.1007485.g003

carrying a floxed null allele for *Rbpj* ($Rbpj^{f/f}$), the Notch transcriptional mediator, and the R26-CreERT2 transgene [29, 30]. $Ik^{L/L}$ $Rbpj^{+/+}$ Cre^{+} ($Ik^{L/L}$ RBPJ WT) and $Ik^{L/L}$ $Rbpj^{f/f}$ Cre^{+} ($Ik^{L/L}$ RBPJ KO) mice, along with control animals, were treated with tamoxifen for 5 days to delete *Rbpj*, and analyzed 5 days after the last injection. Deletion was confirmed by Western

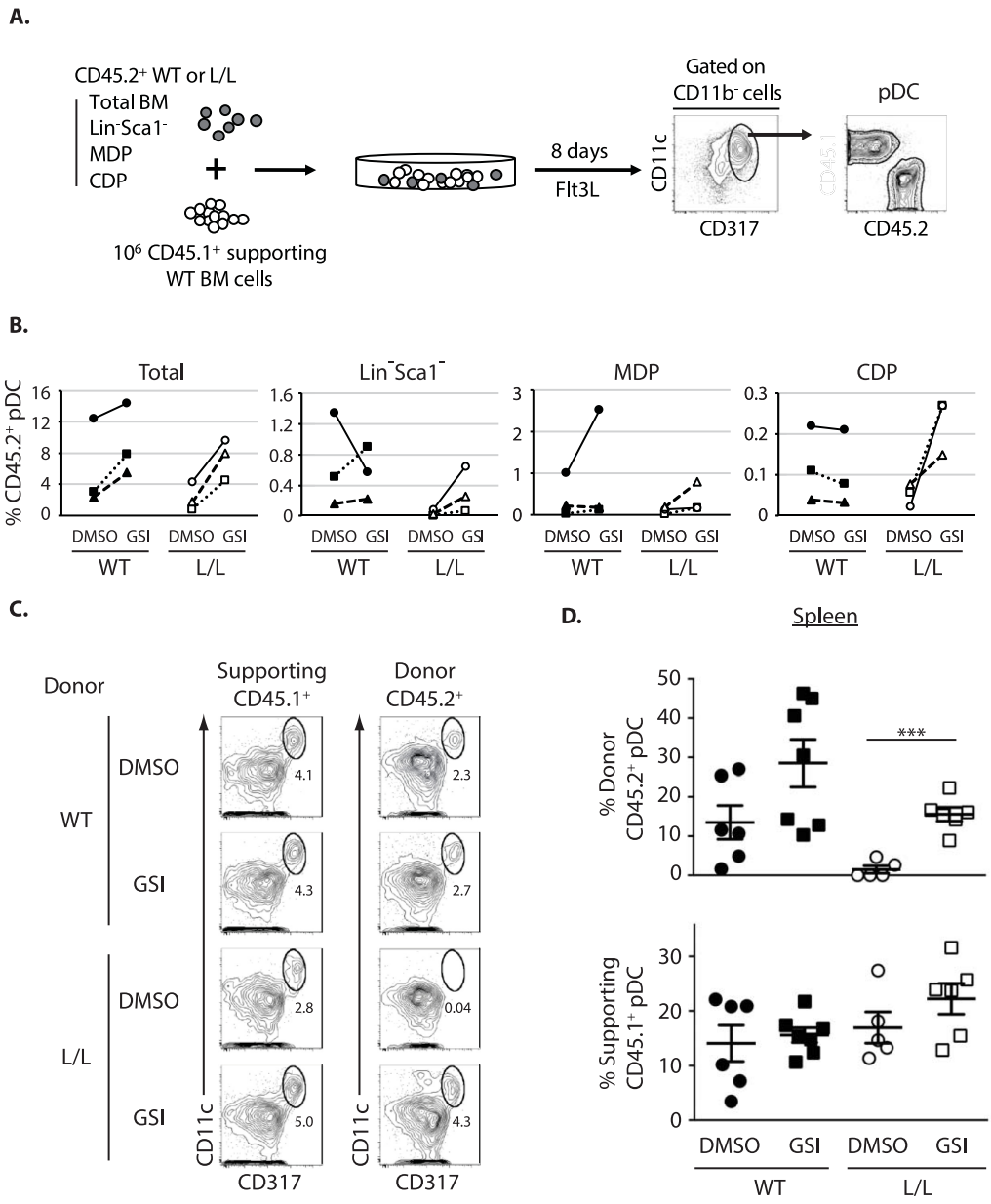
A.
CD45.2+ WT or L/L
Total BM
Lin-Sca1-
MDP
CDP
+
10^6 CD45.1+ supporting
WT BM cells
8 days
Flt3L
Gated on
CD11b- cells
CD11c
CD317
pDC
CD45.1
CD45.2
B.
Total
Lin-Sca1-
MDP
CDP
% CD45.2+ pDC
DMSO GSI
WT
L/L
C.
Donor
Supporting
CD45.1+
Donor
CD45.2+
WT
L/L
DMSO
GSI
4.1
4.3
2.8
5.0
2.3
2.7
0.04
4.3
CD11c
CD317
D.
Spleen
% Donor
CD45.2+ pDC
% Supporting
CD45.1+ pDC
***
DMSO GSI DMSO GSI
WT
L/L

Fig 4. GSI acts on DC progenitors and rescues $Ik^{L/L}$ pDC maturation in vivo. (A) Experimental scheme: the indicated cell populations from WT or $Ik^{L/L}$ BM ($CD45.2^+$) were cultured with supporting $C57BL/6^{CD45.1}$ ($CD45.1^+$) WT BM cells. Cultures were treated with GSI or DMSO at d0, and the percentage of $CD45.2^+$ pDCs were analyzed at d8. **(B)** Percentage of $CD45.2^+$ pDCs ($CD11c^+CD317^+CD11b^-$) after 8 days of co-culture. Data from cells of the same mouse treated with DMSO or GSI were connected by lines. Data from 3 independent experiments. **(C)** Representative analysis of splenic pDCs from $CD45.2^+$ WT or $Ik^{L/L}$ BM cells, cultured with Flt3L in the presence or absence of GSI for 2d, and then transplanted ($2x10^5$ cells per recipient) into lethally-irradiated $CD45.1^+CD45.2^+$ recipient mice, in the presence of supporting $CD45.1^+$ WT BM cells ($2x10^5$ cells). The presence of pDCs was analyzed 9 days after transplantation. Representative of 2 independent experiments, 2–4 animals per condition per experiment. **(D)** Frequency of splenic $CD45.1^+$ and $CD45.2^+$ pDCs ($CD11c^+CD317^+CD11b^-$) in the recipient mice, as described in (A). $^{***}p \leq 0.001$ (Student's t-test).

https://doi.org/10.1371/journal.pgen.1007485.g004

blot (S3 Fig). BM cells from the tamoxifen-treated mice were cultured with Flt3L for 8 days, in the presence or absence of GSI, and cell expansion and pDC development were studied (Fig 5A and 5B). In these experiments, we reasoned that if GSI rescues pDC development by inhibiting Notch signaling, then (i) *Rbpj* inactivation should mimic the effects of GSI, and (ii) GSI should not have additional effects when *Rbpj* is deleted.

When cell numbers were evaluated, we observed that the samples treated with GSI contained significantly higher numbers of cells, regardless of RBPJ and/or Ikaros status (Fig 5B). This suggested that GSI inhibits the function of pathways other than Notch. Likewise, when pDC development was evaluated (Fig 5A and 5B), *Rbpj* deletion by itself did not enhance the differentiation of Ik^{WT} DMSO-treated cells, indicating that Notch activation is not required to limit pDC development when Ikaros is present. Further, in Ik^{WT} cells, GSI treatment enhanced pDC differentiation in both RBPJ WT and KO conditions, suggesting that GSI enhances pDC differentiation in the absence of Notch. Interestingly, when similar experiments were performed in $Ik^{L/L}$ conditions, GSI treatment rescued pDC development in the RBPJ WT samples, as expected, but no rescue was observed when both RBPJ and Ikaros were mutated. GSI nevertheless still increased total cell numbers in the cultures from the RBPJ-Ikaros double mutant cells, indicating that its effects on pDC differentiation and cell expansion are separable.

To determine why GSI treatment did not rescue pDC development in $Ik^{L/L}$ RBPJ KO BM cultures, we analyzed the BM DC progenitor populations of tamoxifen-treated $Ik^{L/L}$ RBPJ KO mice and littermate controls (Fig 5C and 5D). Specifically, we evaluated the CDP population in the double mutant mice, as GSI rescues $Ik^{L/L}$ CDP differentiation. These experiments revealed that MDPs and CDPs were barely detectable in most of the $Ik^{L/L}$ RBPJ KO BM samples (4 out of 5), while the BM from single mutant mice contained easily recognizable MDP and CDP cells. These results indicated that the GSI target population is absent in the $Ik^{L/L}$ RBPJ KO BM, and suggested that Ikaros and Notch activation cooperate to generate or maintain MDP and CDP cells in the BM.

Collectively, our results demonstrate that GSI treatment inhibits a Notch-independent pathway important for CDP development.

The TGFβ pathway is activated in Ikaros-deficient CDPs

To further investigate the molecular pathways targeted by Ikaros and γ-secretase in CDPs, we studied the transcriptome profiles of WT and $Ik^{L/L}$ MDPs and CDPs, cultured in the presence or absence of GSI. We used a protocol similar to the one above, and co-cultured $CD45.2^+$ WT or $Ik^{L/L}$ MDPs, and CDPs, with supporting $CD45.1^+$ WT BM cells. $CD45.2^+$ cells were purified after 24h, and their transcriptomes were analyzed by microarray.

In the vehicle-treated samples, 963 genes were differentially expressed >1.5-fold between $Ik^{L/L}$ CDPs and all WT populations (Fig 6A). Approximately 30% of these genes were deregulated in both $Ik^{L/L}$ MDPs and CDPs (clusters III and IV), and 70% were deregulated only in the $Ik^{L/L}$ CDPs (clusters I and II). To determine how these genes are expressed during WT DC development, we compared their levels of expression in $Ik^{L/L}$ CDPs with those in WT

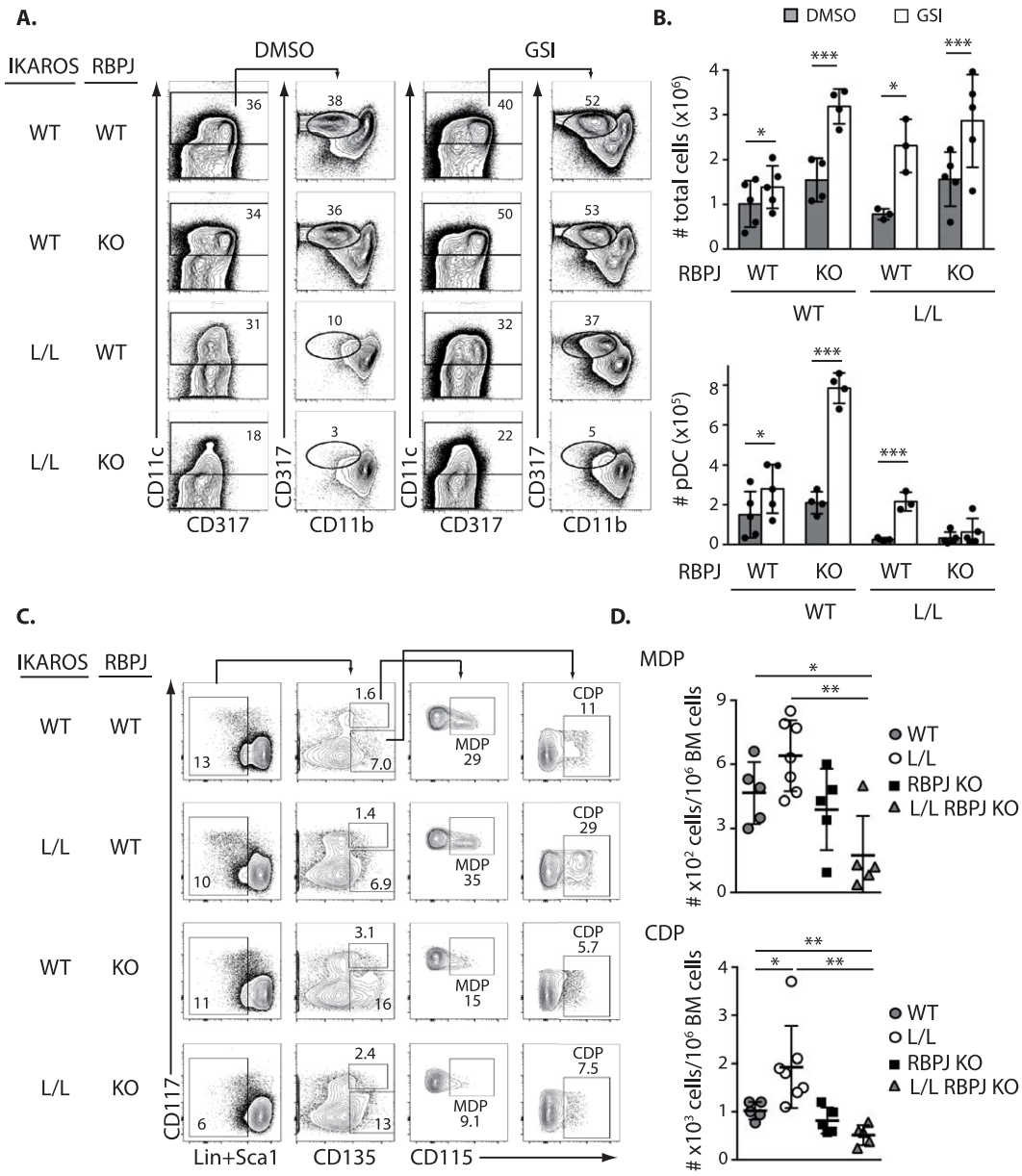
A.
IKAROS
RBPJ
WT
WT
WT
KO
L/L
WT
L/L
KO
DMSO
GSI
36
38
40
52
34
36
50
53
31
10
32
37
18
3
22
5
CD11c
CD317
CD317
CD11b
CD11c
CD317
CD317
CD11b
B.
DMSO
GSI
total cells (x10⁶)
pDC (x10⁵)
RBPJ
WT
KO
WT
KO
WT
L/L
C.
IKAROS
RBPJ
WT
WT
L/L
WT
WT
KO
L/L
KO
13
1.6
7.0
MDP 29
CDP 11
10
1.4
6.9
MDP 35
CDP 29
11
3.1
16
MDP 15
CDP 5.7
6
2.4
13
MDP 9.1
CDP 7.5
CD117
Lin+Sca1
CD135
CD115
D.
MDP
CDP
x10² cells/10⁶ BM cells
x10³ cells/10⁶ BM cells
WT
L/L
RBPJ KO
L/L RBPJ KO

Fig 5. Genetic deletion of RBPJ does not rescue $Ik^{L/L}$ pDC differentiation. (A) Representative analysis of Flt3L-supplemented cultures of BM cells from compound mutant mice with $Ik^{L/L}$ and/or RBPJ KO alleles, after addition of DMSO or GSI at day 0. Cultures were analyzed 8d later. **(B)** Numbers of total cells and pDCs obtained from cultures described in (A) (mean±SD from 3–5 mice per genotype; p values were obtained by paired Student's t-test). **(C)** Analysis and **(D)** relative numbers of MDPs and CDPs from the BM of Ikaros-RBPJ compound mutant mice (representative of 2 independent experiments with 2–5 mice per genotype and per experiment; p values were obtained by Student's t-test). $^{*}p\leq0.05$; $^{**}p\leq0.01$; $^{***}p\leq0.001$.

https://doi.org/10.1371/journal.pgen.1007485.g005

progenitors and mature DC populations, as reported by the ImmGen Compendium (GSE15907), using unsupervised clustering [7]. Interestingly, this revealed that, among the genes up-regulated in $Ik^{L/L}$ CDPs (Fig 6B), the large majority (>70%) were related to mature cDC genes, and not pDCs. The remainder of the genes were DC progenitor-related. In contrast, among the genes down-regulated in $Ik^{L/L}$ CDPs (S4A Fig), most were related to DC progenitor (CMP, MDP, CDP) genes. Further, gene set enrichment analyses (GSEA) indicated that both the up- and down-regulated genes in the $Ik^{L/L}$ CDPs correlated with those normally expressed in WT cDCs (S4B Fig). Thus, Ikaros is required to repress the premature expression of cDC-associated genes in CDPs. We then asked if the cDC transcriptional hallmarks that characterize the $Ik^{L/L}$ CDPs were also retained in the BM pDCs from $Ik^{L/L}$ mice. Indeed, GSEA analysis showed that genes up- or down-regulated in $Ik^{L/L}$ pDCs (transcriptome data from [14]) were also up- or down-regulated in mature cDCs (S4C Fig), thereby confirming our hypothesis.

Among the genes deregulated in $Ik^{L/L}$ CDPs, only 70 were differentially expressed between GSI and DMSO treated samples (Fig 6C, S1 Table). To identify the potential upstream pathways involved in the regulation of their expression in DC progenitors, we performed Ingenuity Pathway Analysis (Fig 6D). This revealed Ikaros to be a significant probable regulator, which validated our approach, and showed the importance of Ikaros in CDPs. The top candidate, however, was TGFβ1, which was interesting because TGFβ1 was previously reported to skew CDP differentiation towards the cDC lineage at the expense of pDCs [9]. We therefore asked if the deregulated genes found in $Ik^{L/L}$ CDPs were enriched for TGFβ-associated genes, by GSEA. These results showed a strong and direct correlation between the genes down-regulated in $Ik^{L/L}$ CDPs and those down-regulated by TGFβ1 signaling (Fig 6E) [9]. Conversely, the genes up-regulated in $Ik^{L/L}$ CDPs were up-regulated by TGFβ1 activation (Fig 6F). Thus, Ikaros expression is correlated with reduced TGFβ1 signaling in CDP cells.

To determine if Ikaros directly regulates the TGFβ pathway, we investigated its capacity to bind TGFβ target genes. The low number of CDPs in WT mice did not allow us to directly investigate Ikaros binding in these cells. We therefore compared Ikaros binding to chromatin from 2 unrelated precursor cell types (pre-B cells and DN3 thymocytes) [31, 32], because conserved binding might indicate that Ikaros regulates similar elements across hematopoietic cell types. These analyses showed strong and conserved Ikaros binding to several TGFβ target genes implicated in DC differentiation (eg. *Axl*, *Irf1*, *Irf4*, *Nfkb2*, *Nfkbie*, *Rel*, *Relb*) (Fig 6G and S4 Fig), and suggested that Ikaros may directly regulate the expression of TGFβ target genes in CDPs.

Inhibition of TGFβ signaling rescues Ikaros-deficient pDC development

To determine if the TGFβ pathway is activated in $Ik^{L/L}$ CDPs, we studied the mRNA expression of genes encoding upstream components of this pathway. Although the level of transcripts encoding the type I and type II TGFβ receptors, and the downstream SMAD proteins, were similar between WT and $Ik^{L/L}$ MDPs and CDPs, we found that the mRNA levels of *Eng*, encoding the type III TGFβ receptor Endoglin, was higher in $Ik^{L/L}$ MDPs (2x) and CDPs (2.8x), regardless of GSI treatment (Fig 6A). Endoglin (CD105), is an auxiliary receptor for the TGFβ receptor complex, which has been shown to positively modulate TGFβ signaling [33].

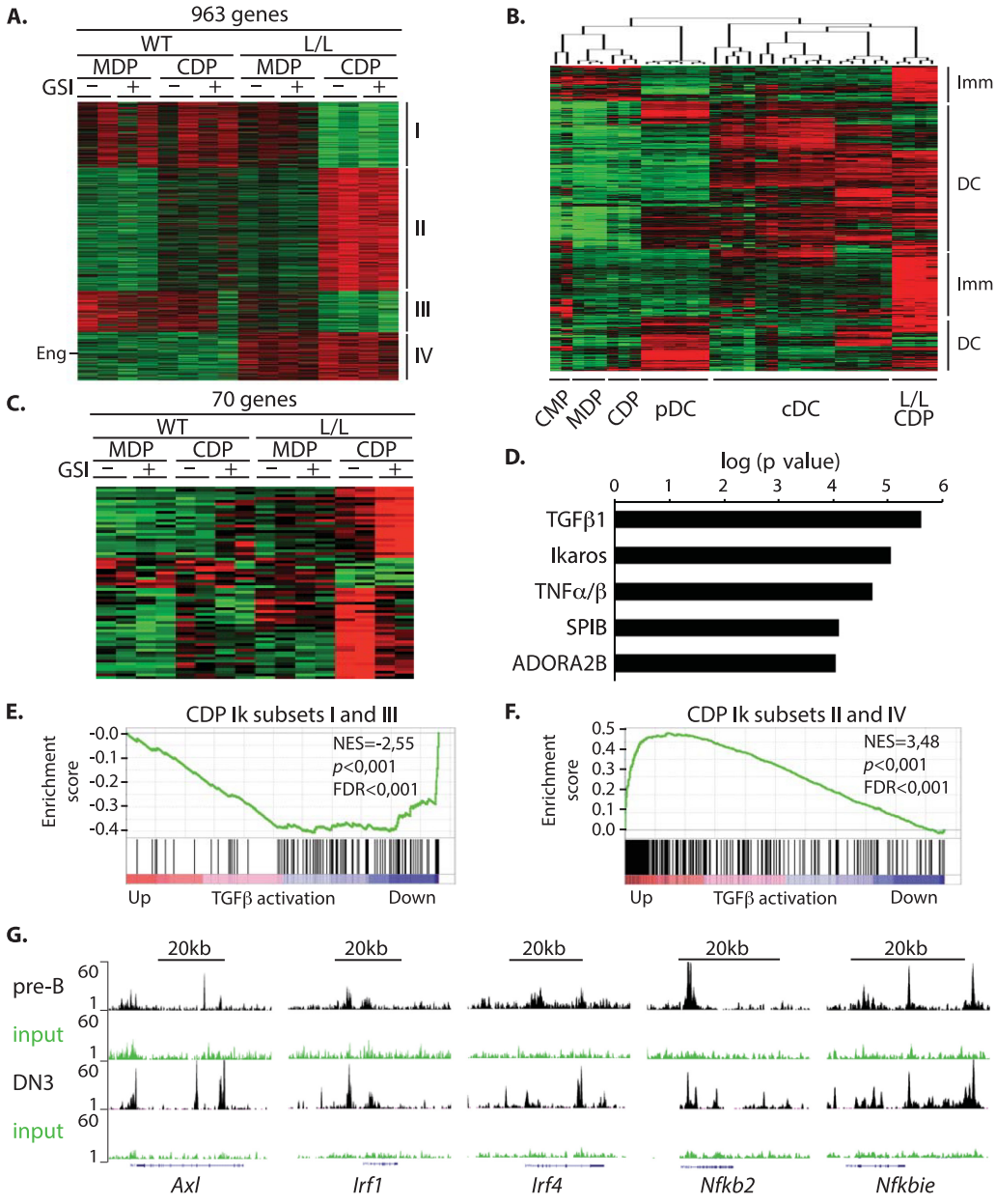
A.
963 genes
WT
L/L
MDP
CDP
MDP
CDP
GSI
− + − + − + − +
I
II
III
IV
Eng
B.
Imm
DC
Imm
DC
CMP
MDP
CDP
pDC
cDC
L/L
CDP
C.
70 genes
WT
L/L
MDP
CDP
MDP
CDP
GSI
− + − + − + − +
D.
log (p value)
0 1 2 3 4 5 6
TGFβ1
Ikaros
TNFα/β
SPIB
ADORA2B
E.
CDP Ik subsets I and III
Enrichment score
-0.0
-0.1
-0.2
-0.3
-0.4
NES=-2,55
p<0,001
FDR<0,001
Up
TGFβ activation
Down
F.
CDP Ik subsets II and IV
Enrichment score
0.5
0.4
0.3
0.2
0.1
0.0
NES=3,48
p<0,001
FDR<0,001
Up
TGFβ activation
Down
G.
20kb
20kb
20kb
20kb
20kb
pre-B
input
DN3
input
60
1
Axl
Irf1
Irf4
Nfkb2
Nfkbie

Fig 6. The TGFβ1 pathway is activated in $Ik^{L/L}$ CDPs. $CD45.2^+$ WT or $Ik^{L/L}$ MDPs, and CDPs, were co-cultured with supporting $CD45.1^+$ WT BM cells for 24h with Flt3L and GSI (or DMSO). $CD45.2^+$ cells were then re-purified and their transcriptomes analyzed. 2 mice per condition. **(A)** Heat map representing K-means clustering of 963 genes differentially expressed between WT or $Ik^{L/L}$ CDPs [fold change (FC)>1.5]. Clusters I and II are deregulated specifically in $Ik^{L/L}$ CDPs. Clusters III and IV are deregulated in all $Ik^{L/L}$ DC progenitors. Eng indicates the Endoglin gene. Red and green indicate high and low expression, respectively. **(B)** Hierarchical clustering of the genes from clusters II and IV in (A), using Immgen transcriptome data for DC progenitors and mature subsets (GSE15907). Clusters of genes similarly expressed between $Ik^{L/L}$ CDPs and DC progenitors (Imm) or mature DCs (DC) are indicated. **(C)** K-means clustering of 70 genes differentially expressed between WT and $Ik^{L/L}$ CDPs, and deregulated by GSI (FC>1.5). **(D)** Top 5 putative upstream regulators related to the 70 genes from (C), as identified by the Ingenuity Pathways Analysis software. **(E)** GSEA enrichment plots of genes specifically down-regulated [clusters I and III in (A)] and **(F)** up-regulated (clusters II and IV) in $Ik^{L/L}$ CDPs. The ranked gene list corresponds to TGFβ1-regulated genes in CDPs, as identified by Felker et al (2010). NES: normalized enrichment score; FDR: false discovery rate. **(G)** Genome browser tracks showing Ikaros binding to loci associated with TGFβ activation in pre-B cells (BH1-Ik1-ER-Bcl2 cell line) and immature DN3 thymocytes (GEO GSE114629 and GSE61148 accession numbers).

https://doi.org/10.1371/journal.pgen.1007485.g006

Higher CD105 expression was also detected on $Ik^{L/L}$ MDPs, CDPs and pDCs (Fig 7A and 7B). In contrast, CD105 levels were stable in other BM populations, including $CD11c^+CD317^-$ cDCs (Fig 7B), indicating that Endoglin expression is specifically increased in $Ik^{L/L}$ pDCs and DC progenitors. In addition, we observed that Ikaros bound to the *Eng* locus in pre-B and DN3 cells, suggesting that it is an Ikaros target gene (S5A Fig).

Lastly, we analyzed the functional consequence of TGFβ inhibition on pDC development. WT and $Ik^{L/L}$ BM cells were cultured with Flt3L for 8 days, in the presence or absence of a TGFβR1 inhibitor (SB431542), and/or GSI. SB431542 treatment alone did not affect total cell numbers (S5B Fig), but increased pDC numbers in both WT and $Ik^{L/L}$ cultures (Fig 7C and 7D). In contrast, GSI treatment alone increased both total cell numbers and pDC numbers. The combination of SB431542 and GSI gave similar total and pDC numbers, compared with GSI alone. These results suggested that TGFβ inhibition promotes pDC differentiation in $Ik^{L/L}$ CDPs.

Discussion

Here we identify Ikaros as a promoter of early DC development. We show that Ikaros cooperates with Notch signaling to enhance the emergence and/or survival of MDPs and CDPs in the BM (Fig 7E). We also show that Ikaros is required to promote CDP differentiation and cell fate specification towards the pDC and cDC lineages, in large part by correctly regulating the expression of DC-specific target genes, and secondly, by antagonizing TGFβ function. These results indicate that the general absence of mature DCs in Ikaros null mice [13, 34], as well as the selective absence of pDCs in Ikaros hypomorphic animals [14], are due at least in part to CDP defects.

Our results suggest that Ikaros antagonizes a TGFβ-dependent gene expression program in CDPs. TGFβ was previously reported to skew CDP differentiation towards the cDC lineage at the expense of pDCs, in part because it induces the expression of Id2, which inhibits the master pDC regulator E2.2 [9, 35–37]. We show that Ikaros-deficient CDPs display a premature cDC gene expression signature, indicating that Ikaros represses the expression of mature cDC-associated genes in DC progenitors. In addition, Ikaros-deficient BM pDCs also display a cDC signature, suggesting that the mutant CDPs that commit to the pDC lineage continue to express a promiscuous cDC gene expression program. Neither *Id2* nor *E2.2* are affected at the mRNA level in Ikaros-deficient CDPs and pDCs, suggesting that Ikaros promotes CDP differentiation independently of E2.2.

How Ikaros antagonizes TGFβ function remains only partially understood. Certain TGFβ target genes are enriched among the genes deregulated by GSI in CDPs. Furthermore, Ikaros-deficient CDPs ectopically express high levels of endoglin which can potentiate TGFβ signaling [38]. Because no other TGFβ receptors or downstream SMAD factors are deregulated in these cells, endoglin upregulation probably plays an important role in activating the TGFβ pathway

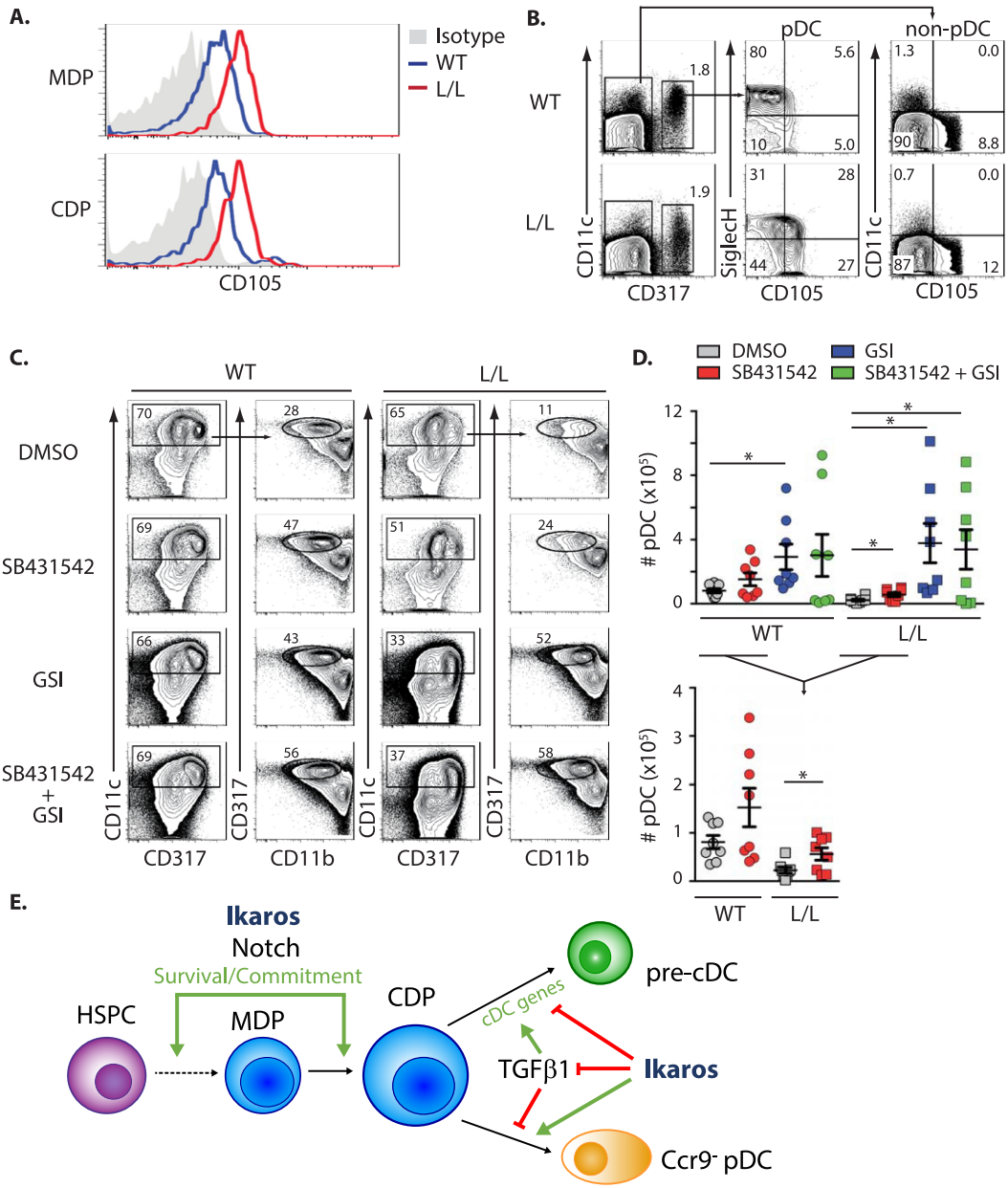
A.
MDP
CDP
Isotype
WT
L/L
CD105
B.
pDC
non-pDC
WT
L/L
1.8
80
5.6
10
5.0
1.3
0.0
90
8.8
1.9
31
28
44
27
0.7
0.0
87
12
CD11c
SiglecH
CD317
CD105
CD11c
CD105
C.
WT
L/L
DMSO
SB431542
GSI
SB431542 + GSI
70
28
65
11
69
47
51
24
66
43
33
52
69
56
37
58
CD11c
CD317
CD317
CD11b
CD11c
CD317
CD317
CD11b
D.
DMSO
SB431542
GSI
SB431542 + GSI
pDC (x10⁵)
WT
L/L
E.
Ikaros
Notch
Survival/Commitment
HSPC
MDP
CDP
pre-cDC
cDC genes
TGFβ1
Ikaros
Ccr9⁻ pDC

Fig 7. TGFβ1 activation inhibits pDC development from $Ik^{L/L}$ CDPs. (A) CD105 expression on WT and $Ik^{L/L}$ DC progenitors. **(B)** SiglecH vs. CD105 expression on BM pDCs ($CD317^+$) and non-pDCs ($CD317^-$). Representative of 4 independent experiments. **(C)** Effect of the TGFβR1 inhibitor SB431542 on pDC differentiation in Flt3L-supplemented WT and $Ik^{L/L}$ BM cultures. Cells were treated at d0 with SB431542 and/or GSI and analyzed at d8. Percentages of cells in the corresponding gates are indicated. Representative of 4 independent experiments. **(D)** Number of pDCs obtained from experiments described in (C). Data of the SB431542 treatments are shown at a larger scale in the lower panel. Representative of 4 independent experiments; 2 mice per genotype per experiment; p values were obtained with a Student's t-test. $^*p \leq 0.05$. **(E)** Schematic representation of Ikaros function during DC development in the BM. Ikaros and Notch signaling are required for the onset of DC differentiation and the appearance of MDPs and CDPs. Later, in CDPs, Ikaros promotes pDC development by antagonizing TGFβ1 signaling and by repressing the cDC gene expression program. HSPC: Hematopoietic stem/progenitor cell.

https://doi.org/10.1371/journal.pgen.1007485.g007

in the mutant DC progenitors. Interestingly, betaglycan, a type III TGFβ receptor closely related to endoglin in structure and function, is a substrate of γ-secretase, and GSI inhibits TGFβ2-mediated reporter gene expression via betaglycan inactivation in HepG2 cells [39]. γ-secretase cleavage of type III TGFβ receptors may therefore inhibit TGFβ receptor signaling in Ikaros-deficient cells. If true, this suggests that Ikaros may be a novel upstream regulator of TGFβ signaling.

In addition to its role in CDP differentiation, Ikaros is also required for MDP and CDP homeostasis. Observed only in compound mutants deficient for Ikaros and RBPJ where both populations are absent, our results demonstrate that Ikaros cooperates with Notch activation to maintain DC progenitor survival and/or expansion. Notch signaling by itself was previously found to promote DC development in vitro via up-regulation of the Frizzled family Wnt receptors [10], but the basis for its cooperation with Ikaros remains to be elucidated. We have reported that Ikaros antagonizes Notch function in T cells, and interacts directly with the activated Notch1 protein to control a set of common target genes [40]. Whether Ikaros and Notch regulate common genes in DC progenitors remains to be investigated. Other studies have suggested that the Notch and TGFβ pathways interact to regulate common genes. Indeed, *Hes1* is a common target of both pathways, because it is transcriptionally regulated by the Notch receptor intracellular domain or by Smad3 following TGFβ signaling [41]. In $Ik^{L/L}$ cells, however, *Hes1* up-regulation was observed in pDCs but not in the more immature dendritic progenitors, suggesting that *Hes1* is differentially regulated by Notch and TGFβ activation in these populations.

Finally, our results with γ-secretase inhibitors are unexpected and intriguing, and indicate that these compounds can be exploited to enhance and rescue WT and Ikaros-deficient DC development in vitro, though the effects are stronger in the mutant cells. We showed that transient GSI treatment promotes the generation of $CD11c^-$ cells, probably the upstream precursors of MDPs and CDPs, and pDC differentiation from CDPs. These actions suggest that GSI molecules might be considered as a potential treatment to enhance pDC function during certain viral infections, like chronic HIV or hepatitis C virus. Conversely, it will be important to test if GSI molecules might have a differentiating effect on BPDCN cancers, a rare and fatal leukemia with few options for treatment [42].

Materials and methods

Ethics statement

All mouse procedures were approved by the IGBMC Ethical Committee (Com'Eth); APAFIS#8752–20 170 1261 0337966 v2.

Mice

The mouse lines used in this study were described previously: $Ik^{L/L}$, Hes1-$EmGFP^{SAT}$, $RBPJ^{f/f}$ and R26-CreER(T2) [19, 23, 29, 30]. Mice were used between 6–9 weeks of age. To delete *Rbpj* in vivo, $RBPJ^{f/f}$ R26-$CreET(T2)^+$ or $Ik^{L/L}$ $RBPJ^{f/f}$ R26-$CreET(T2)^+$ mice were injected

intraperitoneally daily for 5 days with 75 mg/kg of tamoxifen dissolved in sunflower oil, and analyzed 10 days after the first injection.

Cell culture

pDC cultures were performed as described [26]. Briefly, BM cells were seeded at $2x10^6$ cells/ml, and cultured in RPMI 1640 containing 10% fetal calf serum, 20 mM HEPES, 2 mM L-glutamine, 2 mM Sodium Pyruvate, 50 μM β-mercaptoethanol, 1x MEM non-essential amino acids, and antibiotics. Cultures were supplemented with conditioned medium from a Flt3L-producing cell line (B16-Flt3L) [43], or rFlt3L at 100 ng/ml (Peprotech). After 4d, half of the medium was replaced with fresh medium containing 2x Flt3L. GSI (Compound E, Calbiochem) and SB431542 (Selleckchem) were used at 5 μM. pDC cultures from DC progenitors were performed as above in 1 ml of Flt3L-supplemented medium using FACS-sorted $Lin^-Sca1^-ckit^+$, MDPs, CDPs or $CD115^-$CDPs from BM cells ($CD45.2^+$) which were co-cultured with 10^6 $CD45.1^+$ whole BM cells. For CpG oligo-deoxynucleotide (ODN) stimulations, pDCs ($CD11c^+CD317^+CD11b^-$) were sorted after 8 days of culture and stimulated at $2x10^6$ cells/ml in 96-well plates. CpG ODN 1585 or an ODN control (InvivoGen) were used at 2.5 μM. Cells were collected after 16h of stimulation.

Transplantations

BM cells from donor mice ($CD45.2^+$) were cultured with Flt3L in the presence or absence of GSI for 48h. $2x10^5$ cells from these cultures were then transplanted with $2x10^5$ supporting WT BM cells ($CD45.1^+$) into lethally-irradiated (9 Gy) $CD45.1^+CD45.2^+$ recipient mice. Mice were sacrificed and analyzed 9 days after the transfer.

RT-qPCR

RNA was extracted with the RNeasy (Qiagen) or Nucleospin RNA (Macherey-Nagel) kits, and reverse transcribed using Superscript II (Invitrogen). *Hes1*, *Ptcra* and *Hprt* were amplified using the QuantiTect SYBR green system with the Mm_Hes1_1SG, Mm_PtcrA_1SG and Mm_Hprt_1SG primer sets (Qiagen). *Ifna* mRNA was amplified using the SYBR green master mix (Roche) with 50 cycles of 10s 95˚C, 30s 66˚C, 15s 72˚C. Primers used to amplify most of the *Ifna* subtypes were 5'-cctgctggctgtgaggaaata and 5'-gcacaggggctgtgtttct. Primers for *Ubiquitin* (*Ubb*) were 5'-tggctattaattattcggtctgcat and 5'-gcaagtggctagagtgcagagtaa. *Hes1* and *Ptcra* levels were normalized to that of *Hprt*, while *Ifna* expression was normalized to that of *Ubb*.

Flow cytometry

We used the following antibodies: anti-CD11b (M1/70) eFluor450 or PE; anti-CD11c (N418) AlexaFluor700; anti-human/mouse CD45R (B220) eFluor650NC; anti- CD59 and Gr1 (RB6-8C5) biotin; anti-CD199 (CCR9) PE/Cy7; anti-CD317 (ebio927) AlexaFluor488 or eFluor450; anti-MHCII (M5/114.15.2) FITC or PE/Cy5; anti-Sca1 (D7) biotin (eBioscience); anti-CD3 (145-2C11) biotin; anti-CD4 (RM4-5) biotin; anti-CD8 (53–6.7) biotin; anti-CD11b (M1/70) biotin; anti-CD45.1 (A20) PE; anti-human/mouse CD45R (B220) biotin; anti-CD115 (c-fms) APC; anti-CD135 (A2F10) PE; anti-CD172a (P84) APC; anti-NK1.1 (PK136) biotin; anti-Ter119 biotin (BD Biosciences); anti-CD11c (N418) biotin or APC; anti-CD19 (6D5) biotin; anti-CD45.1 (A20) FITC; anti-CD45.2 (104.2) PE or AlexaFluor700; anti-CD105 (Endoglin) Alexa488; anti-CD117 (c-kit) APC/Cy7; anti-Ly49Q (2E6) PE (MBL); anti-SiglecH (551.3D3) PE (BioLegend); AlexaFluor™ 405 (InvitroGen) or AlexaFluor488 Streptavidin (Jackson ImmunoResearch). Lineage staining was performed using a mixture of anti-CD3, -CD4, -CD8,

-CD19, -CD11b, -CD11c, -Gr1, -Ter119, -NK1.1 and -B220 antibodies for Lin, and anti-CD3, -CD19, -Ter119, -NK1.1 and -B220 for Lin*. Cells were analyzed on a LSRII analyzer (BD Biosciences) and sorted on a FACSAriaIISORP (BD Biosciences). Sort purity was >98%.

Western blotting

Total protein extracts from 10^6 BM cells were separated on SDS-PAGE gels. Immunoblots were analyzed with anti-RPBJ (T6719; Institute of Immunology, Japan), and anti-β-actin (A5441, Sigma) polyclonal antibodies. All secondary antibodies were horseradish conjugated (Santa Cruz, Jackson ImmunoResearch).

Microarray analysis

Transcriptome analyses were performed with Affymetrix Gene ST 1.0 arrays. Unsupervised hierarchical clustering and K-means clustering were performed using Cluster 3. GSEA was performed using the GSEA 2.0 software [44, 45]. Microarray data are available in the GEO databank (GSE114108).

Supporting information

S1 Fig. GSI does not act on CD115$^-$ CDPs to stimulate pDC differentiation. (A) Representative analysis of CD115$^-$ CDPs from WT and Ik$^{L/L}$ BM, by flow cytometry. **(B)** Relative numbers of CD115$^-$ CDPs (as gated in A). ns: not significant (Student's t-test). **(C)** Experimental scheme: CD115$^-$ CDPs from WT or Ik$^{L/L}$ BM (CD45.2$^+$) were cultured with supporting C57BL/6$^{CD45.1}$ (CD45.1$^+$) WT BM cells. Cultures were treated with GSI or DMSO at d0, and the percentage of CD45.2$^+$ pDCs analyzed at d8. **(D)** Percentage of CD45.2$^+$ pDCs (CD11c$^+$CD317$^+$CD11b$^-$) after 8 days of co-culture. Data from cells of the same mouse treated with DMSO or GSI were connected by lines. Data from 3 independent experiments.
(EPS)

S2 Fig. Frequency of GSI-treated pDCs after transplantation. Frequencies of pDCs (CD11c$^+$CD317$^+$CD11b$^-$) from CD45.1$^+$ BM and CD45.2$^+$ GSI-treated WT and Ik$^{L/L}$ cells in the BM of recipient mice 9 days post-transplantation.
(EPS)

S3 Fig. Conditional deletion of RBPJ by tamoxifen in Ik$^{L/L}$ mice. Western blot of RBPJ expression in total BM cells from Ikaros-RBPJ compound mutant mice. Actin was used as a loading control.
(EPS)

S4 Fig. Gene expression changes in Ik$^{L/L}$ CDPs. Transcriptome profiling of purified MDPs and CDPs from WT or Ik$^{L/L}$ BM, treated beforehand with GSI or DMSO for 24h. **(A)** Hierarchical clustering of the genes from clusters I and III in Fig 6A, using Immgen transcriptome data for DC progenitors and mature subsets (GSE15907). **(B)** GSEA enrichment plots of genes up- or down-regulated in Ik$^{L/L}$ CDPs compared with WT (clusters II and IV, and clusters I and III in Fig 6A, respectively). **(C)** GSEA enrichment plots of genes specifically up- or down-regulated in Ik$^{L/L}$ pDCs compared with WT (FC>2; p≤0,05) [14]. In (B) and (C), the ranked gene list corresponds to the differential gene expression between WT cDCs and pDCs (Immgen GSE15907). NES: normalized enrichment score; FDR: false discovery rate. **(D)** Genome browser tracks showing Ikaros binding sites in the *Rel* and *Relb* loci in pre-B cells and DN3 thymocytes (GEO GSE114629 and GSE61148 accession numbers).
(EPS)

S5 Fig. TGFβ1 signaling during pDC development in $Ik^{L/L}$ CDPs. (A) Genome browser tracks showing Ikaros binding in the *Eng* locus in pre-B cells and DN3 thymocytes (GEO GSE114629 and GSE61148 accession numbers). **(B)** Total numbers of cells after 8 days of Flt3L-supplemented cultures of WT and $Ik^{L/L}$ BM cells treated with SB431542 and/or GSI. See experiments shown in Fig 7C and 7D. Representative of 4 independent experiments; 2 mice per genotype per experiment; p values were obtained by a Student's t-test. $^{*}p \leq 0.05$; $^{***}p \leq 0.001$.
(EPS)

S1 Table. FC of the 70 genes deregulated in $Ik^{L/L}$ CDPs vs. WT cells, and sensitive to GSI treatment.
(EPS)

Acknowledgments

We thank Silvia Fre, Spyros Artavanis-Tsakonas and Tasuku Honjo for the Hes1-GFP and floxed RBPJ mouse lines, Marc Dalod for the B16-Flt3L cell line, Patricia Marchal for technical assistance, Claudine Ebel and Muriel Philipps for cell sorting, Cathy Herouard for microarray experiments, Michael Gendron for mouse husbandry, and members of the Kastner-Chan lab for discussions.

Author Contributions

Conceptualization: Jérôme Mastio, Philippe Kastner, Susan Chan, Peggy Kirstetter.

Data curation: Jérôme Mastio, Peggy Kirstetter.

Formal analysis: Jérôme Mastio, Peggy Kirstetter.

Funding acquisition: Philippe Kastner, Susan Chan, Peggy Kirstetter.

Investigation: Jérôme Mastio, Célestine Simand, Giovanni Cova, Peggy Kirstetter.

Methodology: Jérôme Mastio, Philippe Kastner, Susan Chan, Peggy Kirstetter.

Project administration: Philippe Kastner, Susan Chan, Peggy Kirstetter.

Resources: Jérôme Mastio, Célestine Simand, Peggy Kirstetter.

Supervision: Philippe Kastner, Susan Chan, Peggy Kirstetter.

Validation: Jérôme Mastio, Célestine Simand, Peggy Kirstetter.

Visualization: Peggy Kirstetter.

Writing – original draft: Philippe Kastner, Susan Chan, Peggy Kirstetter.

Writing – review & editing: Philippe Kastner, Susan Chan, Peggy Kirstetter.

References

1. Hespel C, Moser M. Role of inflammatory dendritic cells in innate and adaptive immunity. Eur J Immunol. 2012; 42(10):2535–43. https://doi.org/10.1002/eji.201242480 PMID: 23042650.
2. Colonna M, Trinchieri G, Liu YJ. Plasmacytoid dendritic cells in immunity. Nat Immunol. 2004; 5 (12):1219–26. https://doi.org/10.1038/ni1141 PMID: 15549123.
3. Merad M, Sathe P, Helft J, Miller J, Mortha A. The dendritic cell lineage: ontogeny and function of dendritic cells and their subsets in the steady state and the inflamed setting. Annu Rev Immunol. 2013; 31:563–604. https://doi.org/10.1146/annurev-immunol-020711-074950 PMID: 23516985; PubMed Central PMCID: PMCPMC3853342.

4. Fogg DK, Sibon C, Miled C, Jung S, Aucouturier P, Littman DR, et al. A clonogenic bone marrow progenitor specific for macrophages and dendritic cells. Science. 2006; 311(5757):83–7. https://doi.org/10.1126/science.1117729 PMID: 16322423.
5. Naik SH, Sathe P, Park HY, Metcalf D, Proietto AI, Dakic A, et al. Development of plasmacytoid and conventional dendritic cell subtypes from single precursor cells derived in vitro and in vivo. Nature immunology. 2007; 8(11):1217–26. Epub 2007/10/09. https://doi.org/10.1038/ni1522 PMID: 17922015.
6. Onai N, Obata-Onai A, Schmid MA, Ohteki T, Jarrossay D, Manz MG. Identification of clonogenic common Flt3+M-CSFR+ plasmacytoid and conventional dendritic cell progenitors in mouse bone marrow. Nature immunology. 2007; 8(11):1207–16. Epub 2007/10/09. https://doi.org/10.1038/ni1518 PMID: 17922016.
7. Miller JC, Brown BD, Shay T, Gautier EL, Jojic V, Cohain A, et al. Deciphering the transcriptional network of the dendritic cell lineage. Nat Immunol. 2012; 13(9):888–99. https://doi.org/10.1038/ni.2370 PMID: 22797772; PubMed Central PMCID: PMCPMC3985403.
8. Murphy TL, Grajales-Reyes GE, Wu X, Tussiwand R, Briseno CG, Iwata A, et al. Transcriptional Control of Dendritic Cell Development. Annu Rev Immunol. 2016; 34:93–119. https://doi.org/10.1146/annurev-immunol-032713-120204 PMID: 26735697; PubMed Central PMCID: PMCPMC5135011.
9. Felker P, Sere K, Lin Q, Becker C, Hristov M, Hieronymus T, et al. TGF-beta1 accelerates dendritic cell differentiation from common dendritic cell progenitors and directs subset specification toward conventional dendritic cells. J Immunol. 2010; 185(9):5326–35. Epub 2010/10/01. https://doi.org/10.4049/jimmunol.0903950 PMID: 20881193.
10. Zhou J, Cheng P, Youn JI, Cotter MJ, Gabrilovich DI. Notch and wingless signaling cooperate in regulation of dendritic cell differentiation. Immunity. 2009; 30(6):845–59. https://doi.org/10.1016/j.immuni.2009.03.021 PMID: 19523851; PubMed Central PMCID: PMCPMC2700307.
11. Xiao J, Zhou H, Wu N, Wu L. The non-canonical Wnt pathway negatively regulates dendritic cell differentiation by inhibiting the expansion of Flt3(+) lymphocyte-primed multipotent precursors. Cell Mol Immunol. 2016; 13(5):593–604. https://doi.org/10.1038/cmi.2015.39 PMID: 26051474; PubMed Central PMCID: PMCPMC5037275.
12. Belz GT, Nutt SL. Transcriptional programming of the dendritic cell network. Nat Rev Immunol. 2012; 12(2):101–13. https://doi.org/10.1038/nri3149 PMID: 22273772.
13. Wu L, Nichogiannopoulou A, Shortman K, Georgopoulos K. Cell-autonomous defects in dendritic cell populations of Ikaros mutant mice point to a developmental relationship with the lymphoid lineage. Immunity. 1997; 7(4):483–92. PMID: 9354469.
14. Allman D, Dalod M, Asselin-Paturel C, Delale T, Robbins SH, Trinchieri G, et al. Ikaros is required for plasmacytoid dendritic cell differentiation. Blood. 2006; 108(13):4025–34. https://doi.org/10.1182/blood-2006-03-007757 PMID: 16912230.
15. Cytlak U, Resteu A, Bogaert D, Kuehn HS, Altmann T, Gennery A, et al. Ikaros family zinc finger 1 regulates dendritic cell development and function in humans. Nat Commun. 2018; 9(1):1239. https://doi.org/10.1038/s41467-018-02977-8 PMID: 29588478; PubMed Central PMCID: PMCPMC5869589.
16. Lucioni M, Novara F, Fiandrino G, Riboni R, Fanoni D, Arra M, et al. Twenty-one cases of blastic plasmacytoid dendritic cell neoplasm: focus on biallelic locus 9p21.3 deletion. Blood. 2011; 118(17):4591–4. https://doi.org/10.1182/blood-2011-03-337501 PMID: 21900200.
17. Menezes J, Acquadro F, Wiseman M, Gomez-Lopez G, Salgado RN, Talavera-Casanas JG, et al. Exome sequencing reveals novel and recurrent mutations with clinical impact in blastic plasmacytoid dendritic cell neoplasm. Leukemia. 2014; 28(4):823–9. https://doi.org/10.1038/leu.2013.283 PMID: 24072100.
18. Tzankov A, Hebeda K, Kremer M, Leguit R, Orazi A, van der Walt J, et al. Plasmacytoid dendritic cell proliferations and neoplasms involving the bone marrow: Summary of the workshop cases submitted to the 18th Meeting of the European Association for Haematopathology (EAHP) organized by the European Bone Marrow Working Group, Basel 2016. Ann Hematol. 2017; 96(5):765–77. https://doi.org/10.1007/s00277-017-2947-4 PMID: 28191591.
19. Kirstetter P, Thomas M, Dierich A, Kastner P, Chan S. Ikaros is critical for B cell differentiation and function. Eur J Immunol. 2002; 32(3):720–30. Epub 2002/03/01. https://doi.org/10.1002/1521-4141(200203)32:3<720::AID-IMMU720>3.0.CO;2-P PMID: 11870616.
20. Dumortier A, Jeannet R, Kirstetter P, Kleinmann E, Sellars M, Dos Santos NR, et al. Notch activation is an early and critical event during T-cell leukemogenesis in Ikaros-deficient mice. Mol Cell Biol. 2006; 26(1):209–20. https://doi.org/10.1128/MCB.26.1.209-220.2006 PMID: 16354692.
21. Kleinmann E, Geimer Le Lay AS, Sellars M, Kastner P, Chan S. Ikaros represses the transcriptional response to Notch signaling in T-cell development. Mol Cell Biol. 2008; 28(24):7465–75. https://doi.org/10.1128/MCB.00715-08 PMID: 18852286.

22. Liu K, Victora GD, Schwickert TA, Guermonprez P, Meredith MM, Yao K, et al. In vivo analysis of dendritic cell development and homeostasis. Science. 2009; 324(5925):392–7. Epub 2009/03/17. https://doi.org/10.1126/science.1170540 PMID: 19286519; PubMed Central PMCID: PMC2803315.

23. Fre S, Hannezo E, Sale S, Huyghe M, Lafkas D, Kissel H, et al. Notch lineages and activity in intestinal stem cells determined by a new set of knock-in mice. PLoS One. 2011; 6(10):e25785. Epub 2011/10/13. https://doi.org/10.1371/journal.pone.0025785 PMID: 21991352; PubMed Central PMCID: PMC3185035.

24. Zhang J, Raper A, Sugita N, Hingorani R, Salio M, Palmowski MJ, et al. Characterization of Siglec-H as a novel endocytic receptor expressed on murine plasmacytoid dendritic cell precursors. Blood. 2006; 107(9):3600–8. https://doi.org/10.1182/blood-2005-09-3842 PMID: 16397130.

25. Schlitzer A, Loschko J, Mair K, Vogelmann R, Henkel L, Einwachter H, et al. Identification of CCR9-murine plasmacytoid DC precursors with plasticity to differentiate into conventional DCs. Blood. 2011; 117(24):6562–70. https://doi.org/10.1182/blood-2010-12-326678 PMID: 21508410.

26. Gilliet M, Boonstra A, Paturel C, Antonenko S, Xu XL, Trinchieri G, et al. The development of murine plasmacytoid dendritic cell precursors is differentially regulated by FLT3-ligand and granulocyte/macrophage colony-stimulating factor. J Exp Med. 2002; 195(7):953–8. https://doi.org/10.1084/jem.20020045 PMID: 11927638.

27. Brawand P, Fitzpatrick DR, Greenfield BW, Brasel K, Maliszewski CR, De Smedt T. Murine plasmacytoid pre-dendritic cells generated from Flt3 ligand-supplemented bone marrow cultures are immature APCs. J Immunol. 2002; 169(12):6711–9. Epub 2002/12/10. PMID: 12471102.

28. Onai N, Kurabayashi K, Hosoi-Amaike M, Toyama-Sorimachi N, Matsushima K, Inaba K, et al. A clonogenic progenitor with prominent plasmacytoid dendritic cell developmental potential. Immunity. 2013; 38(5):943–57. Epub 2013/04/30. https://doi.org/10.1016/j.immuni.2013.04.006 PMID: 23623382.

29. Han H, Tanigaki K, Yamamoto N, Kuroda K, Yoshimoto M, Nakahata T, et al. Inducible gene knockout of transcription factor recombination signal binding protein-J reveals its essential role in T versus B lineage decision. Int Immunol. 2002; 14(6):637–45. Epub 2002/06/01. PMID: 12039915.

30. Badea TC, Wang Y, Nathans J. A noninvasive genetic/pharmacologic strategy for visualizing cell morphology and clonal relationships in the mouse. J Neurosci. 2003; 23(6):2314–22. Epub 2003/03/27. PMID: 12657690.

31. Macias-Garcia A, Heizmann B, Sellars M, Marchal P, Dali H, Pasquali JL, et al. Ikaros Is a Negative Regulator of B1 Cell Development and Function. J Biol Chem. 2016; 291(17):9073–86. https://doi.org/10.1074/jbc.M115.704239 PMID: 26841869; PubMed Central PMCID: PMCPMC4861476.

32. Oravecz A, Apostolov A, Polak K, Jost B, Le Gras S, Chan S, et al. Ikaros mediates gene silencing in T cells through Polycomb repressive complex 2. Nature communications. 2015; 6:8823. https://doi.org/10.1038/ncomms9823 PMID: 26549758.

33. Fonsatti E, Del Vecchio L, Altomonte M, Sigalotti L, Nicotra MR, Coral S, et al. Endoglin: An accessory component of the TGF-beta-binding receptor-complex with diagnostic, prognostic, and bioimmunotherapeutic potential in human malignancies. J Cell Physiol. 2001; 188(1):1–7. https://doi.org/10.1002/jcp.1095 PMID: 11382917.

34. Georgopoulos K, Bigby M, Wang JH, Molnar A, Wu P, Winandy S, et al. The Ikaros gene is required for the development of all lymphoid lineages. Cell. 1994; 79(1):143–56. PMID: 7923373.

35. Hacker C, Kirsch RD, Ju XS, Hieronymus T, Gust TC, Kuhl C, et al. Transcriptional profiling identifies Id2 function in dendritic cell development. Nat Immunol. 2003; 4(4):380–6. https://doi.org/10.1038/ni903 PMID: 12598895.

36. Cisse B, Caton ML, Lehner M, Maeda T, Scheu S, Locksley R, et al. Transcription factor E2-2 is an essential and specific regulator of plasmacytoid dendritic cell development. Cell. 2008; 135(1):37–48. https://doi.org/10.1016/j.cell.2008.09.016 PMID: 18854153; PubMed Central PMCID: PMCPMC2631034.

37. Ghosh HS, Cisse B, Bunin A, Lewis KL, Reizis B. Continuous expression of the transcription factor e2-2 maintains the cell fate of mature plasmacytoid dendritic cells. Immunity. 2010; 33(6):905–16. https://doi.org/10.1016/j.immuni.2010.11.023 PMID: 21145760; PubMed Central PMCID: PMCPMC3010277.

38. Santibanez JF, Letamendia A, Perez-Barriocanal F, Silvestri C, Saura M, Vary CP, et al. Endoglin increases eNOS expression by modulating Smad2 protein levels and Smad2-dependent TGF-beta signaling. J Cell Physiol. 2007; 210(2):456–68. https://doi.org/10.1002/jcp.20878 PMID: 17058229.

39. Blair CR, Stone JB, Wells RG. The type III TGF-beta receptor betaglycan transmembrane-cytoplasmic domain fragment is stable after ectodomain cleavage and is a substrate of the intramembrane protease gamma-secretase. Biochim Biophys Acta. 2011; 1813(2):332–9. Epub 2010/12/21. https://doi.org/10.1016/j.bbamcr.2010.12.005 PMID: 21167215; PubMed Central PMCID: PMC3026071.

40. Geimer Le Lay AS, Oravecz A, Mastio J, Jung C, Marchal P, Ebel C, et al. The tumor suppressor Ikaros shapes the repertoire of Notch target genes in T cells. Sci Signal. 2014; 7(317):ra28. Epub 2014/03/20. https://doi.org/10.1126/scisignal.2004545 PMID: 24643801.

41. Blokzijl A, Dahlqvist C, Reissmann E, Falk A, Moliner A, Lendahl U, et al. Cross-talk between the Notch and TGF-beta signaling pathways mediated by interaction of the Notch intracellular domain with Smad3. J Cell Biol. 2003; 163(4):723–8. https://doi.org/10.1083/jcb.200305112 PMID: 14638857; PubMed Central PMCID: PMCPMC2173673.

42. Ceribelli M, Hou ZE, Kelly PN, Huang DW, Wright G, Ganapathi K, et al. A Druggable TCF4- and BRD4-Dependent Transcriptional Network Sustains Malignancy in Blastic Plasmacytoid Dendritic Cell Neoplasm. Cancer Cell. 2016; 30(5):764–78. https://doi.org/10.1016/j.ccell.2016.10.002 PMID: 27846392; PubMed Central PMCID: PMCPMC5175469.

43. Mach N, Gillessen S, Wilson SB, Sheehan C, Mihm M, Dranoff G. Differences in dendritic cells stimulated in vivo by tumors engineered to secrete granulocyte-macrophage colony-stimulating factor or Flt3-ligand. Cancer Res. 2000; 60(12):3239–46. PMID: 10866317.

44. Subramanian A, Tamayo P, Mootha VK, Mukherjee S, Ebert BL, Gillette MA, et al. Gene set enrichment analysis: a knowledge-based approach for interpreting genome-wide expression profiles. Proc Natl Acad Sci U S A. 2005; 102(43):15545–50. Epub 2005/10/04. doi: 0506580102 [pii] https://doi.org/10.1073/pnas.0506580102 PMID: 16199517; PubMed Central PMCID: PMC1239896.

45. Mootha VK, Lindgren CM, Eriksson KF, Subramanian A, Sihag S, Lehar J, et al. PGC-1alpha-responsive genes involved in oxidative phosphorylation are coordinately downregulated in human diabetes. Nat Genet. 2003; 34(3):267–73. https://doi.org/10.1038/ng1180 PMID: 12808457.

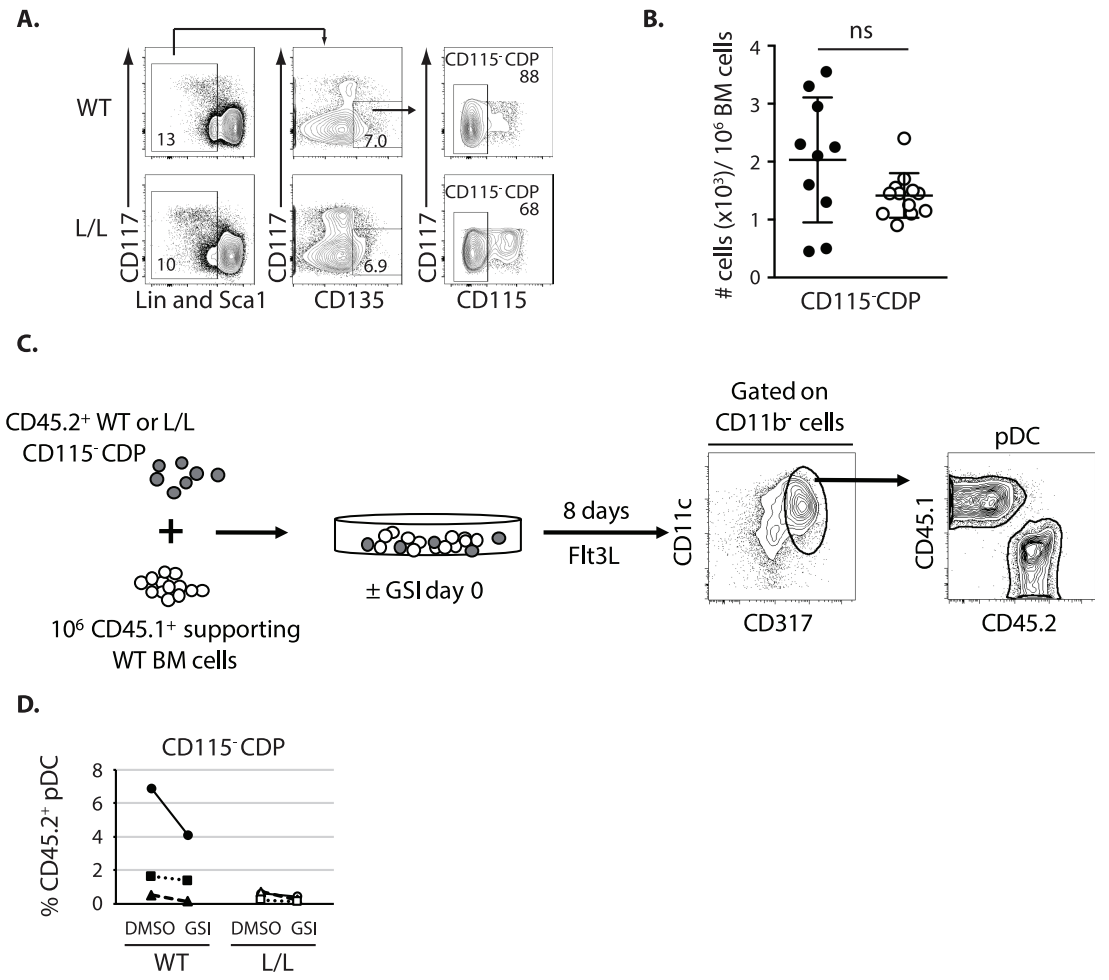

S1 Fig. GSI does not act on CD115$^-$ CDPs to stimulate pDC differentiation.
(A) Representative analysis of CD115$^-$ CDPs from WT and Ik$^{L/L}$ BM, by flow cytometry. **(B)** Relative numbers of CD115$^-$ CDPs (as gated in A). ns: not significant (Student's t-test). **(C)** Experimental scheme: CD115$^-$ CDPs from WT or Ik$^{L/L}$ BM (CD45.2$^+$) were cultured with supporting C57BL/6$^{CD45.1}$ (CD45.1$^+$) WT BM cells. Cultures were treated with GSI or DMSO at d0, and the percentage of CD45.2$^+$ pDCs analyzed at d8. **(D)** Percentage of CD45.2$^+$ pDCs (CD11c$^+$CD317$^+$CD11b$^-$) after 8 days of co-culture. Data from cells of the same mouse treated with DMSO or GSI were connected by lines. Data from 3 independent experiments.

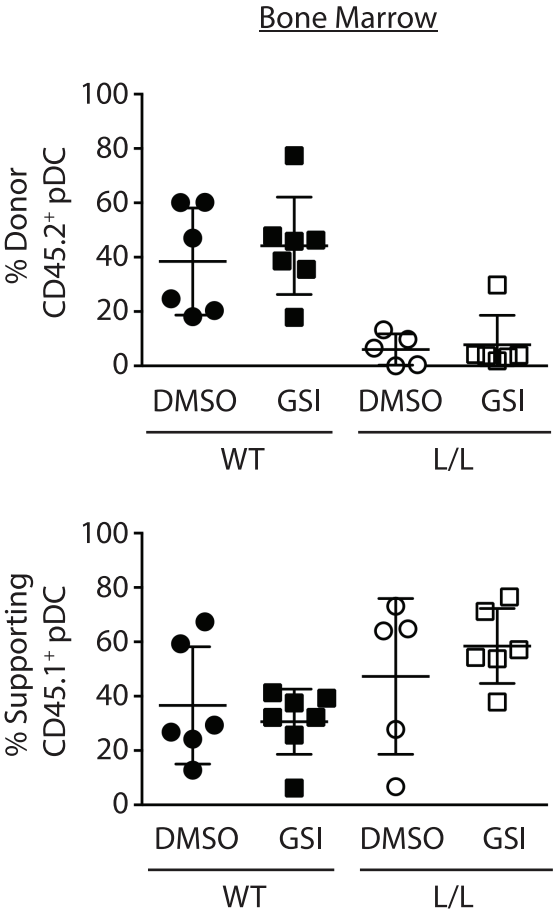

S2 Fig. Frequency of GSI-treated pDCs after transplantation.
Frequencies of pDCs ($CD11c^+CD317^+CD11b^-$) from $CD45.1^+$ BM and $CD45.2^+$ GSI-treated WT and $Ik^{L/L}$ cells in the BM of recipient mice 9 days post-transplantation.

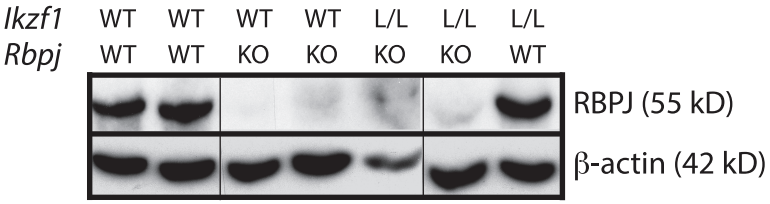

S3 Fig. Conditional deletion of RBPJ by tamoxifen in $Ik^{L/L}$ mice.
Western blot of RBPJ expression in total BM cells from Ikaros-RBPJ compound mutant mice. Actin was used as a loading control

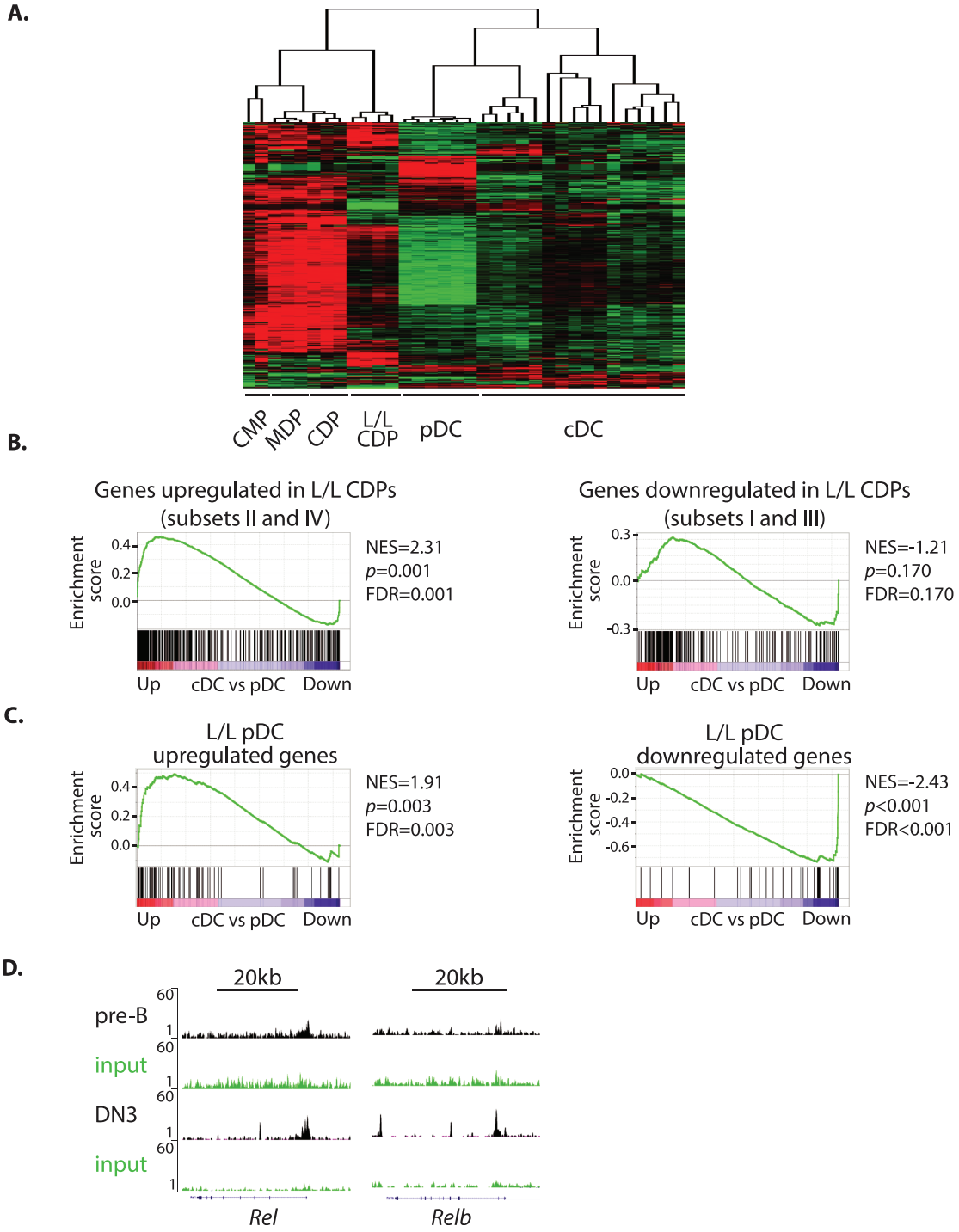

S4 Fig. Gene expression changes in Ik$^{L/L}$ CDPs.
Transcriptome profiling of purified MDPs and CDPs from WT or Ik$^{L/L}$ BM, treated beforehand with GSI or DMSO for 24h. **(A)** Hierarchical clustering of the genes from clusters I and III in Fig 6A, using Immgen transcriptome data for DC progenitors and mature subsets (GSE15907). **(B)** GSEA enrichment plots of genes up- or down-regulated in Ik$^{L/L}$ CDPs compared with WT (clusters II and IV, and clusters I and III in Fig 6A, respectively). **(C)** GSEA enrichment plots of genes specifically up- or down-regulated in Ik$^{L/L}$ pDCs compared with WT (FC>2; p≤0,05) [14]. In (B) and (C), the ranked gene list corresponds to the differential gene expression between WT cDCs and pDCs (Immgen GSE15907). NES: normalized enrichment score; FDR: false discovery rate. **(D)** Genome browser tracks showing Ikaros binding sites in the *Rel* and *Relb* loci in pre-B cells and DN3 thymocytes (GEO GSE114629 and GSE61148 accession numbers).

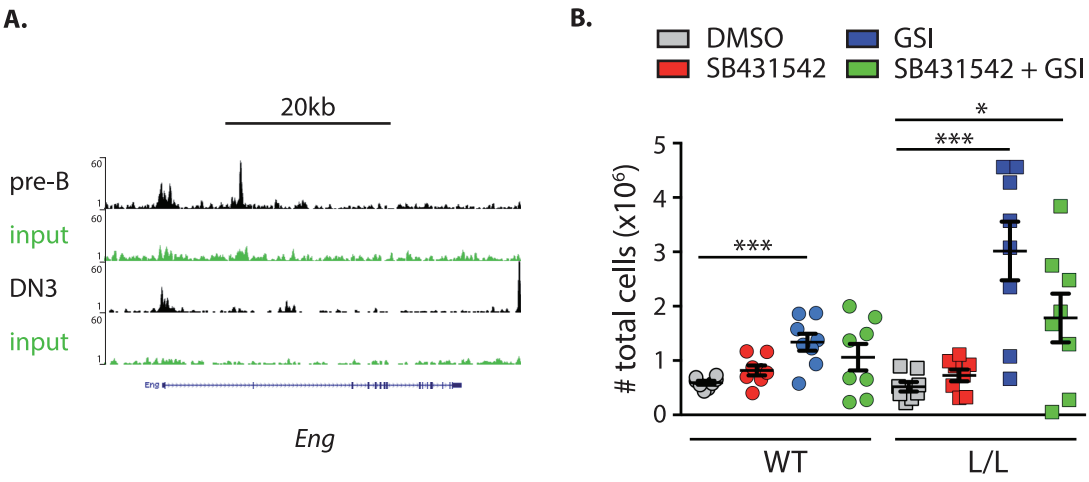

S5 Fig. TGFβ1 signaling during pDC development in $Ik^{L/L}$ CDPs.
(A) Genome browser tracks showing Ikaros binding in the *Eng* locus in pre-B cells and DN3 thymocytes (GEO GSE114629 and GSE61148 accession numbers). **(B)** Total numbers of cells after 8 days of Flt3L-supplemented cultures of WT and $Ik^{L/L}$ BM cells treated with SB431542 and/or GSI. See experiments shown in Fig 7C and 7D. Representative of 4 independent experiments; 2 mice per genotype per experiment; p values were obtained by a Student's t-test. *p≤0.05; ***p≤0.001

	Probe Set ID	Gene Symbol	FC L/L vs WT CDPs (Log2)	FC L/L CDPs GSI vs DMSO (Log2)
1	10575052	Cdh1	1,972	7,476
2	10576799	Cd209e	1,972	6,928
3	10583056	Mmp12	2,718	3,994
4	10598976	Timp1	1,844	3,965
5	10487021	Slc30a4	1,822	3,096
6	10598093	Tarm1	0,423	3,028
7	10469358	Mrc1	6,238	2,799
8	10497381	Cyp7b1	2,875	2,793
9	10438769	Cldn1	7,789	2,775
10	10576332	Tubb3	1,716	2,557
11	10498350	P2ry14	2,014	2,515
12	10374197	Ramp3	10,961	2,266
13	10560294	Ceacam15	1,545	2,250
14	10499394	Lmna	1,682	2,210
15	10390075	Gm11545	2,959	2,097
16	10546631	Frmd4b	2,266	2,057
17	10350159	Lad1	2,032	2,037
18	10377774	Mgl2	7,310	2,022
19	10375472	Timd4	12,849	1,963
20	10475544	Sema6d	6,404	1,746
21	10467842	Got1	1,979	1,741
22	10408227	Hfe	1,641	1,728
23	10363735	Egr2	2,710	1,708
24	10484318	Nckap1	1,602	1,706
25	10425040	Apol7b	1,508	1,656
26	10520950	Pdlim1	0,649	1,627
27	10412298	Itga1	0,432	1,589
28	10571036	Ppapdc1b	0,631	1,556
29	10476314	Prnp	2,444	1,533
30	10584712	Hyou1	1,575	1,516
31	10367982	Gpr126	1,892	0,666
32	10411622	Naip6	0,663	0,658
33	10497122	Depdc1a	0,337	0,656
34	10445338	Enpp5	2,163	0,656
35	10486026	Zfp770	1,651	0,655
36	10599174	Il13ra1	2,940	0,645
37	10390103	Pdk2	1,665	0,643
38	10555862	Trim34a	1,578	0,641
39	10565570	Ddias	0,425	0,641
40	10403229	Itgb8	3,774	0,637
41	10480238	St8sia6	1,744	0,616
42	10396402	Prkch	1,820	0,614
43	10486061	Rasgrp1	2,094	0,612
44	10576639	Nrp1	1,529	0,608
45	10532741	Tmem119	1,823	0,608
46	10486112	Bmf	1,766	0,604
47	10527940	Cdk14	1,699	0,603
48	10581434	Dpep2	2,071	0,593
49	10568001	Sult1a1	2,564	0,591
50	10441233	Mx1	1,842	0,589
51	10531610	Rasgef1b	2,608	0,582
52	10585085	---	0,630	0,581
53	10485633	Gm10796	0,593	0,580
54	10420483	Phf11a	3,055	0,578
55	10351623	F11r	6,065	0,577
56	10541575	Clec4a4	5,272	0,557
57	10352905	Cd34	0,594	0,551
58	10591614	Dock6	1,860	0,542
59	10451054	Enpp4	1,686	0,530
60	10598750	Gpr34	1,725	0,525
61	10385504	Gm5431	2,515	0,497
62	10548422	Klri2	3,066	0,495
63	10547153	Alox5	8,793	0,479
64	10444223	H2-Oa	2,159	0,445
65	10473399	Prg2	1,793	0,433
66	10542140	Klrb1f	0,268	0,423
67	10512470	Cd72	3,032	0,423
68	10523128	Ppbp	4,911	0,416
69	10561104	Axl	2,042	0,281
70	10351792	Slamf9	4,508	0,275

S1 Table. FC of the 70 genes deregulated in $Ik^{L/L}$ CDPs vs. WT cells, and sensitive to GSI treatment.

TITRE

Rôle d'Helios dans la biologie des cellules souches et des progéniteurs hématopoïétiques.

CONTEXTE

Les cellules souches hématopoïétiques (CSH), situées dans la moelle osseuse (MO), donnent naissance aux cellules sanguines matures tout au long de la vie adulte d'un individu[1]. Les deux fonctions importantes des CSH et de leurs progéniteurs en aval sont (1) leur capacité à générer des cellules lymphoïdes, des cellules myéloïdes et des érythro-mégacaryocytes[1], et (2) leur capacité à préserver une intégrité du génome suite aux dommages de l'ADN[2,3]. La perte de la première fonction peut entraîner des immunodéficiences ou une anémie tandis que la perte de la seconde fonction est souvent associée au développement de leucémies[4,6].

Dans la hiérarchie simplifiée, les CSH sont divisées en CSH à long terme (LT-) ($Lin^-Sca1^+cKit^+CD48^-CD150^+$), qui se s'auto-renouvellent et se différencient rarement, et les CSH à court terme en aval (ST-) ($Lin^-Sca1^+cKit^+CD48^-CD150^-$), qui s'auto-renouveler de manière plus importante et se différencient en cellules progénitrices multi-potentes (MPP). Récemment, il a été démontré que les MPP constituaient une population hétérogène, qui peut être divisée en 3 sous-populations: les MPP2, 3 et 4[4,5]. Les cellules MPP2 ($Lin^-Sca1^+cKit^+Flt3^-CD48^+CD150^+$) donnent naissance principalement à la lignée érythroïde et mégacaryocytaire. Les cellules MPP3 ($Lin^-Sca1^+cKit^+Flt3^-CD48^+CD150^-$) sont limitées aux cellules de la lignée myéloïde et deviennent des progéniteurs des monocytes et des granulocytes (GMP), tandis que les MPP4 ($Lin^-Sca1^+cKit^+Flt3^+CD48^+CD150^-$) sont principalement composées de progéniteurs lymphoïdes (CLP) qui vont se différencier en cellules lymphoïdes matures. Chez les souris adultes jeunes (<6 mois), les cellules MPP3 et MPP4 sont présentent dans les mêmes proportions parmi les MPP, tandis que les cellules MPP2 ne représentent qu'environ 10% de cette population. La régulation de l'ensemble de ces premières étapes de différenciation par les facteurs transcriptionnels reste encore largement méconnue.

Notre laboratoire s'intéresse à la régulation moléculaire de l'expression des gènes au cours de l'hématopoïèse normale et pathologique. En particulier, nous étudions la famille des facteurs de transcription Ikaros [Ikaros (IKZF1), Helios (IKZF2), Aiolos (IKZF3), Eos (IKZF4)], qui jouent un rôle crucial dans le développement de différentes cellules hématopoïétiques. Ces protéines, qui se lient à l'ADN par l'intermédiaire d'un motif à un doigt de zinc, sont également impliquées en tant que suppresseurs de tumeurs[7]. Chez la souris, ces facteurs sont nécessaires pour la différenciation de plusieurs types de cellules hématopoïétiques. Chez l'homme, les mutations des gènes IKZF sont corrélées aux leucémies aiguës lymphoblastiques. Des délétions ou des mutations dominantes négatives d'IKZF1 sont plus étroitement associées aux leucémies aiguës lymphoblastiques à cellules B. En revanche, des délétions d'IKZF2 ont été observées dans plus de 50% des leucémies aiguës lymphoblastiques dites hypodiploïde avec seulement 32 à 39 chromosomes; ces leucémies ont des pronostics très médiocres[7].

Les protéines Ikaros et Helios sont fortement exprimées dans les CSH. S'il a été montré qu'Ikaros est nécessaire à l'auto-renouvellement et à la différenciation des progéniteurs des CSH[8], la fonction d'Helios dans ces cellules reste inconnue.

Mon projet au laboratoire a consisté à étudier la fonction d'Helios dans les CSH, à l'aide d'un modèle murin où le gène IKZF2 est supprimé dans la lignée germinale. Mon travail a révélé qu'Helios influence le développement des cellules souches et progénitrices hématopoïétiques en favorisant la différenciation de ces cellules vers la lignée lymphoïde.

RÉSULTATS

Pour déterminer le rôle d'Helios dans l'hématopoïèse, j'ai d'abord étudié son expression au niveau protéique dans les CSH et leurs progéniteurs en aval dans la MO par cytométrie en flux. J'ai montré qu'Helios est fortement exprimé dans les cellules Lineage$^-$cKit$^+$Sca1$^+$ (LSK), qui comprennent les CSH à long terme (LT) et à court terme (ST), ainsi que les progéniteurs débutants multi-potents (MPP). Au contraire, Helios est largement absent des cellules hématopoïétiques matures et des cellules de la niche hématopoïétique. Ces résultats suggèrent qu'Helios joue un rôle

important dans la biologie des cellules souches et des progéniteurs hématopoïétiques.

Pour déterminer son rôle dans l'hématopoïèse, nous avons analysé le phénotype des CSH et des progéniteurs hématopoïétiques chez les souris sauvages (WT) et déficientes pour Helios ($He^{-/-}$) âgées de 7 à 20 semaines. Au cours de l'analyse par cytométrie de flux de l'expression des marqueurs de surfaces des CSH, nous avons constaté une forte réduction du nombre total de cellules B matures et des progéniteurs lymphoïdes engagés ainsi qu'une augmentation accrue des progéniteurs myéloïdes et de mégacaryocytaires, ce phénotype ressemble fortement à un celui observé lors du vieillissement des CSH.

Nous avons découvert en analysant les premiers progéniteurs multi-potents une diminution significative du nombre de progéniteurs engagés vers le lignage lymphoïde (LMPP ou MPP4) accompagnée d'une augmentation des progéniteurs myéloïdes (MPP3) dans la MO des souris $He^{-/-}$. De plus, les progéniteurs érythroïdes / mégakaryocytaires (MPP2) sont biaisées vers le lignage megacaryocytaire. Ces résultats suggèrent qu'Helios joue un rôle précoce dans la différenciation hématopoïétique.

Pour valider ce déséquilibre de différenciation hématopoïétique au niveau fonctionnel, nous avons étudié la capacité des cellules totales ou des CSH et / ou MPP purifiées de la MO $He^{-/-}$ à se différencier en cellules lymphoïdes, myéloïdes et mégacaryocytaires in vivo (expériences de greffe de la MO) et ex vivo (formation de colonies en culture). In vivo, nous avons constaté qu'après la greffe de cellules totales de MO ou de CSH purifiées chez les souris receveuses irradiées de manière létale, les cellules $He^{-/-}$ engendrent moins de cellules lymphoïdes B et plus de cellules myéloïdes que les cellules donneuses WT. Des résultats similaires ont été obtenus in vitro lorsque des CSH et des MPP purifiés $He^{-/-}$ ont été mis en cultures. Dans toutes les expériences effectuées, les cellules $He^{-/-}$ génèrent un nombre plus important de cellules myéloïdes et de mégacaryocytes comparés aux cellules WT. Ces résultats suggèrent qu'Helios est nécessaire pour que la différentiation des cellules hématopoïétiques à partir des CSH et des MPP s'effectue proprement et de manière équilibrée.

Pour étudier la régulation génique plus en profondeur, nous avons effectué un séquençage des transcrits de cellules purifiées LT-CSH, MPP3 et MPP4 à partir de MO de souris $He^{-/-}$ et WT. Nous avons découvert que les populations les plus

affectées par la déficience d'Helios sont les LT-CSH tandis que le profil transcriptionel des MPP est modérément affecté. En outre, nous avons constaté, en effectuant des analyses GSEA (gene set enrichment analysis), que les LT-CSH $He^{-/-}$ ont un profil transcriptionnel similaire à celui observé chez les CSH WT âgées et aux CSH biaisées vers le lignage megacaryocytaire. Une réduction de la transcription des gènes spécifiques du lignage lymphoïde a été observé dans les MPP3 et MPP4 $He^{-/-}$.

Dans l'ensemble, ces résultats supportent qu'Hélios est un acteur décisif dans le chez choix des cellules hématopoïétiques précoces dès les premières étapes de l'hématopoïèse.

Nous effectuons actuellement des analyses moléculaires plus détaillées afin de déterminer si la différence d'expression de transcrit est due aux changements d'expression génique intrinsèque aux cellules souches hématopoïétiques ou due à une différence composition de la population étudiée. De plus, pour caractériser directement les gènes cibles d'Helios, nous testons de nouvelles techniques pour déterminer les gènes directement régulés par Helios (Cut&Run, ChIP).

Références

1. Laurenti E, Göttgens B. **From haematopoietic stem cells to complex differentiation landscapes**. Nature. 2018 Jan 24, 553(7689):418-426
2. Beerman I, Seita J, Inlay MA, Weissman IL, Rossi DJ. **Quiescent hematopoietic stem cells accumulate DNA damage during aging that is repaired upon entry into cell cycle**. Cell Stem Cell. 2014 Jul 3, 15(1):37-50
3. Flach J, Bakker ST, Mohrin M, Conroy PC, Pietras EM, Reynaud D, Alvarez S, Diolaiti ME, Ugarte F, Forsberg EC, Le Beau MM, Stohr BA, Méndez J, Morrison CG, Passegué E. **Replication stress is a potent driver of functional decline in ageing haematopoietic stem cells**. Nature. 2014 Aug 14
4. Akunuru S, Geiger H. **Aging, Clonality, and Rejuvenation of Hematopoietic Stem Cells.** Trends Mol Med. 2016 Aug, 512(7513):198-202
5. Pietras EM, Reynaud D, Kang YA, Carlin D, Calero-Nieto FJ, Leavitt AD, Stuart JM, Göttgens B, and Passegué E. **Functionally distinct subsets of lineage-biased multipotent progenitors control blood production in normal and regenerative conditions**. Cell Stem Cell. 2015 Jul 2, 17(1):35-46

6. Rodriguez-Fraticelli AE, Wolock SL, Weinreb CS, Panero R, Patel SH, Jankovic M, Sun J, Calogero RA, Klein AM, Camargo FD. **Clonal analysis of lineage fate in native haematopoiesis.** Nature. 2018 Jan 112018 Jan 3, 553(7687):212-216
7. Heizmann B, Kastner P, Chan S. **The Ikaros family in lymphocyte development.** Curr Opin Immunol. 2017 Dec 23, 51:14-23
8. Yoshida T, Ng SY, Zuniga-Pflucker JC, Georgopoulos K. **Early hematopoietic lineage restrictions directed by Ikaros**. Nat Immunol. 2006 Apr, 7(4):382-91

Giovanni Cova

THE ROLE OF HELIOS IN THE HEMATOPOIETIC STEM AND PROGENITOR CELL DEVELOPMENT

Hematopoietic Stem and Progenitor Cells (HSPC) engender all the mature blood cells throughout life. They are subdivided in undifferentiated stem cells (HSC) and primed multipotent progenitors (MPP). MPP are heterogeneous and composed of erythro-megakaryocytes (MMP2), myeloid (MPP3) and lymphoid (MPP4) primed cells. Despite the fact that these populations are well defined, the molecular mechanisms underlying their differentiation remain unclear. We showed that the transcription factor Helios, highly expressed in the HSPC, is crucial for HSPC specification and aging. Bone marrow transplantation, ex-vivo differentiation and flow cytometry assays revealed that Helios deficient mice have reduced MPP4 as well as lymphoid progenitors. This deficiency is offset by an increase in MPP3, granulo-monocyte and megakaryocyte progenitors. Moreover, transcriptional analysis of HSPC revealed that Helios deficiency affects mainly HSC with an enrichment of megakaryocyte and old HSC genes signatures, whereas Helios deficient MPP express lower levels of lymphoid specific genes. Our work reveals Helios as a novel regulator of HSC specification and aging.

Les cellules souches et progénitrices hématopoïétiques (CSPH) produisent les cellules sanguines durant toute la vie. Elles sont divisées en cellules souches indifférenciées (CSH) et en cellules progénitrices multipotentes engagées (MPP). Les MPP sont hétérogènes et composées de cellules progénitrices multipotentes engagées vers les lignages érythro-mégacaryocytaires (MPP2), myéloïdes (MPP3) et lymphoïdes (MPP4). Malgré que ces populations cellulaires soient bien définies, les mécanismes moléculaires gouvernants leurs différenciations restent en grande partie encore inconnus. Nous avons montré que le facteur de transcription Hélios, exprimé fortement dans les CSPH, est crucial pour la spécification et le vieillissement des CSPH. Les greffes de moëlle osseuse et les expériences de différenciation ex-vivo et de cytométrie en flux montrent que les souris déficientes pour Hélios possèdent un nombre réduit de MPP4 et de progéniteurs lymphoïdes. Ce déficit est compensé par une augmentation du nombre de MPP3 et de progéniteurs granulo-monocytaires et mégacaryocytaires. De plus l'analyse transcriptionnelle des CSPH indique que la déficience pour Hélios affecte principalement les CSH exprimant des gènes spécifiques aux mégacaryocytes et aux vieilles CSH, tandis que les MPP déficients pour Hélios expriment faiblement les gènes spécifiques aux cellules lymphoïdes. Notre travail montre que Hélios est un nouveau régulateur de la spécification et du vieillissement des HSC.